

BARBITURATES AND MODIFIED HAMILTON RECEPTORS FOR
SUPRAMOLECULAR CATALYSIS, SENSING, AND MATERIALS APPLICATIONS

by

DANIEL THOMAS SEIDENKRANZ

A DISSERTATION

Presented to the Department of Chemistry and Biochemistry
and the Graduate School of the University of Oregon
in partial fulfillment of the requirements
for the degree of
Doctor of Philosophy

September 2018

DISSERTATION APPROVAL PAGE

Student: Daniel Thomas Seidenkranz

Title: Barbiturates and Modified Hamilton Receptors for Supramolecular Catalysis, Sensing, and Materials Applications

This dissertation has been accepted and approved in partial fulfillment of the requirements for the Doctor of Philosophy degree in the Department of Chemistry and Biochemistry by:

Michael M. Haley	Chairperson
Michael D. Pluth	Advisor
Victoria J. DeRose	Core Member
John S. Conery	Institutional Representative

and

Janet Woodruff-Borden	Vice Provost and Dean of the Graduate School
-----------------------	--

Original approval signatures are on file with the University of Oregon Graduate School.

Degree awarded September 2018

© 2018 Daniel Thomas Seidenkranz

DISSERTATION ABSTRACT

Daniel Thomas Seidenkranz

Doctor of Philosophy

Department of Chemistry and Biochemistry

September 2018

Title: Barbiturates and Modified Hamilton Receptors for Supramolecular Catalysis, Sensing, and Materials Applications

Supramolecular chemistry (chemistry beyond the molecule) is the study and synthesis of complex molecular architectures from simple subunits using non-covalent interactions. The types of non-covalent interactions that are used for the self-assembly of these complex molecular architectures include electrostatic interactions (e.g. ionic, halogen, and hydrogen bonding), π -effects, van der Waals interactions, metal coordination, and hydrophobic effects. While these interactions are often used in concert, some of the most successful and ubiquitous approaches for the design and construction of new host-guest architectures are the incorporation of hydrogen bonding motifs. A popular class of molecules capable of making strong, highly directional hydrogen bonds is barbiturates.

Barbiturates have a well-known reputation as potent hypnotics, anticonvulsants, and anxiolytics but recent years have seen a renewed interest in these molecules due to their unique, symmetric acceptor-donor-acceptor hydrogen bonding motif. In addition, receptors with complementary hydrogen bonding motifs capable of binding barbiturates have also been reported, namely those based on the work of Hamilton *et al.* Collectively, barbiturates and their receptors have seen widespread use in a variety of applications including sensing, optoelectronics, catalysis, and the design of soft materials.

The work presented in this dissertation describes the development of novel Hamilton receptors for supramolecular catalysis and barbiturate sensing, as well as the design of new synthetic barbiturates. Together this body of research aims to extend the utility of these types of host–guest systems as well as continue to develop and refine the supramolecular design principles that govern the binding interactions between barbiturates and a variety of Hamilton-type receptors.

This dissertation includes both previously published/unpublished and co-authored material.

CURRICULUM VITAE

NAME OF AUTHOR: Daniel Thomas Seidenkranz

GRADUATE AND UNDERGRADUATE SCHOOLS ATTENDED:

University of Oregon, Eugene
University of Minnesota, Morris

DEGREES AWARDED:

Doctor of Philosophy, Chemistry, 2018, University of Oregon
Bachelor of Arts, Chemistry, 2013, University of Minnesota, Morris

AREAS OF SPECIAL INTEREST:

Organic Synthesis and Materials
Supramolecular Chemistry
Organometallic Chemistry

PROFESSIONAL EXPERIENCE:

Teaching Assistant for Topics in Magnetic Resonance (University of Oregon,
CH 613)

Teaching Assistant for Major's Organic Chemistry Lecture (University of
Oregon, CH 341, CH 342)

Teaching Assistant for Major's and Non-Major's Organic Chemistry Laboratory
(University of Oregon)

Undergraduate Teaching Assistant for Organic and General Chemistry
(University of Minnesota, Morris)

GRANTS, AWARDS, AND HONORS:

University of Oregon Graduate Student Award for Excellence in the Teaching of
Chemistry, University of Oregon, 2015

NSF Graduate Research Fellowship Honorable Mention, University of Oregon,
2014

Outstanding Scholarship in Chemistry Award, University of Minnesota, Morris
2014

Scholar of the College, University of Minnesota, Morris, 2012

PUBLICATIONS:

Seidenkranz, D. T.; McGrath, J. M.; Zakharov, L.N.; Pluth, M.D. Supramolecular bidentate phosphine ligand scaffolds from deconstructed Hamilton receptors. *Chem. Commun.* **2017**, 53, 561–564.

Kendall, A. J.; Seidenkranz, D. T.; Tyler, D. R. Improved Synthetic Route to Heteroleptic Alkylphosphine Oxides. *Organometallics* **2017**, 36, 2412–2417.

Kendall, A. J.; Barry, J. T.; Seidenkranz, D. T.; Ryerson, A.; Hiatt, C.; Salazar, C. A.; Bryant, D. J.; Tyler, D. R. Highly efficient biphasic ozonolysis of alkenes using a high-throughput film-shear flow reactor. *Tetrahedron Lett.* **2016**, 57, 1342–1345.

Hammers, M. D.; Taormina, M. J.; Cerda, M. M.; Montoya, L. A.; Seidenkranz, D. T.; Parthasarathy, R.; Pluth, M. D. A Bright Fluorescent Probe for H₂S Enables Analyte-Responsive, 3D Imaging in Live Zebrafish Using Light Sheet Fluorescence Microscopy. *J. Am. Chem. Soc.* **2015**, 137, 10216–10223.

Pappenfus, T. M.; Seidenkranz, D. T.; Lovander, M. D.; Beck, T. L.; Karels, B. J.; Ogawa, K.; Janzen, D. E. Synthesis and Electronic Properties of Oxidized Benzo[1,2-b:4,5-b']dithiophenes. *J. Org. Chem.* **2014**, 79, 9408–9412

Pappenfus, T. M.; Seidenkranz, D. T.; Reinheimer, E. W. One-Pot Synthesis of 4,8-Dialkylbenzo[1,2-b:4,5-b']dithiophenes. *Heterocycles* **2012**, 85, 355–364.

ACKNOWLEDGMENTS

Graduate school is by far the most challenging event I've encountered thus far in my life. Completing this daunting task would not have been possible without help and guidance from many people. Firstly, I wish to express my sincere appreciation to the teachers and professors whose passion for science inspired me to pursue a formal education in chemistry. Specifically, I would like to acknowledge my high school chemistry teacher, Teri Hei, and my undergraduate advisors, Dr. Nancy Carpenter and Dr. Ted Pappenfus.

Next, I would like to express my appreciation to the mentors I had early on in my graduate career including; Dr. Alex Kendall, Dr. Gabe Rudebusch, and Dr. Jonathan Marshall. Without their mentorship, I would not be the scientist I am today. While in graduate school I was also fortunate to make many friends and have many colleagues who believed in me, even when I didn't believe in myself. I'd like to make special acknowledgements to Justin Barry, Josh Barker, Claire Otteson, Carrie Levinn, and Brittany White for their unending support and friendship. In addition to great mentorship and friendship, I received much guidance from several PIs including, Prof. Mike Pluth, Prof. Mike Haley, Prof. Dave Tyler, and Prof. Ramesh Jasti. Thank you all for the instruction and direction you provided me over the past years.

Lastly, I'd like to thank my family and friends for their patience and support during all my academic pursuits and the funding (NSF - CHE-1506221, CHE-0923589, CHE-1427987) that made this dissertation possible.

Dedicated to all those that helped me along the way

TABLE OF CONTENTS

Chapter	Page
I. SUPRAMOLECULAR APPLICATIONS OF MODIFIED HAMILTON RECEPTORS.....	1
1.1 Introduction to Supramolecular Chemistry and Molecular Recognition.....	1
1.2 An Introduction to the Hamilton Receptor	2
1.3. Understanding the Supramolecular Design Principles of Hamilton Receptors.....	4
1.4. Applications of the Hamilton Receptor Beyond Barbiturate Binding.....	6
1.4.2 Catalysis, Metal Coordination, and Sensing Applications.....	7
1.4.3. Surface Functionalization and Optoelectronic Materials Applications	9
1.4.4. Macromolecular Applications: Poly(oligo)meric scaffolds and mechanically interlocked molecules.....	13
1.5. Conclusions and Outlook.....	15
1.6. Bridge.....	16
II. SUPRAMOLECULAR BIDENTATE PHOSPHINE LIGAND SCAFFOLDS FROM DECONSTRUCTED HAMILTON RECEPTORS.....	17
2.1. Introduction.....	17
2.2 Results and Discussion	20
2.3 Conclusions.....	26
2.4 Bridge.....	26

Chapter	Page
III. DIRECT SYNTHESIS OF 5,5'-DISUBSTITUTED BARBITURIC ACIDS FROM BENZYL AND ALLYL HALIDES.....	27
3.1 Introduction.....	27
3.2 Results and Discussion	29
3.3 Conclusions.....	35
3.4 Bridge.....	36
IV. PROGRESS TOWARDS THE HYDROFORMYLATION OF 1-OCTENE USING SUPRAMOLECULAR PHOSPHINE LIGANDS BASED ON THE HAMILTON RECEPTOR.....	37
4.1 Introduction.....	37
4.2 Results and Discussion	41
4.3 Conclusions.....	49
4.4 Bridge.....	49
V. SINGLE-COMPONENT, LOW MOLECULAR WEIGHT ORGANIC SUPERGELATORS BASED ON CHIRAL BARBITURATE SCAFFOLDS.....	51
5.1 Introduction.....	51
5.2 Results and Discussion	54
5.3 Conclusions.....	60
5.4 Bridge.....	60
VI. SUBSTITUENT EFFECTS OF FLUORESCENT ARYLETHYNYL HAMILTON RECEPTORS FOR BARBITURATE SENSING.....	61
6.1 Introduction.....	61
6.2 Results and Discussion	64
6.3 Conclusions.....	71

Chapter	Page
6.4 Concluding Remarks.....	72
APPENDICES	73
APPENDIX A: SUPPORTING INFORMATION FOR CHAPTER II	73
APPENDIX B: SUPPORTING INFORMATION FOR CHAPTER III	98
APPENDIX C: SUPPORTING INFORMATION FOR CHAPTER IV	125
APPENDIX D: SUPPORTING INFORMATION FOR CHAPTER V	147
APPENDIX E: SUPPORTING INFORMATION FOR CHAPTER VI	161
REFERENCES CITED.....	183

LIST OF FIGURES

Figure	Page
1.1 Equilibrium of the original Hamilton receptor and the binding of a common barbiturate, barbital. The group in blue is often referred to as the linker between the 2,6-diamidopyridine groups. The red subunit is referred to as the macrocyclizing group.	3
1.2 Modified acyclic Hamilton receptor used for acyl transfer catalysis.	4
1.3 Modified Hamilton receptors showing various levels of pre-organization and the corresponding association constants for the binding of barbital in CDCl ₃ . *K _a values are in M ⁻¹ and were measured in CD ₂ Cl ₂	5
1.4 a) Effect of steric size on the binding of barbital. b) structure of bifurcated Hamilton receptor used to measure electronic influence of R group on barbital binding.	6
1.5 Bipyridine modified Hamilton receptor showing allosteric inhibition of barbiturate binding through Zn ^{II} coordination.	7
1.6 Hamilton receptor modified Au surfaces for Au nanoparticle attachment via barbiturate modification.	10
1.7 Hamilton receptor modified metalloporphyrin, cyanurate functionalized fullerene donor-acceptor system developed by Hirsch.	11
1.8 Supramolecular metalloporphyrinoid:fullerene donor-acceptor molecular wires with various conjugated linkers.	12

Figure	Page
1.9 a) polymeric subunits of supramolecular polymers pioneered by Binder. b) Hamilton modified monomers for the construction of supramolecular polymers via RAFT polymerization.	14
2.1 Metal-assisted self-assembling of a bifurcated, phosphine modified Hamilton receptor.	19
2.2 a) Synthesis of <i>cis</i> -PtL ₂ Cl ₂ complexes 4b-c . b) ³¹ P{ ¹ H} NMR (202 MHz) of free 3b c) ³¹ P{ ¹ H} NMR (202 MHz) of <i>cis</i> -PtL ₂ Cl ₂ , 4b	22
2.3 ORTEP representations of 4b with thermal ellipsoids drawn at 50% probability. Dimeric form of structure showing intra- and inter-molecular hydrogen bonds with non-hydrogen bonding hydrogens omitted for clarity.	24
2.4 Sample ¹ H NMR titration of 4b and 5a in H ₂ O sat. CDCl ₃	25
3.1 Various tautomers of the barbituric acid anion showing <i>O</i> , <i>N</i> , and <i>C</i> nucleophilic centers, respectively.	29
3.2 (a) Absorbance and fluorescence ($\lambda_{\text{ex}} = 346 \text{ nm}$) spectra of compound 2 in degassed THF at 14 μM and 28 μM , respectively. (b) Absorbance and fluorescence ($\lambda_{\text{ex}} = 393 \text{ nm}$) spectra of 3 in THF at 15 μM and 30 μM , respectively..	32

Figure	Page	
3.3	<p>ORTEP representations of compounds 1-3 and 4a with thermal ellipsoids drawn at 50% probability. All non-hydrogen bonding hydrogens omitted for clarity. a) Dimer of compound 4a ; b) dimer of compound 2; c) profile and portrait view of compound 1 with the THF molecules omitted for clarity; d) solid state structure of compound 3 showing profile view of hydrogen bonding motif and view showing π-π interactions with THF molecules omitted for clarity</p>	34
3.4	<p>Synthesis of unsymmetrical barbiturate 5 and ORTEP representations with thermal ellipsoids drawn at 50% probability. Both the profile view of the hydrogen bonding motif and view showing the π-π interactions have the non-hydrogen bonding hydrogens and water molecule omitted for clarity.....</p>	35
4.1	<p>Supramolecular bidentate phosphine ligand scaffolds popularized by Breit and Reek.....</p>	40
4.2	<p>a) Synthesis of <i>cis</i>-PtL₂Cl₂ (L = 6a). b) ¹H NMR titration of 4b and 7a in H₂O sat. CDCl₃ at 25 °C.</p>	46
4.3	<p>ORTEP representations of 7a with thermal ellipsoids drawn at 50% probability. Hydrogen bonds have been eliminated for clarity. Left) side-on view. Right) straight-on view showing the lack of pre-organization of the host binding pocket..</p>	46
4.4	<p>Generic metal-ligand complex with perfluorinated aryl groups showing secondary interactions with a barbiturate guest.....</p>	47

Figure	Page
5.1	Previously reported organogelators based on the melamine·barbiturate/ cyanurate motifs (left) and a new chiral, single-component LMOG based on a barbiturate scaffold (right).. 53
5.2	a) Synthesis of (<i>S</i>)/(<i>R</i>)-BINABarb from barbituric acid with (<i>S</i>)-stereochemistry shown. b) Structures of control compounds that are not organogelators..... 54
5.3	Plot of diffusion coefficient vs barbiturate concentration in CDCl ₃ at 25 °C. Values reported are an average of at least 3 independent trials ($\pm \sigma$)..... 58
5.4	a) Space-filling representation of tetrameric columnar stack from single crystal x-ray diffraction data with H-bonds omitted for clarity b) ORTEP of tetrameric columnar stack with molecules colored by symmetry equivalence showing the helical nature of the column. Thermal ellipsoids shown at 50% probability with hydrogen atoms omitted for clarity.. 59
5.5	VP-SEM images of a) 1a (<i>S</i>)-BINABarb CHCl ₃ gel with inset of an inverted vial containing the gel, b) 1b (<i>R</i>)-BINABarb CHCl ₃ gel, c) crystalline solid of 1b 59
6.1	Structures of original and selected modified Hamilton receptors..... 62
6.2	Emission spectra of 3e in different solvents ($[3e] = 5 \mu\text{M}$, $\lambda_{\text{ex}} =$ absorbance λ_{max} for the given solvent)..... 66

Figure	Page
6.3	a) Emission spectra of hosts 3b–e (1 μ M) in H ₂ O sat. CHCl ₃ . b) Emission spectra of hosts 3b–e (1 μ M) in the presence of 200 equivalents 4b in H ₂ O sat. CHCl ₃ 67
6.4	¹ H NMR (500 MHz) titration of 3e with barbital (4b) in H ₂ O sat. CDCl ₃ at 25 °C. 68
6.5	Emission spectra of 3b in the presence of 4d showing a ratiometric response to the addition of AcOH..... 69
6.6	Binding affinities of guests 4a–e and receptor 3b at 25 °C in H ₂ O sat. CHCl ₃ . Binding isotherms fit to a 1:1 binding model. The error shown is $\pm \sigma$ 71

LIST OF TABLES

Table	Page
3.1 Solvent screening study using benzyl bromide. All reactions conducted with barbituric acid concentrations of 390 mM. The reported yields are from isolated yields based on barbituric acid.	29
3.2 Electrophile screening using DMSO as the solvent. Reported yields are isolated yields based on barbituric acid. ^a 100 °C for 22 hours, ^b room temperature for 1 hour.	30
4.1 Linear to branched (<i>l:b</i>) aldehyde ratio from the hydroformylation of 1-octene at 50 °C using classic monodentate and supramolecular bidentate phosphine ligand assemblies. Conditions: [Rh] = 100 μM, [ligand] = 2.0 mM, [1-octene] = 100 mM, [decane] = 50 mM.	43
4.2 Results from the hydroformylation of 1-octene at rt using classic monodentate and supramolecular bidentate phosphine ligand assemblies. Conditions: [Rh] = 100 μM, [ligand] = 2.0 mM, [1-octene] = 100 mM, [decane] = 50 mM.	44
4.3 Effect of methylene spacer and regioisomerism of phosphorus donor atom on the linear to branched (<i>l:b</i>) aldehyde ratio from the hydroformylation of 1-octene at rt for four days. Conditions: [Rh] = 100 μM, [ligand] = 2.0 mM, [1-octene] = 100 mM, [decane] = 50 mM.	45

Table	Page
4.4 Results from the hydroformylation of 1-octene with supramolecular bidentate ligands capable of secondary interactions and different guest molecules at 50 °C. Conditions: [Rh] = 100 μM, [ligand] = 2.0 mM, [1-octene] = 100 mM, [decane] = 50 mM.....	48
5.1 Gelation properties of compounds 1-3 at r.t. G = gel, S = soluble, ppt = precipitate formed, SS = slightly soluble, I = insoluble.	57
6.1 Photophysical Properties of Hosts 3a-3e in the presence and absence of barbital guest. λ_{\max} measured with [H] = 5 μM in H ₂ O sat. CHCl ₃ . ϵ were measured in H ₂ O sat. CHCl ₃ . λ_{em} in the presence of barbital measured with [H] = 1 μM in H ₂ O sat. CHCl ₃ and 200 equivalents of barbital.....	65
6.2 Binding affinities of hosts 3b-e with barbital at 25 °C in H ₂ O sat. CHCl ₃ . The error shown is $\pm \sigma$	70

LIST OF SCHEMES

Scheme	Page
2.1	Synthesis of phosphine ligands 3a-c 20
3.1	Synthesis of new metal-coordinating and fluorescent barbiturates. 31
3.2	Synthesis of (<i>R</i>) and (<i>S</i>)-BINABARB with (<i>R</i>)-stereochemistry shown. 33
4.1	General scheme for the hydroformylation reaction. 38
4.2	General mechanism of Rh-catalyzed hydroformylation. 39
4.3	Synthesis of phosphine functionalized bifurcated Hamilton receptor ligands 3a-c and structures of barbiturate guests used for initial screenings..... 42
4.4	Generalized reaction scheme for the hydroformylation of 1-octene using the new bifurcated Hamilton receptor supramolecular ligand scaffold. 43
4.5	Synthesis of benzyl-modified bifurcated Hamilton receptor ligands. 45
4.6	Synthesis of benzyl and perfluorobenzyl substituted phosphine modified Hamilton receptors..... 48
6.1	Synthesis of substituted arylethynyl Hamilton receptors..... 65

CHAPTER I

SUPRAMOLECULAR APPLICATIONS OF MODIFIED HAMILTON RECEPTORS

Chapter I is an overview of the field of supramolecular chemistry as it pertains to Hamilton receptors and their applications. This chapter contains co-authored unpublished work. The content of this chapter was researched and written by me. Michael D. Pluth provided editorial assistance.

1.1 Introduction to Supramolecular Chemistry and Molecular Recognition

Supramolecular chemistry is the study of molecular recognition events that exploit the use of non-covalent interactions to assemble complex molecular architectures from simple subunits.^{1,2} Often inspired by the efficiency and complexity of self-assembled biological systems, supramolecular chemists are continually developing new supramolecular assemblies to better understand the subtle, yet powerful, non-covalent interactions responsible for the self-assembly of these intricate systems. Using supramolecular approaches, chemists have developed a vast array of programmed molecular assemblies for applications including small molecule sensing, drug delivery, and the design of molecular machines, which was awarded the 2016 Nobel prize in chemistry.¹

In contrast to covalent linkages, non-covalent interactions used in supramolecular chemistry are highly reversible and often weak (1-5 kcal/mol).³ The inventory of non-covalent interactions available include electrostatic interactions (e.g. ionic, halogen, and hydrogen bonding), π -effects, van der Waals interactions, metal coordination, and hydrophobic effects.⁴ While these interactions are often used in concert, some of the most successful and ubiquitous approaches for the design and construction of new host–guest architectures are the incorporation of hydrogen bonding motifs.⁵ In contrast to other non-covalent interactions, hydrogen bonds are highly directional and often exhibit high cooperativity leading to strong association of guest molecules.

1.2 An Introduction to the Hamilton Receptor

Some of the most prominent hydrogen bonding host–guest scaffolds are those based on synthetic receptors pioneered by Hamilton *et al.* (Figure 1.1), commonly referred to as Hamilton receptors, wedges, or clefts.⁶ Originally devised as a platform for studying the molecular recognition of barbiturates, a widely used class of pharmaceuticals known for their sedative and anticonvulsant properties,⁷ these types of receptors are characterized by the two-fold symmetric hydrogen-bonding arrays formed between the complementary donor-acceptor-donor (DAD) units of Hamilton receptor and the acceptor-donor-acceptor (ADA) units of the barbiturate guest. Initial reports on these receptors showed large association constants between the host and a variety of barbiturate guests in non-polar solvents (e.g. CDCl_3 and CD_2Cl_2) ranging from 10^4 - 10^6 M^{-1} .^{6, 8} The binding strength of these systems is dependent on several factors including the identity of

the macrocyclizing group (Figure 1 red), number of hydrogen bonding groups available in the barbiturate guest, and the orientation of these hydrogen bonding groups in the guest. A more detailed discussion of these factors is presented in the following section.

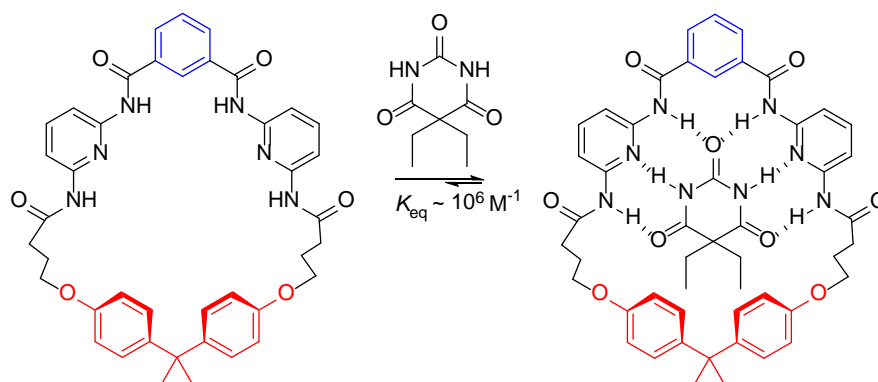


Figure 1.1. Equilibrium of the original Hamilton receptor and the binding of a common barbiturate, barbitol. The group in blue is often referred to as the linker between the 2,6-diamidopyridine groups. The red subunit is referred to as the macrocyclizing group.

In addition to molecular recognition, early reports of these systems demonstrated their application as catalysts for acyl transfer reactions and synthetic analogues for understanding protease enzymes (Figure 1.2).⁹ Model reactions between an ester-functionalized barbiturate and thiol-functionalized Hamilton receptor showed more than a 10^4 fold rate enhancement for the acyl transfer reaction compared to the control reaction in the absence of the receptor

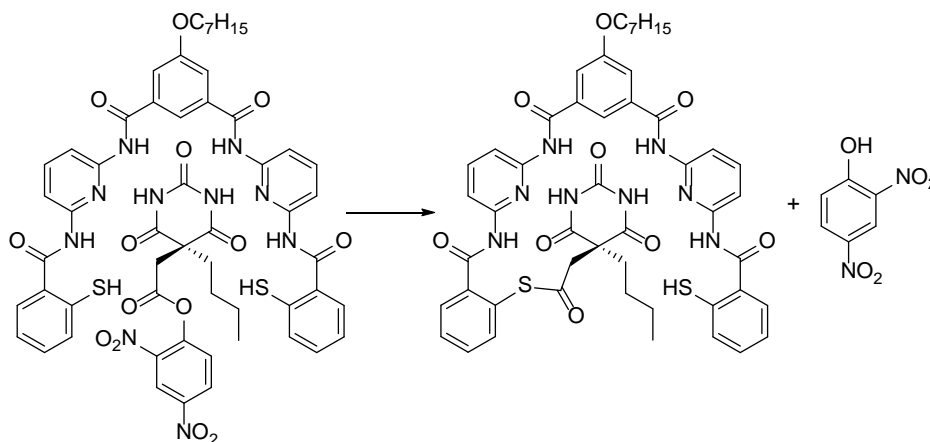


Figure 1.2. Modified acyclic Hamilton receptor used for acyl transfer catalysis.

Additionally, a structural analogue of the barbiturate guest incorporating only three hydrogen bonds showed an eight-fold increase in rate, demonstrating the cooperativity observed in the hydrogen bonding network between the host and guest.

1.3. Understanding the Supramolecular Design Principles of Hamilton Receptors

Since the first report of the Hamilton receptor, efforts continue to be made toward understanding the physical organic chemistry principles that govern the molecular recognition of these systems with the intent of developing design strategies that allow for the evolution of more efficient and versatile systems. Initial studies concerned with understanding the structural elements that significantly impact the binding affinity of these systems towards barbiturates showed over a 100-fold difference in the association of barbital between the macrocyclic (Figure 1.3, **1**) and acyclic forms (Figure 1.3, **2**).^{6, 8} Furthermore, changing the number of available hydrogen bonds in the barbiturate guest by simple methyl substitution of one of the imide N-H moieties lowers the binding affinity by more than 1000-fold.⁸ In addition, substitution of the carbonyl oxygen of

barbital with a weaker hydrogen bond accepting sulfur atom leads to a dramatic 1800-fold decrease in affinity.

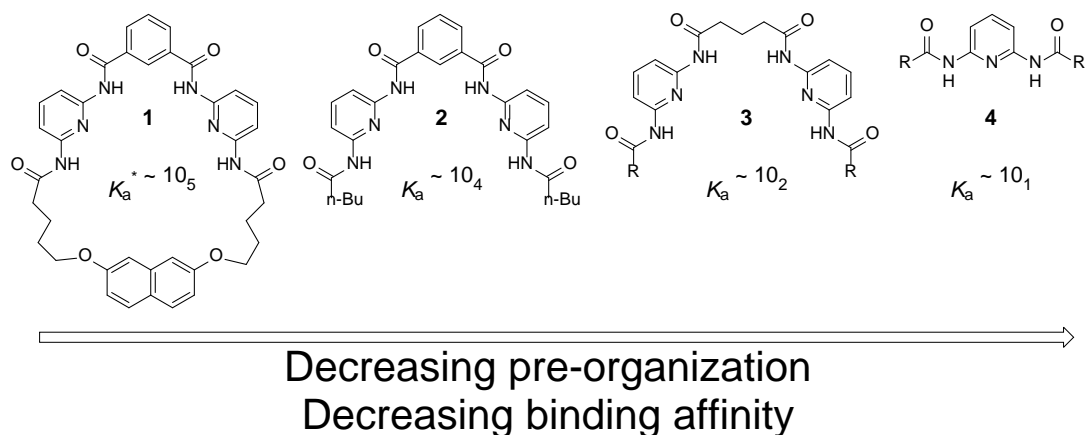


Figure 1.3. Modified Hamilton receptors showing various levels of pre-organization and the corresponding association constants for the binding of barbital in CDCl_3 . * K_a values are in M^{-1} and were measured in CD_2Cl_2 .

Recent work by our group has shown that a dramatic effect on binding is observed upon changing the flexibility of the 2,6-diamidopyridine linker.¹⁰ By reducing the preorganization of the host system via replacement of the isophthaloyl group with a more flexible alkyl linker, attenuation of guest binding is observed (Figure 1.3, **3**). Complete bifurcation of the receptor leads to almost complete attenuation of binding, but interestingly maintains a 1:1 binding stoichiometry, suggesting that the entropic penalty for the formation of a three-component system is more unfavorable than the formation of three additional hydrogen bonds.

The identity of the peripheral groups in the acyclic forms of the Hamilton receptor play a large role in guest binding. Our group has also shown that increasing the steric size of these groups leads to weaker association of barbiturate guest due to the steric

congestion around the hydrogen bonding groups and the negative steric interactions with the 5,5' substituents of the guest (Figure 1.4a).¹⁰ In addition to the steric influence of the R groups, the bifurcated system also show a linear free energy relationship when substituted by electron withdrawing and electron donating groups (Figure 1.4b).¹¹ Notably, a break is observed in the Hammett plot for these systems. Through computational studies, our group showed that while the proximal N-H...O(barbital) exhibits a linear change upon increasing the electron donating character in these groups, changes in the pyridyl N...H-N(barbital) were not linear thus leading the observable break.

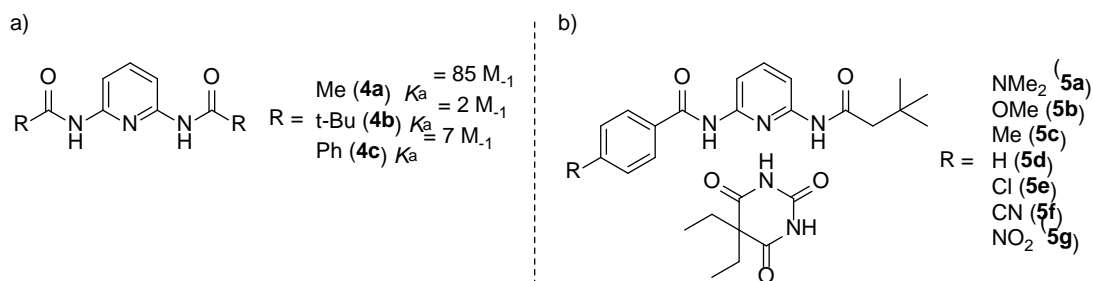


Figure 1.4. a) Effect of steric size on the binding of barbital. b) structure of bifurcated Hamilton receptor used to measure electronic influence of R group on barbital binding.

1.4. Applications of the Hamilton Receptor Beyond Barbiturate Binding

Using the established design principles that effect guest binding researchers have developed a variety of acyclic Hamilton receptors to enhance the application of these systems beyond simple barbiturate binding. The following sections provide a brief overview of selected classes of chemical applications where these types of receptors have

seen success. For a more extensive review on the applications of the Hamilton receptor, the authors recommend the work of Tron *et al.*¹²

1.4.2 Catalysis, Metal Coordination, and Sensing Applications

As noted previously, the first reports utilizing the Hamilton receptor as a catalyst focused primarily on acyl transfer reactions. Since these initial reports, much work has been done to incorporate these types of receptors into metal coordination complexes in an effort to influence the geometry and reactivity of the metal centers, as well as, the geometry of the receptor itself. Early efforts towards these goals demonstrated that through incorporation of pendent bipyridyl groups to an acyclic Hamilton receptor, barbiturate binding could be allosterically controlled through the addition of Zn^{II} (Figure 1.5).¹³ Upon the addition of Zn^{II} to the receptor, a conformational change of the host binding pocket is observed due to coordination of the bipyridyl groups to the zinc cation resulting in complete attenuation of binding

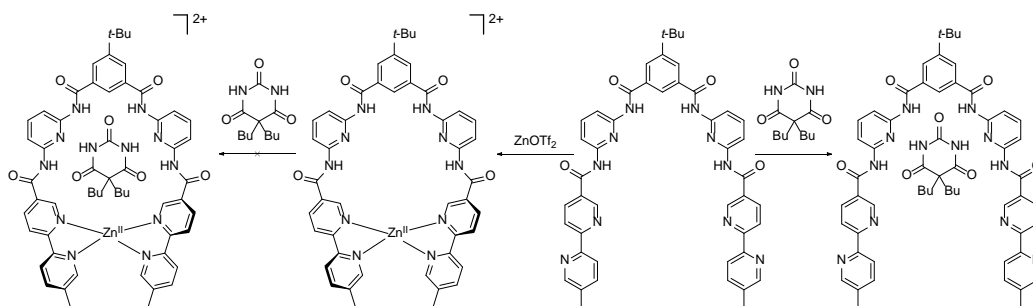


Figure 1.5. Bipyridine modified Hamilton receptor showing allosteric inhibition of barbiturate binding through Zn^{II} coordination.

Phosphine modification of the Hamilton receptor is another approach used for the construction of new supramolecular catalytic systems. Appendage of diphenylphosphine moieties to acyclic receptors has produced new ligands systems capable of forming supramolecular metallocycles with palladium.¹⁴ Additionally, these ligands systems in some cases show enhanced reactivity towards Heck couplings compared to their PPh₃ analogues. Furthermore, these types of phosphine ligands exhibit unique oxidative addition reactivity in the presence of palladium and arylido-functionalized barbiturates.¹⁵ Inverse regioselectivity of the oxidative addition is observed when compared to a simple aryl iodide, highlighting the capacity of such functionalized Hamilton receptors to influence the coordination geometry about a metal center.

Further derivatization of the receptor has expanded the potential of these receptors for use as enantioselective catalysts. Chiral phosphite-functionalized dendritic Hamilton receptors have been used as ligands for the Rh-catalyzed asymmetric hydrogenation of enamides and α -dehydroamino acid derivatives with enantioselectivities between 80-90%.¹⁶ In addition to the good enantioselectivity, this system exhibited high recyclability with maintained levels of activity. The catalysts could be recovered via precipitation through the addition of hexanes and subsequently reused up to five times before any loss in selectivity or activity was observed. Other chiral BINOL derivatives of the Hamilton receptor have been used for nitrile oxide cyclizations of functionalized barbiturates. While effective, these systems were not shown to be catalytic.¹⁷

In addition to barbiturates, Hamilton receptors have been used to bind a variety of other small molecule analytes including nucleotides, carboxylic acids, sulfoxides, and cyanurates. Some of the most noteworthy applications of these receptors for non-

barbiturate binding are used as chiral recognition reagents. Examples of chiral resolution of carboxylic acid, oxazolidinone, lactone, alcohol, sulfoxide, sulfoximine, isocyanate, or epoxide moieties have been reported¹⁸. In some cases as little as 5 mol% receptor is required to achieve sufficient resolution.¹⁹ More recently, similar BINOL functionalized Hamilton receptors have been used for linear discriminant analysis (LDA) of chiral anions demonstrating its potential for use in microsensor arrays.²⁰

1.4.3. Surface Functionalization and Optoelectronic Materials Applications

Precise spatial control over the binding of small molecules to surfaces is a continual challenge for material scientists. Achieving molecular level control over the positioning of ligands on surfaces is critical for the successful development of nano(bio)technology. Currently, there exist many methods in which researchers have attempted to achieve this control, much of which is through covalent modification of surfaces. In contrast to typical covalent modifications, supramolecular approaches aimed at addressing this issue allow for greater tunability and modularity of scaffolds used to study the surface interactions, while maintaining high degrees of spatial control through the use of complementary recognition units. Hamilton receptors have been utilized in this manner to evaluate the self-assembly of thio-functionalized barbiturate Au nanoparticles onto a planar Au surface bearing a modified Hamilton receptor (Figure 1.6).²¹ Through control of the receptor concentration, tunable surface coverage up to 100% area coverage was achieved.

Application of this method to thin films of statistical block copolymers was also demonstrated and shown to have concentration dependent coverage at receptor concentrations less than 1 mol %.²² A similar design strategy was used for the addition of CdSe nanoparticles and nanorods to polymer thin films. The addition could be mediated by the addition of methanol, thereby eroding the hydrogen bonding network between the host and receptor.²³ Extension of these types of systems to include conjugated linkers for potential nanowire electronic applications has also been reported.²⁴ Further modification of these types of systems to include other inorganic-organic hybrid nanostructures such as ZnO nanorods²⁵ and TiO₂ nanoparticles²⁶ have been reported demonstrating the generality of this approach for ligand immobilization.

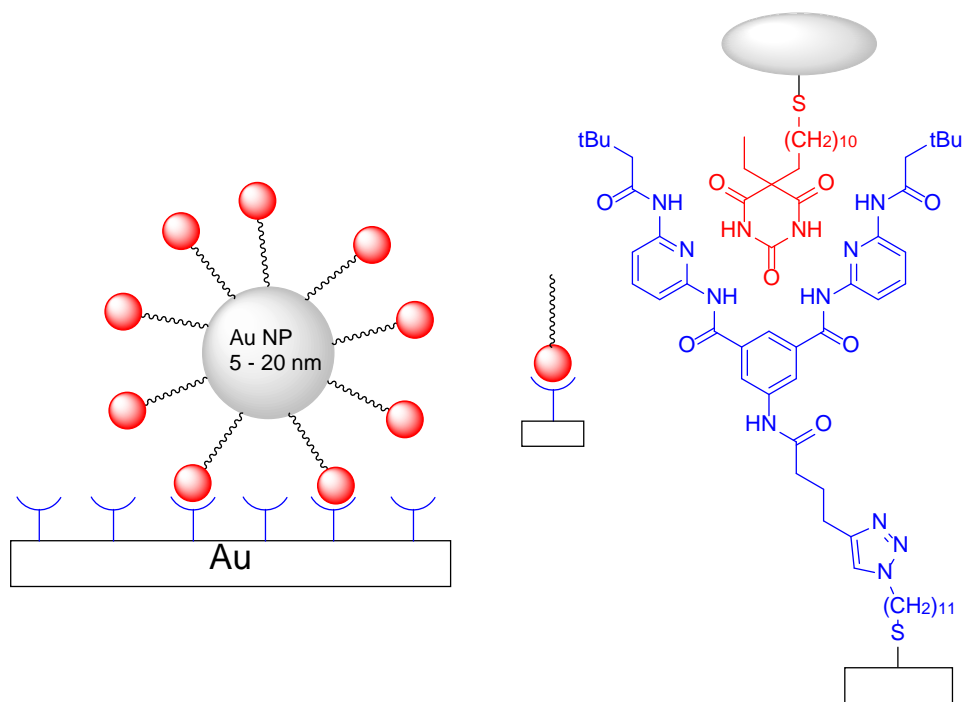


Figure 1.6. Hamilton receptor modified Au surfaces for Au nanoparticle attachment via barbiturate modification.

complexation of metalloporphyrin functionalized Hamilton receptors and cyanurate functionalized fullerenes.²⁸ Building upon these results, the substitution of the alkyl linkers for conjugated systems including *p*-phenylene-vinylene²⁹, oligophenylenevinylene^{30,31}, and fluorene²⁹ linkers has produced systems with even better electron transfer between the donor and acceptor units akin to that of a molecular wire (Figure 1.8).

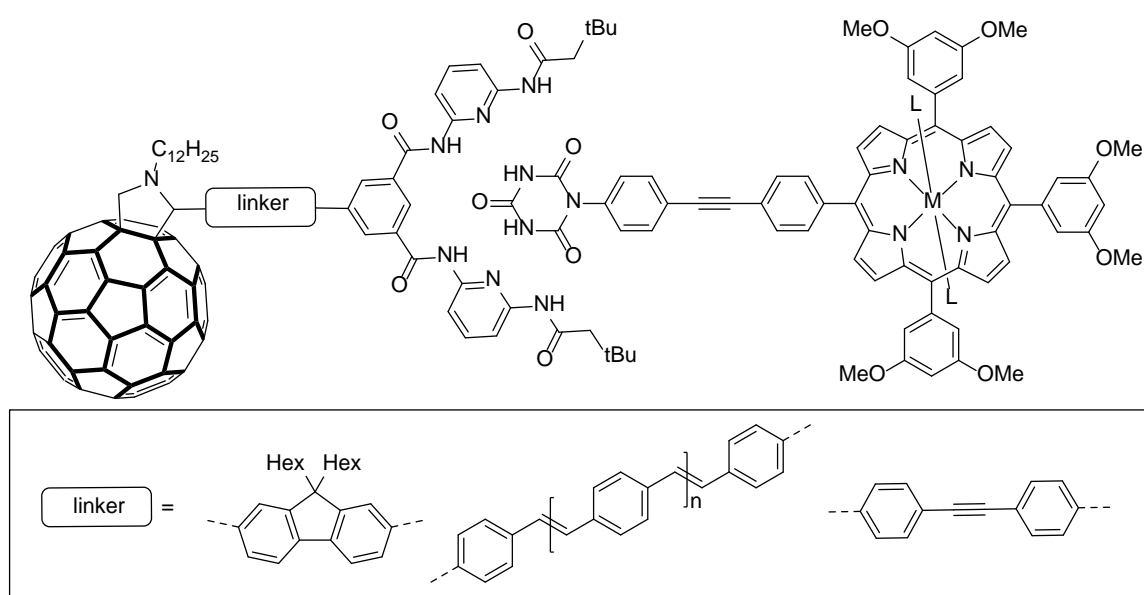


Figure 1.8. Supramolecular metalloporphyrinoid:fullerene donor-acceptor molecular wires with various conjugated linkers.

Further use of this architecture by Grimm *et al.* demonstrated that an energy-transfer:electron-transfer cascade could be achieved through a three-component system consisting of a perylenedimide-functionalized Hamilton receptor, and a cyanurate-functionalized metalloporphyrin with an axial fullerene ligand.³² In addition to fullerenes, these types of systems have been used for the dissolution and separation of

Hamilton receptor-functionalized single-walled carbon nanotubes for similar optoelectronic and solar applications.³³

1.4.4. Macromolecular Applications: Poly(oligo)meric scaffolds and mechanically interlocked molecules

Hamilton-type receptors have been widely incorporated into numerous macromolecular systems including polymers,³⁴⁻³⁷ oligomers,^{30, 38, 39} and dendrimers.^{16, 27,}³³ The earliest reports of oligomeric Hamilton-type receptors reported by Lehn investigated the propensity of these systems to adopt helical conformations in the presence of cyanurate guests.³⁹ Furthermore, the homoditopic Hamilton receptors and homoditopic cyanurate analogues have been shown to self-assemble into supramolecular polymers that display tunable polymer properties such as viscosity, dispersity, and even reversible polymerization by changing simple external stimuli such as temperature, solvent, concentration and stoichiometry.⁴⁰ Building upon these initial reports, the Binder laboratory has produced a plethora of self-assembling polymers containing Hamilton-type recognition units. Most notable are the Hamilton receptor functionalized telechelic polyisobutylenes for the development of composite materials,⁴¹ functional gel materials,^{42,43} and self-healing polymers (Figure 1.9).^{44, 45} Other examples of block copolymers that exhibit unique phase separation have also been reported.^{34,35} Importantly, use of these types of systems has allowed polymer chemists to better understand single-chain folding dynamics^{46,47} and entropic effects⁴⁸ on the self-assembly of macromolecules. The self-assembly of macromolecular structures functionalized with

Hamilton receptors has also been utilized to create complex helix-helix block copolymers.⁴⁹

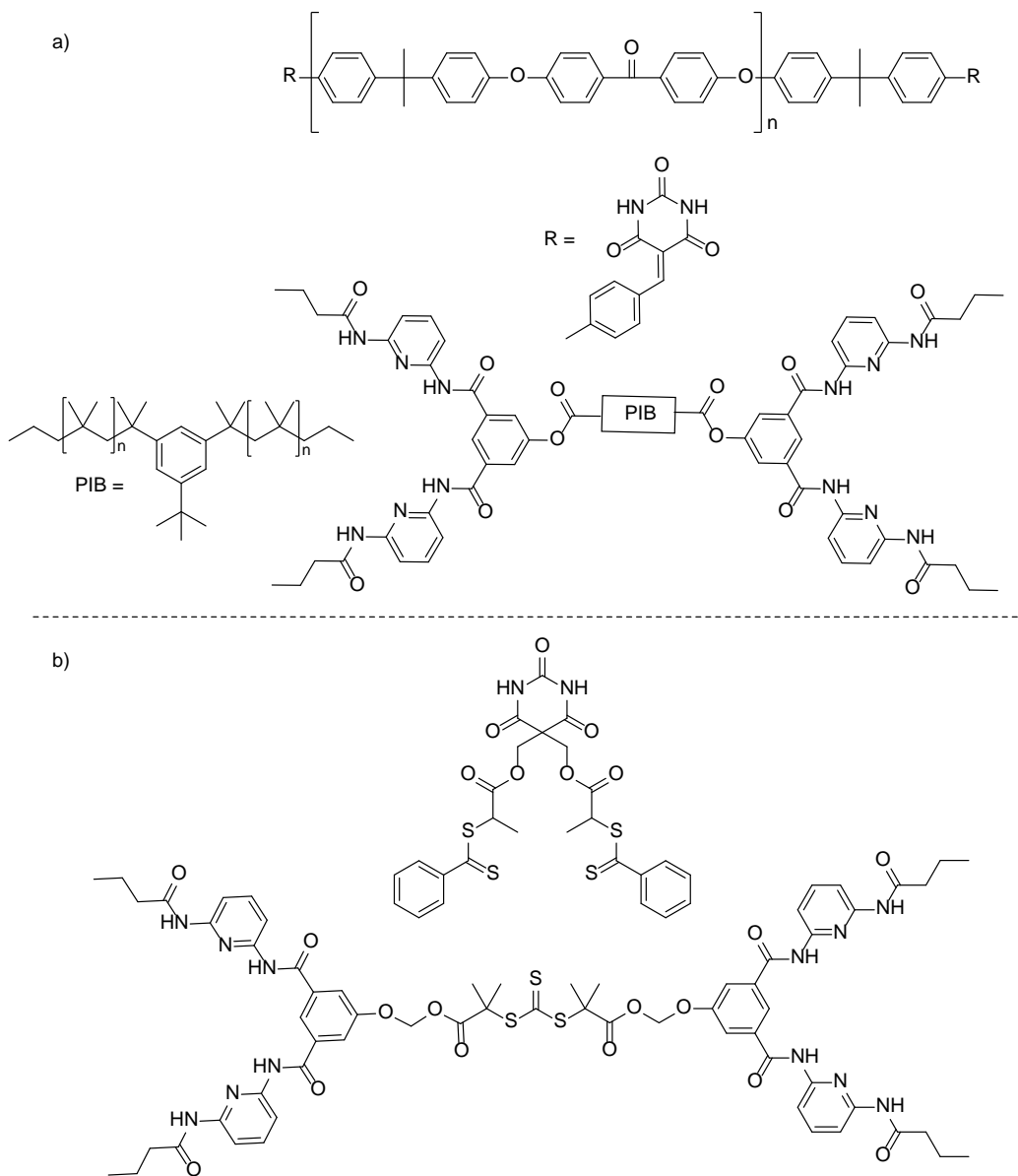


Figure 1.9. a) polymeric subunits of supramolecular polymers pioneered by Binder. b) Hamilton modified monomers for the construction of supramolecular polymers via RAFT polymerization.

In addition to polymeric applications, the use of the Hamilton receptor has also seen successful application to the generation of mechanically interlocked molecules (MIMs). Largely pioneered by the work of the McClenaghan group, the first reports of a [2]rotaxane incorporating a Hamilton receptor utilizes an azide functionalized barbiturate thread, followed by a 1,3-dipolar cycloaddition to append the corresponding stopper moieties.⁵⁰ Further derivatization of this type of scaffold to include photoactivatable anthracene groups along the Hamilton receptor resulted in the formation of a photoactivated and thermally reversible [2]rotaxane.⁵¹ Most recently, this photoactivated system has been used as a molecular effector for the photoregulated ring gliding of an orthogonal [2]rotaxane with multiple docking sites.^{52, 53}

1.5. Conclusions and Outlook

Supramolecular chemistry and molecular recognition have become central themes in the design and implementation of new molecular architectures and materials design. While there have been many host–guest systems developed over the last century, one of the most ubiquitous host–guest scaffolds based primarily on hydrogen bonding is the Hamilton receptor. Since its inception over 30 years ago, much work has been done to develop design principles to aid in the construction of tailored Hamilton receptor analogues for use in a diverse range of applications including polymers, optoelectronics, and catalysis. Future work in this field will likely continue to improve on our understanding of the physical organic principles that govern guest recognition events, in addition to the continued adaptation of this scaffold for the design of new materials and

supramolecular applications. Currently, some of the most underexplored applications of the Hamilton receptor are in the new area of molecular machines and use in aqueous media. Overcoming the associated challenges with utilizing hydrogen bonding motifs with controlled molecular motion and the attenuated binding in aqueous environments would be a tremendous advancement for the implementation of the Hamilton receptor and its continued use as a prominent host architecture.

1.6 Bridge

Using the known design principles for construction of new Hamilton receptors and building upon their existing applications, the research discussed in this dissertation aims to extend the utility of these types of host–guest systems. These applications include supramolecular catalysts for the hydroformylation of alkenes, the development of new barbiturate based organogelators, and the design of new fluorescent receptors for barbiturates detection.

CHAPTER II

SUPRAMOLECULAR BIDENTATE PHOSPHINE LIGAND SCAFFOLDS FROM DECONSTRUCTED HAMILTON RECEPTORS

Chapter II of this dissertation is a modified form of a previously published manuscript. I performed a majority of the analytical and synthetic chemistry and wrote the manuscript. Coauthors include Jacqueline M. McGrath, Lev N. Zakharov, and Michael D. Pluth. The citation for this article is as follows: Seidenkranz, D. T.; McGrath, J. M.; Zakharov, L.N.; Pluth, M.D. Supramolecular bidentate phosphine ligand scaffolds from deconstructed Hamilton receptors. *Chem Commun.* **2017**, *53*, 561–564.

2.1. Introduction

New ligand architectures provide valuable platforms on which inorganic and organometallic chemistry can be supported, controlled, and leveraged for applications including bioinorganic chemistry, materials science, and catalysis. Of the numerous ligand platforms available, phosphine ligands are among the most ubiquitous not only in chemical catalysis,¹ but also the construction of metal organic hybrid systems including metal-organic frameworks,²⁻⁴ supramolecular coordination complexes,^{5,6} and molecular capsules.⁷⁻⁹ Yet the design and diversity of self-assembling architectures based on

phosphine ligands is frequently limited by challenging phosphine derivatization. This drawback is particularly acute for the design and derivatization of bidentate phosphine ligands. To combat these obstacles, researchers have begun to employ supramolecular techniques in ligand design.¹⁰⁻¹⁴ In addition to creating large, meaningful ligand libraries from fewer components,^{15, 16} supramolecular ligand libraries are more amenable to the implementation of high throughput screening methodologies for identifying unique chemical structures, reactivity, and materials with novel properties.

Supramolecular approaches to the construction of functional bidentate ligands employ principles of molecular recognition to develop ligands with compatible donor-acceptor sites inherent in the ligand framework. Pioneering work by Breit,¹⁶⁻¹⁸ as well as van Leeuwen and Reek,^{19, 20} demonstrated that functional bidentate ligands can be created through incorporation of non-covalent interactions in the ligand scaffold, such as hydrogen bonding and metal ligation. However, few supramolecular approaches to bidentate ligand construction are based on self-assembling host-guest systems. Moreover, a self-assembling ligand system that uses host-guest interactions to control the magnitude of bidentate character of monodentate ligands would enable precise tuning of the shape and size of new metal-organic hybrid systems based on host-guest binding affinities and guest characteristics. Furthermore, control over typical bidentate ligand parameters, such as bite angle, can be achieved through the use of different host-guest combinations making this approach amenable to combinatorial screening techniques.

Of the many host-guest architectures, the synthetic barbiturate receptor first synthesized by Hamilton²¹ lends itself well to phosphine modification.^{22, 23} The receptor is characterized by six hydrogen bonds formed between the two complimentary donor-

acceptor-donor (DAD) and acceptor-donor-acceptor (ADA) faces of the host and guest, respectively. We envisioned that bifurcation of the ligand scaffold would create a more flexible and accommodating host pocket upon metal ligation, as well as allow for precise control over the “bidentate” nature of the ligand through the use of derivatized barbiturate guests. Additionally, coordination of the ligands to the metal would provide the necessary pre-organization required for guest binding, thus favoring complete assembly of the supramolecular ligand structure (Figure 2.1). This design strategy would generate a new class of multicomponent self-assembled phosphine ligands that mimic bidentate structures upon guest binding. Herein, we report the design, synthesis, characterization, metal coordination, and binding affinities of such self-assembled ligand scaffolds and demonstrate that host-guest chemistry can be used to access bidentate coordination motifs from simple, modular, monodentate ligand components.

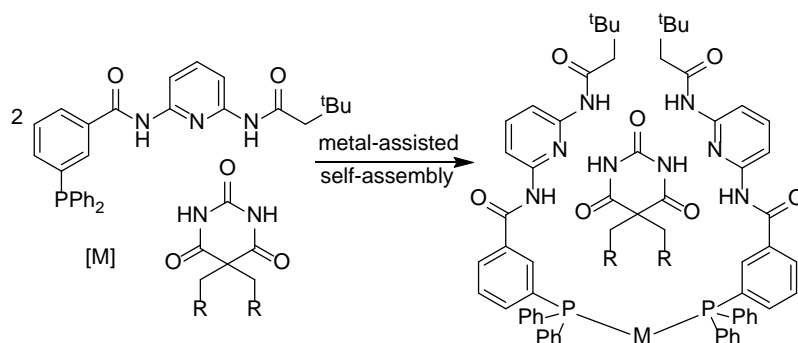
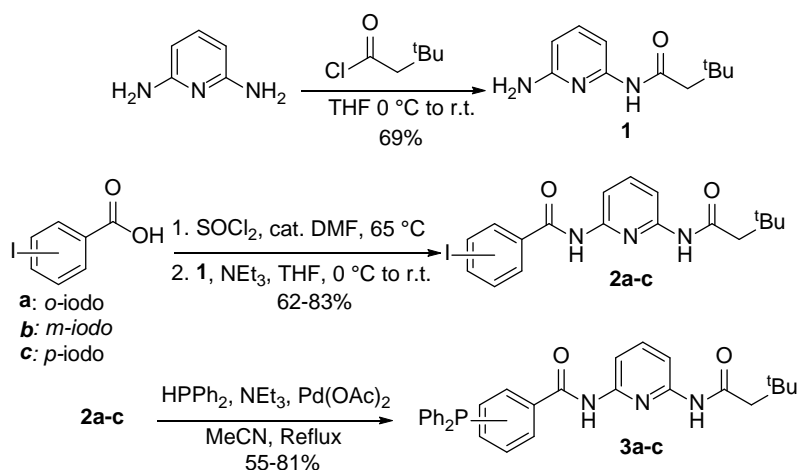


Figure 2.1 Metal-assisted self-assembling of a bifurcated, phosphine modified Hamilton receptor.

2.2. Results and Discussion

The effects of Hamilton receptor bifurcation and backbone rigidity on guest binding have been previously reported and indicate that substitution at the distal amide and the rigidity of the backbone have significant effects on guest binding and host aggregation.²⁴ To encourage guest inclusion, while limiting host aggregation, we hypothesized that neopentyl substitution at the host distal amide would result in optimal binding affinities. Moreover, we envisioned that the regioisomerism of the appended phosphorus group in the bifurcated receptor system would play a critical role in the geometry and size of the host binding pocket. Specifically, we hypothesized that the *meta*-substituted ligand would provide the most pre-organized host pocket but may be sterically congested upon metal complexation. Therefore, the *para*-substituted isomer could alleviate the steric congestion and have minor effects on host pocket pre-organization. To investigate these postulates, a suite of regioisomers containing neopentyl substituted distal amides was synthesized according to Scheme 2.1.



Scheme 2.1 Synthesis of phosphine ligands **3a-c**.

2,6-Diaminopyridine was subjected to mono-amidation conditions using 3,3-dimethylbutyryl chloride to give the mono-substituted pyridine (**1**), which was then used for subsequent amidation of the *ortho*-, *meta*-, and *para*-substituted iodobenzoyl chlorides to afford compounds **2a-c**, respectively. Palladium-mediated couplings of HPPH₂ and **2a-c** in the presence of base resulted in the desired phosphine ligands **3a-c** in moderate to good yields. This highly modular, three-step synthesis allows for fine control over the electronic and steric parameters of the ligand scaffold through substitution at both the phosphorus and diaminopyridine backbone.

Single crystals suitable for X-ray diffraction of all three isomers were grown from THF/pentane vapor diffusion under an inert atmosphere (Appendix A, Figure A.1). Notably, all regioisomers co-crystallized with one molecule of THF, which was hydrogen bonded to the proximal amide N-H and THF oxygen. The preference for the hydrogen bond at the proximal amide is likely due to the potential negative steric interactions between the neopentyl group and the THF molecule. This observation is in agreement with our hypothesis that bulky substituents discourage host aggregation, but allow for guest inclusion.

To generate a host scaffold with two properly oriented DAD faces to bind the incoming barbiturate guest, the ligands must adopt a *cis*-geometry about the metal center. A common method for determining ligand geometry is to use Pt(II) salts that form square planar complexes upon the addition of two equivalents of ligand. These square planar, d⁸ Pt complexes display distinct ¹J_(Pt-P) couplings constants for their *cis*- (>3000 Hz) or *trans*- (< 3000 Hz) isomers.²⁵ To investigate the coordination properties of our ligand

scaffold, Pt(II) complexes **4b-c** were prepared using one equivalent of $[\text{Cl}_2\text{Pt}(\text{COD})]$ with two equivalents of the desired ligand in CH_2Cl_2 (Figure 2.2a). Following the complexation via $^{31}\text{P}\{^1\text{H}\}$ NMR spectroscopy shows clean conversion upon the addition of ligand to the $\text{Pt}(\text{COD})\text{Cl}_2$ (Figure 2.2b–c). Analysis of the $^1J_{(\text{Pt-P})}$ coupling constants confirms a *cis*-geometry of both complexes with coupling constants of 3666 Hz and 3647 Hz for **4b** and **4c**, respectively. Attempts to synthesize Pt complexes with ligand **3a**, however, resulted in the complete disappearance of a phosphorus resonance, suggesting decomposition or possible formation of polymeric species causing significant peak broadening. The inability to form discrete species with **3a** is likely due to the steric crowding about the metal center that would occur in a *cis*- arrangement of the ligands.

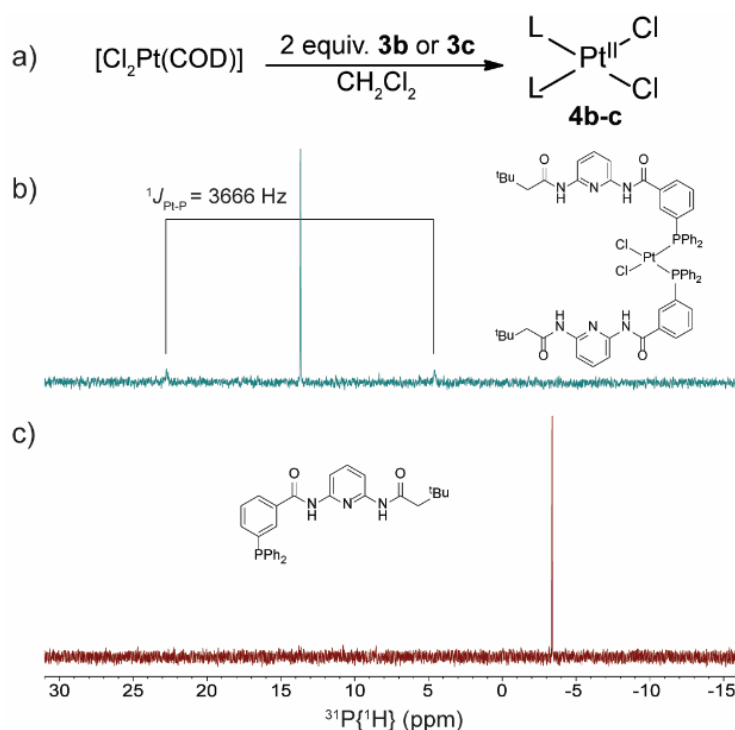


Figure 2.2 a) Synthesis of *cis*-PtL₂Cl₂ complexes **4b-c**. b) $^{31}\text{P}\{^1\text{H}\}$ NMR (202 MHz) of free **3b** c) $^{31}\text{P}\{^1\text{H}\}$ NMR (202 MHz) of *cis*-PtL₂Cl₂, **4b**.

To further study the ligand isomerism and host pocket geometry, single crystals of **4b** were grown from THF/MeCN:pentane via vapor diffusion and analyzed by X-ray diffraction. Analysis of the structure confirms the *cis*-orientation about the Pt center (Figure 2.3). Interestingly, the complex co-crystallizes with two molecules of THF, each bound to a different phosphine ligand and amide. Consequently, the structure adopts a dimeric motif with both intra- and intermolecular hydrogen bonds. The intramolecular hydrogen bonds occur between the proximal amide N-H of one phosphine and the distal amide oxygen of the other phosphine, with a calculated distance of 2.922 Å, to effectively encapsulate the THF guests. The intermolecular hydrogen bonds between the THF molecules and the upper and lower amides have calculated distances of 2.947 Å and 2.811 Å, respectively. The positioning of the host pocket *cis* to the chloride ligands may help to explain the low association constants (*vide infra*) as potential negative steric interactions would occur between the chloride ligands and incoming guest.

Previous work in our lab has shown that deconstructed Hamilton receptors display 1:1 binding motifs, similar to the original Hamilton receptor.²⁴ The free rotation around the host P-C bond, however, could allow for a 2:1 binding motif if the enthalpic gain from hydrogen bond formation is greater than the entropic cost of creating a three component system. To confirm which binding motif was present, a Job plot for **4b** and **5a** was constructed using ¹H NMR spectroscopy. Following the chemical shift of the guest N-H resonance, the data support a 1:1 binding motif as evidenced by a maximum in the Job plot at 0.5 in H₂O sat. CDCl₃ and 1% DMSO in CDCl₃ (Appendix A, Figures A.4 and A.6).

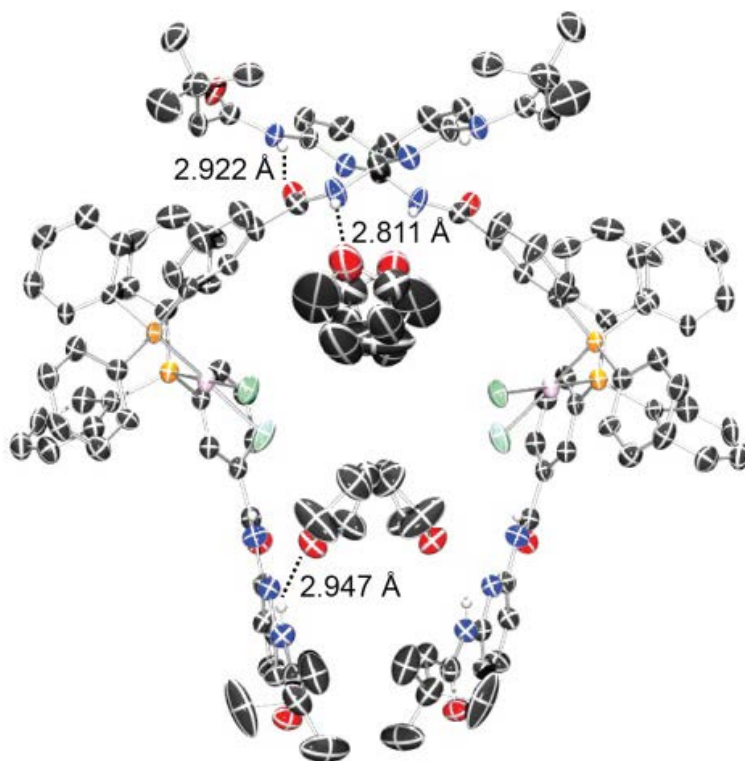


Figure 2.3. ORTEP representations of **4b** with thermal ellipsoids drawn at 50% probability. Dimeric form of structure showing intra- and inter-molecular hydrogen bonds with non-hydrogen bonding hydrogens omitted for clarity.

To assess the efficacy of our self-assembling ligand system, ^1H NMR titrations of host complex **4b** and a synthetic barbiturate **5a** were performed and fit to a 1:1 model using the Thordarson method.²⁶ Due to solubility constraints of the guest, inverse titrations (excess host with constant guest) were required to generate adequate signal in the ^1H NMR experiments to accurately determine small chemical shift changes. Following the N-H resonance of the guest in a H_2O saturated CDCl_3 solvent system, a significant downfield shift is observed with a measured association constant of $800 \pm 100 \text{ M}^{-1}$ (Figure 2.4). Switching to a more competitive solvent such as MeCN resulted in attenuated, but measurable, binding constant of $19 \pm 5 \text{ M}^{-1}$ demonstrating the propensity

of this system to self-assemble even in a competitive hydrogen bonding environment. Comparison between hosts **4b** and **4c** revealed that para-substitution of the phosphorus group leads to a less pre-organized host pocket, indicated by the lower association constant of $260 \pm 20 \text{ M}^{-1}$. Taken together, these binding data demonstrate that ligand coordination facilitates barbiturate guest binding and that the geometry of the ligand architecture can be used to tune guest binding fidelities.

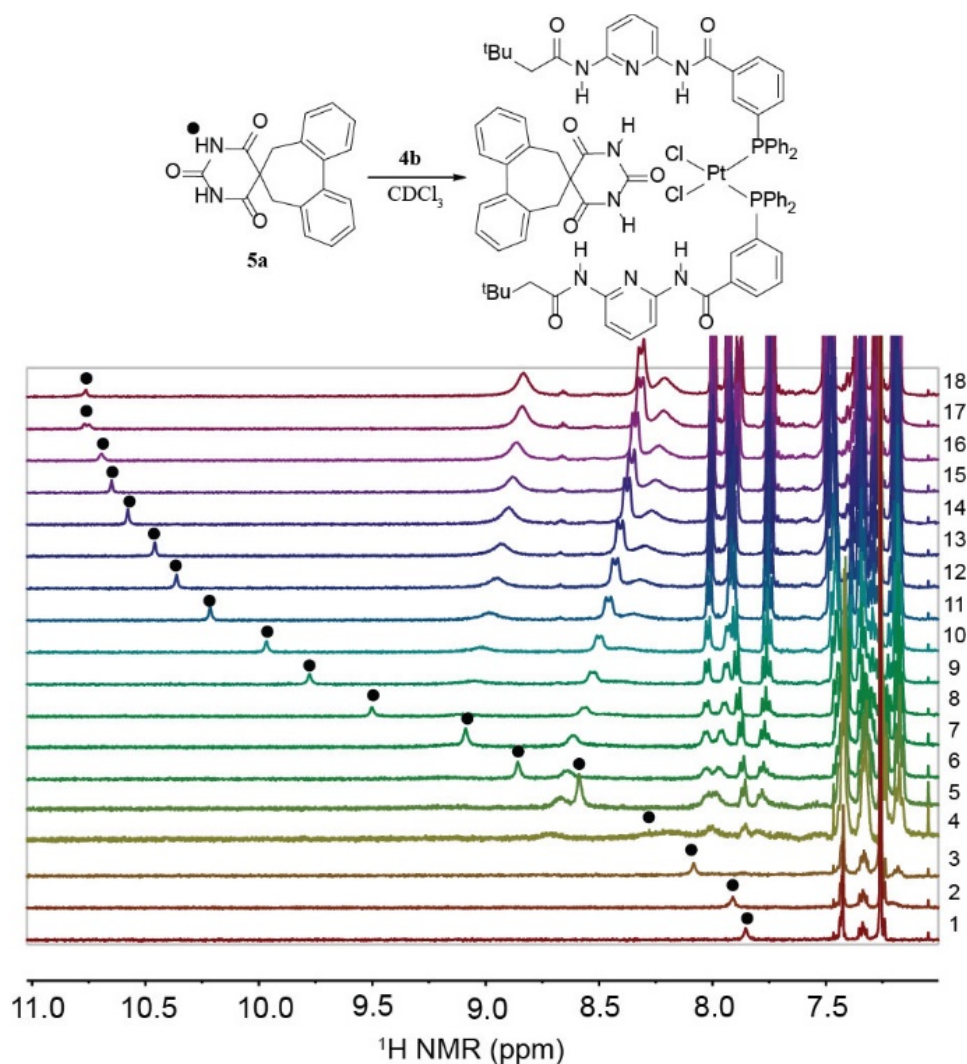


Figure 2.4. Sample ^1H NMR titration of **4b** and **5a** in H_2O sat. CDCl_3 .

2.3. Conclusions

In summary, we have developed a new supramolecular, self-assembling ligand scaffold motif based on a deconstructed Hamilton receptor. *Cis*-PtL₂Cl₂ host complexes that bind synthetic barbiturate guests were synthesized and characterized both in solution and the solid state. This supramolecular system displays a 1:1 binding mode consistent with a deconstructed Hamilton receptor, and guest binding was observed in both competitive and non-competitive solvents. The ease and high modularity of the host synthesis as well as the guest tunability make this scaffold poised for diverse applications ranging from acting as a building block for larger self-assembled structures and materials as well as applications in high-throughput and combinatorial screenings of catalytic reactions.

2.4. Bridge

The contents of this chapter outline the initial design strategy, synthesis, and basic self-assembly properties of a new supramolecular bidentate phosphine ligand scaffold. These new ligands act as host components for potential supramolecular bidentate catalyst libraries. However, these ligands alone can only act as monodentate ligands. Chapter III of this dissertation will describe the development of a small library of new synthetic barbiturate guest molecules that act as the second component in the supramolecular catalyst system.

CHAPTER III

DIRECT SYNTHESIS OF 5,5'-DISUBSTITUTED BARBITURIC ACIDS FROM BENZYL AND ALLYL HALIDES

Chapter III of this dissertation contains co-authored unpublished work that was written by me. The synthesis and photophysical experiments were performed by me and the results were also interpreted by me. Zakharov, L. collected and interpreted the x-ray diffraction data. Pluth, M. provided editorial assistance.

3.1. Introduction

Substituted barbituric acids have long held a privileged role as potent hypnotics, anticonvulsants, and anxiolytics.¹ More recently, their use as functional materials (e.g. organo-gelators,² non-linear optics materials,^{3,4} metal-ion sensors^{5,6}) and components in supramolecular coordination assemblies⁷ has renewed interest in this molecular scaffold. During our development of supramolecular bidentate phosphine ligands based on the Hamilton receptor,⁸ we became interested in easily accessible 5,5'-disubstituted barbiturates. Although there have been a multitude of barbiturates synthesized since their initial discovery by von Baeyer in 1863,⁹ straightforward synthetic routes to these molecules remain under-reported. This dearth is particularly true when considering the direct synthesis of 5,5'-disubstituted barbiturates from commercially available barbituric

acid. Building from this need, we report here the direct synthesis of diverse 5,5'-disubstituted barbituric acids from benzyl and allyl halides and barbituric acid for potential use in materials applications and construction of supramolecular assemblies.

Traditional syntheses of substituted barbiturates involve condensation of substituted malonates with urea under basic conditions.^{7, 10} Notably, these procedures involve prior functionalization of the malonates, and the subsequent condensations with urea to form the desired barbiturate remains challenging.¹¹ Alternatively, the relatively acidic methylene hydrogens of barbituric acid (BA) ($pK_a = 4.00$, H_2O)¹² allows for simple substitution reactions via deprotonation using a weak base. The numerous tautomers present in the anionic form of barbituric acid, however, make both *N*- and *O*-alkylation possible (Figure 3.1), thus often complicating the preparation of the target molecules. Additionally, under most reaction conditions, the resulting anion from deprotonation is insoluble in the organic solvents typically used to solubilize the subsequent electrophile. More recent approaches that utilize commercially available barbituric acid require the use of phase transfer conditions.¹³ In our hands, however, this methodology proved unreliable with different electrophiles, and we found that the presence of a phase transfer catalyst (PTC) significantly complicated purification. Therefore, we sought to develop a simple protocol for the synthesis of 5,5'-disubstituted barbiturates from barbituric acid in the absence of a phase transfer catalyst that could be used to provide access to commonly-used, as well as new more difficult to access, derivatives.

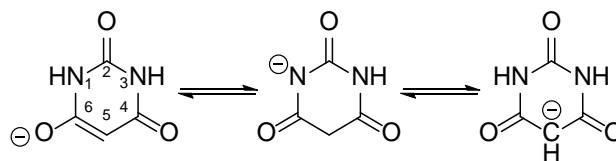
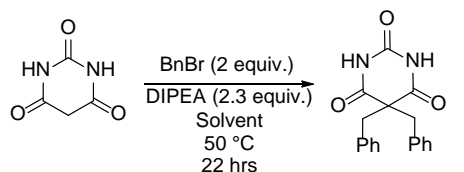


Figure 3.1. Various tautomers of the barbituric acid anion showing *O*, *N*, and *C* nucleophilic centers, respectively.

3.2. Results and Discussion

As a test system, we began by investigating the solvent effects on the reaction between benzyl bromide and barbituric acid in the presence of *N,N*-diisopropylethylamine (DIPEA) (Table 3.1). In all cases, pure product was isolated without the need for column chromatography by simple trituration in a DCM:hexanes mixture (see Appendix B, Figure B.1). As expected, polar solvents gave higher yields, with DMSO, MeOH, and DMF providing the highest yields, which we attributed the increased solubility of both the anion and electrophile.

Table 3.1. Solvent screening study using benzyl bromide. All reactions conducted with barbituric acid concentrations of 390 mM. The reported yields are from isolated yields based on barbituric acid.



Solvent	Yield	Solvent	Yield
MeOH	62%	THF	22%
<i>i</i> PrOH	31%	MeCN	19%
<i>n</i> BuOH	33%	Toluene	11%
DMSO	79%	Pyridine	0%
DMF	51%		

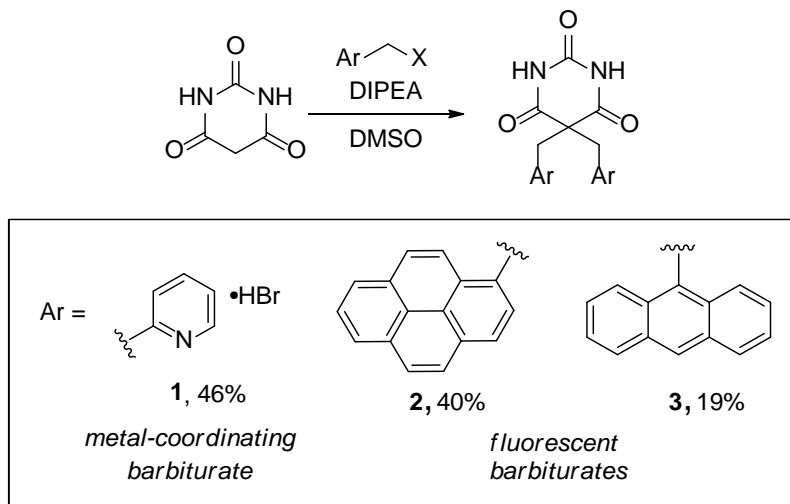
Using the best conditions from our solvent screening, we then screened different electrophiles to determine the tolerance to different electrophiles of this method (Table 3.2). Gratifyingly, clean alkylation at the C5 position was observed for all benzyl halides and allyl bromides, with reactions using benzyl iodide complete in an hour at room temperature. Alkyl halides, however, failed to provide any of the desired alkylated products. In addition to the halide substrates shown in Table 3.2, use of pseudo halides, alkyl tosylates, also failed to generate the desired product, which is likely due to the multiple reactive sites of the resultant barbituric anion, thus resulting in complex *N*- and *O*-alkylation mixtures.

Table 3.2. Electrophile screening using DMSO as the solvent. Reported yields are isolated yields based on barbituric acid. ^a 100 °C for 22 hours, ^b room temperature for 1 hour.

Entry	R-X	Yield	Entry	R-X	Yield
1		70% ^a	6		0%
2		78%	7		0%
3		76% ^b	8		0%
4		57%	9		0%
5		51%	10		0%

Having elucidated the scope of this method to access simple 5,5'-disubstituted barbituric acid derivatives, we next focused on preparing novel barbiturates that could

have utility in potential materials and supramolecular applications, particularly scaffolds with metal coordination and fluorescent properties. To this end, reacting 2-bromomethylpyridine hydrogen bromide, 1-bromomethylpyrene, and 9-chloromethylanthracene with barbituric acid under similar reaction conditions to those described in Table 3.2, yielded compounds **1-3** respectively (Scheme 3.1). The absorbance spectra of **2** and **3** exhibit the characteristic fine structure of acene-type aromatics with $\lambda_{\text{max}} = 346$ nm and 393 nm for **2** and **3**, respectively. Additionally, the emission maxima at 379 nm and 425 nm for compounds **2** and **3** make them good candidates for reporter molecules for supramolecular assembly and recognition.¹⁴⁻¹⁶



Scheme 3.1. Synthesis of new metal-coordinating and fluorescent barbiturates.

In addition to barbiturates with well-defined optical properties, we were also interested accessing chiral barbiturates. Typically, such molecules involve desymmetrization of barbituric acid by asymmetric substitution at the N1/N3 position and C5 position. Alternatively, barbiturate functionalization with point chiral precursors can yield chiral barbiturates, but this approach is underutilized because of the limited

accessibility to the required chiral precursors.¹⁷ To overcome these obstacles, we hypothesized that simple prefunctionalization of commercially available, enantiopure BINOL would provide simple access to a rare example of an axially chiral barbiturate. Starting with BINOL, triflation with PhN(Tf)₂, followed by a Kumada cross coupling with MeMgI, and bromination with NBS afforded the desired bis(methylbromide), which was subsequently coupled to barbituric acid in DMSO to afford **4a** (*R*) and **4b** (*S*), as shown in Scheme 3.2. Under these standard reaction conditions, **4a** and **4b** could be isolated in pure form after column chromatography and recrystallization from ethanol.

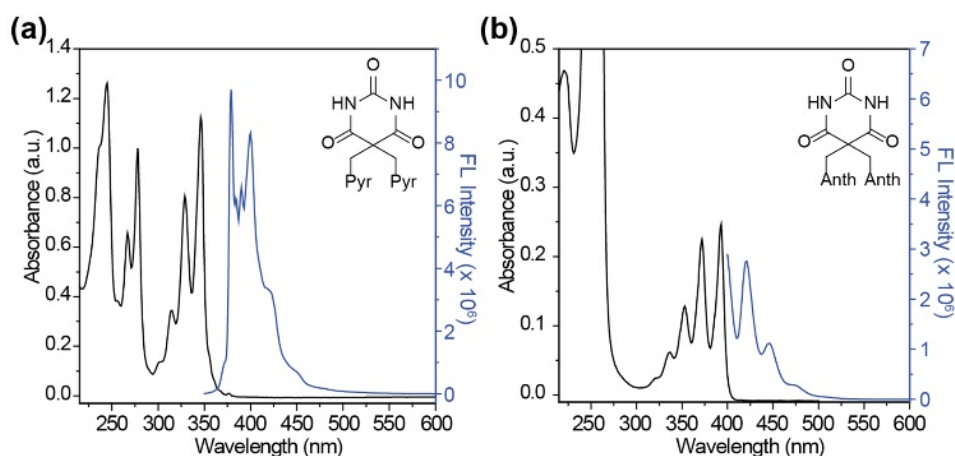
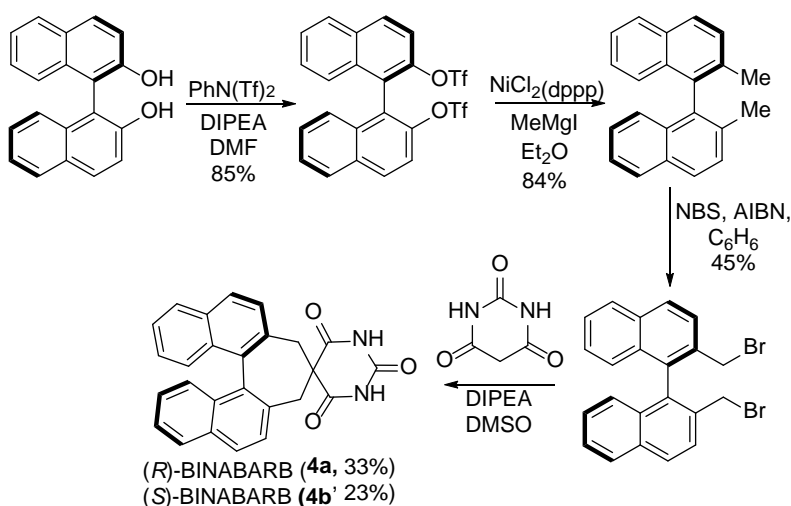


Figure 3.2. (a) Absorbance and fluorescence ($\lambda_{\text{ex}} = 346$ nm) spectra of compound **2** in degassed THF at 14 μM and 28 μM , respectively. (b) Absorbance and fluorescence ($\lambda_{\text{ex}} = 393$ nm) spectra of **3** in THF at 15 μM and 30 μM , respectively.

Having prepared a variety of substituted barbiturates with different substitution in the 5-position, we next sought to investigate the solid-state interactions of **1-3** and **4**. In addition to applications in materials science, barbiturates are used extensively in crystal engineering,¹⁸ pharmaceutical co-crystallization,^{19, 20} and crystal polymorphism.²¹⁻²⁵ For the prepared barbiturates, suitable single crystals for X-ray diffraction were grown from

THF:pentane vapor diffusion (Figure 3.3). All new barbiturates crystallized as the tri-keto tautomer with C-N and C-O bond lengths ranging from 1.35-1.38 Å and 1.21-1.22 Å, respectively. Compound **4a** displays two N-H...O=C hydrogen bonding motifs between adjacent barbiturates in the crystal lattice, with N-H...O=C bond distances of 2.905 and 2.726 Å, which is common in many barbiturates.^{18,24} For compound **1**, introduction of a competitive hydrogen bond acceptor like pyridine perturbs the hydrogen bonding network and provides an alternative packing motif.



Scheme 3.2. Synthesis of (*R*) and (*S*)-BINABARB with (*R*)-stereochemistry shown.

In **1**, a N-H...N(pyridine) hydrogen bond is formed with a distance of 2.907 Å, with the second N-H from the barbiturate hydrogen bonding to the THF solvent molecule in the crystal lattice. Further changes in the crystal lattice are observed upon increasing the size of the planar π surface as in **2** and **3**. For both compounds, the N-H...O=C hydrogen bonding network is completely eroded and instead only N-H...O(THF) motifs are observed. In these systems, the π - π interactions dominate the packing structure with an

interplanar distances of 3.449 Å and 3.419 Å between the two offset pyrenes in **2** and 3.365 Å in **3**.

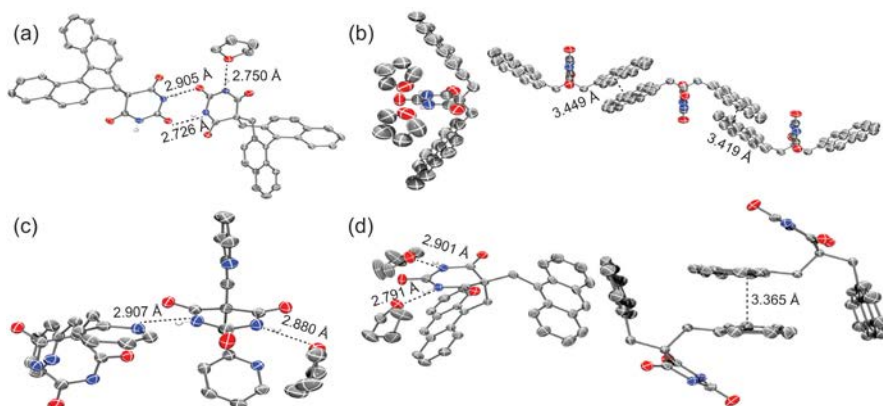


Figure 3.3. ORTEP representations of compounds **1-3** and **4a** with thermal ellipsoids drawn at 50% probability. All non-hydrogen bonding hydrogens omitted for clarity. a) Dimer of compound **4a** ; b) dimer of compound **2**; c) profile and portrait view of compound **1** with the THF molecules omitted for clarity; d) solid state structure of compound **3** showing profile view of hydrogen bonding motif and view showing π - π interactions with THF molecules omitted for clarity.

To further examine the extent that the π - π interactions could affect the solid-state structure, we synthesized an unsymmetrical barbiturate, **5**, which has one perfluorinated phenyl ring, with the goal of evaluating how the arene-perfluoroarene interactions would affect the typical N-H \cdots O=C hydrogen bonding networks (Figure 3.4). In this case, X-ray quality crystals of **5** were obtained from a slow evaporation from acetone.

Interestingly, the solid state structure contains both an extensive arene-perfluoroarene network as well as a hydrogen bonding network. The centroid to centroid distance between the arene-perfluoroarene moieties is 3.644 Å, while the distance between the centroid of the arene ring to the plane of perfluoroarene ring is 3.444 Å. The hydrogen bonding network is characterized by a traditional N-H \cdots O=C hydrogen bond of 2.751 Å with the other imide N-H bound to adventitious water. Lastly, the conformations of the

new barbiturates range from highly planar (0.16° for compound **2**) to highly enveloped (32.6° for compound **3**), however, no trend is immediately apparent (Appendix B, Table B.1). Altogether, the solid-state structures of this new suite of barbiturates confirms that substitution at the 5-position of the barbiturate greatly impacts the crystal packing of these molecules and can be tuned by modifying the type non-covalent interactions present.

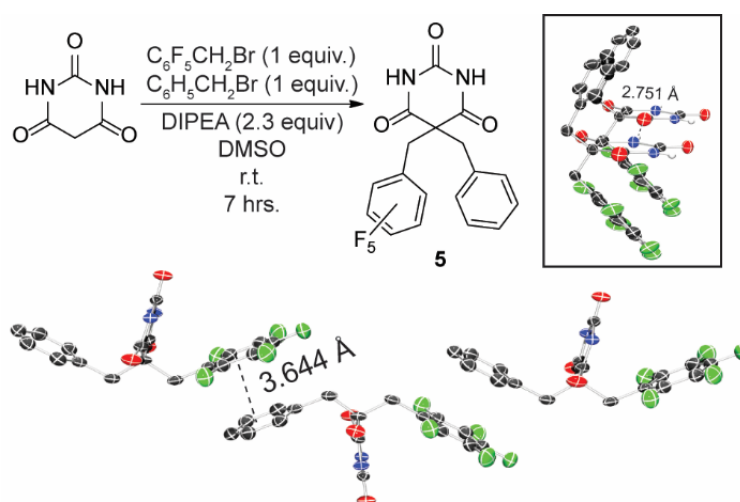


Figure 3.4. Synthesis of unsymmetrical barbiturate **5** and ORTEP representations with thermal ellipsoids drawn at 50% probability. Both the profile view of the hydrogen bonding motif and view showing the π - π interactions have the non-hydrogen bonding hydrogens and water molecule omitted for clarity.

3.3 Conclusions

In conclusion, we have shown that 5,5'-disubstituted barbiturates can be synthesized directly from barbituric acid without the use of phase transfer catalysts to provide moderate to good yields for benzyl and allyl electrophiles. Using this methodology, we prepared new fluorescent and chiral barbiturates with properties that

make them potentially useful for materials and supramolecular applications. Additionally, the solid-state analysis shows that varying the substitution at the 5-position has a dramatic impact on the observed hydrogen-bonding motifs.

3.4 Bridge

In Chapter II of this dissertation we reported the design and synthesis of a new supramolecular phosphine ligands as the host component of our new supramolecular ligand scaffold. In this chapter, we reported the design and synthesis of new and previously reported barbiturates as the guest components of our new supramolecular ligand scaffold. Chapter IV will discuss the applications of this combined supramolecular ligand platform for the hydroformylation of 1-octene. This model reaction will serve as a method for evaluating the efficacy of this new ligand design strategy and its application towards allosteric control of catalysis.

CHAPTER IV

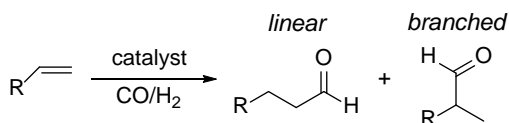
PROGRESS TOWARDS THE HYDROFORMYLATION OF 1-OCTENE USING SUPRAMOLECULAR PHOSPHINE LIGANDS BASED ON THE HAMILTON RECEPTOR

This chapter contains co-authored unpublished work that was written by me. The majority of the experiments were performed by me and the results were also interpreted by me. Barker, J. performed the synthesis for compounds 8-10 in this chapter. Zakharov, L. collected and interpreted the x-ray diffraction data. Pluth, M. provided editorial assistance.

4.1. Introduction

Hydroformylation is one of the most important catalytic processes of both academic interest and industrial relevance. By volume, it is the largest industrial process in homogenous catalysis.¹ Since its original discovery in 1938 by Roelen, hydroformylation has been the subject of numerous academic reports, including the subject of many recent reviews.¹⁻⁸ Formally, the hydroformylation reaction involves the addition of CO and H₂ to an alkene to generate aldehyde products (Scheme 4.1). Most often, this process is mediated by Rh-phosphine complexes however, many other metals⁶ (e.g. Ru, Ir, Pd, Pt, Fe, etc) and ligands⁹⁻¹¹ have been reported. Asymmetric hydroformylation, although much less developed, continues to be a blossoming area of research.¹²⁻¹⁸ Additionally, because many of the substrates used in these processes

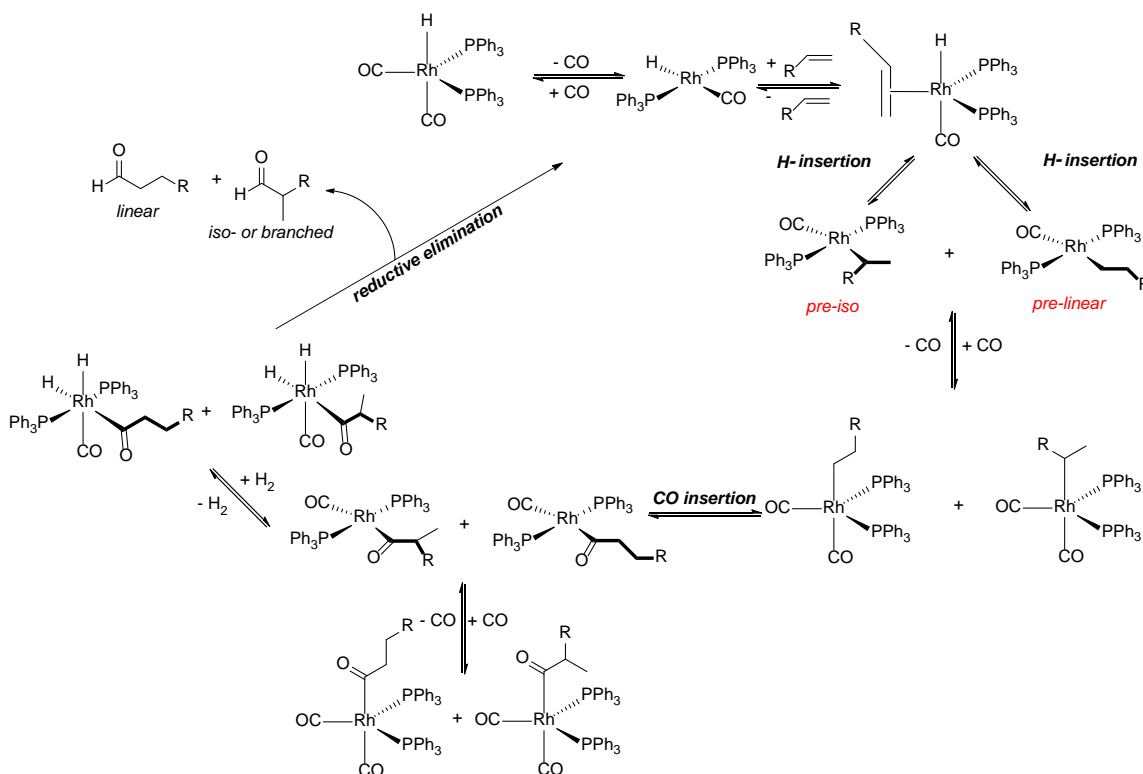
contain unsaturated units, in addition to the production of reactive aldehyde products, hydroformylation has been a ubiquitous component in tandem reactions.¹⁹⁻²²



Scheme 4.1. General scheme for the hydroformylation reaction.

The mechanism of hydroformylation proposed by Heck and Breslow remains the most widely accepted and well-established (Scheme 4.2). While there continue to be mechanistic improvements, the current general reaction scheme provides a clear understanding of the production of branched and linear aldehyde products. Importantly, the reversibility of almost all of the steps in the mechanism has the potential to result in many unwanted and isomerized by-products such as internal olefins, branched alcohols, and alkanes from over reduction. Moreover, the reversible hydride-migration is the primary step in determining the regioisomerism of the final aldehyde products. The resulting aldehydes are important precursors for the synthesis of bulk chemicals such as alcohols, amines, and esters with the linear aldehydes often being the preferred regioisomer. Additionally, the aldehyde products have wide applications in the fragrance industry.⁴ Therefore, understanding the factors that control this selectivity has been a major focus of hydroformylation research. Currently, one of the most effective ways to control the regioselectivity is through the use of bidentate phosphine ligands, as the bite angle of the phosphine has been well-correlated with the linear to branched aldehyde ratio (*l:b*).^{23,24} However, bidentate ligands often achieve this enhanced selectivity at the cost of decreased activity. Moreover, the synthesis of large libraries of bidentate ligands

is typically much more tedious and difficult compared to their monodentate analogues. These synthetic drawbacks make combinatorial approaches to ligand screening more difficult and less amenable to high-throughput screenings. Thus, there is a continual demand to find new, readily accessible ligand platforms for applications in hydroformylation and beyond.



Scheme 4.2. General mechanism of Rh-catalyzed hydroformylation.

A relatively new area of ligand design is that of supramolecular bidentate ligands.^{1, 25-27} Using supramolecular design principles, formation of functional bidentate ligands can be achieved through the self-assembly of two monodentate ligand subunits. This activity is often achieved through the incorporation of non-covalent interactions and complementary recognition motifs inherent in the ligand architecture. This new class of ligands benefits from the simplified synthetic design strategies for monodentate ligands

while exploiting the chelation abilities of bidentate ligands. Pioneering work by the independent groups of Breit and Reek have popularized this strategy and developed new, highly efficacious ligand platforms based on different types of non-covalent interactions (Figure 4.1). The work of Breit has primarily focused on the construction of supramolecular bidentate ligands assemblies using hydrogen bond forming tautomers.²⁸⁻³² The most popular and efficacious scaffolds are those based on the phosphine functionalized-2-pyridone/2-hydroxypyridine tautomer. When in the presence of a metal ion, these monodentate ligands selectively form heterodimeric metal-ligand complexes. Conversely, work by Reek utilizes secondary metal ligation of pyridyl-functionalized phosphines to direct coordination of bis-Zn-porphyrin scaffolds.³³⁻⁴⁰ Importantly, both approaches show high efficiency towards the hydroformylation of alkenes showing selectivity for linear aldehydes over branched similar to traditional bidentates. Additionally, because of the synthetic accessibility of these subunits, combinatorial approaches to catalytic screenings are not only possible, but can generate more meaningful structure-function studies.³²

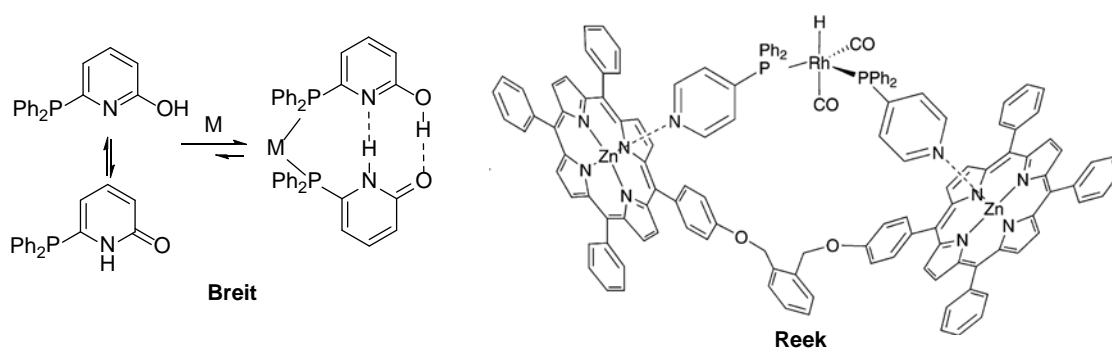
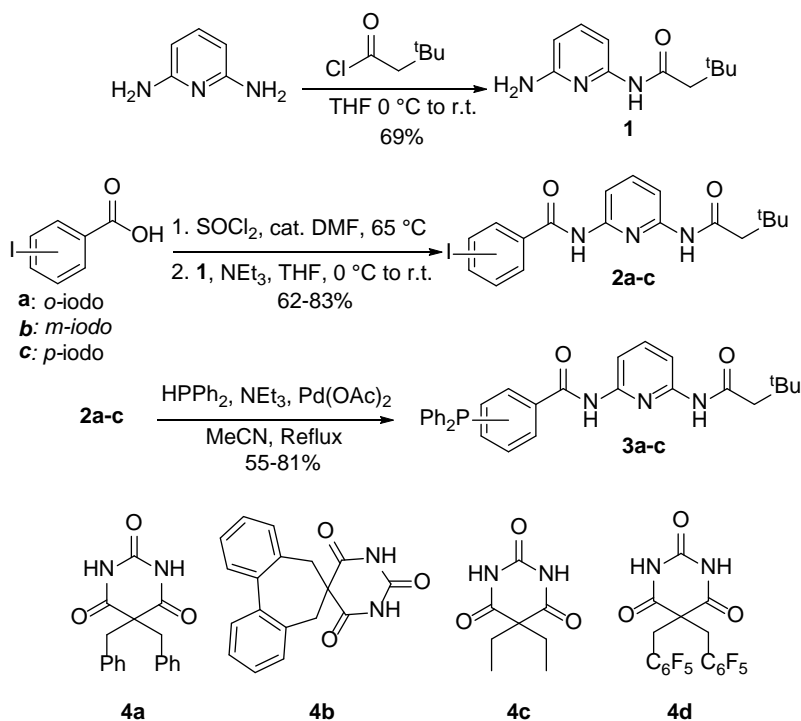


Figure 4.1. Supramolecular bidentate phosphine ligand scaffolds popularized by Breit and Reek.

In an effort to expand the types of supramolecular ligand platforms capable of self-assembly to give functional bidentate ligands, we recently reported a new host–guest approach to supramolecular ligand designed based on bifurcated Hamilton receptors and barbiturate guests.⁴¹ Initial results showed that model *cis*-PtL₂Cl₂ (L = phosphine functionalized bifurcated Hamilton receptor) systems do undergo self-assembly in the presence a barbiturate guest with the binding affinities controlled by the regioisomerism of the appended phosphine. To evaluate the efficacy of our new supramolecular ligand system, we chose to perform the Rh-catalyzed hydroformylation of 1-octene as a model reaction. We hypothesized that through evaluation of the linear:branched aldehyde ratio, we could gain a better understanding of the structural features of our new ligand platform that controlled the tunable bidentate character. Herein, we report our initial results towards these aims as well as the synthesis, coordination properties, binding affinities, and catalytic efficiencies of new benzyl and fluorinated structural analogues to our original bifurcated receptors.

4.2. Results and Discussion

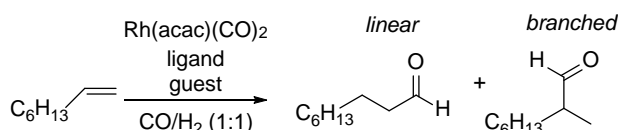
The synthesis of the phosphine functionalized bifurcated Hamilton receptors has been reported by us previously⁴¹ and is shown in Scheme 4.3. Using the currently accepted mechanism of hydroformylation, we knew that to achieve effective bidentate type behavior, a *cis* geometry of these ligands about the metal center was required. Therefore, we elected to exclude the ortho-isomer **3a** from our catalytic screenings due to its inability to form *cis*-PtL₂Cl₂ model complexes.



Scheme 4.3 Synthesis of phosphine functionalized bifurcated Hamilton receptor ligands **3a–c** and structures of barbiturate guests used for initial screenings.

To begin our studies, we elected to use hydroformylation conditions similar to those reported by Reek³⁷ and Breit²⁸ to investigate the efficacy of our new ligand platform towards the hydroformylation of 1-octene (Scheme 4.4). Initial screenings focused on ligand **3b** with increasing equivalents of a dibenzylbarbiturate guest (**4a**). Compound **3b** was chosen as the primary screening ligand as it was shown to have the largest binding affinity for a synthetic barbiturate guest during our previous studies.⁴¹ The Rh catalysts were prepared in-situ by mixing a Rh(acac)(CO)₂ precursor with 200 equivalents of ligand, 1–1000 equivalents of guest, and charged with 1000 equivalents of 1-octene in THF under an inert atmosphere. The reaction vessel was then pressurized (150 PSI) with H₂/CO (1:1). The catalyst was allowed to form with an initial heating at 50 °C for 90 minutes at which point the headspace was recharged with H₂/CO (1:1, 150 PSI) and stirred at 50 °C overnight (12-24 hours). The ratio of linear to branched

aldehyde products was then determined using GC-MS, the results of which are given in Table 4.1. From the initial results we were able to determine that while the presence of barbiturate guest has little effect on the *l:b* ratio when using traditional monodentate ligands (PPh₃), no increase in selectivity observed when using **3b** with up to 100 equivalents of guest.



Scheme 4.4. Generalized reaction scheme for the hydroformylation of 1-octene using the new bifurcated Hamilton receptor supramolecular ligand scaffold.

Table 4.1. Linear to branched (*l:b*) aldehyde ratio from the hydroformylation of 1-octene at 50 °C using classic monodentate and supramolecular bidentate phosphine ligand assemblies. Conditions: [Rh] = 100 μM, [ligand] = 2.0 mM, [1-octene] = 100 mM, [decane] = 50 mM.

Ligand	Guest (Equiv.)	<i>l:b</i>
PPh ₃	--	2.82
PPh ₃	4a (1)	2.70
3b	4a (1)	2.66
3b	4a (5)	2.72
3b	4a (10)	2.73
3b	4a (100)	2.67

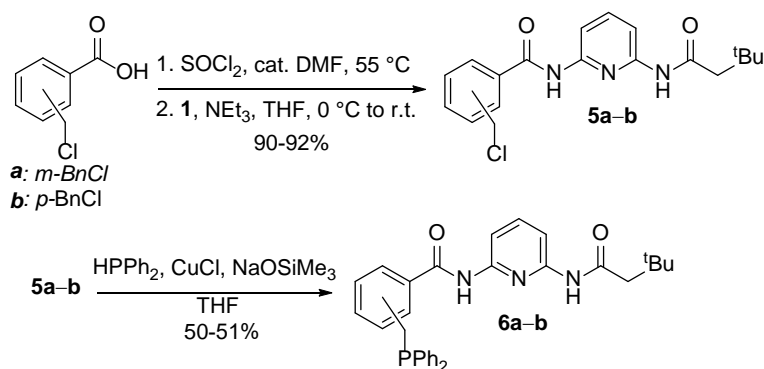
We hypothesized this lack of selectivity could be caused by the attenuation of hydrogen bond formation between the ligand host and barbiturate guest due to the elevated reaction temperatures at which the reactions were run. In an attempt to increase the observed selectivity, the reactions were allowed to stir overnight at room temperature after pre-activation of the catalyst at 50 °C for 90 min. The results are shown in Table 4.2. Again, no increase in selectivity of linear over branched aldehyde product was observed using ligand **3b** with up to 100 equivalents of **4a**.

Table 4.2. Results from the hydroformylation of 1-octene at rt using classic monodentate and supramolecular bidentate phosphine ligand assemblies. Conditions: [Rh] = 100 μ M, [ligand] = 2.0 mM, [1-octene] = 100 mM, [decane] = 50 mM.

Ligand	Guest (Equiv.)	<i>l:b</i>
PPh ₃	--	3.4
PPh ₃	4a (6)	3.3
3b	4a (5)	3.1
3b	4a (56)	2.9
3b	4a (108)	3.0

Further attempts to improve the selectivity were made by revisiting our initial ligand design. After looking closely at the crystal structure of the *cis*-PtL₂Cl₂ (L = **3b**), we hypothesized that the direct aryl linkage of the phosphorus donor atom could be too rigid and therefore impose an unfavorable binding pocket for the incoming barbiturate guest. To improve the flexibility of this scaffold, we synthesized the methylene spaced, benzyl analogues **6a–b** (Scheme 4.5). Using similar methods for the synthesis of **2a–c**, we were able to construct the benzyl halide isomers **5a–b**. Attempts to synthesis the ortho isomer resulted in isolation of the oxindole (cyclized) byproducts and was therefore not pursued further. Using a Cu^I mediated substitution reaction with diphenylphosphine in the presence of a mild base (NaOSiMe₃), benzyl-modified ligands **5a–b** were isolated after column chromatography.

With these new receptors in hand, we then subjected ligands **3c** and **6a–b** to similar hydroformylation condition as those used for **3b** to evaluate the effects of regioisomerism and host flexibility on selectivity (Table 4.3). The results again show no increase in selectivity for these new ligands compared to PPh₃ and **3b** confirming that binding pocket flexibility and regioisomerism are not responsible for the poor selectivity.

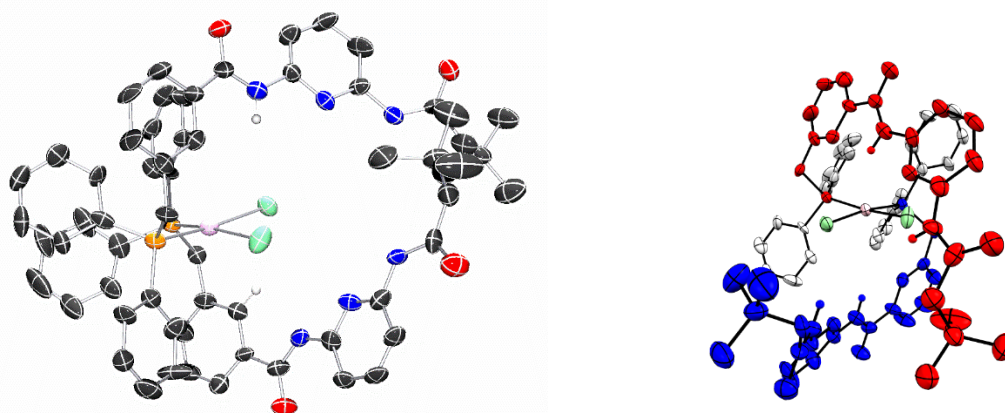
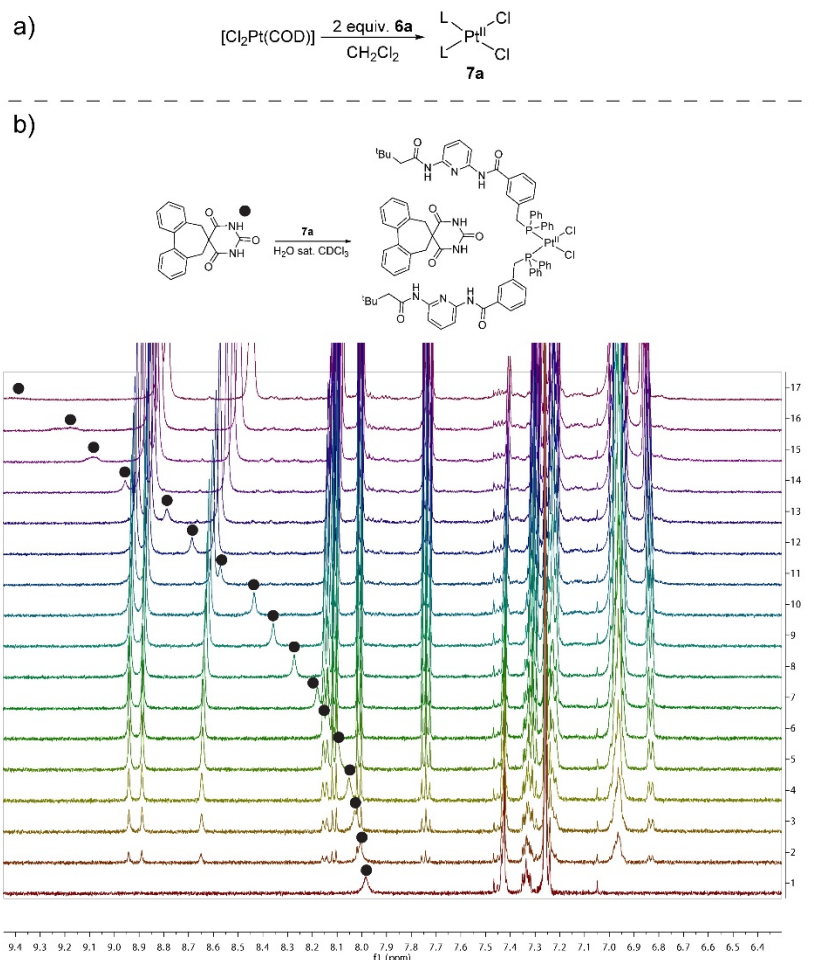


Scheme 4.5. Synthesis of benzyl-modified bifurcated Hamilton receptor ligands.

Table 4.3. Effect of methylene spacer and regioisomerism of phosphorus donor atom on the linear to branched (*l:b*) aldehyde ratio from the hydroformylation of 1-octene at rt for four days. Conditions: [Rh] = 100 μM , [ligand] = 2.0 mM, [1-octene] = 100 mM, [decane] = 50 mM.

Ligand	Guest (Equiv.)	<i>l:b</i>
PPh ₃	--	3.07
3b	4a (55)	3.06
3c	4a (55)	3.23
6a	4a (55)	2.49
6b	4a (55)	2.56

In an attempt to investigate the root cause of the poor selectivity of the benzyl-modified ligands, *cis*-PtL₂Cl₂ model complexes were constructed and ¹H NMR titrations were performed to measure the binding affinity towards guest **4b** (Figure 4.2). Fitting the resultant binding isotherm to a 1:1 binding model resulted in a drastically attenuated binding affinity ($K_a = 66 \text{ M}^{-1}$) compared to that of **3b** ∪ **4b** ($K_a = 800 \text{ M}^{-1}$). Further insight into the cause of this attenuation was provided by single crystal x-ray diffraction (Figure 4.3). The structure of *cis*-PtL₂Cl₂ (L = **6a**) (**7a**) clearly shows a distorted binding pocket with the two recognition units of the host arms trans to the phosphorus donor atom. This erosion of preorganization likely explains the attenuated binding affinity and similar hydroformylation activity compared to **3b**.



In a final attempt to increase the binding affinity and improve the efficacy of this new ligand platform, an alternative approach to hydrogen-bonding was taken. Typically, the distal substitution of the receptor arms is chosen such that the steric bulk of the appended groups prevents self-aggregation. We hypothesized that instead of neo-pentyl substitution, using perfluorinated arene rings would result in positive secondary non-covalent interactions (arene-perfluoroarene) between the host and guest resulting in increased binding affinities (Figure 4.4). Synthesis of these types of ligands and the proto-analogues was achieved using similar amide couplings and phosphination conditions as previously reported (Scheme 4. 6).

These new ligands were then subjected to similar hydroformylation conditions as before and compared directly to a traditional bidentate ligand (Xantphos). Additionally, other types of synthetic barbiturates (**4a–d**) were screened to evaluate the effect of guest on the *l:b* ratio. Unfortunately, these ligands again showed no increase in selectivity when compared to ligands **3b–c**, **6a–b**, or PPh₃.

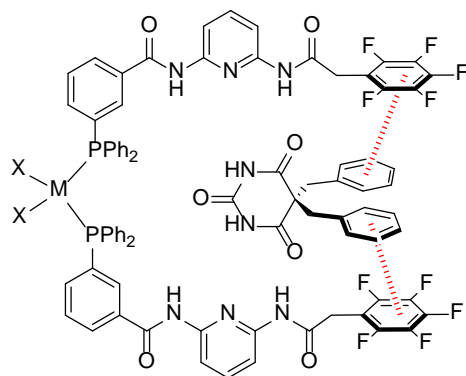
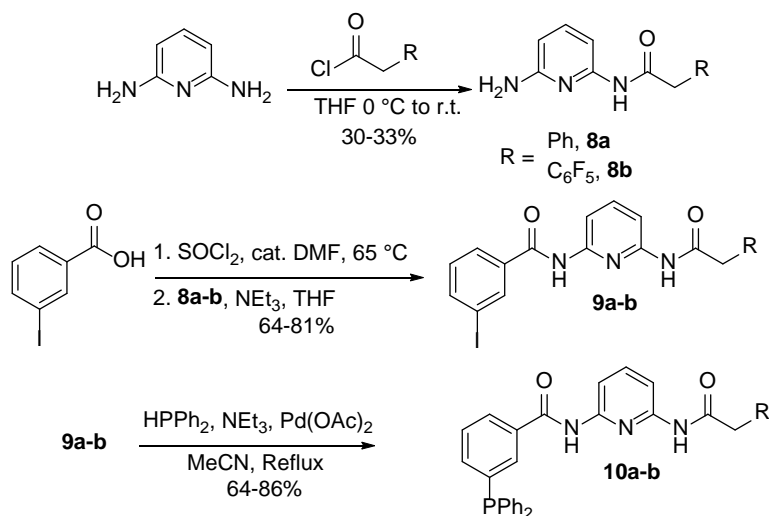


Figure 4.4. Generic metal-ligand complex with perfluorinated aryl groups showing secondary interactions with a barbiturate guest.



Scheme 4.6. Synthesis of benzyl and perfluorobenzyl substituted phosphine modified Hamilton receptors.

Both ligands **10a** and **10b** showed similar selectivity when used with their complementary guest (**4d** and **4a**, respectively). Additionally, barbiturates of different sizes also had little to no effect on aldehyde selectivity indicating that negative steric interactions between the host and guest are either minimal or prohibiting binding altogether.

Table 4.4. Results from the hydroformylation of 1-octene with supramolecular bidentate ligands capable of secondary interactions and different guest molecules at 50 °C. Conditions: [Rh] = 100 μM , [ligand] = 2.0 mM, [1-octene] = 100 mM, [decane] = 50 mM.

Ligand	Guest (Equiv.)	<i>l:b</i>
PPh ₃	--	2.82
PPh ₃	4a (27)	2.57
Xantphos	--	> 99:1
10a	4a (27)	2.63
10a	4d (27)	2.84
10b	4a (27)	2.64
10b	4d (27)	2.78
3b	4c (27)	2.73

4.3. Conclusions

In conclusion we report the synthesis and binding affinities of new phosphine modified Hamilton receptors as an additional supramolecular phosphine ligand platform. Hydroformylation of 1-octene with these ligands in the presence of a variety of barbiturate guests showed no enhanced selectivity over traditional monodentate ligands. Numerous design methods were employed and tested in an attempt to improve this lack of selectivity, but were unsuccessful. These results are likely due to the suboptimal preorganization of the host-binding pocket preventing strong association of the barbiturate guest resulting in little effective chelation of the phosphorous donor atoms. Future attempts at improving the efficacy of this scaffold should focus on alternative secondary interaction between barbiturate guest and ligand receptor to improve the binding affinity. Additionally, substitution of the 4-position on the pyridyl ring with electron rich moieties could increase the binding affinity of the guest by increasing the basicity of the pyridyl lone pair.

4.4. Bridge

After understanding the limitations of our current supramolecular ligand platform, we switched our attention to understanding the potential supramolecular interactions between individual barbiturate guest molecules. Many barbiturates are known to dimerize in the solid-state and we were interested in understanding their self-association in solution as well. In Chapter II we reported the synthesis of new chiral barbiturates. A

unique observation was made that these molecules form gels when dissolved in chlorinated solvents. The contents of Chapter V elaborate on this observation and provide initial insights into the molecular/physical parameters that cause this unique gelation behavior. Additionally, we investigate the types of microstructures formed from the self-association of these new barbiturates.

CHAPTER V

SINGLE-COMPONENT, LOW MOLECULAR WEIGHT ORGANIC SUPERGELATORS BASED ON CHIRAL BARBITURATE SCAFFOLDS

This chapter contains co-authored unpublished work that was written by me. The majority of the experiments were performed by me and the results were also interpreted by me. SEM imaging experiments were performed with the assistance of Langworthy, K. Zakharov, L. collected and interpreted the x-ray diffraction data. Pluth, M. provided editorial assistance.

5.1. Introduction

Supramolecular gels are an emerging class of soft materials with unique and tunable rheological and thermal properties. Due to their viscoelastic properties, supramolecular gels capable of gelating organic solvents (organogels) have found widespread application in sensing and stimuli responsive materials,¹⁻¹⁰ optoelectronics,¹¹⁻²⁰ drug delivery,^{21, 22} and as templates for nanoparticles and other inorganic structures.^{23, 24} Structurally, organogelators range from polymeric to single small molecules or low molecular-weight organic gelators (LMOGs). In addition, multicomponent gel systems have also been reported.²⁵⁻²⁸ In LMOGs and multicomponent systems, gel formation

typically occurs through the self-assembly of individual units to produce one-dimensional fibers that become three-dimensionally entangled or crosslinked. The delicate balance required to favor gelation over crystallization or dissolution is typically achieved through careful tailoring of the non-covalent interactions, H-bonding, π - π stacking, metal-coordination, and van der Waals interaction, to guide self-assembly. Here, we report a simple approach to accessing chiral, single-component, supergelators using simple and readily-accessible starting materials.

Among the most popular strategies for creating new organogelators is incorporation of long, single chain alkyl groups or cholesteryl moieties to a specific scaffold of interest.^{25, 29} Application of these strategies has produced organogelators capable of gelating an array of organic liquids but has limited the potential for further understanding of the physical processes that drive gelation. Another popular motif for the construction of supramolecular gels is the melamine-barbiturate/cyanurate binary system (Figure 5.1).³⁰⁻³⁴ Such systems are characterized by the complementary donor-acceptor-donor hydrogen bonding motif of the melamine unit, and the acceptor-donor-acceptor motif of the barbiturate/cyanurate. Although these systems show promising gelation behavior, functionalization with long alkyl chains or large cholesteryl groups is required for efficient gelation.³³ A rare example of a strategically modified, self-complementary barbiturate/receptor has been reported, but the gelation ability of this system was poor and limited to specific solvent conditions and required a high weight percent (8 wt %) of gelator.³⁵

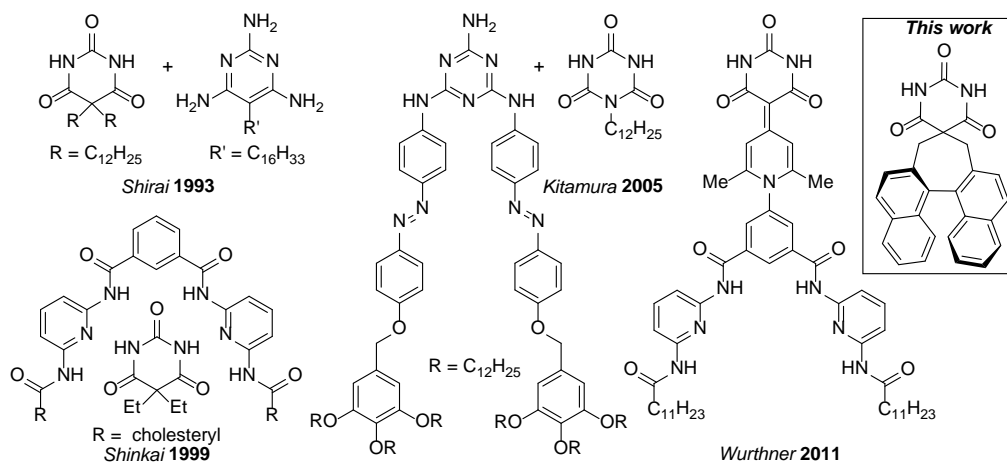


Figure 5.1. Previously reported organogelators based on the melamine·barbiturate/cyanurate motifs (left) and a new chiral, single-component LMOG based on a barbiturate scaffold (right).

Adding to the inherent gelation properties, the inclusion of chirality is also a common feature of organogelators.³⁶ Unfortunately, the useful properties of chiral gelators are often eroded when used as racemic mixtures with most racemates showing no gelation behavior. Additionally, by studying the self-assembly of these chiral building blocks, researchers can begin to understand the mechanisms of chirality transfer from single molecules to self-assembled, chiral nanostructures.³⁷⁻⁴¹ Therefore, there is significant interest in developing new chiral organogelators that do not require large alkyl and steroidal groups to induce gelation behavior. Aligned with this need, we report a chiral barbiturate that functions as a single component LMOG in various organic solvents with low loading requirements for gelation (0.3 wt%), which classify it as a supergelator. Notably, this construct lacks the large alkyl chains or cholesteryl groups commonly employed to induce gelation, and instead utilizes a simple, planar chiral, aromatic backbone with a polar H-bonding head group to induce gelation thus providing a versatile platform for future expansion and application.

5.2. Results and Discussion

Because barbiturates are capable of forming large hydrogen bonding networks, we reasoned that incorporation of chiral groups could provide access to homochiral self-assembled networks. To provide contrasting molecular interactions to the hydrogen bonding barbiturate core, we chose to incorporate aromatic subunits to provide the potential for additional long-range order through π -stacking interactions. Combining these design principles, we reasoned that use of axially-chiral binaphthyl (BINAP) groups could be used to increase molecular complexity. To prepare the target barbiturate, we treated barbituric acid with the *bis*(methylbromide) of BINAP to prepare enantiopure BINABarb (Figure 5.2a).

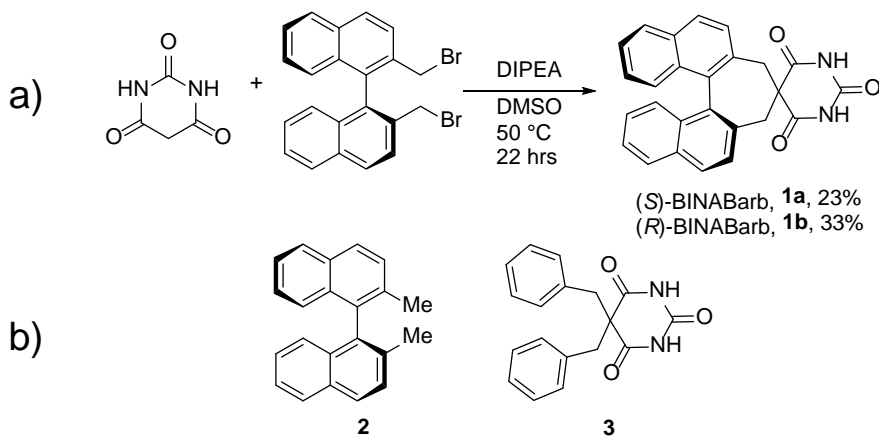


Figure 5.2. a) Synthesis of (*S*)/(*R*)-BINABarb from barbituric acid with (*S*)-stereochemistry shown. b) Structures of control compounds that are not organogelators.

Upon preparation of **1**, we observed that dilute CH₂Cl₂ solutions formed gels, whereas similar solutions of benzyl barbiturate (**3**) failed to gelate. Building from these initial observations, we sought to determine the gelation ability of **1** towards other

organic solvents and compare this to structural analogues of **1** (Figure 5.2b). The results from the screening show that **1** forms organogels in different chlorinated solvents (Table 5.1, Entries 1-4) and substituted aromatic solvents (Table 5.1, entries 8-11). Solvents such as tetrachloroethane, CCl₄, and benzene showed no gelation behavior suggesting a fine balance between solubility, crystallization, and gelation. The apparent trend that requires at least one substituent on the aromatic ring for gelation is unusual and is currently under further investigation in our laboratory. Solvents containing either hydrogen bond accepting or donating groups eroded the gelation behavior, which is consistent with the requirement of a barbiturate hydrogen bonding network for successful gelation. In addition, we probed the potential gelation behavior of structurally-similar compounds **2**, which contains the BINAP moiety but lacks the barbiturate, and in **3**, which contains the barbiturate but lacks the BINAP moiety, and failed to observe gelation behavior of either of these compounds in any of the solvents investigated.

To investigate the self-assembly of BINABarb on the molecular level we performed diffusion-ordered NMR spectroscopy (DOSY) on compounds **1-3** in CDCl₃. We hypothesized that if significant self-assembly was occurring, then a significant change in the diffusion coefficient could be measured. Using this technique also provided another opportunity to elucidate some of the structural requirements for gelation by comparing the diffusion coefficients of **1** to structural analogues **2** and **3**. The effects of gelator concentration on diffusion coefficient for **1a** and control compounds **2** and **3** are shown in Figure 5.3. The sharp break in the measured diffusion coefficient of **1a** is indicative of significant self-assembly and the formation of higher order nanostructures.^{42, 43} The minimum gelation concentration was observed to be 10 mM or

0.3 wt%, which classifies **1a** as a supergelator.⁴⁴ Increasing the concentration beyond the minimum gelation concentration (15-25 mM) showed no significant change in diffusion coefficient. Gelation was also confirmed for all samples > 10 mM by a simple inversion test. The critical gelation temperature (T_{gel}) for **1a** was also measured using VT-DOSY and found to be ~50 °C. In addition, VT-DOSY confirmed the thermal reversibility of the self-assembly (Figure D.10). In contrast, neither **2** nor **3** show any significant change in diffusion coefficient within a similar concentration regime. These results support the necessity of both a polar head and an aromatic tail for self-assembly to occur.

Additionally, the biphenyl derivative of BINABarb shows no gelation properties and could not be further studied due to poor solubility in the required concentration regime. Therefore, we attribute the unique gelation behavior observed by **1a** and **1b** over other barbiturates to the inherent chirality of the binaphthyl backbone, which allows for extension of the individual molecular units into an extended nanostructure. Attempts to measure racemic mixtures of the barbiturate at concentrations above 10 mM resulted in precipitation rather than gel formation, further suggesting that the chiral backbone is critical to gelation.

In an effort to understand key interactions at the molecular level that could be responsible for the gel formation of **1**, we turned to x-ray crystallography. Attempts to grow single crystals from dilute solutions of chloroform or other solvents that induced gelation were unsuccessful, highlighting the propensity of these systems to gelate rather than crystallize. We were, however, able to grow crystals of **1b** from THF/pentane vapor diffusion. Although these were not the gelation conditions, we surmised that analysis of

the crystallographic details could provide additional information on the types of intramolecular interactions present in these systems.

Table 5.1. Gelation properties of compounds 1-3 at r.t. G = gel, S = soluble, ppt = precipitate formed, SS = slightly soluble, I = insoluble.

entry	solvent	1a	2	3
1	chloroform	G	S	S
2	chlorobenzene	G	S	ppt
3	dichloromethane	G	S	SS
4	dichloroethane	G	S	S
5	tetrachloromethane	I	S	ppt
6	tetrachloroethane	S	S	S
7	benzene	I	S	ppt
8	toluene	G	S	ppt
9	o-xylene	G	S	ppt
10	m-xylene	G	S	ppt
11	p-xylene	G	S	ppt
12	nitrobenzene	S	S	S
13	pyridine	S	S	S
14	tetrahydrofuran	S	S	S
15	ethyl acetate	S	S	S
16	acetone	S	S	S
17	acetonitrile	S	S	S
18	ethanol	ppt	S	S
19	methanol	ppt	S	S
20	water	I	I	ppt

Analysis of the crystal structure shows clear dimerization between the two pyrimidine heads with the other hydrogen bonds satisfied by a THF co-solvent (Figure D.11). Expansion of the asymmetric unit shows long range order, driven by hydrogen bonding and π -stacking, that could result in the fiber formation that could occur upon gelation (Figure 5.4). From these representations, correlations to the helicity of the fibers observed in the VP-SEM can be made. The barbiturate polar head groups are held together by H-bonding interactions between a neighboring barbiturate and the THF co-

solvent, while there is a short, T-shaped contact (3.451 Å) between the aromatic π -faces of the binaphthyl backbone in neighboring columns. This arrangement leads to the formation of two intertwining chains that could explain the helicity of the fibers formed in solution. It can also then be rationalized why polar solvents inhibit gel formation. Erosion of the hydrogen bonding motif by strong H-bond donors and acceptors interrupts dimerization of the barbiturate and thus prevents the growth of one-dimensional fibers.

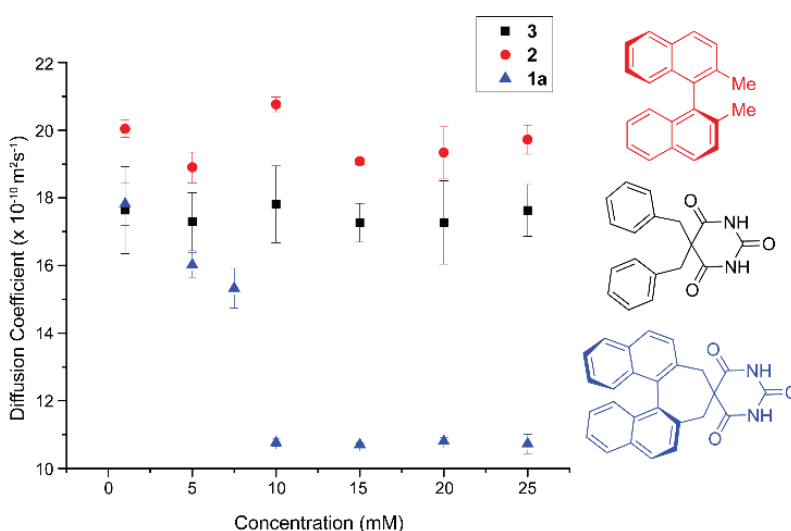


Figure 5.3. Plot of diffusion coefficient vs barbiturate concentration in CDCl_3 at 25 °C. Values reported are an average of at least 3 independent trials ($\pm \sigma$).

To further investigate the supramolecular ordering at the microscale level, we used a variable pressure scanning electron microscopy (VP-SEM) to visualize the type of microstructures (tapes, ribbons, sheets, fibers, coils, etc.) that were formed. Figure 5.5 shows the difference between the microcrystalline material before dissolution in CHCl_3 and the supramolecular fibers formed from either (*S*)-BINABarb or (*R*)-BINABarb. These fibers showed a diverse size range from 3-15 μm in diameter with various levels of entanglement. Notably, the images clearly show microstructures with helical twists,

demonstrating that the axial molecular chirality of the individual subunits is translated into microstructures.

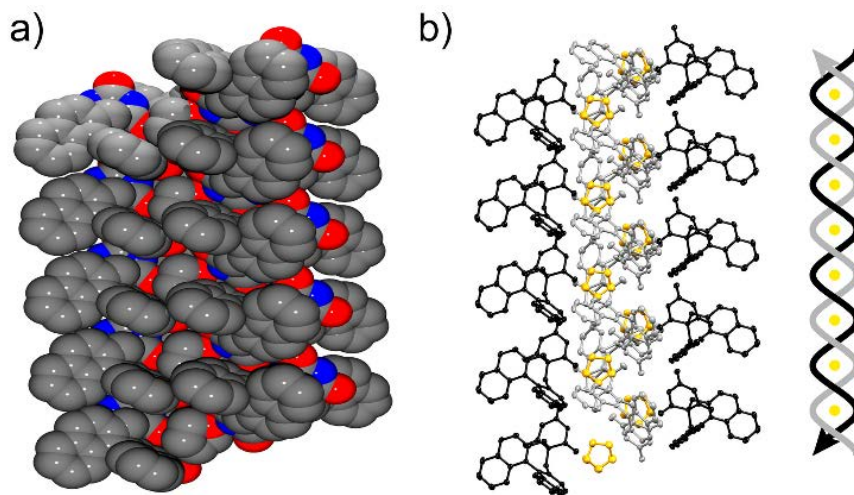


Figure 5.4. a) Space-filling representation of tetrameric columnar stack from single crystal x-ray diffraction data with H-bonds omitted for clarity b) ORTEP of tetrameric columnar stack with molecules colored by symmetry equivalence showing the helical nature of the column. Thermal ellipsoids shown at 50% probability with hydrogen atoms omitted for clarity.

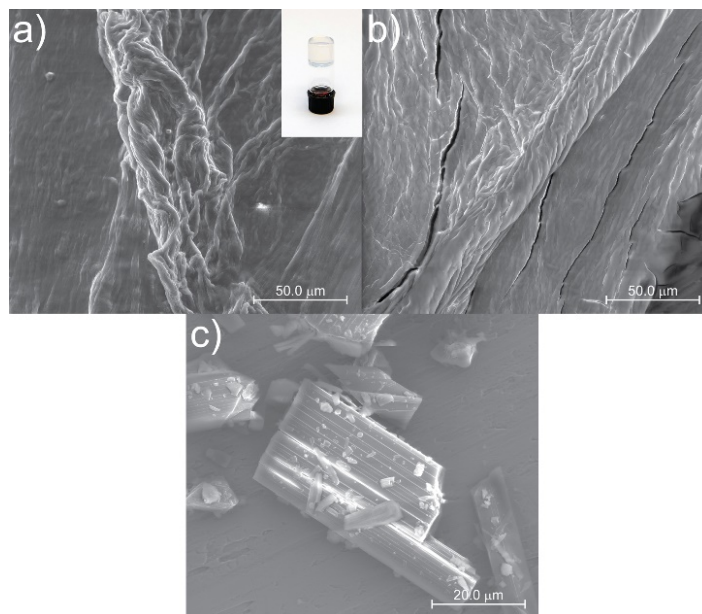


Figure 5.5. VP-SEM images of a) **1a** (*S*)-BINABarb CHCl_3 gel with inset of an inverted vial containing the gel, b) **1b** (*R*)-BINABarb CHCl_3 gel, c) crystalline solid of **1b**.

5.3. Conclusions

In conclusion, we report the first chiral barbiturate to act as a single-component LMOG. This new LMOG can be classified as a super gelator and is capable of gelating a variety of chlorinated and aromatic solvents. The structural requirements for gelation when compared to other non-gelating analogs appear to be both a polar H-bonding head group and chiral aromatic backbone. VP-SEM and XRD experiments show the self-assembly of **1** results in the production of fiber type microstructures likely promoted by the dimerization of individual barbiturate units. Potential applications of this new LMOG include use as chiral dopants for liquid crystals and use as chiral shift/transfer reagents. These, as well as other potential applications, are currently being investigated by our laboratory.

5.4. Bridge

After investigating the structure and properties of new, chiral barbiturate based organogels, we moved our attention back to the developing the supramolecular design principles for acyclic Hamilton receptors. Specifically, Chapter VI focuses on the development of new fluorescent Hamilton receptors whose photophysical properties can be modulated by varying the electronic properties of the appended arylethynyl fluorophores.

CHAPTER VI

SUBSTITUENT EFFECTS OF FLUORESCENT ARYLETHYNYL HAMILTON RECEPTORS FOR BARBITURATE SENSING

This chapter contains co-authored unpublished work that was written by me. All of the experiments were performed by me and the results were also interpreted by me. Pluth, M. provided editorial assistance.

6.1. Introduction

Hydrogen bonding is a ubiquitous theme in the fields of self-assembly and molecular recognition. Owing to the high directionality of H-bonds, host–guest systems incorporating these types of non-covalent interactions often exhibit significant cooperativity leading to strong association constants. Of the numerous host–guest architectures that incorporate hydrogen bonding as the primary recognition motif,¹ one of the most ubiquitous scaffolds is that based on the synthetic barbiturate receptor developed by Hamilton (Figure 6.1).²

This highly-utilized class of macrocyclic 2,6-diamidopyridine receptors is characterized by the two symmetric donor-acceptor-donor H-bonding schemes of the host that align with the two, symmetric acceptor-donor-acceptor H-bonding scheme of barbiturates. These types of systems exhibit large associations constants (K_a) for

barbituric acid derivatives ranging from 10^5 - 10^6 M^{-1} in aprotic solvents such as $CHCl_3$ and CH_2Cl_2 .^{2,3} Although the preorganization imposed by the macrocyclizing component is required for the largest binding affinities, non-macrocyclic forms of the receptor also display relatively large binding affinities ($\sim 10^4$ M^{-1}).³ Our group has previously investigated the impacts of steric⁴ and electronic⁵ effects on non-macrocyclic Hamilton receptors. Similarly, other groups have also utilized different acyclic derivatives for a variety of applications including the construction of supramolecular dendrimers^{6,7} and polymeric materials,⁸⁻¹⁰ applications as optoelectronic materials,¹¹⁻¹⁴ and sensing.¹⁵⁻¹⁷

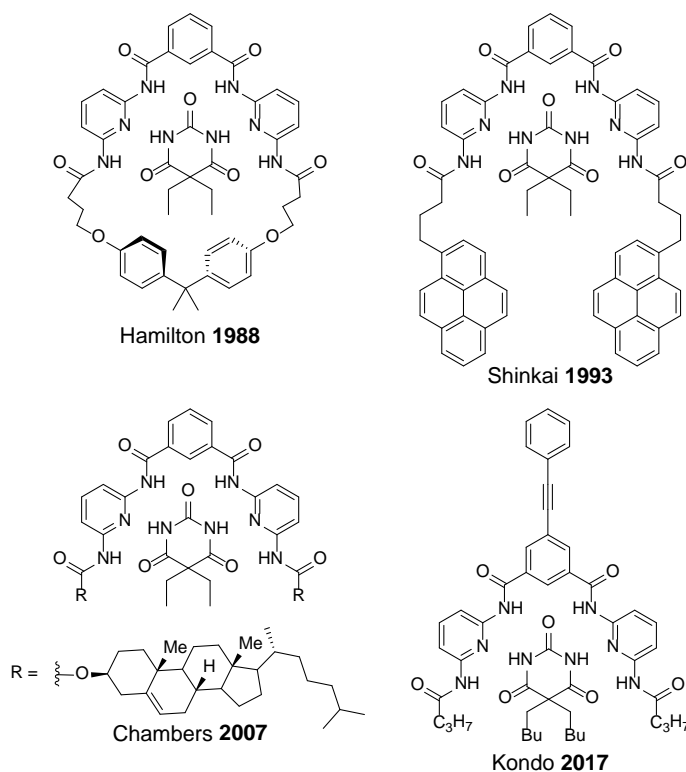


Figure 6.1. Structures of original and selected modified Hamilton receptors.

Although many of these receptors exhibit high selectivity and affinity for barbiturate guests, relatively few of these systems have desirable photophysical

properties for sensing applications (e.g. low energy absorbances, strong emission profiles, etc). Therefore, derivatized Hamilton receptors are needed that contain fluorogenic and other chromophoric groups. Towards these aims, prior work by Izuo *et al.* demonstrated that appending pyrene moieties to an acyclic Hamilton receptor results in a strong fluorescence turn-on that can be monitored by fluorescence spectroscopy.¹⁸ The efficacy of this system is largely due to solvent effects that cause disaggregation of the host molecule in the presence of barbiturates. Chambers *et al.* have shown that cholesteryl modified Hamilton receptors can be incorporated into liquid crystal display technologies that respond with relatively large changes in maximum reflectance wavelengths in the presence of barbital.¹⁹ Other approaches for barbiturate detection include electrochemical methods²⁰ and Fe spin-crossover complexes that in the presence of barbiturates produce a visible colorimetric response that is selective for barbiturates over structural analogues.²¹

More recently, the Kondo group demonstrated that appendage of a phenylethynyl group on the 4-position of the isophthalimide backbone results in a turn-on fluorescent probe for barbiturates.²² While simultaneously working on a similar design strategy, we hypothesized that appending arylethynyl groups to the 4-position of the diamidopyridine backbone would have two positive effects over the isophthalyl linkage. First, the turn-on response could be easily tuned through the identity of the R-group due to the inherent “push-pull” nature of the fluorophore and greater differences in the ground and excited electronic state between the bound and unbound receptor. Secondly, the binding affinities of the receptor could be tuned through the incorporation of electron-donating groups or electron-withdrawing groups in the 4-position of the arylethynyl moiety thereby changing the basicity of the pyridyl nitrogen lone pair. Herein, we report the synthesis,

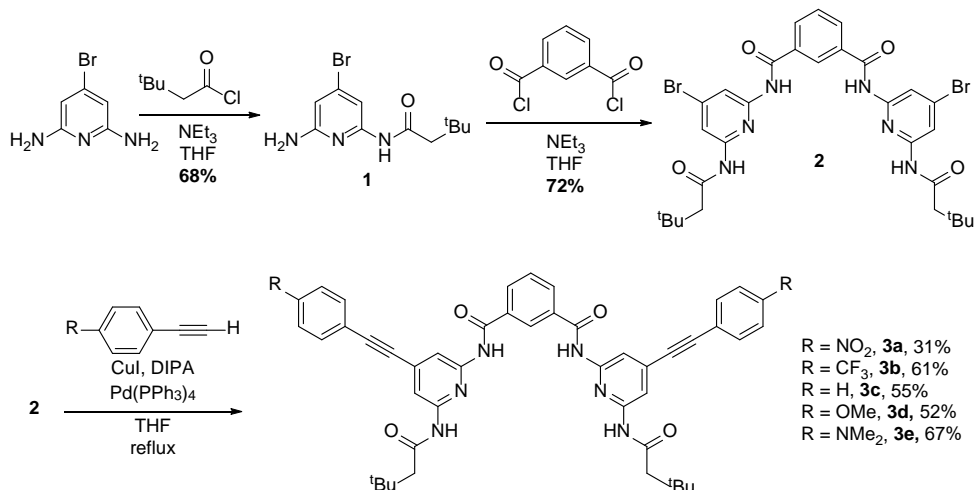
optoelectronic properties, and binding affinities of a suite of arylethynyl Hamilton receptors that function as fluorescent barbiturate sensors and provide insights into the design principles required for efficient fluorogenic properties in Hamilton-based receptors.

6.2. Results and Discussion

The synthesis of the new arylethynyl-containing Hamilton receptors is relatively straightforward. We envisioned that a variety of aryl-ethynyl groups could be appended using typical Sonogashira cross-coupling conditions using the corresponding 4-bromopyridyl precursor (**2**). Using methods similar to those reported previously,^{4, 23} we were able to prepare the brominated analogue of a typical acyclic Hamilton receptor, **2**. This precursor was then subjected to standard Sonogashira cross-coupling conditions to yield the final products in moderate yields from commercially available materials (Scheme 6.1). Purification of these molecules could be obtained through column chromatography or in some cases recycling GPC to remove any unreacted starting material or mono-substituted products. Using this methodology, we prepared a variety of 4-substituted arylethynyl Hamilton receptors that included strongly electron-donating and strongly electron-withdrawing groups, **3a–e**.

With these new receptors in hand, we first examined their optical properties (Table 6.1). The absorption maxima of **3a–e** range from 321–368 nm with receptor **3e** showing the most red-shifted absorption. As we hypothesized, the emission spectra exhibit notable differences upon substitution of the arylethynyl moiety (Figure 6.3a). Receptors **3a–d** exhibited very weak emission profiles in the absence of guest. In

contrast, **3e** shows a strong emission maximum at 451 nm in the absence of guest. This change in emission behavior is likely due to the charge transfer between the strongly electron donating dimethyl amino group and electron poor pyridine ring, which has been observed in other push-pull pyridine-containing systems.^{24, 25}



Scheme 6.1. Synthesis of substituted arylethynyl Hamilton receptors.

Table 6.1. Photophysical Properties of Hosts **3a-3e** in the presence and absence of barbital guest. λ_{\max} measured with $[H] = 5 \mu\text{M}$ in H_2O sat. CHCl_3 . ϵ were measured in H_2O sat. CHCl_3 . λ_{em} in the presence of barbital measured with $[H] = 1 \mu\text{M}$ in H_2O sat. CHCl_3 and 200 equivalents of barbital.

Host	λ_{\max} (nm)	<i>without barbital</i>	
		ϵ ($\times 10^4 \text{ M}^{-1} \text{ cm}^{-1}$)	λ_{em} (nm)
3a	321	7.68 ± 0.03	-
3b	303	7.36 ± 0.02	-
3c	306	9.04 ± 0.05	-
3d	324	8.27 ± 0.06	-
3e	368	7.6 ± 0.1	451
<i>with barbital</i>			
3a	321	n/a	-
3b	305	n/a	380
3c	306	n/a	372
3d	327	n/a	449
3e	374	n/a	454

Further supporting the charge-transfer behavior, we also observed that receptors **3a-d** displayed solvatochromic properties common to other charge transfer systems in both the absorbance (Figure E.2) and fluorescence spectra (Figure 6.2) In addition to the absorbance and emission bathochromic shifts, the fluorescence intensity decreases as the solvent polarity increases (Figure E.3). This behavior has been exhibited in other fluorogenic charge transfer systems and is caused by the increase in non-radiative pathways available in the excited state that is stabilized by the polar solvent molecules.²⁶

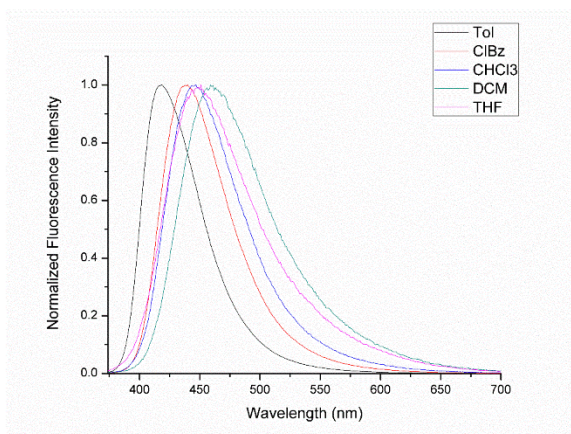


Figure 6.2. Emission spectra of **3e** in different solvents ($[3e] = 5 \mu\text{M}$, $\lambda_{\text{ex}} = \text{absorbance } \lambda_{\text{max}}$ for the given solvent).

With the photophysical properties of new hosts **3a-e** measured, we sought to probe the changes of these photophysical properties to the addition of guest molecules. Previously reported systems based on unsubstituted-arylethynyl systems show a turn-on fluorescent response to the addition of barbiturate guests, in addition to small changes in the absorption spectra.²² We observed similar spectral changes for our substituted-arylethynyl hosts upon the addition of barbital (Figure 6.3b). The absorption spectra show small red shifts ranging from 3-6 nm upon the addition of barbital (Figure E.4), while the changes in the emission spectra are much more dynamic. Unsurprisingly the fluorescence

of **3a** remains quenched due to the presence of the nitro group. However, other electron withdrawing substituents such as the CF_3 moiety of **3b** show a moderate fluorescent turn-on (6.7 fold) at 380 nm upon the addition of barbital. Similar behavior is exhibit for the H-substituted receptor, **3c** (4.9 fold turn-on). Upon increasing to more electron donating substituents, a dramatic red-shifting in the emission profile occurs with receptor **3d** exhibiting an λ_{em} at 449 nm in addition to a much stronger fluorescence turn-on (17 fold). In contrast, the even more electron rich NMe_2 substituted receptor **3e** shows a turn-off response to the addition of barbital.

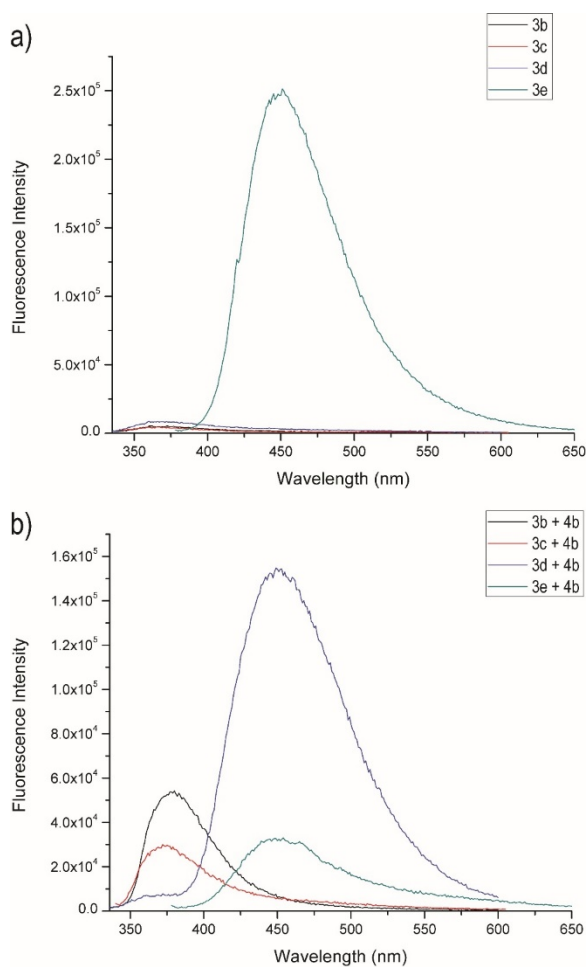


Figure 6.3. a) Emission spectra of hosts 3b–e (1 μM) in H_2O sat. CHCl_3 . b) Emission spectra of hosts 3b–e (1 μM) in the presence of 200 equivalents 4b in H_2O sat. CHCl_3 .

To explain the quenching effect observed for **3e** in the presence of barbital, we reasoned that protonation of the dimethylamino group by the barbiturate N-H could be responsible. Using ^1H NMR spectroscopy, we performed a titration experiment with barbital and **3e** in H_2O sat. CDCl_3 . However, upon increasing the equivalence of guest, there was no observable change in the dimethylamino resonance indicating that protonation of the group was not occurring. Instead, typical down-field shifts are observed for the two amide N-H groups (Figure 6.4).

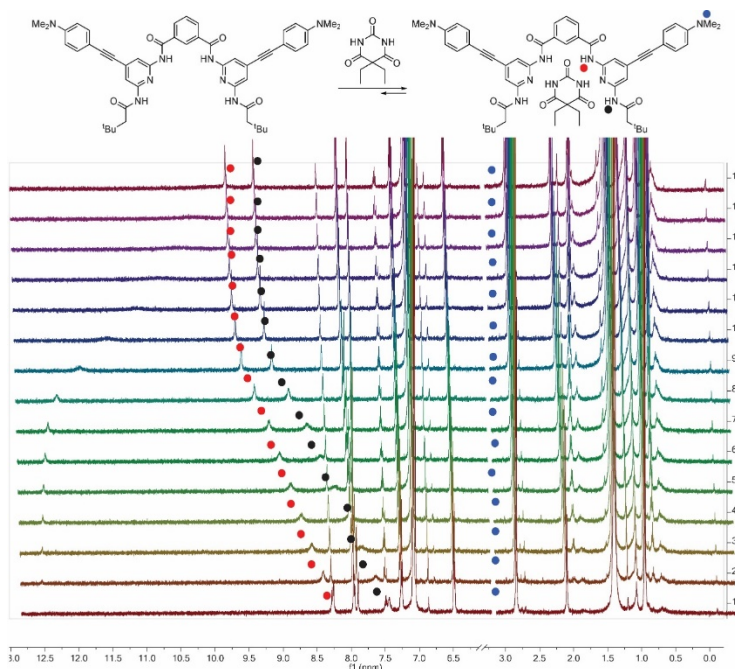


Figure 6.4. ^1H NMR (500 MHz) titration of **3e** with barbital (**4b**) in H_2O sat. CDCl_3 at 25 $^\circ\text{C}$.

To further probe the differences between the emission profiles of our receptors we hypothesized that protonation of the pyridyl nitrogen could be responsible for the emission feature at 445 nm. Therefore, the emission profiles of electron poor receptors, such as **3b**, could be caused by weak proton transfer between the barbiturate N-H and the

pyridine. To determine the effect of protonation at the pyridyl nitrogen we preformed a fluorescence titration between receptor **3b** and dibenzylbarbital (**4d**), followed by acetic acid. Upon addition of barbital we observe a fluorescence turn-on at 380 nm.

Interestingly, the subsequent addition of acetic acid to the same solution containing **3b** and **4d**, yields a ratiometric response with an increasing emission band at 453 nm and a decrease in the band at 380 nm. (Figure 6.5). An isobestic point is observed at 425 nm confirming a direct conversion of the H:G complex to the protonated host complex.

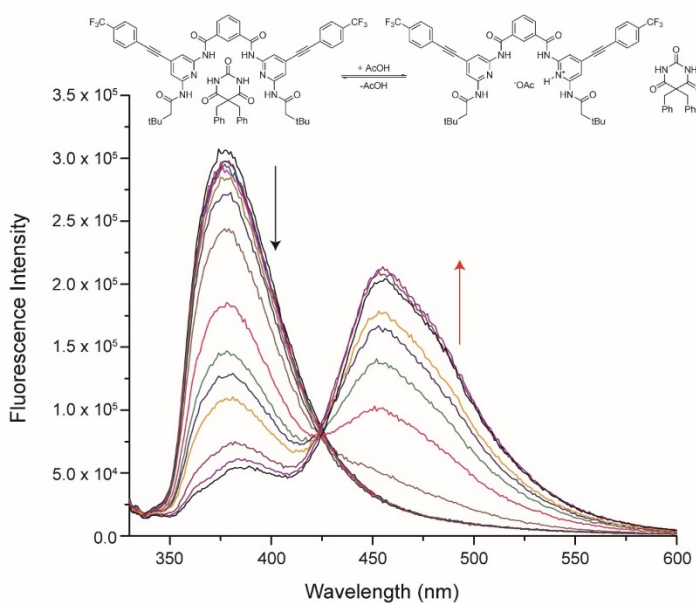


Figure 6.5. Emission spectra of **3b** in the presence of **4d** showing a ratiometric response to the addition of AcOH.

After determining the photophysical properties of our new receptor library, we wanted to determine the effect of R group on the binding of barbital. Fluorescence titrations were performed and the total integrated fluorescence data were fit to a 1:1 binding model. The results are summarized in Table 6.2. The measured binding constants are similar to those reported previously for similar systems.²² As we hypothesized, the

binding affinities could be tuned through substitution of the R group on the arylolethynyl moiety. EDGs effectively increase the basicity of the nitrogen lone pair, making the system a better H-bond acceptor, while EWGs decrease the pyridyl lone pair basicity leading to a lower binding affinity.

We next constructed a Hammett plot from the titration data to determine whether this system exhibits a linear free energy relationship. The data show a moderately correlated linear trend (Figure E.5). The negative slope ($\rho = -0.10$) is indicative of an increase in positive charge upon barbiturate binding, corroborating the partial proton transfer between the barbiturate N-H and pyridyl nitrogen. The magnitude of the slope indicates that the R groups have a weak influence on the binding affinity of the guests and is likely due to the relatively large distance between the R group and the pyridyl nitrogen.

Table 6.2. Binding affinities of hosts **3b-e** with barbital at 25 °C in H₂O sat. CHCl₃. The error shown is $\pm \sigma$.

Host	K_a ($\times 10^4 \text{ M}^{-1}$)
3b	3.04 ± 0.04
3c	3.3 ± 0.2
3d	3.80 ± 0.06
3e	4.0 ± 0.03

In addition, we also investigated whether barbiturate substitution impacted binding to the receptor motifs. We chose receptor **3b** as the model host and measured the change in fluorescence upon titration with guests **4a-d** (Figure 6.6). Although the size of these barbiturates changed significantly, there were not large changes or correlations between the size of the barbiturate and binding affinity. We did observe, however, that guest **4a** exhibited a 2-fold stronger binding compared to other guests, which we attribute

to the locked confirmation of the 5,5' groups on the barbiturate which help preorganize the guest to have minimal negative steric interactions with the distal neopental groups of the host.

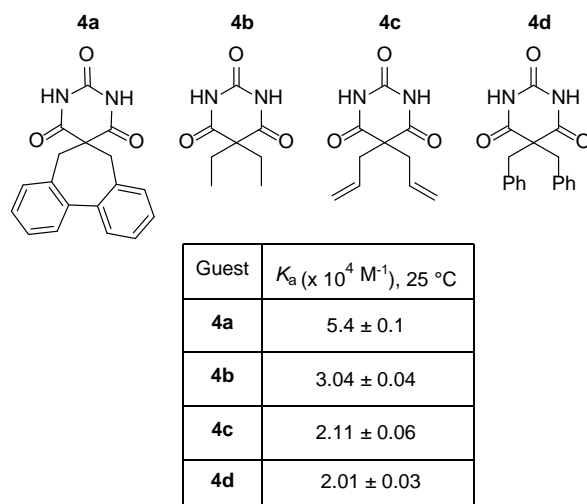


Figure 6.6. Binding affinities of guests **4a–e** and receptor **3b** at 25 °C in H₂O sat. CHCl₃. Binding isotherms fit to a 1:1 binding model. The error shown is ± σ .

6.3. Conclusion

In summary we have prepared small library of substituted arylethynyl Hamilton receptors via simple Sonogashira couplings in moderate yields. These new receptors exhibit tunable photophysical properties dependent on the identity of arylethynyl substituents. Electron withdrawing substituents show a moderate fluorescent turn-on in the presences of barbiturate guests with λ_{em} between 372-380 nm. Electron donating substituents exhibit bimodal behavior. In the case of the OMe substituted host, (**3d**) a stronger, red shifted fluorescence turn-on at 449 nm is observed. In contrast the most electron donating NMe₂ host (**3e**) shows a turn-off fluorescence response in the presence of guest. Additionally, the fluorescence of this compound exhibits mild solvatochromic

behavior. The binding affinity of these new receptors towards barbiturates can be modulate by the electron donating/withdrawing nature of the arylethynyl substituents and exhibits a moderately correlated linear free energy relationship. Overall, these findings demonstrate the fine control of photophysical and binding properties that can be achieved through careful tailoring of the electronics of appended fluorophores to acyclic Hamilton receptors. Specifically, the electron density at the pyridyl nitrogen plays an important role in both the optical properties as well as guest binding.

6.4. Concluding Remarks

In this dissertation, I have described work aimed at expanding the utility of the Hamilton receptor and barbiturates for a variety of applications. While the initial goal was to develop a new supramolecular bidentate ligand scaffold for catalytic applications, we were able to investigate alternative applications for new barbiturates and receptors that were synthesized along the way. Additionally, our continual interested in the transfer of chirality in supramolecular systems, while not discussed in this dissertation, led use to pursue a variety of chromophoric and fluorogenic derivatives of acyclic Hamilton receptors. These receptors further developed our understanding of the design principles that govern barbiturate binding to these receptors. Future work on these projects should focus on understanding the physical organic chemistry behind the assembly of the chiral barbiturate gels, specifically the differences in gelation and rheological properties between different solvents. Moreover, the new fluorescent probes developed for barbiturate sensing will also provide a unique opportunity to study chirality transfer using circularly polarized luminescence spectroscopy, among other sensing applications.

APPENDIX A

SUPPORTING INFORMATION FOR CHAPTER II

Appendix A is the supporting information for Chapter II of this dissertation. It includes the experimental details and additional spectra relevant to the content of Chapter II.

Experimental Details

General. All commercially-available reagents were used as received. Anhydrous, deoxygenated solvents were collected from a Pure Process Technologies solvent purification system. Triethylamine was dried and distilled over CaH₂ under nitrogen. Reactions were monitored using Merck F₂₅₄ silica gel 60 TLC plates and visualized using UV light or a KMnO₄ stain. Reactions conducted under an inert atmosphere were performed by either using standard Schlenk techniques or a N₂-filled glove box. Chromatographic purification was performed using a Biotage automated flash chromatography purification system. ¹H and ¹³C{¹H} NMR spectra were recorded at the reported frequencies, and chemical shifts are reported in ppm (δ) and referenced to the residual solvent resonance. ³¹P{¹H} chemical shifts are referenced to H₃PO₄. The following naming conventions were used to describe NMR couplings: (s) singlet, (d) doublet, (t) triplet, (q) quartet, (dd) doublet of doublets, (m) multiplet, (b) broad.

General Procedure Binding Constant Determination. Binding studies were performed in CDCl₃ in duplicate or CD₃CN in triplicate for host molecules **4b-c** and were

monitored by ^1H NMR spectroscopy at 25 °C. In a typical H_2O sat. CDCl_3 titration, 10.00 mL of a 1.0 mM barbiturate guest solution was prepared. The guest solution was then divided such that 600 μL was placed into an NMR tube and 1.50 mL was used to create a second solution containing 16 mM host. An initial spectrum of the guest was recorded using the following parameters: $n_t=16$ and $d_1=1\text{s}$, after which aliquots (5-250 μL) of the host solution were added until the N-H resonance of barbiturate no longer shifted. The resultant curves were fit using a 1:1 model and the K_{assoc} obtained. In a typical CD_3CN titration, 3.0 mL of a 1.0 mM Pt host complex solution was prepared. The host solution was then divided such that 600 μL was placed into an NMR tube and the remaining 2.4 mL was used to create a second solution containing 30-60 mM synthetic barbiturate guest. An initial spectrum of the host was recorded using the following parameters: $n_t=16$ and $d_1=1\text{s}$, after which aliquots (5-250 μL) of the guest solution were added until the N-H resonance of the host no longer shifted. The resultant curves were fit using a 1:1 model and the K_{assoc} obtained.

General Procedure for Job Plot Analysis. Stoichiometric binding analysis was performed in H_2O -saturated CDCl_3 or 1% $\text{DMSO}-d_6:\text{CDCl}_3$ and was monitored by ^1H NMR spectroscopy at 25 °C. Total (host + guest) concentrations of 4.0 mM were used for all Job plots. For a typical Job plot, 2.0 mM stock solutions of guest **5a** and host **4b** were divided amongst 10 NMR tubes in 10 mol% increments to a total volume of 600 μL . A pure guest sample was also prepared. A d_1 of 2.0 s and $n_t=8$ were during NMR data collection. Both the shift in host proximal N-H peak and guest N-H peaks were recorded.

Syntheses

N-(6-Aminopyridin-2-yl)-3,3-dimethylbutanamide (**1**). An oven dried flask containing 2,6-diaminopyridine (10.0 g, 91.6 mmol) was charged with anhydrous THF (300 mL) and cooled to 0 °C. A separate solution of 3,3-dimethylbutyryl chloride (6.0 mL, 43 mmol) in anhydrous THF (50 mL) was then added dropwise over 2.5 hours via addition funnel. The reaction mixture was warmed to room temperature and allowed to stir overnight. The crude reaction mixture was then filtered, concentrated via rotary evaporation, and purified via column chromatography (SiO₂, 1:1 EtOAc:Hex, R_f = 0.33) to yield a white solid (6.13 g, 69%) ¹H NMR (500 MHz, CDCl₃) δ: 7.55 (d, *J* = 7.3 Hz, 2H), 7.44 (t, *J* = 7.9 Hz, 1H), 6.23 (d, *J* = 7.9 Hz, 1H), 4.28 (s, 2H), 2.19 (d, *J* = 2.0 Hz, 2H), 1.08 (s, 9H). ¹³C{¹H} NMR (126 MHz, CDCl₃) δ: 170.29, 157.16, 149.93, 140.24, 104.31, 103.37, 51.89, 31.43, 29.94.

N-(6-(3,3-Dimethylbutanamido)pyridin-2-yl)-2-iodobenzamide (**2a**). Excess thionyl chloride (3.0 mL, 41 mmol) was added to a scintillation vial containing 2-iodobenzoic acid (1.01 g, 4.05 mmol). Three drops of anhydrous DMF was added to the reaction mixture, and the reaction was heated to 65 °C, vented through a bubbler containing 1 M KOH, and stirred for 1.5 hours. The excess thionyl chloride was removed under vacuum. The resultant residue was dissolved in anhydrous THF (10 mL) and slowly added to a solution of **1** (0.763 g, 3.68 mmol) and anhydrous triethylamine (770 μL, 5.50 mmol) in THF (150 mL) at 0 °C. The resulting turbid mixture was warmed to room temperature and stirred overnight. The mixture was filtered, diluted with EtOAc, and washed with saturated NaHCO₃ (4 x 50 mL) and then with brine (2 x 50 mL). The organic layer was separated, dried over MgSO₄, filtered, and concentrated under reduced pressure. The crude product was purified via column chromatography (SiO₂, 1:3

EtOAc:Hex, $R_f = 0.18$) to yield a white solid (0.987 g, 62%). ^1H NMR (500 MHz, CDCl_3) δ : 8.21 (s, 1H), 8.01 (d, $J = 8.0$ Hz, 1H), 7.97 (d, $J = 8.1$ Hz, 1H), 7.84 – 7.80 (m, 2H), 7.73 (t, $J = 8.1$ Hz, 1H), 7.60 – 7.57 (m, 3H), 2.23 (s, 2H), 1.10 (s, 9H). ^{13}C NMR (126 MHz, CDCl_3) δ : 170.42, 167.26, 149.76, 149.19, 141.53, 141.02, 140.33, 131.88, 128.45, 110.19, 109.81, 92.34, 51.76, 31.46, 29.90.

N-(6-(3,3-Dimethylbutanamido)pyridin-2-yl)-3-iodobenzamide (**2b**). Excess thionyl chloride (3.0 mL, 41 mmol) was added to an oven-dried flask containing 3-iodobenzoic acid (0.503 g, 2.03 mmol). A drop of anhydrous DMF was added to the reaction mixture, and the mixture was heated to 65 °C, vented through a bubbler containing 1 M KOH, and stirred for 3 hours. The excess thionyl chloride was removed under vacuum. The resultant residue was dissolved in THF (10 mL) and slowly added to a solution of **1** (0.380 g, 1.83 mmol) and anhydrous triethylamine (380 μL , 2.72 mmol) in THF (50 mL) at 0 °C. The resulting turbid mixture was warmed to room temperature and stirred overnight. The mixture was filtered, concentrated under reduced pressure, and purified via column chromatography (SiO_2 , 1:2 EtOAc:Hex, $R_f = 0.46$) to yield a white solid (0.670 g, 84%). ^1H NMR (500 MHz, CDCl_3) δ : 8.22 (s, 1H), 8.15 (s, 1H), 8.03 (d, $J = 8.0$ Hz, 1H), 7.99 (d, $J = 8.0$ Hz, 1H), 7.90 (d, $J = 7.9$ Hz, 1H), 7.85 (d, $J = 7.8$ Hz, 1H), 7.76 (t, $J = 8.0$ Hz, 1H), 7.52 (s, 1H), 7.25 (t, $J = 8.5$ Hz, 1H), 2.25 (s, 2H), 1.12 (s, 9H). $^{13}\text{C}\{^1\text{H}\}$ NMR (126 MHz, CDCl_3) δ : 170.35, 163.90, 149.70, 149.37, 141.29, 141.14, 136.33, 136.25, 130.65, 126.44, 110.05, 109.74, 94.61, 52.00, 31.53, 29.96.

N-(6-(3,3-Dimethylbutanamido)pyridin-2-yl)-4-iodobenzamide (**2c**). Excess thionyl chloride (3.0 mL, 41.3 mmol) was added to scintillation vial containing 3-iodobenzoic acid (0.50 g, 2.0 mmol). A drop of anhydrous DMF was added to the

reaction mixture, and the mixture was heated to 65 °C, vented through a bubbler containing 1 M KOH, and stirred for 4 hours. The excess thionyl chloride was removed under vacuum. The resultant residue was dissolved in anhydrous THF (10 mL) and slowly added to solution of **1** (0.381 g, 1.84 mmol) and anhydrous triethylamine (380 μ L, 2.72 mmol) in THF (100 mL) at 0 °C. The resulting turbid mixture was warmed to room temperature and stirred overnight. The mixture was filtered, concentrated and purified via column chromatography (SiO₂, 1:3 EtOAc:Hex, R_f = 0.42) to yield a white solid (0.668 g, 83%). ¹H NMR (500 MHz, CDCl₃) δ : 8.21 (s, 1H), 8.01 (d, *J* = 8.0 Hz, 1H), 7.97 (d, *J* = 8.1 Hz, 1H), 7.84 – 7.80 (m, 2H), 7.73 (t, *J* = 8.1 Hz, 1H), 7.60 – 7.57 (m, 3H), 2.23 (s, 2H), 1.10 (s, 9H). ¹³C{¹H} NMR (126 MHz, CDCl₃) δ : 170.37, 164.74, 149.68, 149.41, 141.02, 138.20, 133.66, 128.74, 109.98, 109.73, 99.66, 51.85, 31.47, 29.92.

N-(6-(3,3-Dimethylbutanamido)pyridin-2-yl)-2-(diphenylphosphino)benzamide (**3a**). Reactants **2a** (0.152 g, 0.348 mmol), diphenylphosphine (0.081 g, 0.43 mmol), Pd(OAc)₂ (4.8 mg, 21 μ mol), triethylamine (70 μ L, 0.50 mmol, and CH₃CN (20 mL) were combined in a dry flask under N₂. The resulting dark red solution was heated to reflux and stirred overnight. The crude solution was loaded onto dry silica, in air, and purified via column chromatography (dry SiO₂, 1:3 EtOAc:Hex, R_f = 0.29) to yield an off white solid (0.095 g, 55%). ¹H NMR (500 MHz, CDCl₃) δ : 8.18 (bs, 1H), 7.91 (d, *J* = 8.1 Hz, 1H), 7.81 (d, *J* = 8.1 Hz, 1H), 7.72 (bm, 1H), 7.66 (t, *J* = 8.1 Hz, 1H), 7.43 (t, *J* = 7.4 Hz, 1H), 7.38 (t, *J* = 7.5 Hz, 1H), 7.31 (m, 9H), 7.05 (dd, *J* = 7.7, 4.1 Hz, 1H), 2.25 (s, 2H), 1.11 (s, 9H). ³¹P{¹H} NMR (202 MHz, CDCl₃) δ : -9.32. ¹³C{¹H} NMR (126 MHz, CDCl₃) δ : 166.95, 136.57, 136.49, 134.32, 134.09, 133.93, 130.89, 128.95, 128.86,

128.63, 128.57, 127.92, 127.89, 109.59, 109.51, 51.73, 31.38, 29.81.. HRMS (ESI-TOF) m/z : $[M + Na]^+$ Calcd for $C_{30}H_{30}N_3O_2PNa$, 518.1973; found 518.1972.

N-(6-(3,3-Dimethylbutanamido)pyridin-2-yl)-3-(diphenylphosphino)benzamide (**3b**). Reactants **2b** (0.750 g, 1.72 mmol), diphenylphosphine (0.382 g, 2.05 mmol), $Pd(OAc)_2$ (22.7 mg, 101 μ mol), triethylamine (340 μ L, 2.44 mmol), and CH_3CN (35 mL) were combined in a dry flask under N_2 . The resulting dark red solution was heated to reflux and stirred overnight. The crude solution was loaded onto dry silica, in air, and purified via column chromatography (dry SiO_2 , 1:3 EtOAc:Hex, $R_f = 0.41$) to yield a white solid (0.690 g, 81%). 1H NMR (500 MHz, $CDCl_3$) δ : 8.17 (s, 1H), 8.01 (d, $J = 8.0$ Hz, 1H), 7.96 (d, $J = 8.0$ Hz, 1H), 7.89 (d, $J = 8.1$ Hz, 1H), 7.85 (d, $J = 7.5$ Hz, 1H), 7.73 (t, $J = 8.1$ Hz, 1H), 7.54 (s, 1H), 7.45 (t, $J = 7.4$ Hz, 1H), 7.41 (t, $J = 6.8$ Hz, 1H), 7.39 – 7.28 (m, 10H), 2.24 (s, 2H), 1.11 (s, 9H). $^{13}C\{^1H\}$ NMR (126 MHz, $CDCl_3$) δ : 170.24, 165.14, 149.47 (d, $J = 12.9$ Hz), 140.87, 139.07 (d, $J = 13.9$ Hz), 137.06 (d, $J = 13.9$ Hz), 136.22 (d, $J = 10.5$ Hz), 134.44 (d, $J = 7.7$ Hz), 133.79 (d, $J = 19.8$ Hz), 132.23 (d, $J = 25.8$ Hz), 129.15, 129.11, 129.07, 128.75 (d, $J = 7.2$ Hz), 127.58, 109.65 (d, $J = 14.5$ Hz), 51.80, 31.37, 29.82. $^{31}P\{^1H\}$ NMR (202 MHz, $CDCl_3$) δ : -5.23. HRMS (ESI-TOF) m/z : $[M + Na]^+$ Calcd for $C_{30}H_{30}N_3O_2PNa$, 518.1973; found 518.1964.

N-(6-(3,3-Dimethylbutanamido)pyridin-2-yl)-4-(diphenylphosphino)benzamide (**3c**). Reactants **2c** (0.495 g, 1.13 mmol), diphenylphosphine (0.241 g, 1.30 mmol), $Pd(OAc)_2$ (15.7 mg, 69.9 μ mol), triethylamine (230 μ L, 1.65 mmol), and CH_3CN (30 mL) were combined in a dry flask under N_2 . The resulting dark red solution was heated to reflux and stirred overnight. The crude solution was loaded onto dry silica, in air, and purified via column chromatography (dry SiO_2 , 1:3 EtOAc:Hex, $R_f = 0.32$) to yield a

white solid (0.437 g, 78%). ^1H NMR (500 MHz, CDCl_3) δ : 8.20 (s, 1H), 8.05 (d, $J = 8.0$ Hz, 1H), 7.97 (d, $J = 8.0$ Hz, 1H), 7.84 – 7.80 (m, 2H), 7.77 (s, 1H), 7.42 – 7.29 (m, 12H), 2.25 (s, 2H), 1.11 (s, 9H). $^{13}\text{C}\{^1\text{H}\}$ NMR (126 MHz, CDCl_3) δ : 170.33, 165.20, 149.63 (d, $J = 6.8$ Hz), 143.63 (d, $J = 14.6$ Hz), 141.05, 136.20 (d, $J = 10.6$ Hz), 134.17, 134.01, 133.88, 133.73, 129.36, 128.87 (d, $J = 7.3$ Hz), 127.05 (d, $J = 6.4$ Hz), 109.79 (d, $J = 13.2$ Hz), 51.95, 31.50, 29.94. $^{31}\text{P}\{^1\text{H}\}$ NMR (202 MHz, CDCl_3) δ : -5.26. HRMS (ESI-TOF) m/z : $[\text{M} + \text{Na}]^+$ Calcd for $\text{C}_{30}\text{H}_{30}\text{N}_3\text{O}_2\text{PNa}$, 518.1973; found 518.1957.

5,7-dihydro-1'H-Spiro[dibenzo[a,c][7]annulene-6,5'-pyrimidine]-2',4',6'(3'H)-trione (**5a**). Barbituric acid (76.9 mg, 6.00 mmol), 2,2'-bis(bromomethyl)-1,1'-biphenyl (198 mg, 5.83 mmol), triethylamine (170 μL , 1.23 mmol), and DMF (3 mL) were added to a scintillation vial. The reaction mixture was stirred overnight at room temperature. The reaction mixture changed from a clear and colorless solution to cloudy and white and then finally to clear and yellow solution upon completion of the reaction with some precipitate present. The DMF was removed under vacuum with gentle heating. The resultant residue was purified using column chromatography (SiO_2 , 3:1 EtOAc:hexanes, $R_f = 0.58$) to afford an white solid (123 mg, 69%). ^1H NMR (500 MHz, $\text{DMSO}-d_6$) δ : 11.12 (s, 2H), 7.42 – 7.35 (m, 4H), 7.29 (ddd, $J = 7.5, 5.6, 3.1$ Hz, 2H), 7.21 (d, $J = 7.4$ Hz, 2H), 2.93 (bd, $J = 5.5$ Hz, 4H). $^{13}\text{C}\{^1\text{H}\}$ NMR (126 MHz, $\text{DMSO}-d_6$) δ : 172.24, 150.38, 139.60, 134.95, 131.09, 127.87, 127.55, 127.25, 61.71.

General Procedure for the synthesis of cis-PtL₂Cl₂ complexes. In an inert atmosphere, a solution of **3b** (66.2 mg, 134 μmol) in CH_2Cl_2 (2 mL) was added dropwise to a stirring solution of $\text{Pt}(\text{COD})\text{Cl}_2$ (25.3 mg, 67.6 μmol) in CH_2Cl_2 (1 mL). The reaction was stirred at room temperature for one hour, after which the solvent was removed under

vacuum. The resulting solids were triturated three times with hexanes, in air, and filtered to obtain **4b** as an off white solid (63 mg, 75%). ^1H NMR (500 MHz, CDCl_3) δ : 8.39 (s, 2H), 8.03 (d, $J = 11.0$ Hz, 2H), 7.99 (d, $J = 8.1$ Hz, 2H), 7.95 (d, $J = 8.0$ Hz, 2H), 7.89 (s, 2H), 7.79 (d, $J = 7.8$ Hz, 2H), 7.73 (t, $J = 8.1$ Hz, 2H), 7.60 – 7.46 (m, 8H), 7.43 – 7.31 (m, 6H), 7.30 – 7.23 (m, 2H), 7.21 (td, $J = 7.9, 2.1$ Hz, 8H), 2.26 (s, 4H), 1.10 (s, 18H). $^{31}\text{P}\{^1\text{H}\}$ NMR (202 MHz, CDCl_3) δ : 14.55.

Compound **4c**. (white solid, 85 mg, 85%) ^1H NMR (500 MHz, CDCl_3) δ 8.40 (s, 2H), 7.99 (t, $J = 7.5$ Hz, 4H), 7.75 (t, $J = 8.1$ Hz, 3H), 7.62 (d, $J = 8.1$ Hz, 5H), 7.55 (dd, $J = 11.4, 7.7$ Hz, 8H), 7.48 – 7.35 (m, 8H), 7.25 – 7.18 (m, 8H), 2.23 (s, 4H), 1.09 (s, 18H). $^{31}\text{P}\{^1\text{H}\}$ NMR (202 MHz, CDCl_3) δ : 14.32

Additional Crystal Structure Figures and NMR Figures

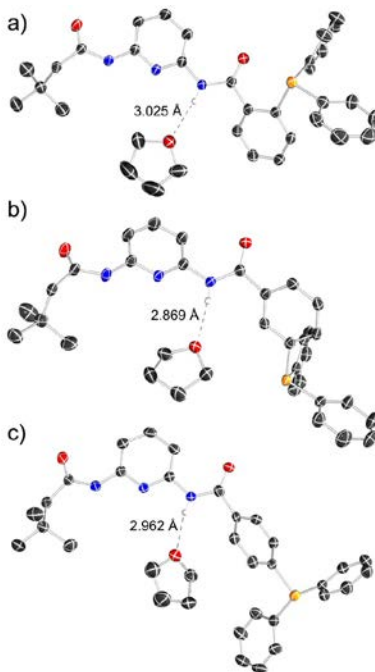


Figure A.1. ORTEP representation of a) *o*- isomer, **3a**, b) *m*-isomer, **3b**, c) *p*-isomer, **3c**, co-crystallized with a molecule of THF. Thermal ellipsoids drawn at 50% probability with non-hydrogen bonding hydrogens omitted for clarity.

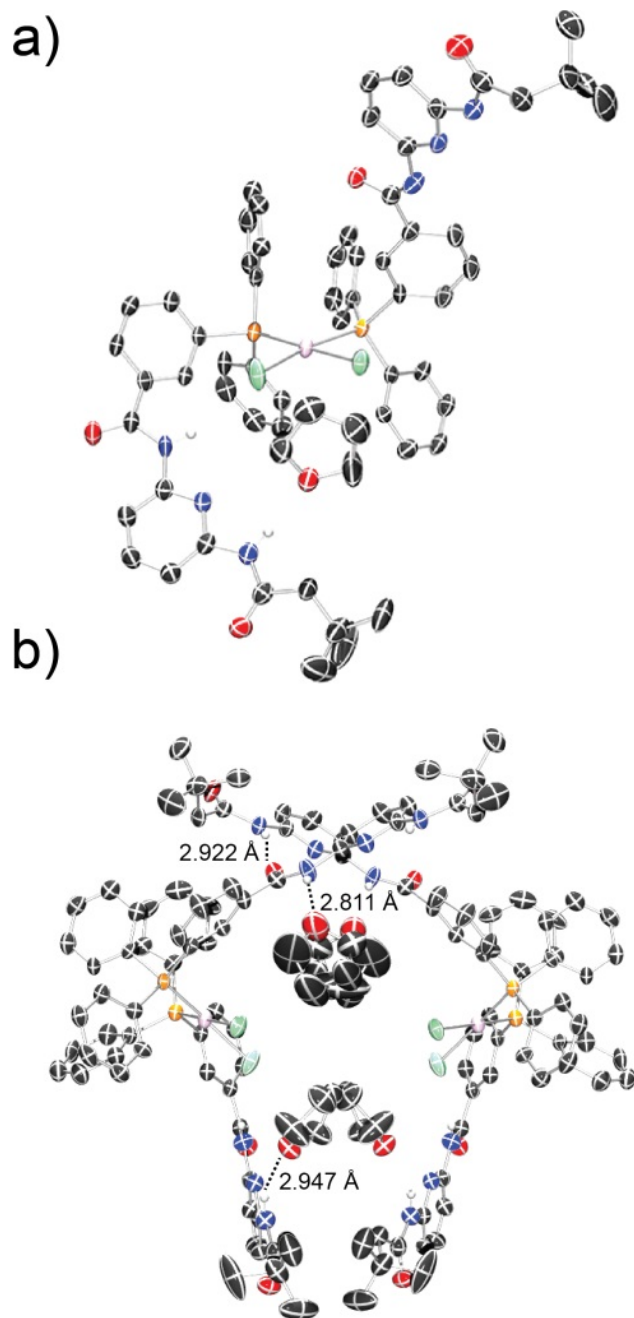


Figure A.2. ORTEP representations of **4b** with thermal ellipsoids drawn at 50% probability. a) Structure viewed face-on with one molecule of THF shown and non-hydrogen bonding hydrogens omitted for clarity. b) Dimeric form of structure showing intra- and inter-molecular hydrogen bonds with non-hydrogen bonding hydrogens omitted for clarity.

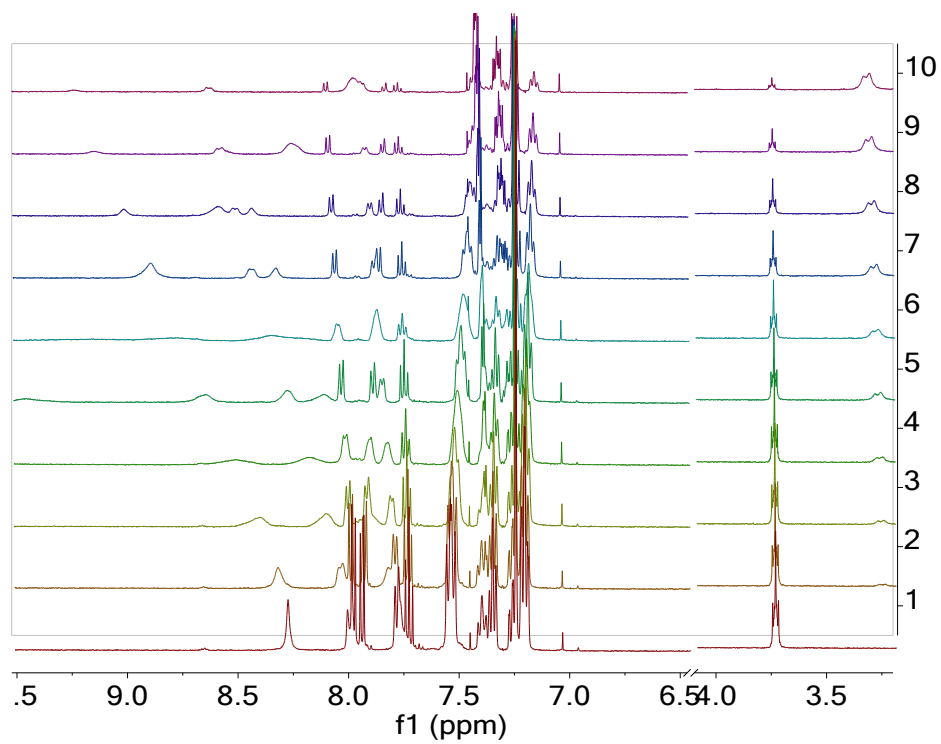


Figure A.3. ^1H NMR data for Job Plot of **4b** and **5a** in CDCl_3 .

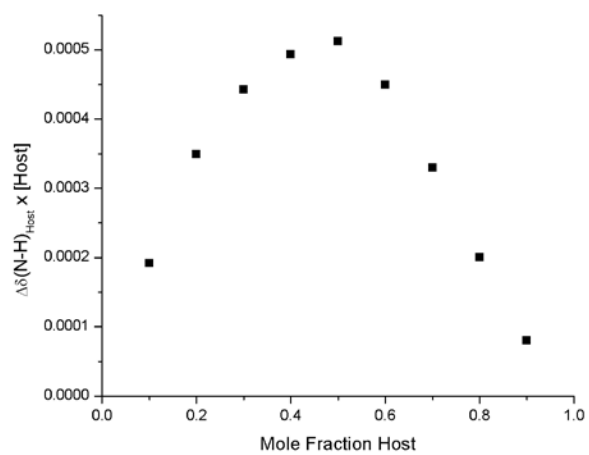


Figure A.4. Job Plot of **4b** and **5a** in CDCl_3 .

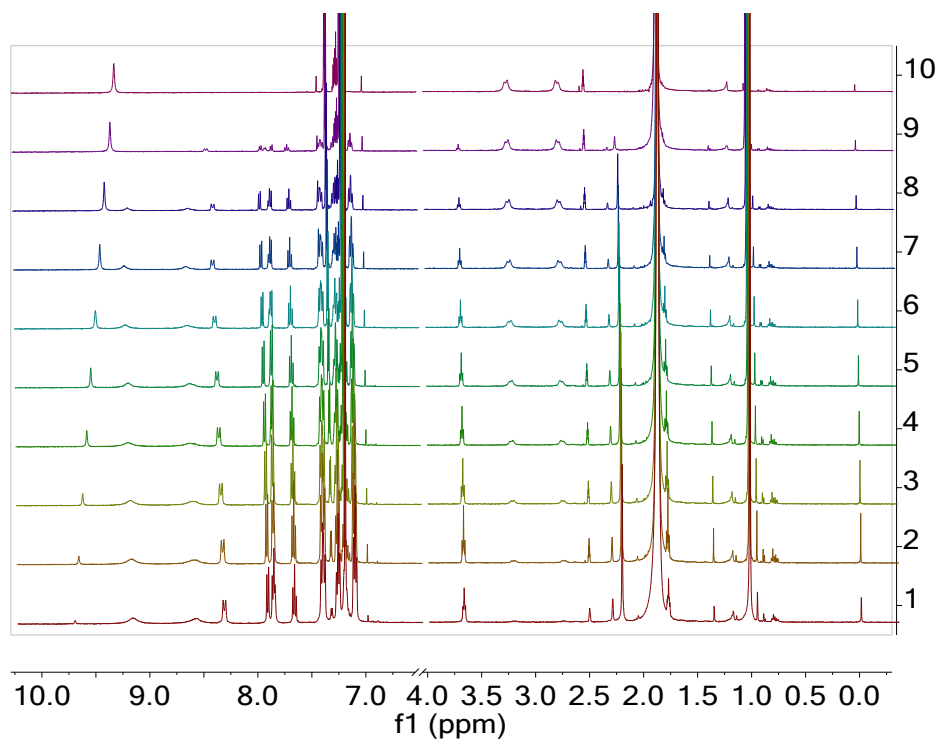


Figure A.5. ¹H NMR data for Job Plot of **4b** and **5a** in 1% DMSO-*d*₆:CDCl₃.

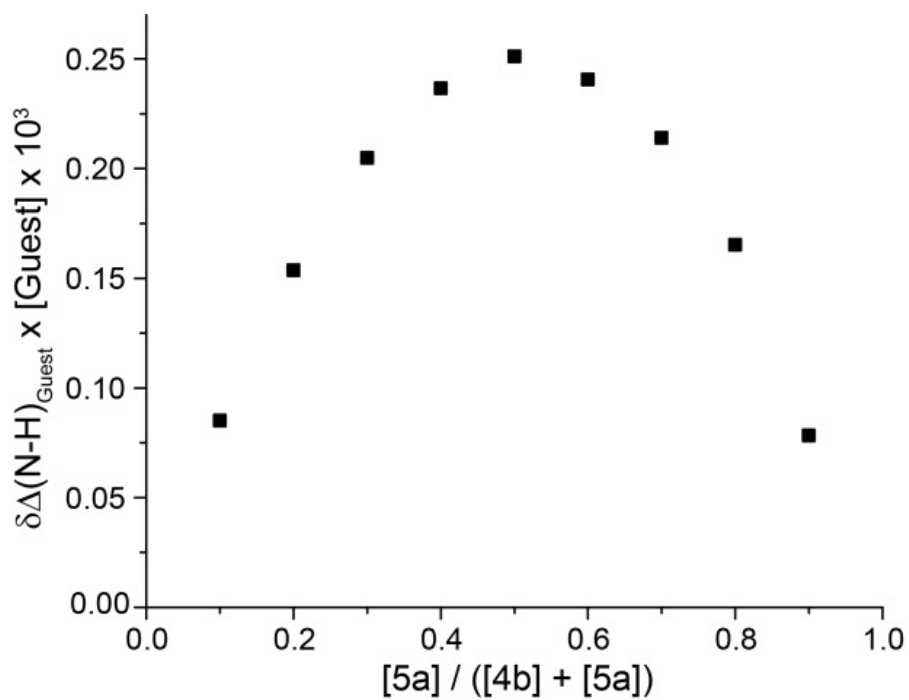


Figure A.6. Job Plot of **4b** and **5a** in 1% DMSO-*d*₆:CDCl₃.

NMR Spectra

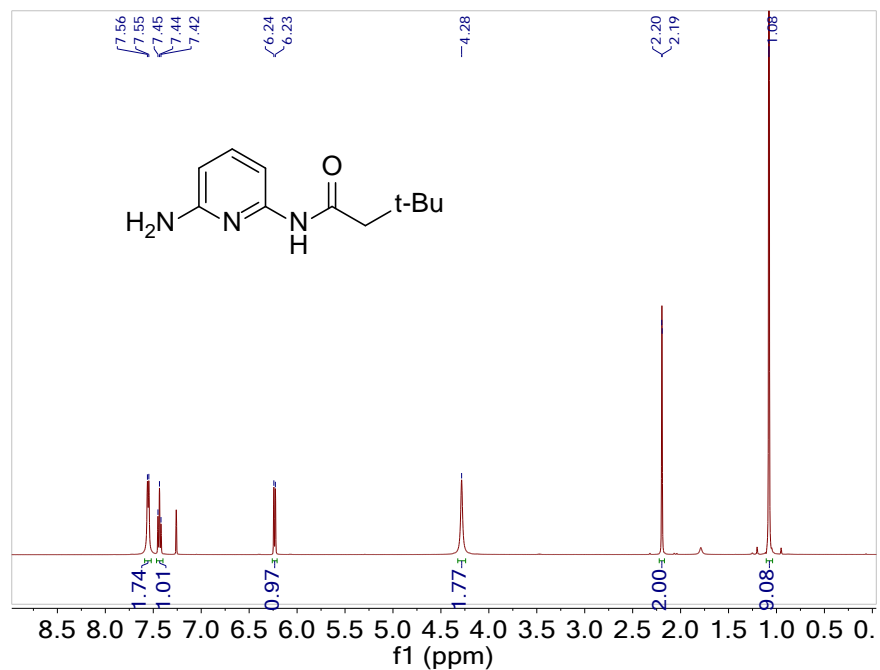


Figure A.7. ^1H (500 MHz) NMR spectrum of **1** in CDCl_3 .

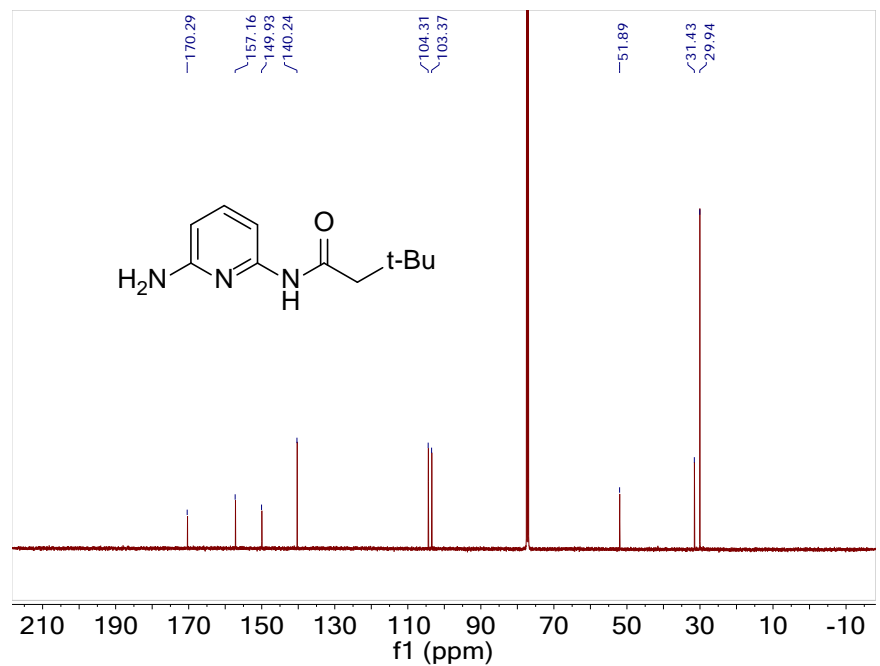


Figure A.8. ^{13}C { ^1H } (126 MHz) NMR spectrum of **1** in CDCl_3 .

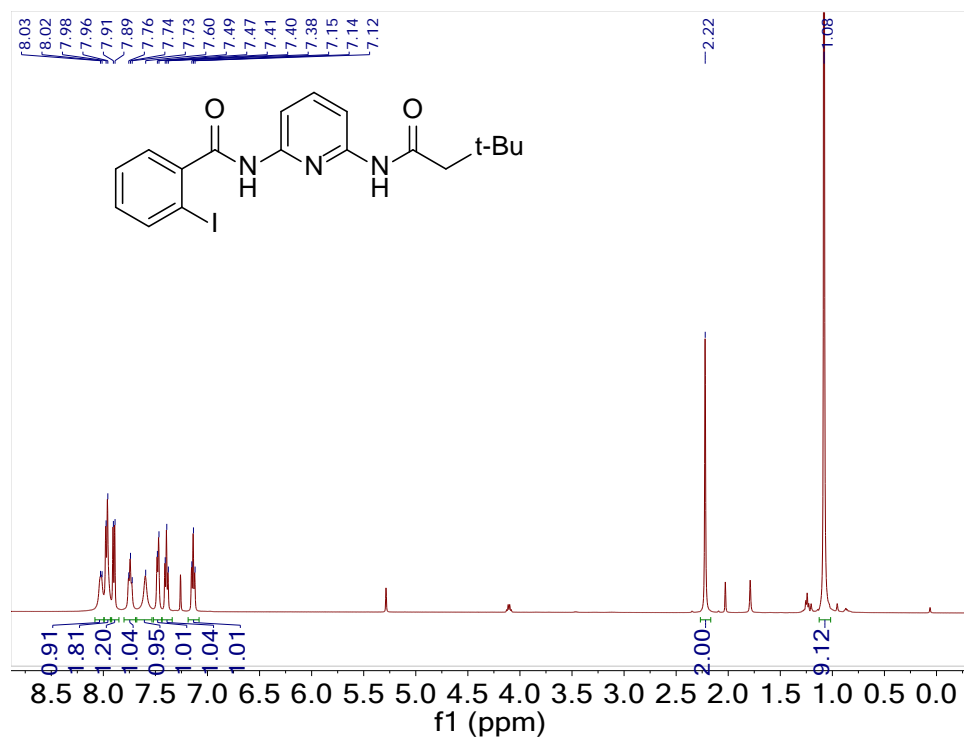


Figure A.9. ^1H (500 MHz) NMR spectrum of **2a** in CDCl_3 .

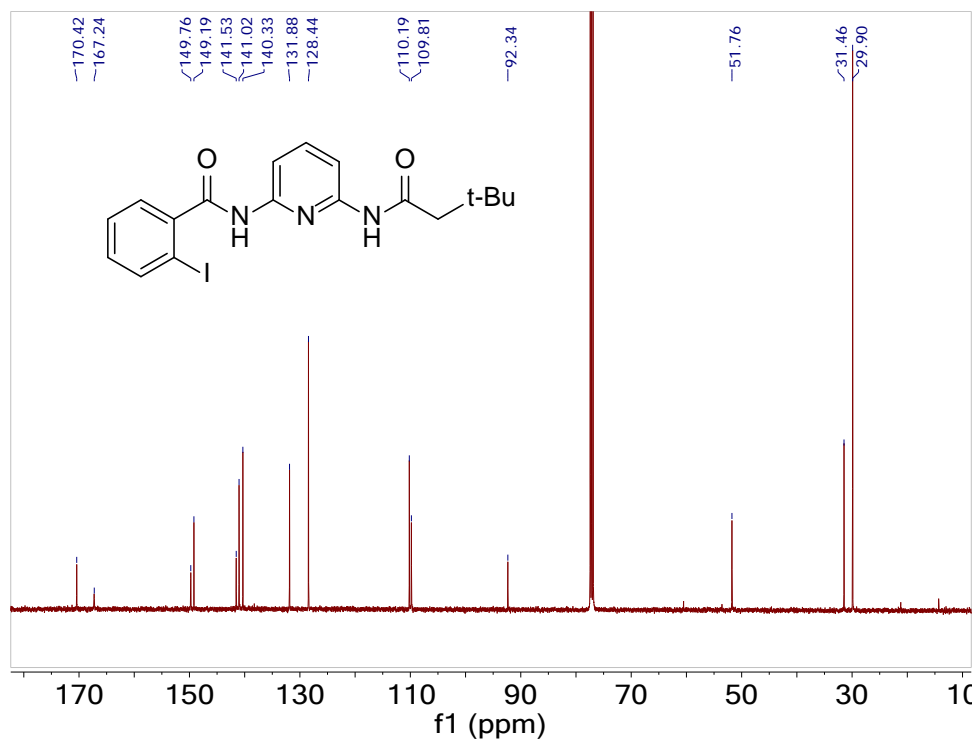


Figure A.10. $^{13}\text{C}\{^1\text{H}\}$ (126 MHz) NMR spectrum of **2a** in CDCl_3 .

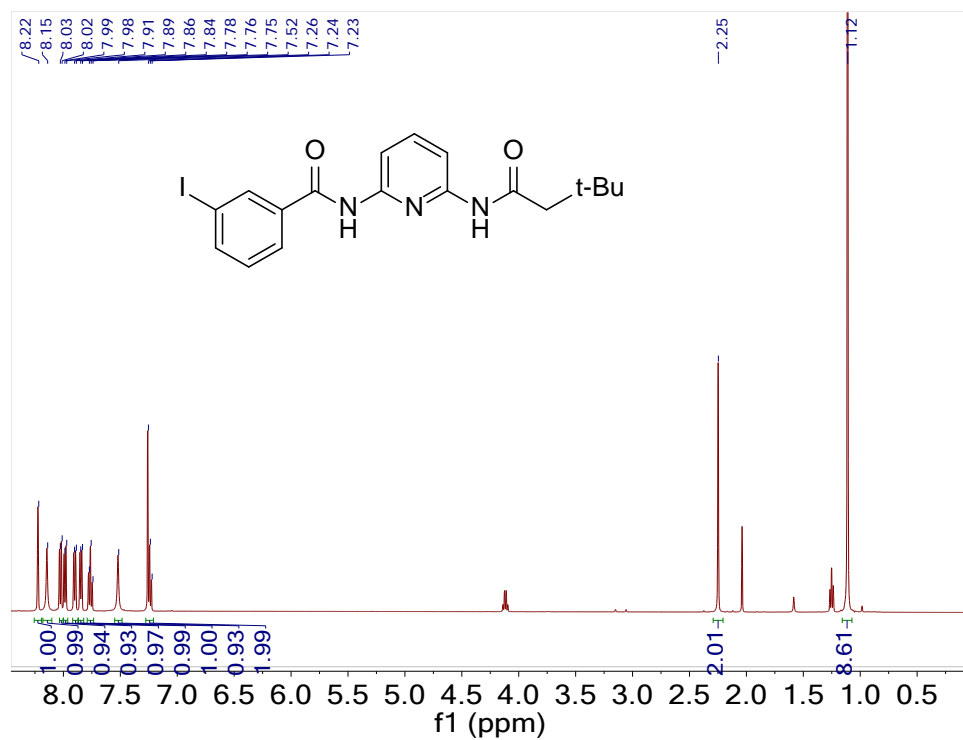


Figure A.11. ^1H (500 MHz) NMR spectrum of **2b** in CDCl_3 .

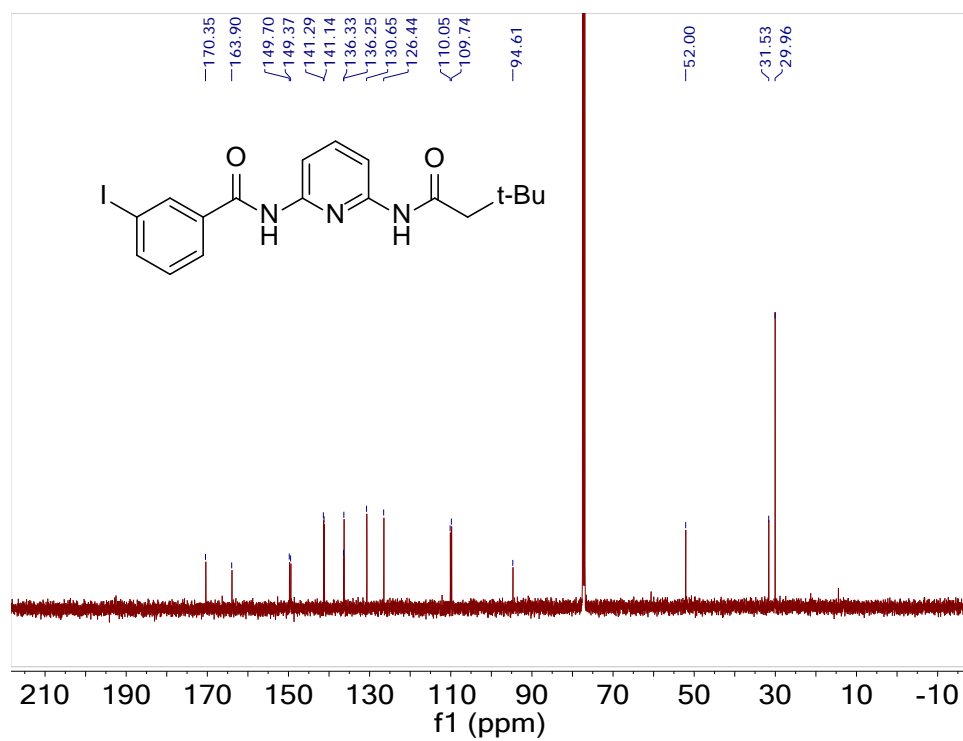


Figure A.12. $^{13}\text{C}\{^1\text{H}\}$ (126 MHz) NMR spectrum of **2b** in CDCl_3 .

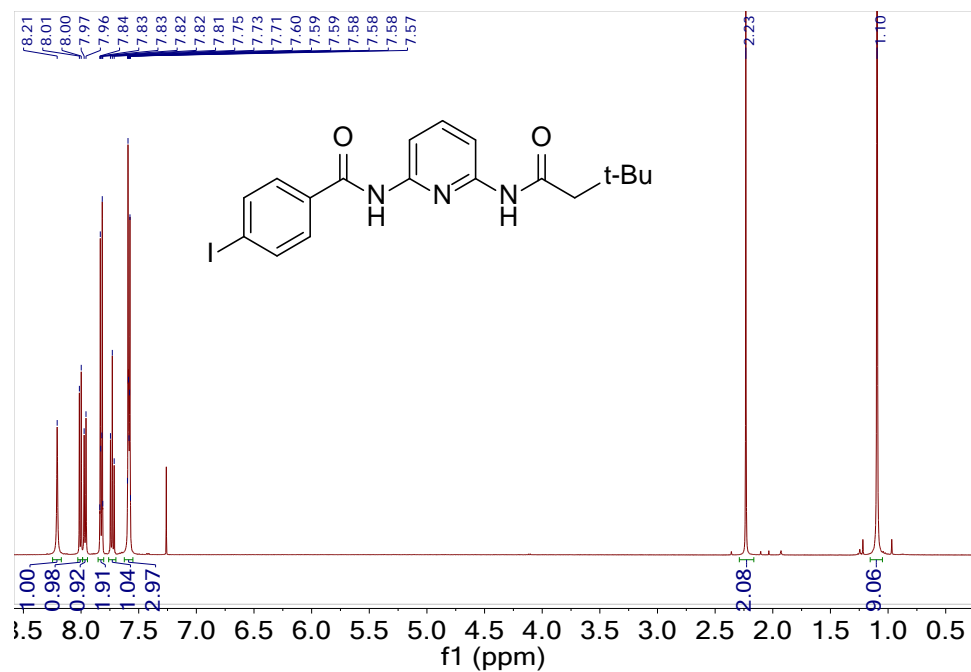


Figure A.13. ^1H (500 MHz) NMR spectrum of **2c** in CDCl_3 .

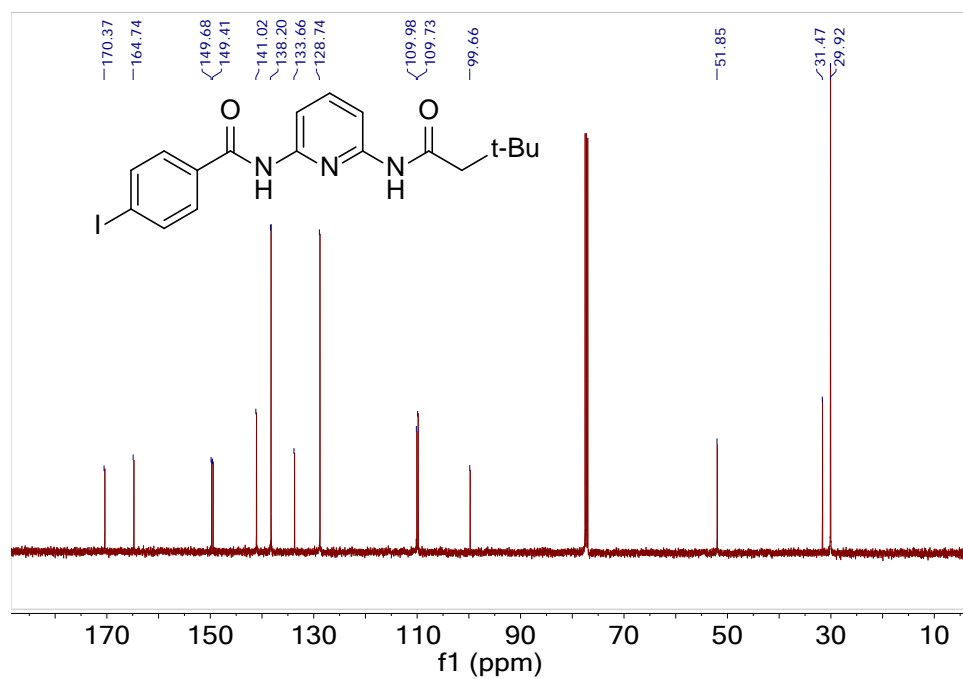


Figure A.14. $^{13}\text{C}\{^1\text{H}\}$ (126 MHz) NMR spectrum of **2c** in CDCl_3 .

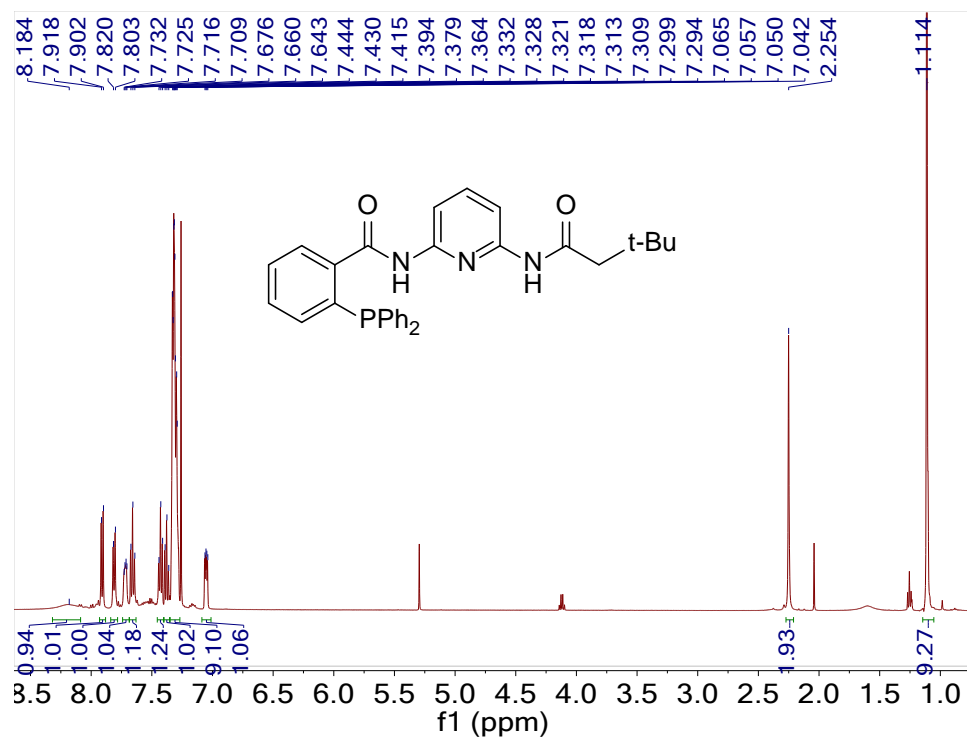


Figure A.15. ^1H (500 MHz), NMR spectrum of **3a** in CDCl_3 .

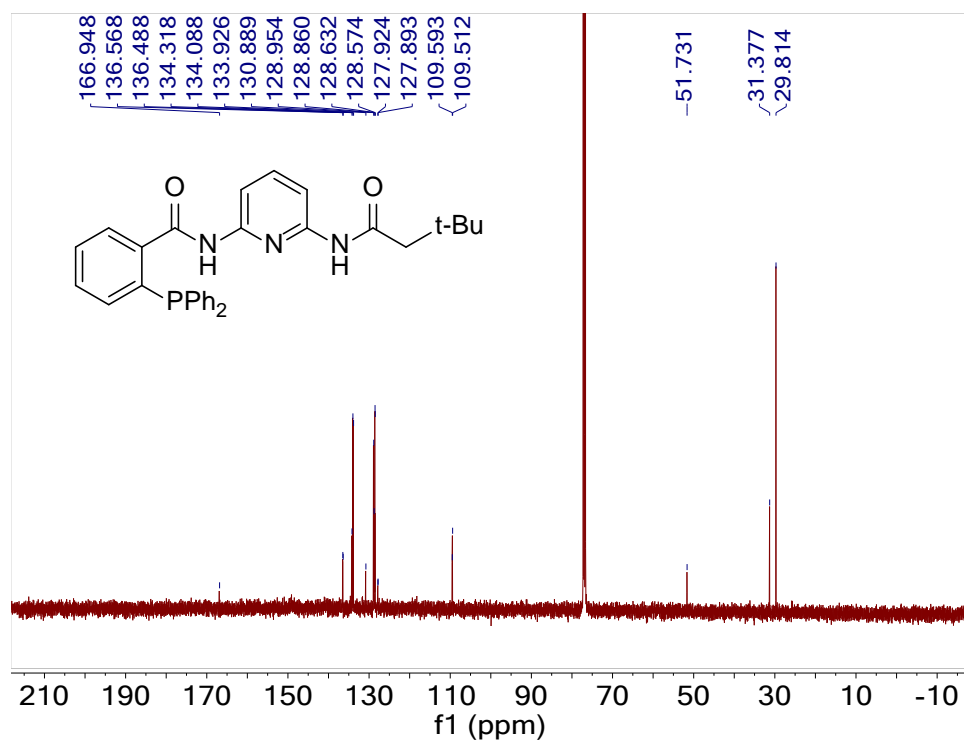


Figure A.16. $^{13}\text{C}\{^1\text{H}\}$ NMR (126 MHz) NMR spectrum of **3a** in CDCl_3 .

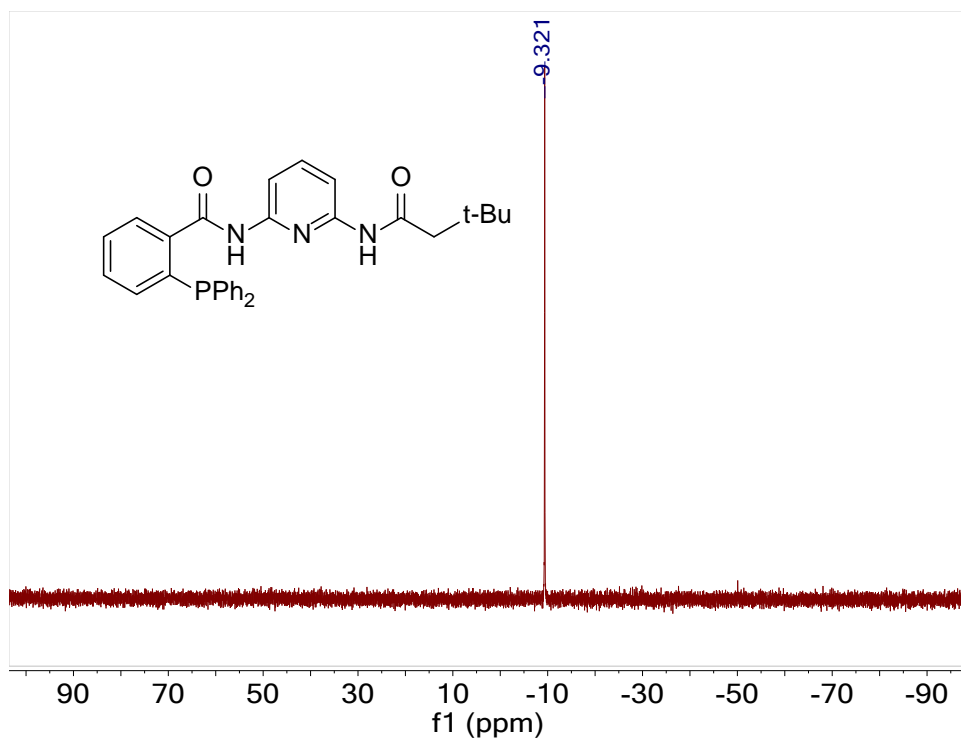


Figure A.17. $^{31}\text{P}\{^1\text{H}\}$ (202 MHz) NMR spectrum of **3a** in CDCl_3 .

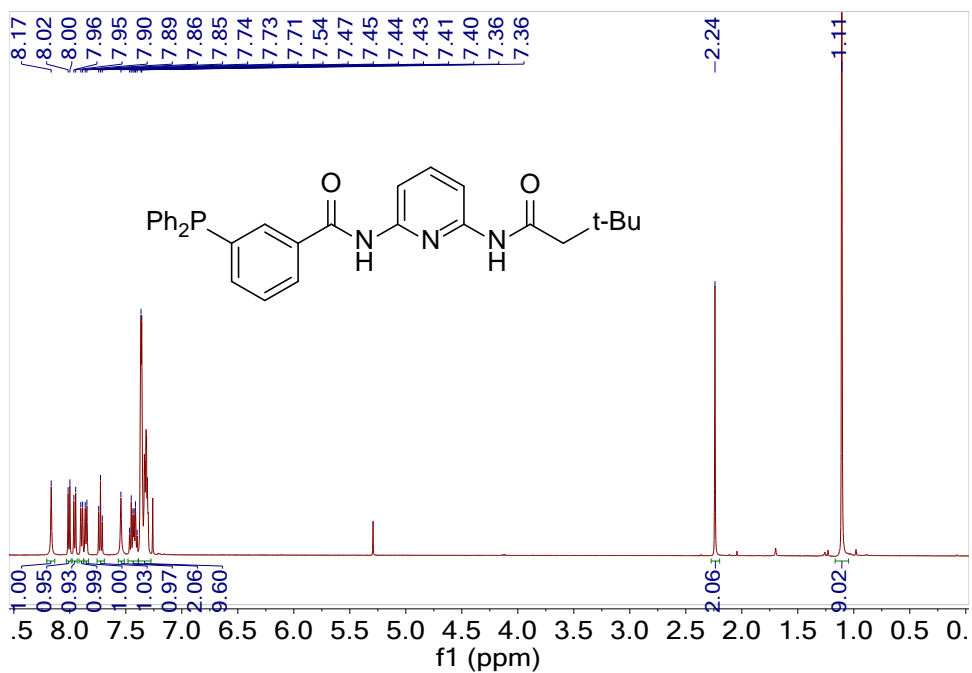


Figure A.18. ^1H (500 MHz) NMR spectrum of **3b** in CDCl_3 .

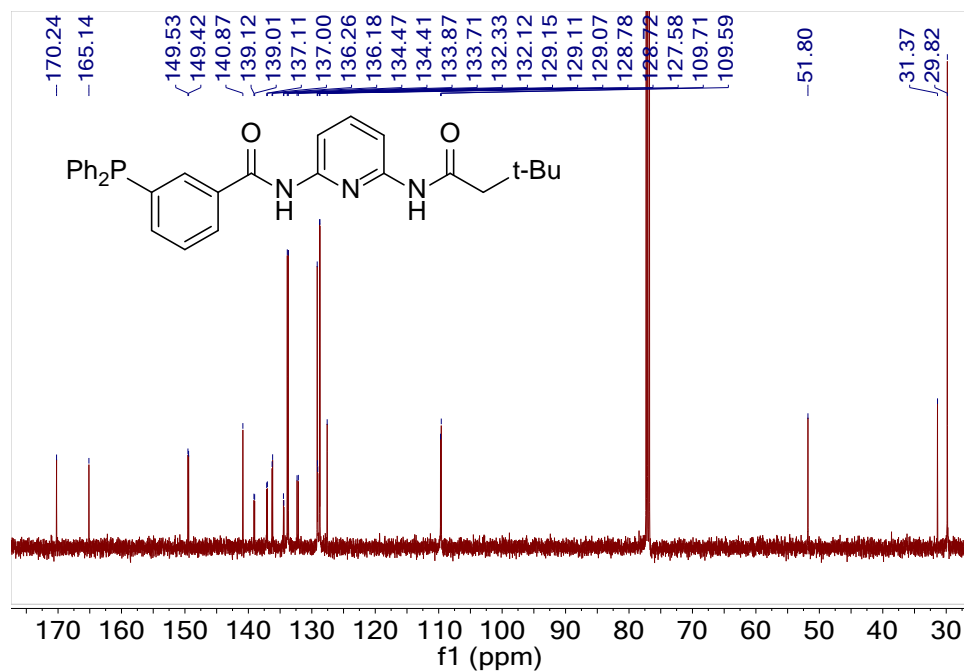


Figure A.19. $^{13}\text{C}\{^1\text{H}\}$ NMR (126 MHz) NMR spectrum of **3b** in CDCl_3 .

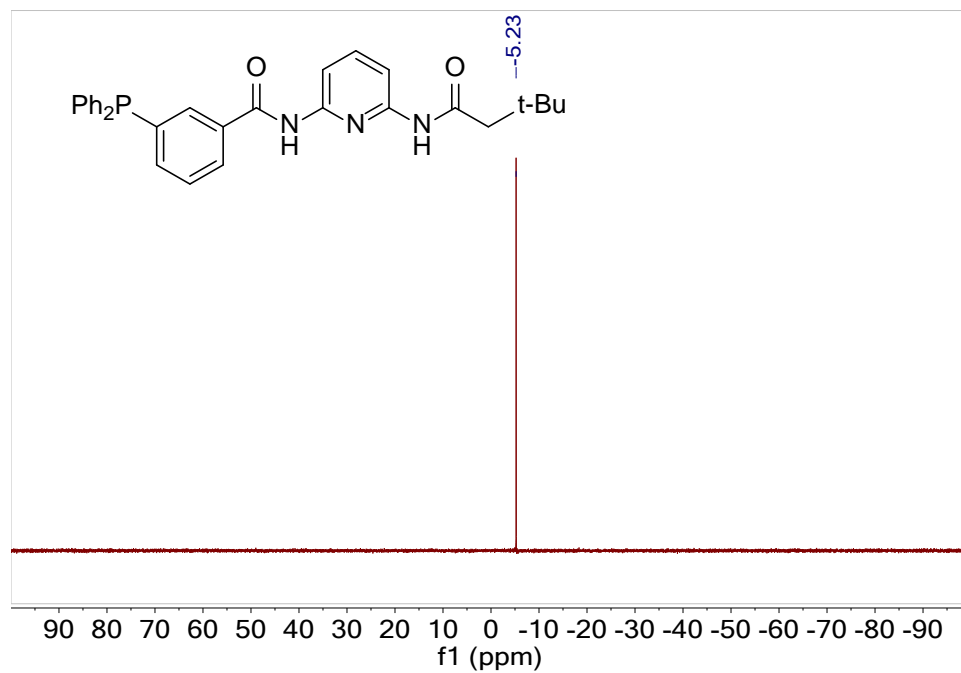


Figure A.20. $^{31}\text{P}\{^1\text{H}\}$ (202 MHz) NMR spectrum of **3b** in CDCl_3 .

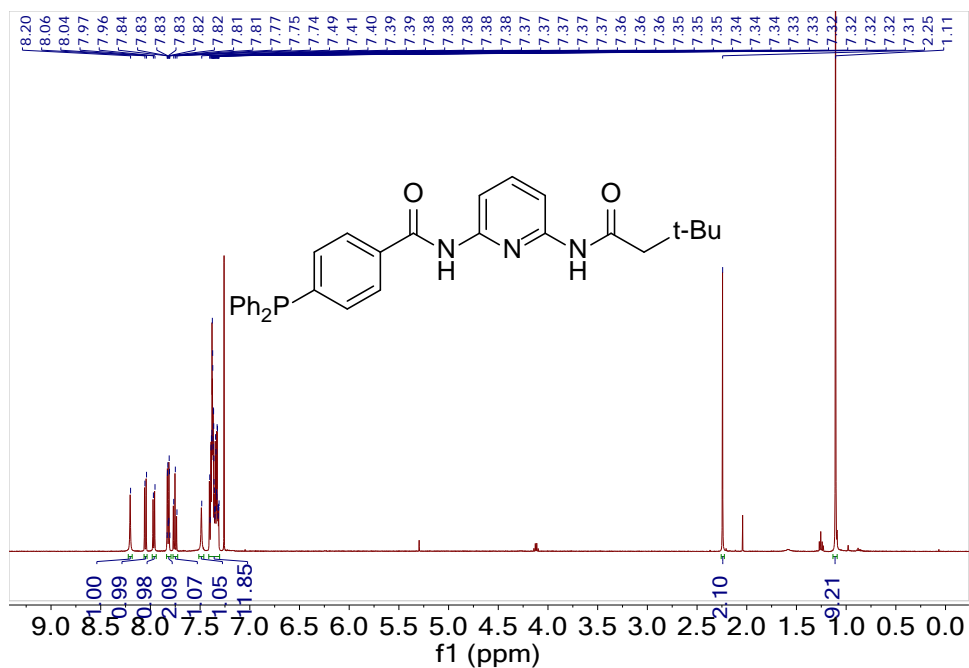


Figure A.21. ¹H (500 MHz) NMR spectrum of **3c** in CDCl₃.

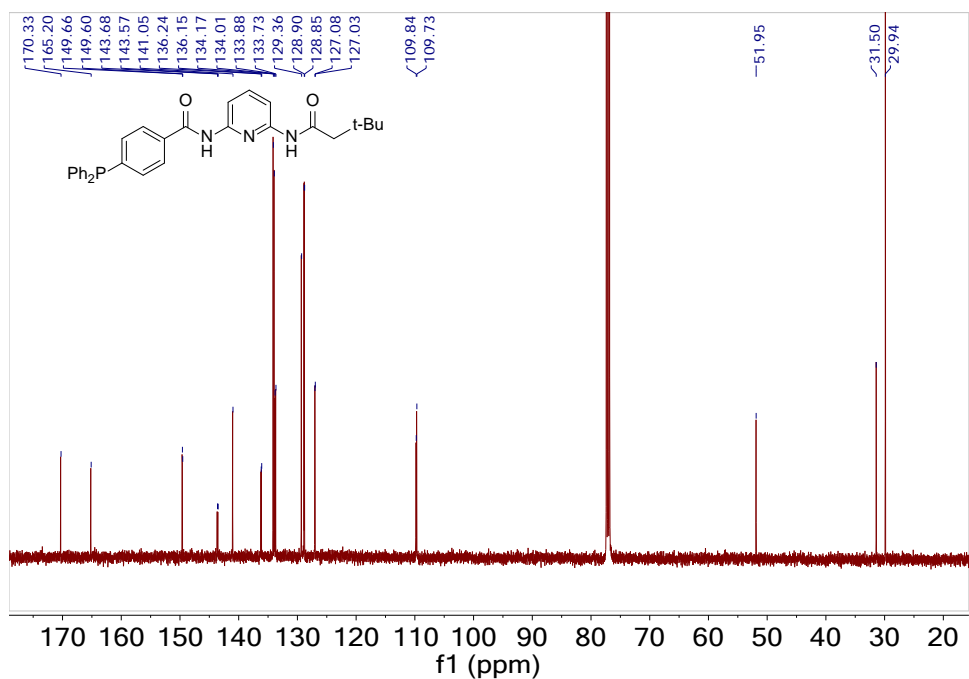


Figure A.22. ¹³C{¹H} (126 MHz) NMR spectrum of **3c** in CDCl₃.

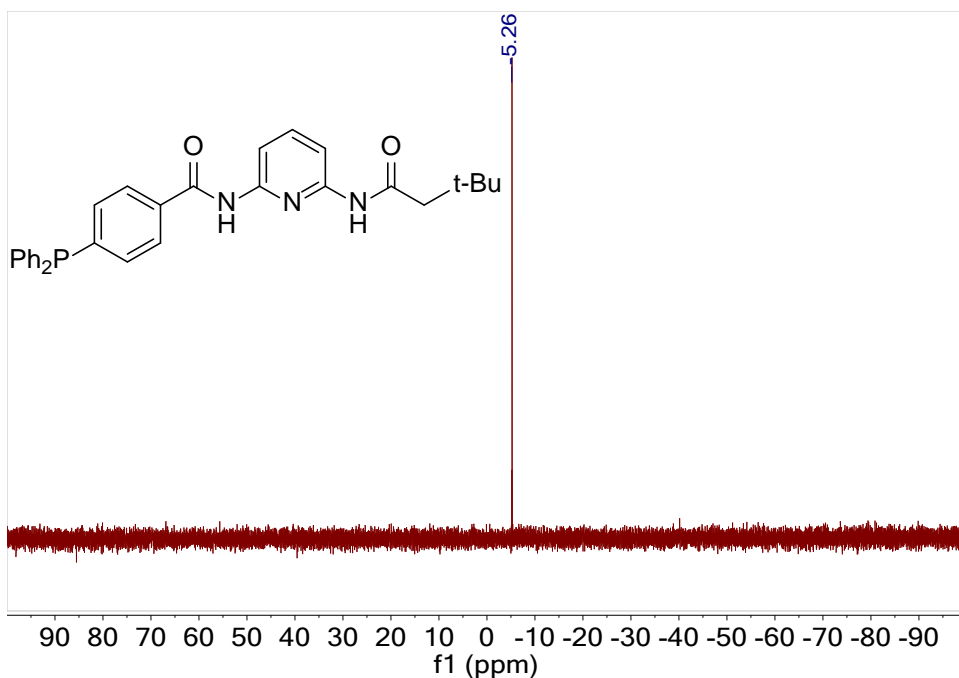


Figure A.23. $^{31}\text{P}\{^1\text{H}\}$ (202 MHz) NMR spectrum of **3c** in CDCl_3 .

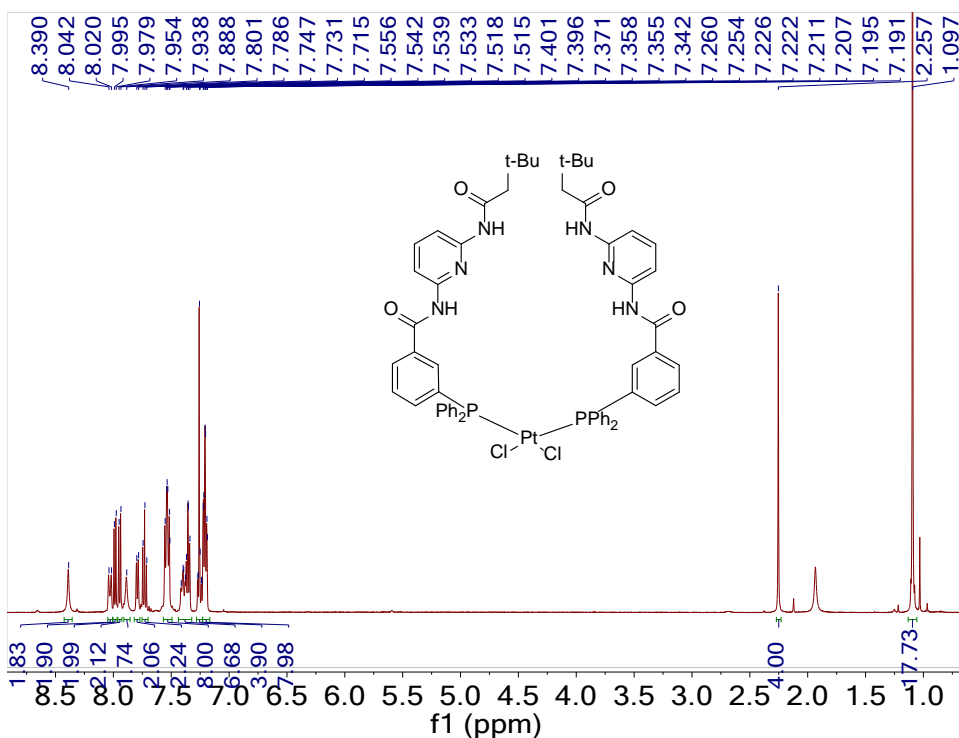


Figure A.24. ^1H (500 MHz) NMR spectrum of **4b** in CDCl_3 .

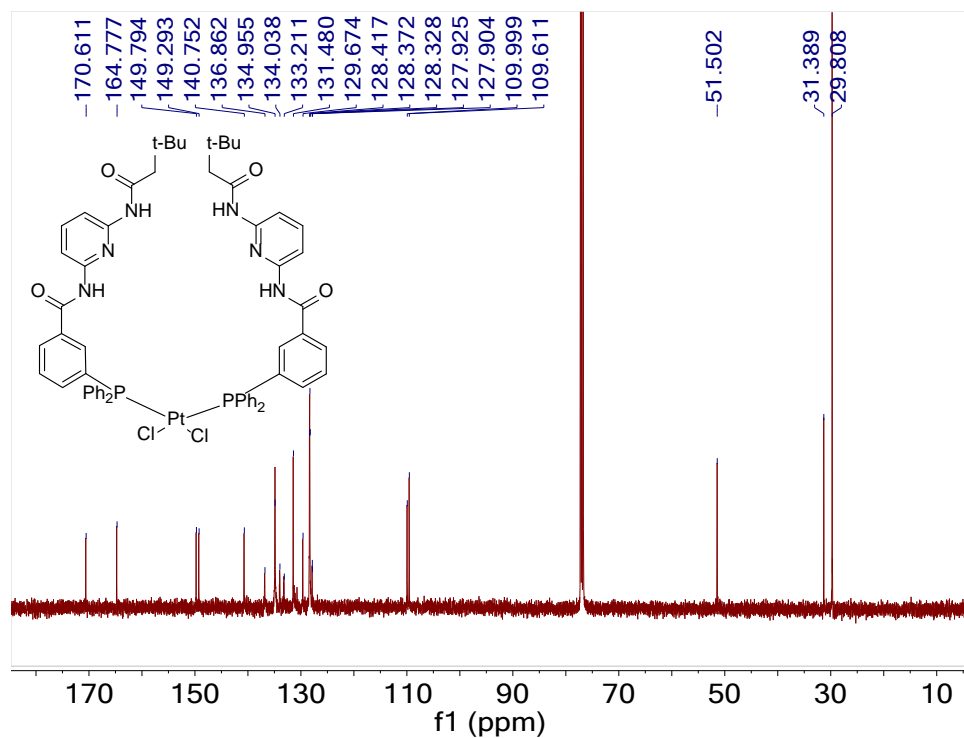


Figure A.25. $^{13}\text{C}\{^1\text{H}\}$ (126 MHz) NMR spectrum of **4b** in CDCl_3 .

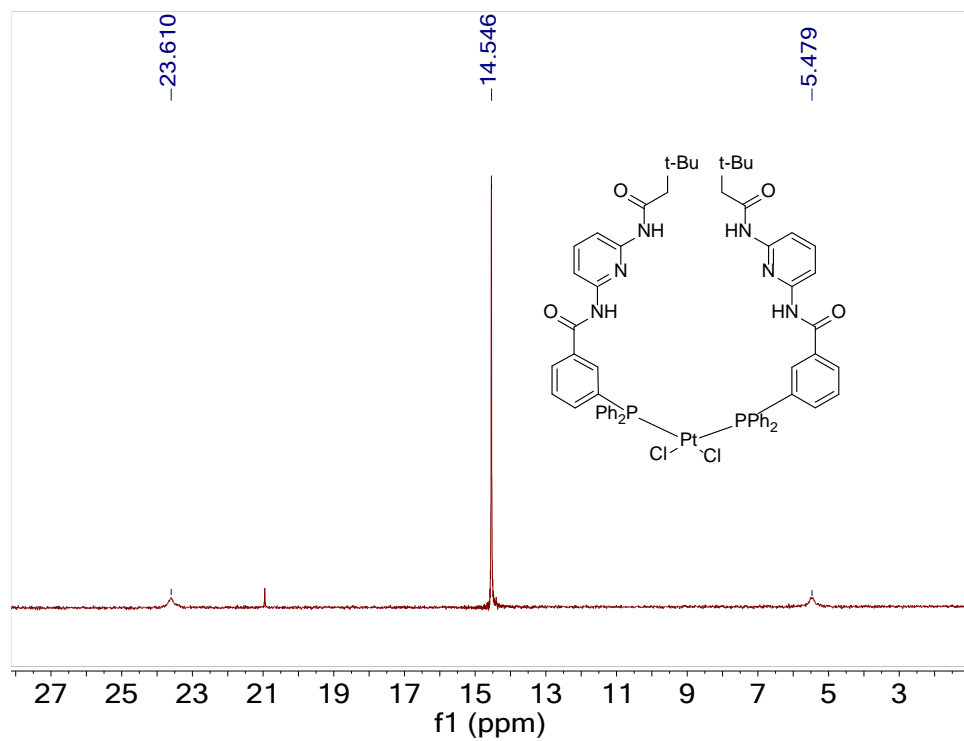


Figure A.26. $^{31}\text{P}\{^1\text{H}\}$ (202 MHz) NMR spectra of **4b** in CDCl_3 .

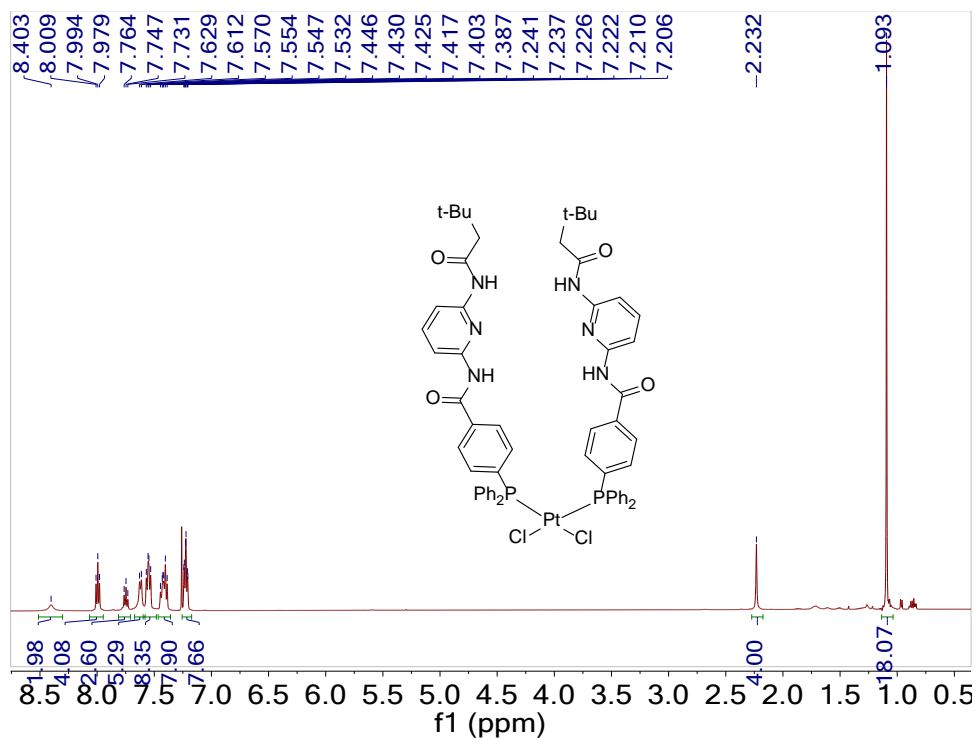


Figure A.27. ¹H (500 MHz) NMR spectrum of **4c** in CDCl₃.

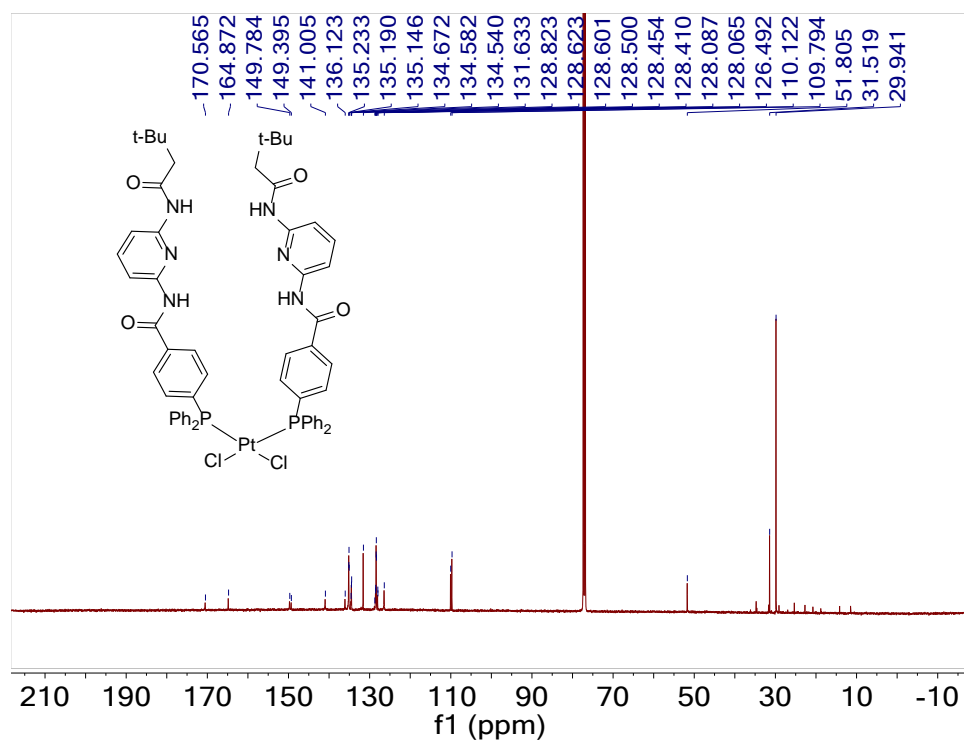


Figure A.28. ¹³C {¹H} (126 MHz) NMR spectrum of **4c** in CDCl₃.

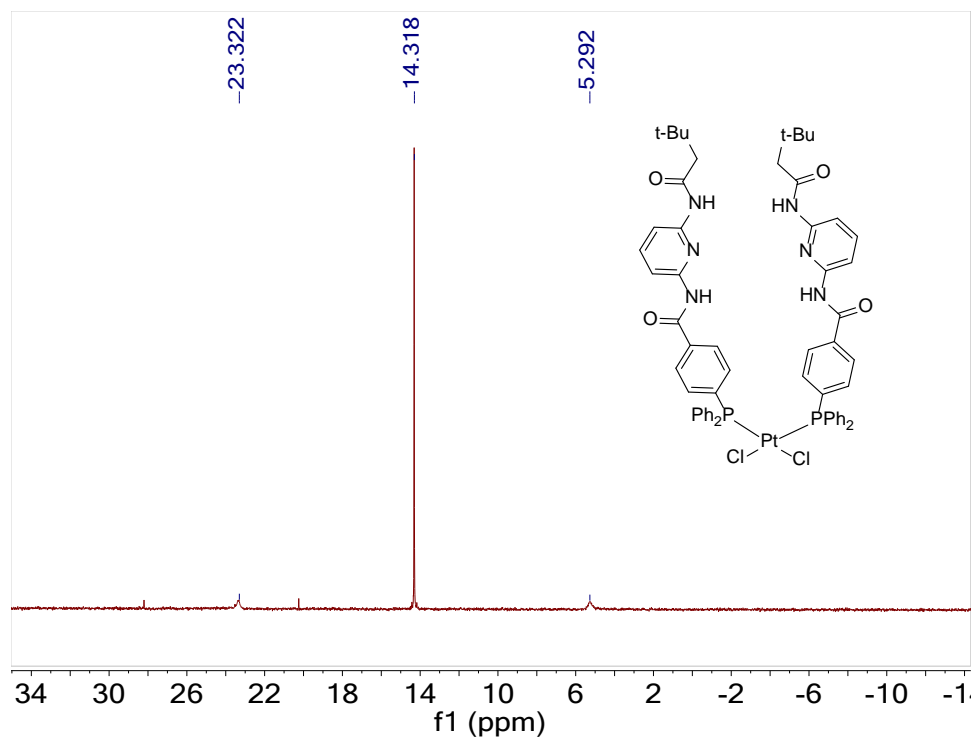


Figure A.29. $^{31}\text{P}\{^1\text{H}\}$ (202 MHz) NMR spectrum of **4c** in CDCl_3 .

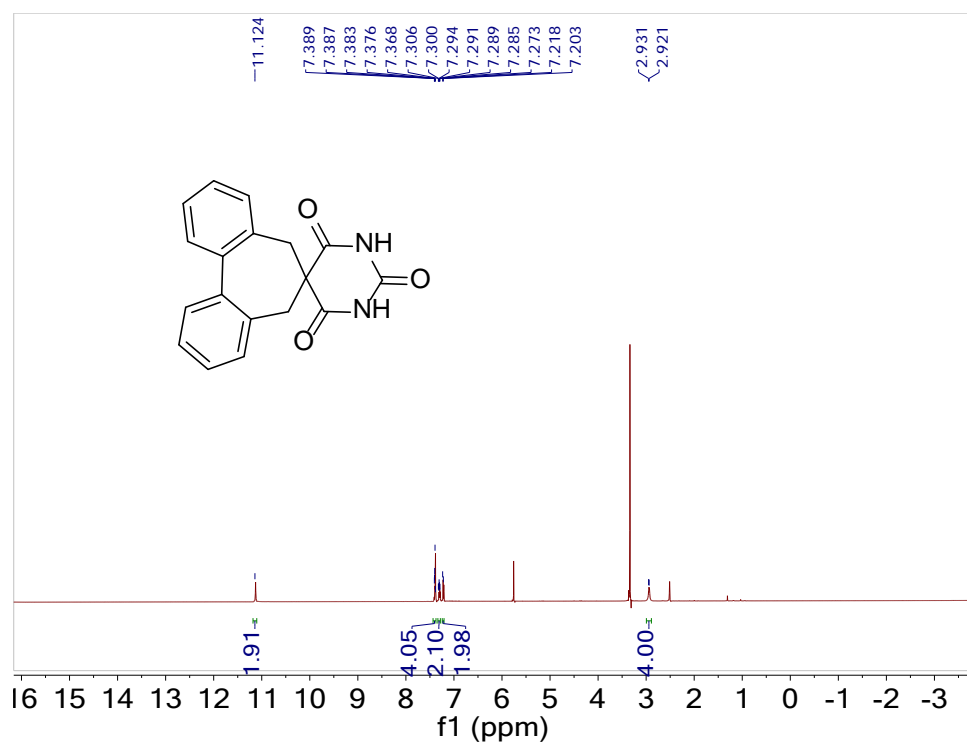


Figure A.30. ^1H (500 MHz) NMR spectra of **5a** in $\text{DMSO}-d_6$.

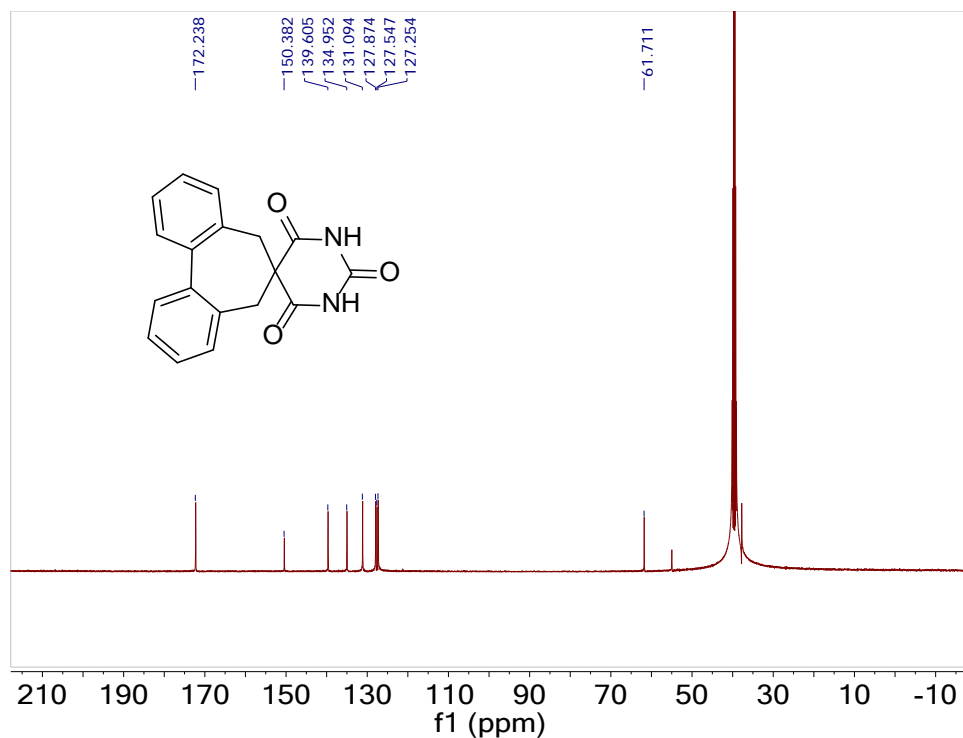


Figure A.31. $^{13}\text{C}\{^1\text{H}\}$ (126 MHz) NMR spectra of **5a** in $\text{DMSO-}d_6$.

Example Binding Isotherms

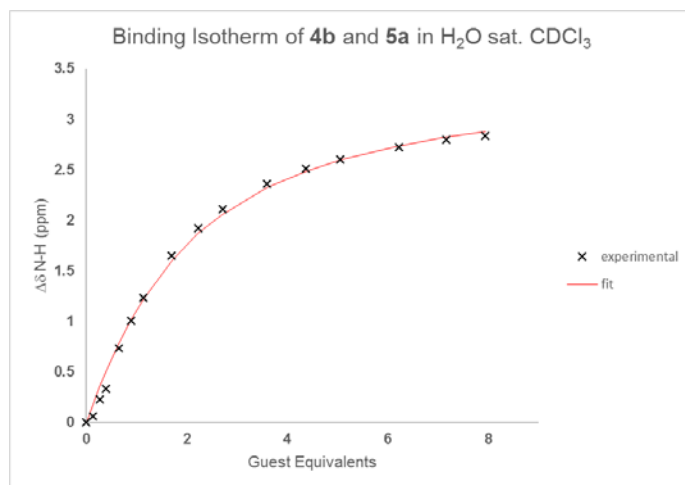


Figure A.32. Binding isotherm from NMR titration of **4b** and **5a** in $\text{H}_2\text{O sat. CDCl}_3$ at 25°C

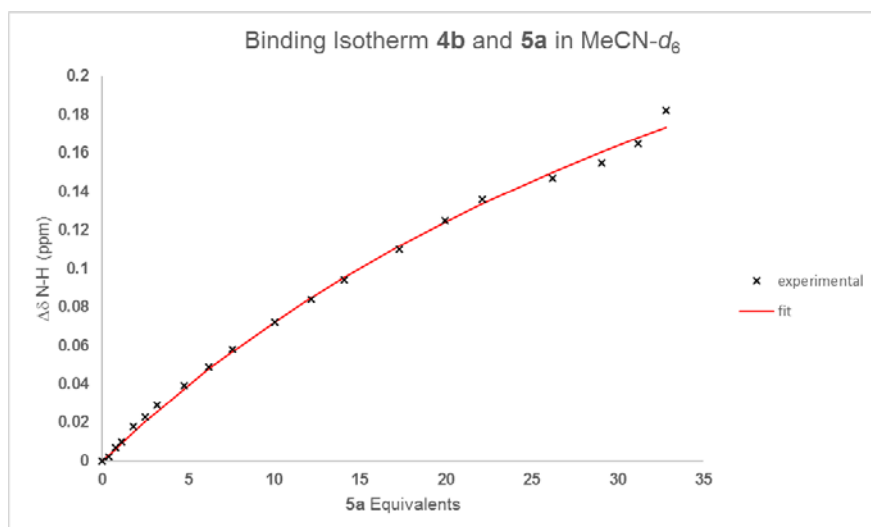


Figure A.33. Binding isotherm from NMR titration of **4b** and **5a** in MeCN-*d*₆ at 25 °C.

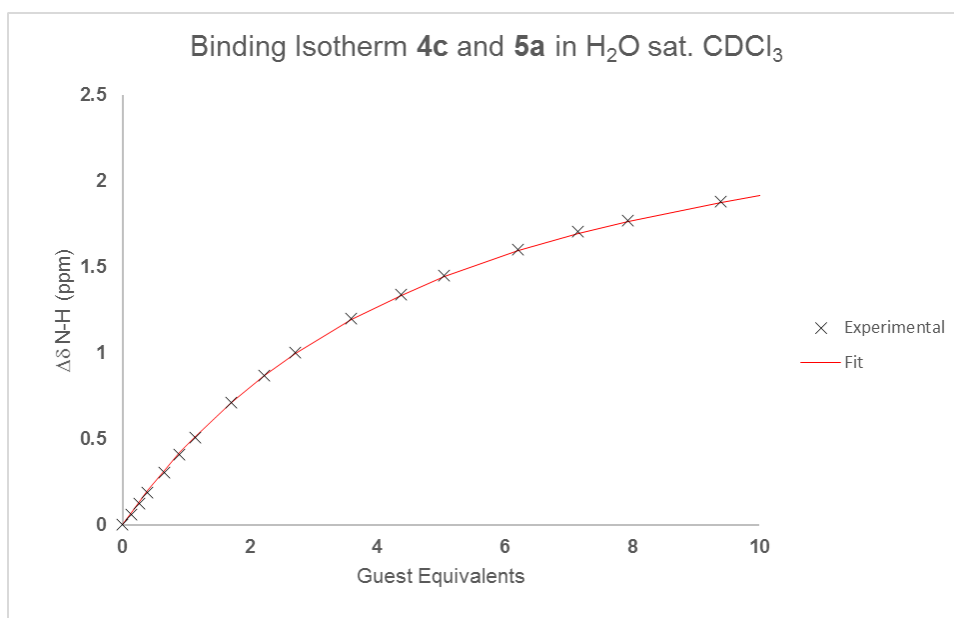


Figure A.34. Binding isotherm from NMR titration of **4c** and **5a** in H₂O sat. CDCl₃ at 25. °C

APPENDIX B

SUPPORTING INFORMATION FOR CHAPTER III

Appendix B is the supporting information for Chapter III of this dissertation. It includes the experimental details and additional spectra relevant to the content of Chapter III.

Experimental Details

General. All commercially-available reagents were used as received. Anhydrous, deoxygenated solvents were collected from a Pure Process Technologies solvent purification system. Reactions were monitored using Merck F₂₅₄ silica gel 60 TLC plates and visualized using UV light or a KMnO₄ stain. Chromatographic purification was performed using a Biotage automated flash chromatography purification system. ¹H and ¹³C{¹H} NMR spectra were recorded at the reported frequencies, and chemical shifts are reported in ppm (δ) and referenced to the residual solvent resonance. All ¹⁹F spectra were indirectly referenced via the Bruker TopSpin 3.5 software suite to CFC₃. The following naming conventions were used to describe NMR couplings: (s) singlet, (d) doublet, (t) triplet, (q) quartet, (dd) doublet of doublets, (m) multiplet, (b) broad. HPLC analysis was performed using an Agilent 1260 Infinity II instrument equipped with an Infinitylab poroshell 120 EC-C18 column (4.6 x 100 mm, 2.7 μm inner diameter) using a MeOH:H₂O gradient for elution.

Procedure for the solvent screening study. To a solution of 250 mg (1.95 mmol) barbituric acid in 5 mL solvent was added 780 μ L (4.48 mmol, 2.3 equiv.) diisopropylethylamine (DIPEA). The mixture was stirred at room temperature for 10 min, after which time a precipitate formed. 470 μ L (3.90 mmol, 2.0 equiv.) of benzyl bromide was then added to the mixture. The mixture was heated to 50 °C and stirred overnight (22 h). The crude, clear orange reaction mixture was diluted with H₂O and extracted 3x with EtOAc. The combined organic extracts were washed 3x with brine, dried over MgSO₄, filtered and concentrated. The residue was triturated with hexanes and the resulting solids collected via vacuum filtration. The final products ranged from white to off white/tan solids.

Syntheses

Synthesis of dibromomethylbinaphthalene precursors: A modified procedure as reported by Ooi *et al.* was used.²⁶ 2,2'-bis(trifluoromethanesulfonyloxy)-1,1'-binaphthyl, [(*R*)-**I**]. (*R*)-BINOL (2.01 g, 7.02 mmol), *N*-phenylbistrifluoromethanesulfonamide (5.02 g, 14.1 mmol), DIPEA (3.60 mL, 21.7 mmol) were combined in 10 mL dry DMF and stirred at r.t. for 24 hours. The reaction was diluted with Et₂O, washed 3x with H₂O and then with brine. The organic layer was dried over MgSO₄, filtered and concentrated under vacuum. The crude product was purified by column chromatography using hexanes:EtOAc gradient (0% - 20%) as the eluent (R_f = 0.12, Hex; R_f = 0.45, 20% EtOAc) to yield the final product as an oil that solidifies to a white solid upon standing (3.27 g, 85%) ¹H NMR (500 MHz, CDCl₃) δ : 8.15 (d, J = 9.1 Hz, 2H), 8.02 (d, J = 8.3 Hz, 2H), 7.66 – 7.57 (m, 4H), 7.43 (t, J = 7.6 Hz, 2H), 7.32 – 7.19 (m, 2H). ¹³C {¹H}

NMR (126 MHz, CDCl₃) δ : 145.51, 133.27, 132.48, 132.12, 128.48, 128.11, 127.45, 126.88, 123.57, 119.46, 118.26 (q, $J = 320.7$ Hz). ¹⁹F NMR (471 MHz, CDCl₃) δ : -74.56.

2,2'-bis(trifluoromethanesulfonyloxy)-1,1'-binaphthyl, [(*S*)-**I**]. Was prepared similar to (*R*)-**I** using the following amounts: (*S*)-BINOL (996 mg, 3.48 mmol), *N*-phenylbistrifluoromethanesulfonamide (2.50 g, 7.00 mmol), DIPEA (1.8 mL, 10 mmol) in 5 mL DMF. The product was isolated as a white solid (1.35 g, 71%). ¹H NMR (500 MHz, CDCl₃) δ : 8.15 (d, $J = 9.1$ Hz, 2H), 8.01 (d, $J = 8.3$ Hz, 2H), 7.62 (d, $J = 9.1$ Hz, 2H), 7.59 (ddd, $J = 8.1, 6.7, 1.0$ Hz, 2H), 7.42 (ddd, $J = 8.2, 6.8, 1.2$ Hz, 2H), 7.32 – 7.19 (m, 2H). ¹³C{¹H} NMR (126 MHz, CDCl₃) δ : 145.51, 133.28, 132.48, 132.12, 128.48, 128.11, 127.45, 126.89, 123.57, 119.53, 118.26 (q, $J = 320.7$). ¹⁹F NMR (471 MHz, CDCl₃) δ : -74.57.

(*R*)-2,2'-Dimethyl-1,1'-binaphthyl, [(*R*)-**II**]. (**R**)-**I** (2.502 g, 4.54 mmol) and NiCl₂(dppp) (82.0 mg, 0.139 mmol) were combined in a Schlenk and evacuated/refilled 3x with and atmosphere of N₂. Dry and degassed Et₂O (25 mL) was added via cannula and cooled to 0 °C. MeMgI (2 M in Et₂O, 6.8 mL, 14 mmol) was added slowly. The reaction mixture was then heated to reflux and stirred for 19 hours. The reaction was then cooled to 0 °C and quenched with 2 mL of 1 M HCl (aq), diluted with Et₂O, and filtered through celite. The organic layer was then washed 3x with H₂O and brine, dried over MgSO₄, filtered, and concentrated under vacuum. The crude mixture was dissolved in hexanes and the residual salts removed via filtration. The product was purified using column chromatography using hexanes as the eluent ($R_f = 0.23$) to yield the final product as a colorless oil that solidifies upon standing (1.08 g, 84%). ¹H NMR (500 MHz, CDCl₃) δ : 7.89 (t, $J = 8.0$ Hz, 4H), 7.51 (d, $J = 8.4$ Hz, 2H), 7.39 (t, $J = 7.5$ Hz, 2H), 7.21 (t, $J =$

7.6 Hz, 2H), 7.05 (d, $J = 8.5$ Hz, 2H), 2.04 (s, 6H). ^{13}C NMR (126 MHz, CDCl_3) δ : 135.26, 134.42, 132.89, 132.35, 128.86, 128.06, 127.56, 126.21, 125.78, 125.02, 20.18.

(*S*)-2,2'-Dimethyl-1,1'-binaphthyl, [(*S*)-**II**]. Was prepared similar to (*R*)-**II** using the following amounts: (*S*)-**I** (4.86 g, 8.83 mmol), $\text{NiCl}_2(\text{dppp})$ (157 mg, 0.265 mmol), degassed Et_2O (40 mL), MeMgI (2 M in Et_2O , 13 mL, 26 mmol). The final product was isolated as an oil that solidified upon standing (2.185 g, 88%) ^1H NMR (500 MHz, CDCl_3) δ : 7.89 (t, $J = 8.0$ Hz, 4H), 7.51 (d, $J = 8.4$ Hz, 2H), 7.39 (ddd, $J = 8.1, 6.6, 1.1$ Hz, 2H), 7.21 (ddd, $J = 8.2, 6.8, 1.3$ Hz, 2H), 7.05 (d, $J = 8.4$ Hz, 2H), 2.04 (s, 6H). $^{13}\text{C}\{^1\text{H}\}$ NMR (126 MHz, CDCl_3) δ : 135.27, 134.43, 132.90, 132.36, 128.86, 128.06, 127.57, 126.22, 125.78, 125.03, 20.18.

(*R*)-2,2'-Bis(bromomethyl)-1,1'-binaphthyl, [(*R*)-**III**]. (*R*)-**II** (428 mg, 1.52 mmol), *N*-bromosuccinimide (594 mg, 3.34 mmol), and AIBN (24.3 mg, 0.148 mmol, 10%) were dissolved in benzene (15 mL) and heated to reflux for 3 hours. The reaction was cooled to room temperature and diluted with Et_2O . The organic layer was washed 3x with H_2O , 3x brine, dried over MgSO_4 and filtered. The crude product was purified using column chromatography ($R_f = 0.23$, Hex). The combined fractions were concentrated and the product was triturated in hexanes and then filtered to yield the final product as a white solid (302 mg, 45%) ^1H NMR (500 MHz, CDCl_3) δ : 8.02 (d, $J = 8.6$ Hz, 2H), 7.93 (d, $J = 8.2$ Hz, 2H), 7.75 (d, $J = 8.6$ Hz, 2H), 7.49 (ddd, $J = 8.2, 6.7, 1.0$ Hz, 2H), 7.32 – 7.18 (m, 2H), 7.08 (d, $J = 8.5$ Hz, 2H), 4.26 (s, 4H). $^{13}\text{C}\{^1\text{H}\}$ NMR (126 MHz, CDCl_3) δ : 134.33, 134.23, 133.41, 132.66, 129.52, 128.17, 127.89, 126.99, 126.97, 126.94, 32.78.

(*S*)-2,2'-Bis(bromomethyl)-1,1'-binaphthyl, [(*S*)-**III**]. Was prepared similar to (*R*)-**III** using the following amounts: (*S*)-**II** (501 mg, 1.77 mmol), *N*-bromosuccinimide (668

mg, 3.75 mmol), and AIBN (32.0 mg, 0.195 mmol), and benzene (15 mL). After 3 hours 125 mg (0.702 mmol) NBS and 5.0 mg (3.0 μ mol) AIBN were added and heated to reflux for an additional hour. The final product was isolated as a white solid (294 mg, 38%). ^1H NMR (500 MHz, CDCl_3) δ : 8.02 (d, J = 8.6 Hz, 2H), 7.93 (d, J = 8.2 Hz, 2H), 7.75 (d, J = 8.6 Hz, 2H), 7.49 (t, J = 7.5 Hz, 2H), 7.28 (t, J = 7.9 Hz, 2H), 7.08 (d, J = 8.5 Hz, 2H), 4.26 (s, 4H). ^{13}C NMR (126 MHz, CDCl_3) δ : 134.33, 134.23, 133.40, 132.65, 129.51, 128.17, 127.89, 126.99, 126.96, 126.94, 32.78.

General Synthesis of 5,5'-disubstituted barbituric acids: To a solution of barbituric acid (1 equiv.) in DMSO was added diisopropylethylamine (DIPEA, 2.3 equiv.) The mixture was stirred at room temperature for 10 min, after which time a precipitate formed (depending on the concentration of barbituric acid). The corresponding benzyl bromide (2 equiv.) was then added to the mixture, which was then heated to 50 $^\circ\text{C}$ and stirred overnight (~22 h). The crude, clear orange reaction mixture was diluted with H_2O and extracted 3x with EtOAc. The combined organic extracts were washed 3x with brine, dried over MgSO_4 , filtered and concentrated. The residue was triturated with a DCM:hexanes mixture and the resulting solids collected via vacuum filtration to yield the final product. In general, this gave acceptably pure product. Further purification could be achieved via recrystallization from EtOH or column chromatography.

5,5'-dibenzylbarbituric acid (**Figure 3.2, Entry 2**). This compound was prepared as described in the general procedure using the following quantities: barbituric acid (253 mg, 1.95 mmol) in 5 mL DMSO, DIPEA (780 μL , 4.45 mmol), and benzyl bromide (470 μL , 3.95 mmol). The product was isolated as a white solid (474 mg, 78%). ^1H NMR (500

MHz, DMSO-*d*₆) δ : 11.19 (s, 2H), 7.35 – 7.17 (m, 6), 7.11 – 7.01 (m, 4H), 3.28 (s, 4H).

¹³C{¹H} NMR (126 MHz, DMSO-*d*₆) δ : 171.99, 148.85, 135.13, 129.26, 128.47, 127.33, 58.99, 43.78.

5,5'-bis((perfluorophenyl)methyl)barbituric acid (**Figure 3.2, Entry 4**). This compound was prepared as described in the general procedure using the following quantities: barbituric acid (100 mg, 0.781 mmol) in 5 mL DMSO, DIPEA (310 μ L, 1.8 mmol), and 2,3,4,5,6-pentafluorobenzyl bromide (240 μ L, 1.58 mmol). This compound was purified by column chromatography (R_f = 0.3, 1:3 EtOAc:Hex, SiO₂) to give the desired product as a white solid (219 mg, 57%). ¹H NMR (500 MHz, DMSO-*d*₆) δ : 11.60 (s, 2H), 3.44 (s, 4H). ¹³C{¹H} NMR (126 MHz, DMSO-*d*₆) δ : 170.17, 149.38, 145.19 (d, J = 245.5 Hz), 139.84 (d, J = 257.1 Hz), 138.16 – 134.98 (m), 109.59 (td, J = 19.4, 19.0, 3.4 Hz), 53.12, 29.68. ¹⁹F NMR (471 MHz, DMSO-*d*₆) δ : -138.81 (dd, J = 23.9, 7.4 Hz, 4F), -154.97 (t, J = 22.3 Hz, 2F), -162.69 (td, J = 23.2, 7.2 Hz, 4F). HRMS (EI-TOF) m/z : [M-H]⁺ Calcd for C₁₈H₅N₂O₃F₁₀, 487.01403; found 487.01331.

5,5'-diallylbarbituric acid (**Figure 3.2, Entry 5**). This compound was prepared as described in the general procedure using the following quantities: barbituric acid (0.502 g, 3.92 mmol) in 10 mL DMSO, DIPEA (1.56 mL, 8.96 mmol), and allyl bromide (680 μ L, 7.87 mmol). The compound was isolated as an off white solid (416 mg, 51%). ¹H NMR (500 MHz, DMSO-*d*₆) δ : 11.50 (s, 2H), 5.56 (ddt, J = 17.4, 10.2, 7.3 Hz, 2H), 5.20 – 4.83 (m, 4H), 2.55 (d, J = 7.4 Hz, 4H). ¹³C{¹H} NMR (126 MHz, DMSO-*d*₆) δ : 172.38, 150.16, 131.78, 120.53, 55.44, 41.92.

5,5'-bis(pyridin-2-ylmethyl)barbituric acid (**1**). This compound was prepared as described in the general procedure using the following quantities: barbituric acid (102

mg, 7.77 mmol) in 5 mL DMSO, DIPEA (580 μ L, 3.3 mmol), and 2-(bromomethyl)pyridine hydrobromide (405 mg, 1.60 mmol). The compound was isolated as a tan solid (111 mg, 46%). ^1H NMR (500 MHz, DMSO- d_6) δ : 10.93 (s, 2H), 8.35 (d, J = 4.7 Hz, 2H), 7.70 (td, J = 7.7, 1.8 Hz, 2H), 7.21 (m, 4H), 3.47 (s, 4H). $^{13}\text{C}\{^1\text{H}\}$ NMR (126 MHz, DMSO- d_6) δ : 172.73, 155.91, 150.27, 148.46, 136.59, 123.59, 122.00, 53.32, 44.72. HRMS (ESI-TOF) m/z : $[\text{M} + \text{H}]^+$ Calcd for $\text{C}_{16}\text{H}_{15}\text{N}_4\text{O}_3$, 311.1144; found 311.1139.

5,5'-bis(pyren-1-ylmethyl)barbituric acid (**2**). This compound was prepared as described in the general procedure using the following quantities: barbituric acid (50.7mg, 0.396 mmol) in 3 mL DMSO, DIPEA (160 μ L, 0.92 mmol), and 1-(bromomethyl)pyrene (231 mg, 0.783 mmol). The compound was purified via column chromatography (R_f = 0.56, 1:1 EtOAc:Hex) followed by recrystallization from a CHCl_3 :EtOH mixture to yield the final product as a white solid (88 mg, 40%). ^1H NMR (500 MHz, DMSO- d_6) δ : 11.08 (s, 2H), 8.62 (d, J = 9.4 Hz, 2H), 8.32 (d, J = 8.0 Hz, 2H), 8.30 (d, J = 7.7 Hz, 2H), 8.27 (d, J = 9.4 Hz, 2H), 8.23 (d, J = 8.0 Hz, 2H), 8.18 (d, J = 8.9 Hz, 2H), 8.13 (d, J = 8.9 Hz, 2H), 8.09 (t, J = 7.7 Hz, 2H), 7.86 (d, J = 8.0 Hz, 2H), 4.40 (s, 4H). $^{13}\text{C}\{^1\text{H}\}$ NMR (126 MHz, DMSO) δ : 172.38, 148.72, 130.82, 130.30, 130.05, 129.83, 129.16, 127.45, 127.37, 127.25, 127.23, 126.35, 125.26, 124.96, 124.76, 124.12, 124.03, 123.77, 58.59. HRMS (ESI-TOF) m/z : $[\text{M} + \text{H}]^+$ Calcd for $\text{C}_{38}\text{H}_{25}\text{N}_2\text{O}_3$, 557.1865; found 557.1874.

5,5'-bis(anthracen-9-ylmethyl)barbituric acid (**3**). This compound was prepared as described in the general procedure except the reaction was stopped after 2 hours. The following quantities were used: barbituric acid (28.3 mg, 0.221 mmol) in 2 mL DMSO,

DIPEA (90 μ L, 0.52 mmol), and 9-(chloromethyl)anthracene (100 mg, 0.441 mmol).

The compound was recrystallized from THF:EtOH to give the final compound as a yellow solid (21 mg, 19%). ^1H NMR (500 MHz, DMSO- d_6) δ : 10.67 (s, 2H), 8.53 (s, 2H), 8.43 (dd, J = 6.5, 3.4 Hz, 4H), 8.03 (dd, J = 6.3, 3.4 Hz, 4H), 7.47 (dd, J = 6.7, 3.2 Hz, 8H), 4.69 (s, 4H). $^{13}\text{C}\{^1\text{H}\}$ NMR (126 MHz, DMSO- d_6) δ : 172.30, 148.67, 130.98, 130.92, 128.68, 128.55, 127.63, 125.54, 125.39, 124.88, 56.66, 35.35. HRMS (ESI-TOF) m/z : $[\text{M} + \text{H}]^+$ Calcd for $\text{C}_{34}\text{H}_{25}\text{N}_2\text{O}_3$, 509.1865; found 509.1858.

5,5'-(*R*)-1,1'-binaphthylbarbituric acid [(*R*)-**BINABARB**, (**4a**)]. This compound was prepared as described in the general procedure using the following quantities: barbituric acid (57.9 mg, 0.452 mmol) in 3 mL DMSO, DIPEA (180 μ L, 1.0 mmol), and (*R*)-**III** (199 mg μ L, 0.452 mmol). The compound was purified by column chromatography (R_f = 0.33, 1:1 EtOAc:Hex) followed by recrystallization from ethanol to yield the final product as a white solid (62 mg, 33%) HRMS (ESI-TOF) m/z : $[\text{M} + \text{Na}]^+$ Calcd for $\text{C}_{26}\text{H}_{19}\text{N}_2\text{O}_3$, 407.1396; found 407.1385.

5,5'-(*S*)-1,1'-binaphthylbarbituric acid [(*S*)-**BINABARB**, (**4b**)]. This compound was prepared as described in the general procedure using the following quantities: barbituric acid (49.7 mg, 0.388 mmol) in 5 mL DMSO, DIPEA (160 μ L, 0.92 mmol), and (*S*)-**III** (172 mg, 0.391 mmol). The compound was purified by column chromatography (R_f = 0.33, 1:1 EtOAc:Hex) followed by recrystallization from ethanol to yield the final product as a white solid (36 mg, 23%). HRMS (ESI-TOF) m/z : $[\text{M} + \text{Na}]^+$ Calcd for $\text{C}_{26}\text{H}_{19}\text{N}_2\text{O}_3$, 407.1396; found 407.1396.

5-benzyl-5-((perfluorophenyl)methyl)barbituric acid (**5**). This compound was using modified procedure as described in the general procedure using the following

quantities: DIPEA (310 μL , 1.80 mmol) was added to barbituric acid (98.8 mg, 0.771 mmol) in 5 mL DMSO and stirred at room temperature for 10 minutes. A separate premixed solution of 2,3,4,5,6-pentafluorobenzyl bromide (120 μL , 0.795 mmol) and benzyl bromide (95 μL , 0.80 mmol) and 1 mL DMSO was then added slowly. The reaction mixture was stirred for 7 hours at room temperature. The reaction mixture was pour into water and extracted 3x with EtOAc. The combined organic layers washed 3x with brine, dried over MgSO_4 , and filtered. Multiple attempts to purify the product via column chromatography and recrystallization from toluene or ethanol were unsuccessful. ^{19}F and ^1H NMR analysis of the impure product indicated a $\sim 3:1:1$ ratio of product: $\text{diCH}_2\text{C}_6\text{H}_5$: $\text{diCH}_2\text{C}_6\text{F}_5$. Potential purification of the product could be achieved via preparatory HPLC, however, this was not attempted.

NMR Spectra.

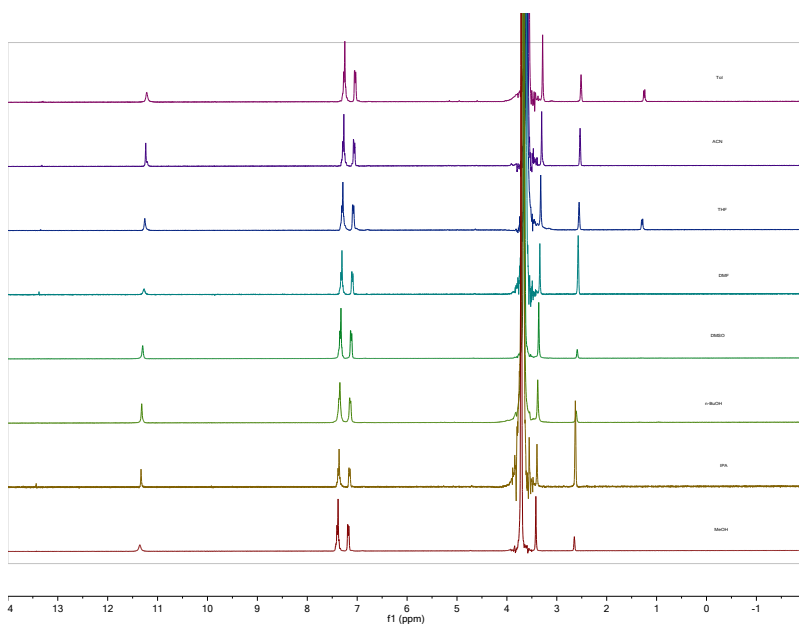


Figure B.1. ^1H NMR spectrum of isolated 5,5'-diphenylbarbituric acid from solvent screening.

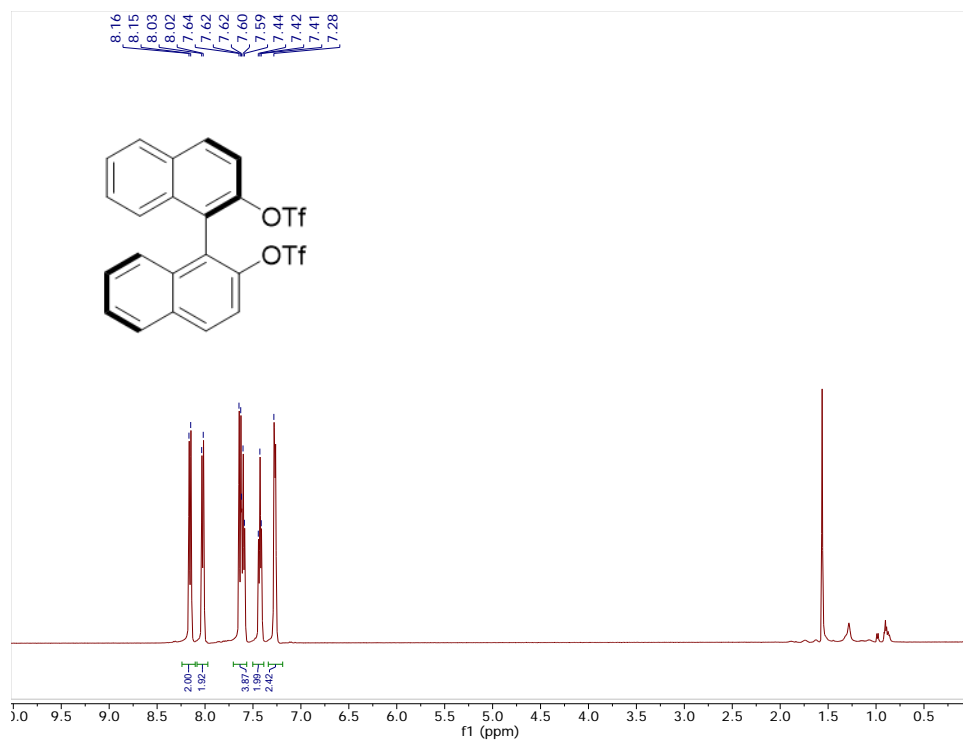


Figure B.2. ¹H (500 MHz) NMR spectrum of (*R*)-I in CDCl₃.

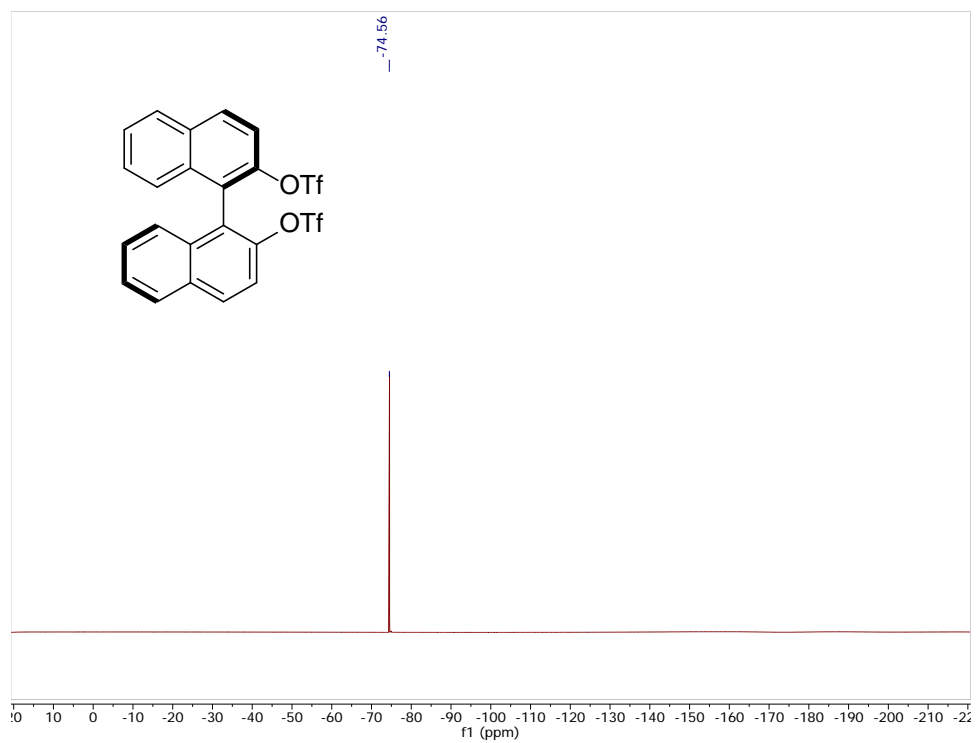


Figure B.3. ¹⁹F (471 MHz) NMR spectrum of (*R*)-I in CDCl₃.

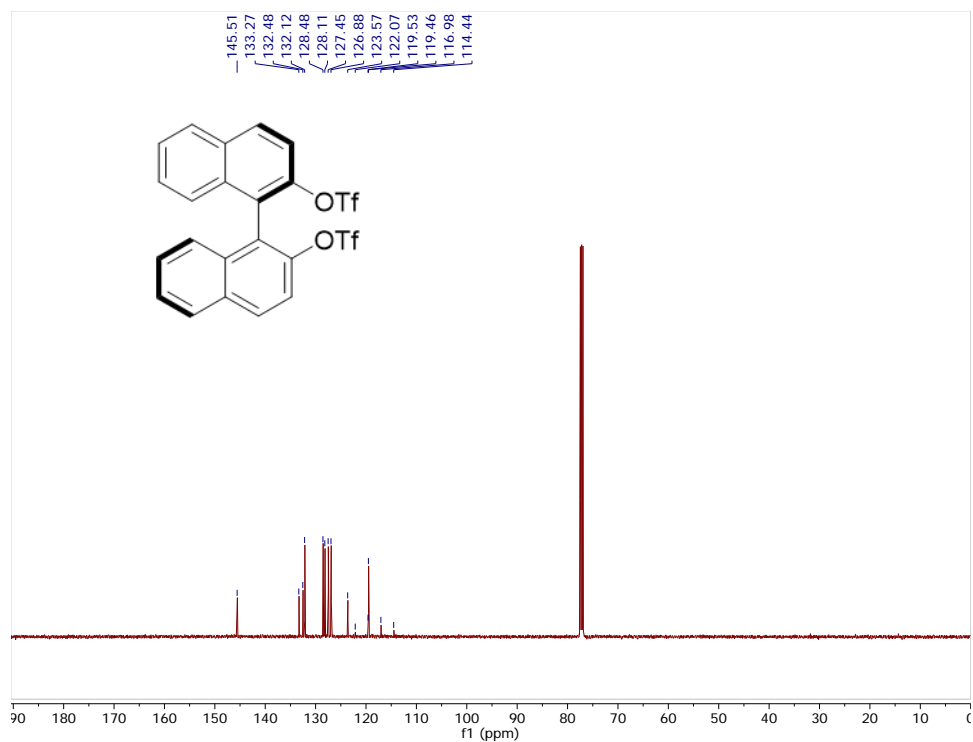


Figure B.4. $^{13}\text{C}\{^1\text{H}\}$ (126 MHz) NMR spectrum of (*R*)-I in CDCl_3 .

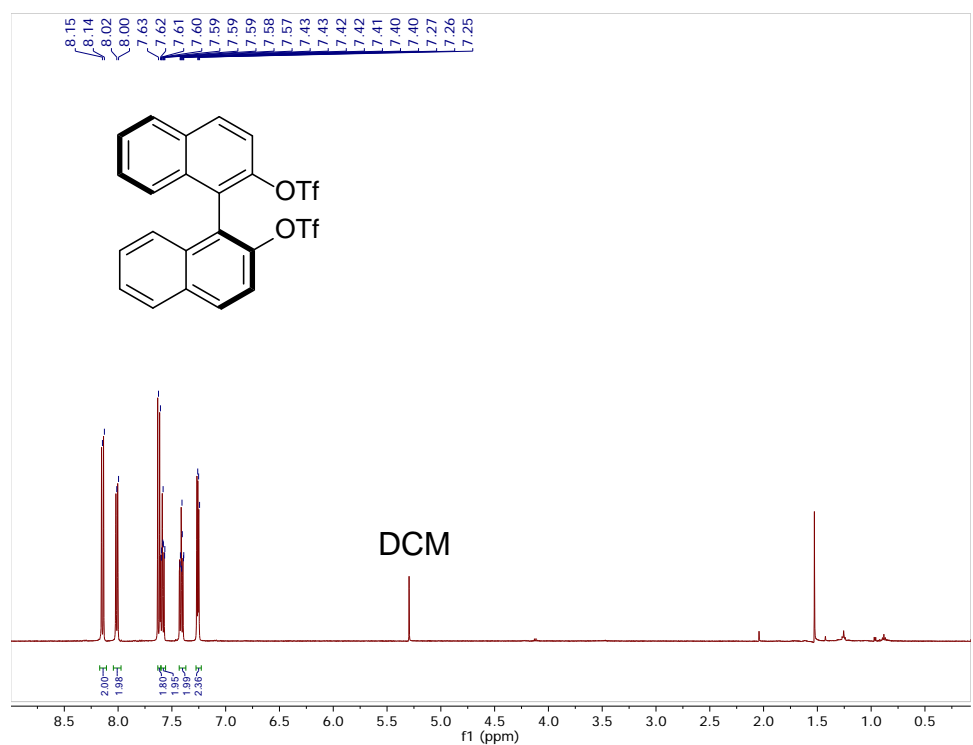


Figure B.5. ^1H (500 MHz) NMR spectrum of (*S*)-I in CDCl_3 .

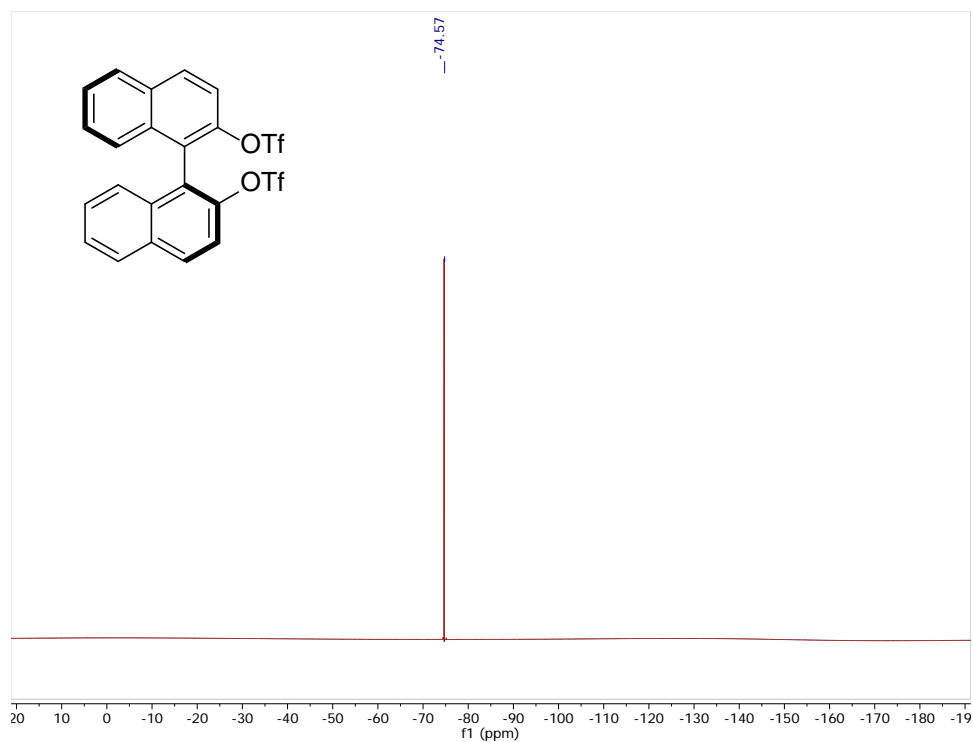


Figure B.6. ^{19}F ((471 MHz) NMR spectrum of (S)-I in CDCl_3 .

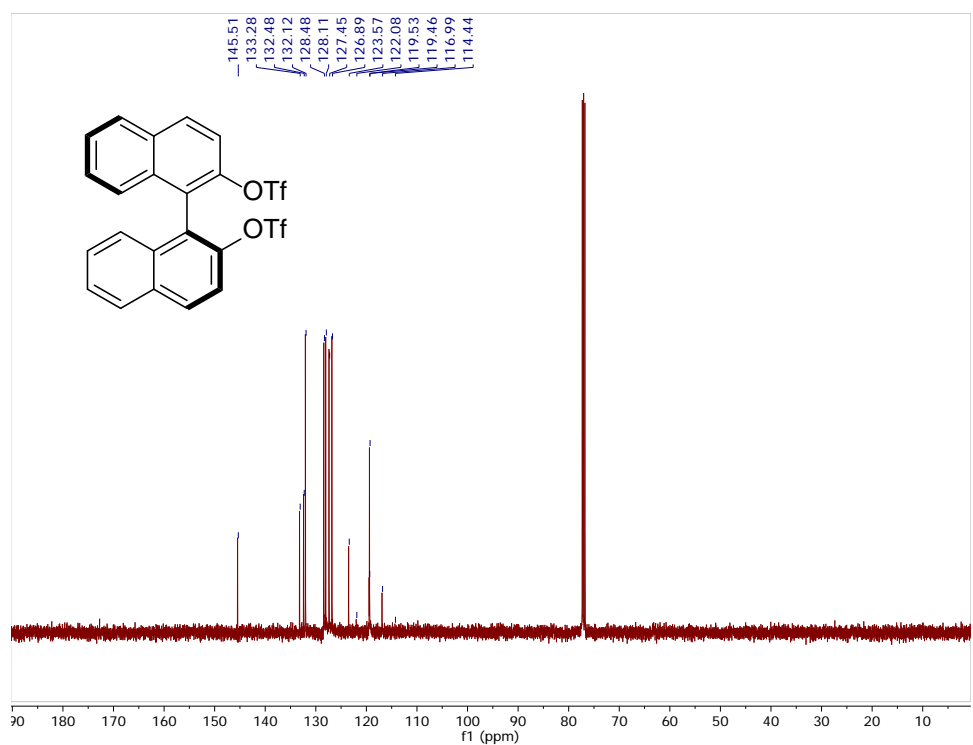


Figure B.7. $^{13}\text{C}\{^1\text{H}\}$ (126 MHz) NMR spectrum of (S)-I in CDCl_3 .

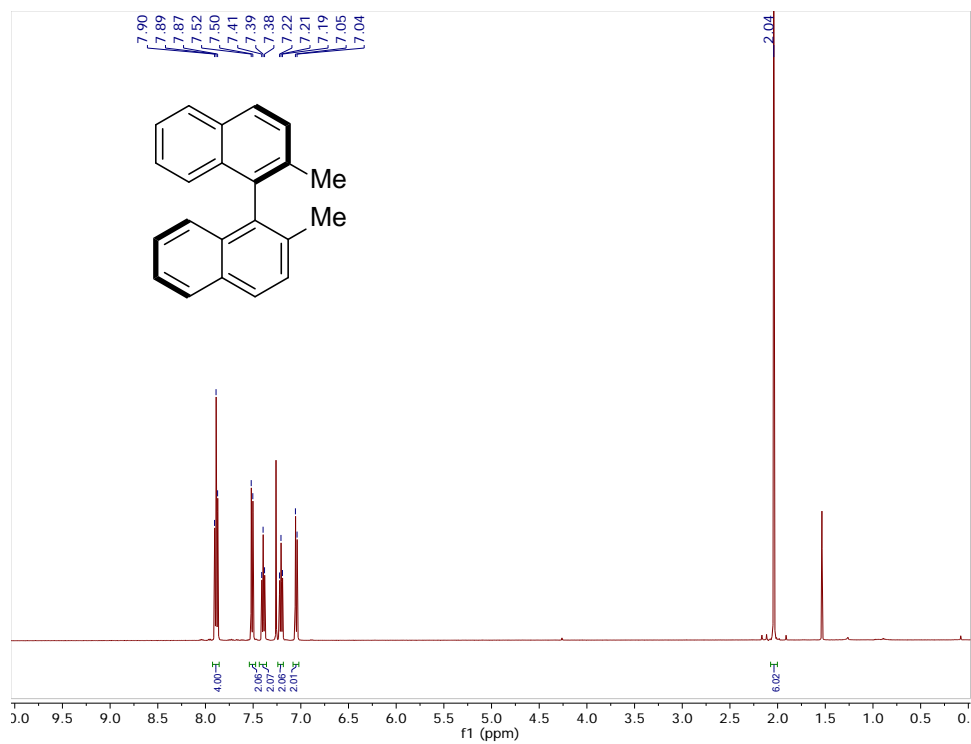


Figure B.8. ¹H (500 MHz) NMR spectrum of (*R*)-II in CDCl₃.

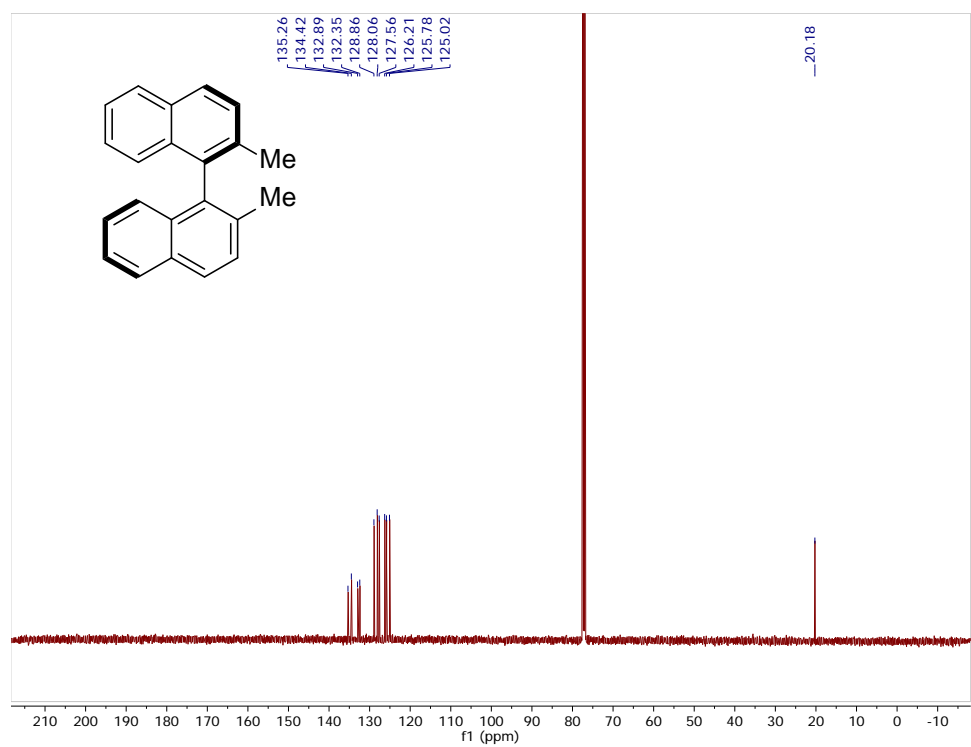


Figure B.9. ¹³C (126 MHz) NMR spectrum of (*R*)-II in CDCl₃.

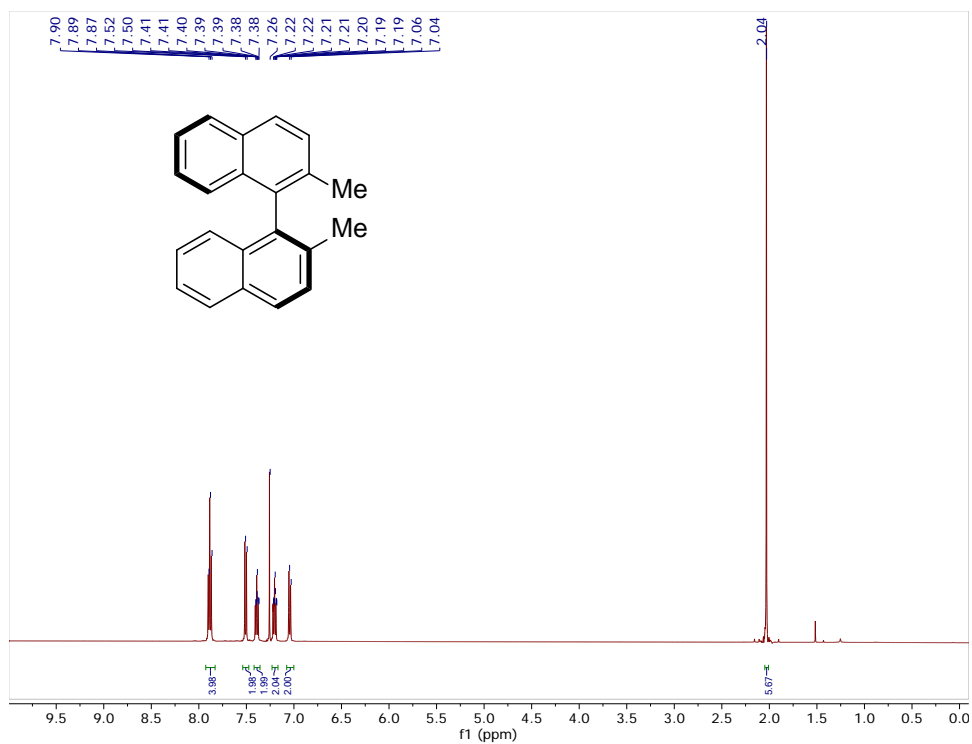


Figure B.10. ^1H (500 MHz) NMR spectrum of (*S*)-II in CDCl_3 .

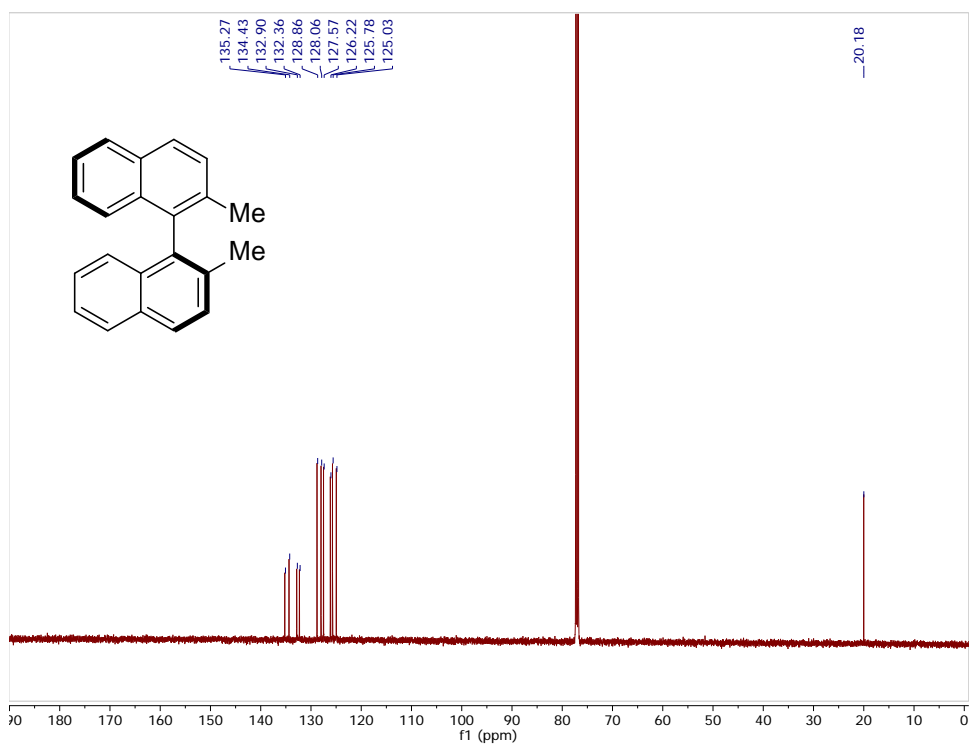


Figure B.11. ^{13}C (126 MHz) NMR spectrum of (*S*)-II in CDCl_3 .

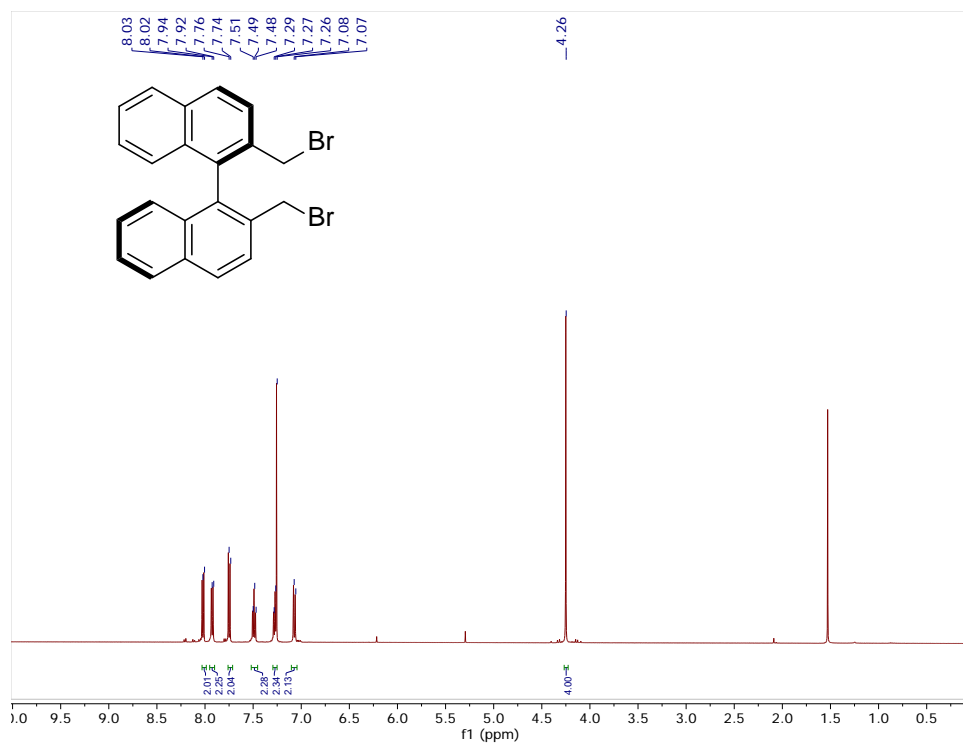


Figure B.12. ^1H (500 MHz) NMR spectrum of (*R*)-III in CDCl_3 .

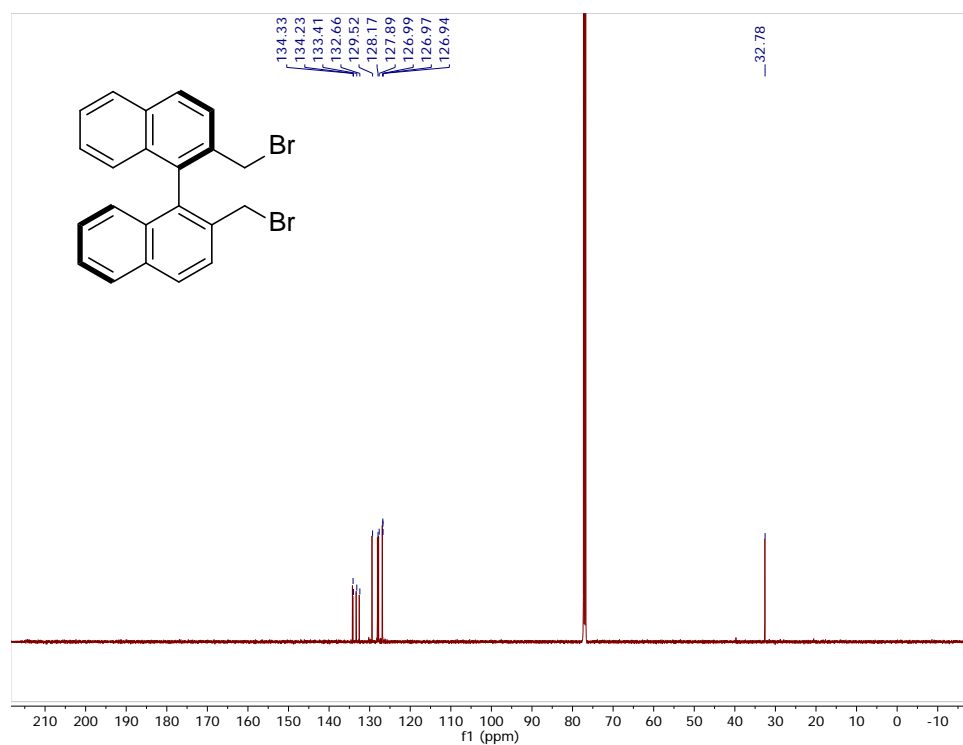


Figure B.13. $^{13}\text{C}\{^1\text{H}\}$ (126 MHz) NMR spectrum of (*R*)-III in CDCl_3 .

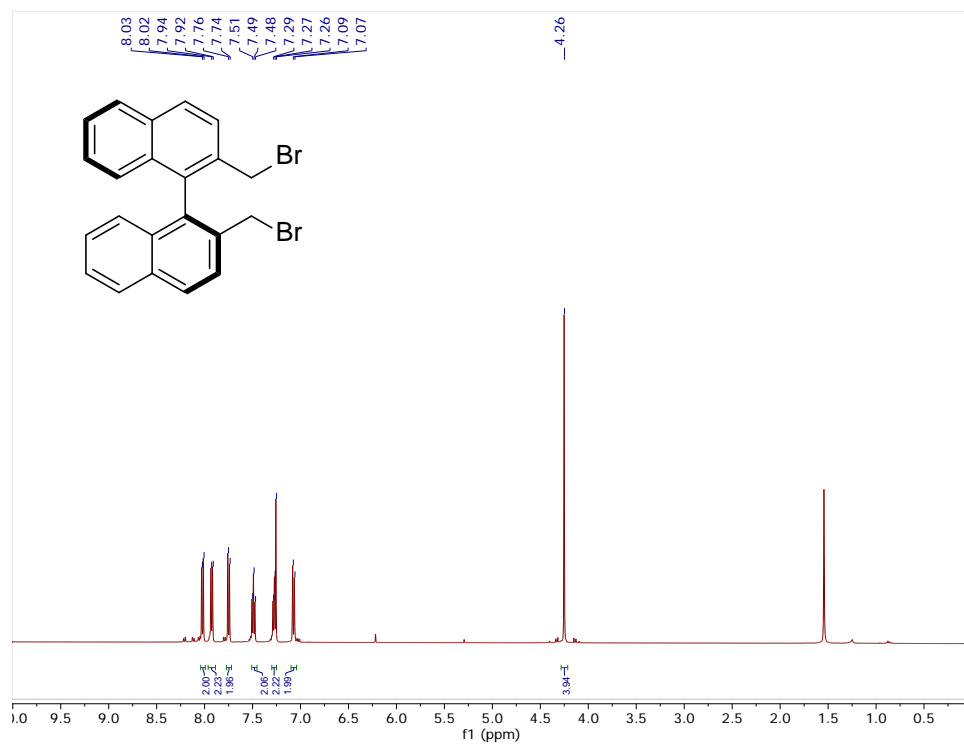


Figure B.14. ^1H (500 MHz) NMR spectrum of (*S*)-III in CDCl_3 .

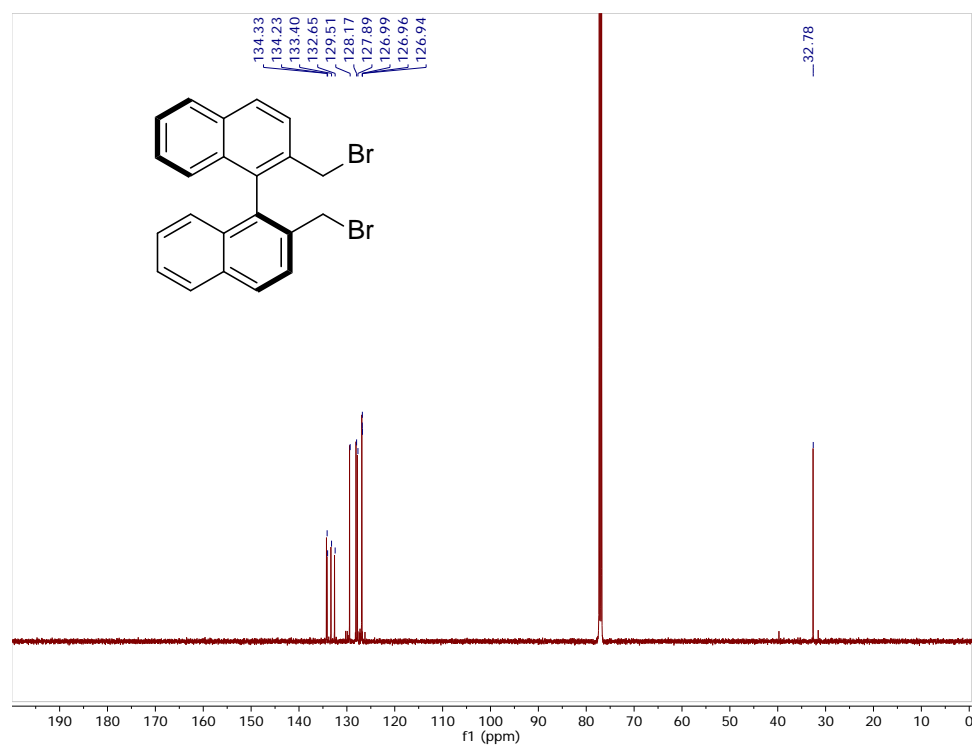


Figure B.15. $^{13}\text{C}\{^1\text{H}\}$ (126 MHz) NMR spectrum of (*S*)-III in CDCl_3 .

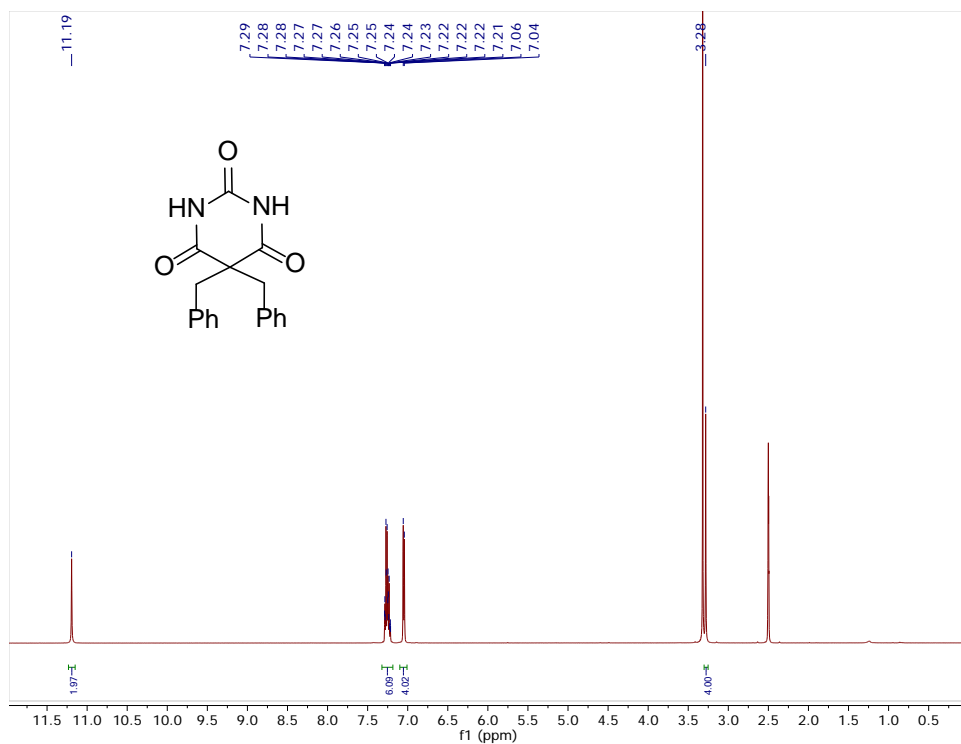


Figure B.16. ^1H (500 MHz) NMR spectrum of 5,5'-diphenyl barbituric acid in d_6 -DMSO.

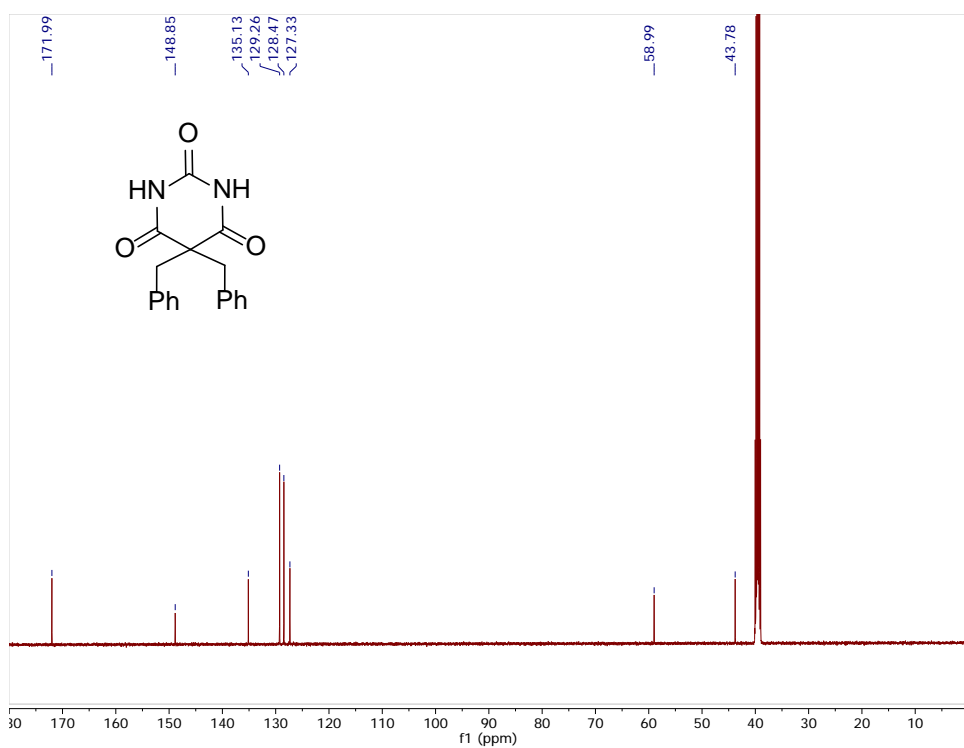


Figure B.17. $^{13}\text{C}\{^1\text{H}\}$ (126 MHz) NMR spectrum of 5,5'-diphenyl barbituric acid in d_6 -DMSO.

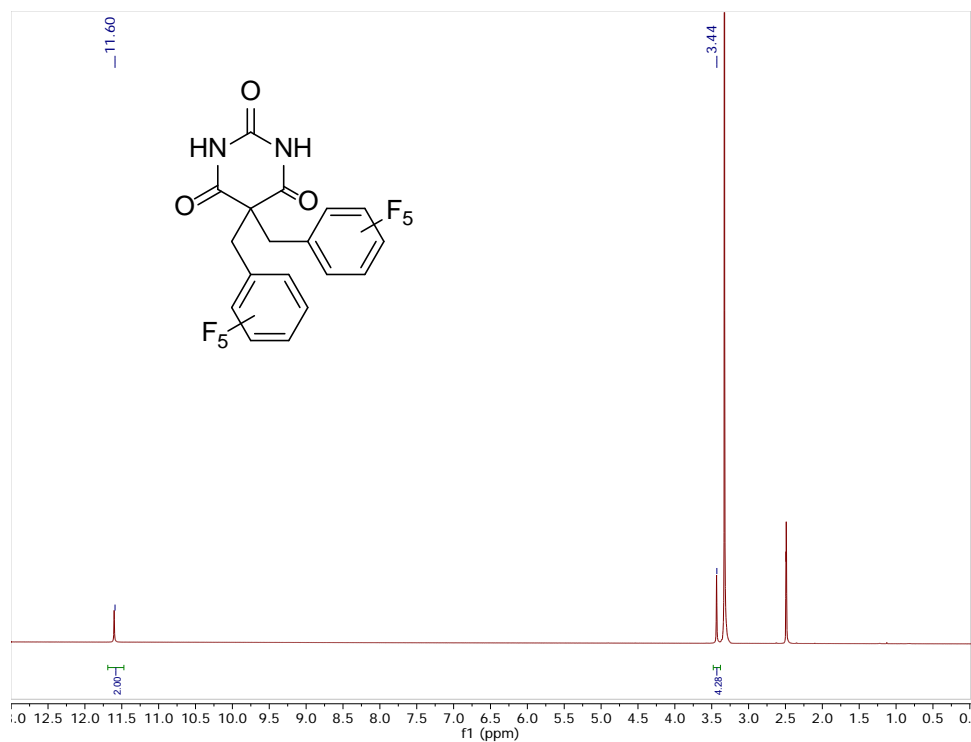


Figure B.18. ^1H (500 MHz) NMR spectrum of 5,5'-bis((perfluorophenyl)methyl) barbituric acid in d_6 -DMSO.

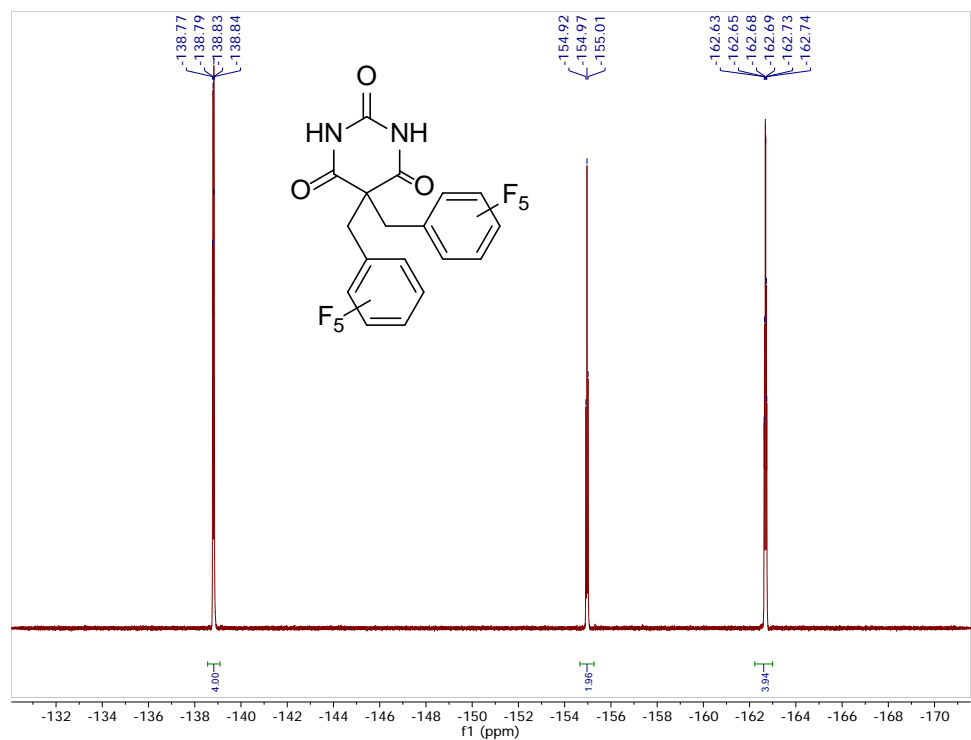


Figure B.19. ^{19}F (471 MHz) NMR spectrum of 5,5'-bis((perfluorophenyl)methyl) barbituric acid in d_6 -DMSO.

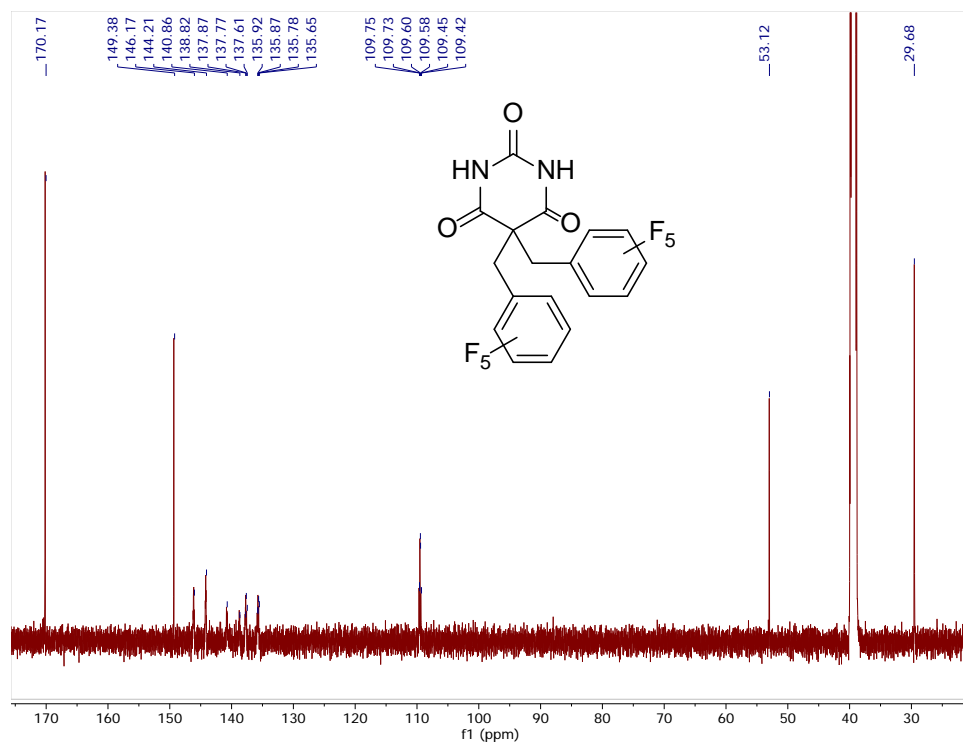


Figure B.20. $^{13}\text{C}\{^1\text{H}\}$ (126 MHz) NMR spectrum of 5,5'-bis((perfluorophenyl)methyl)barbituric acid in d_6 -DMSO.

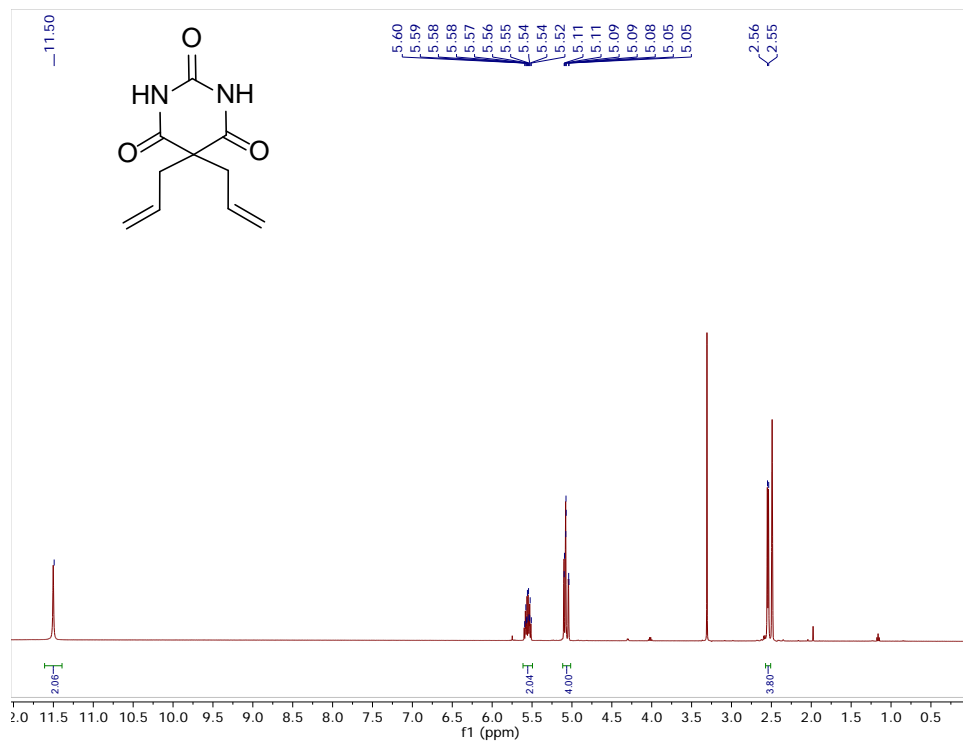


Figure B.21. ^1H (500 MHz) NMR spectrum of 5,5'-diallylbarbituric acid in d_6 -DMSO.

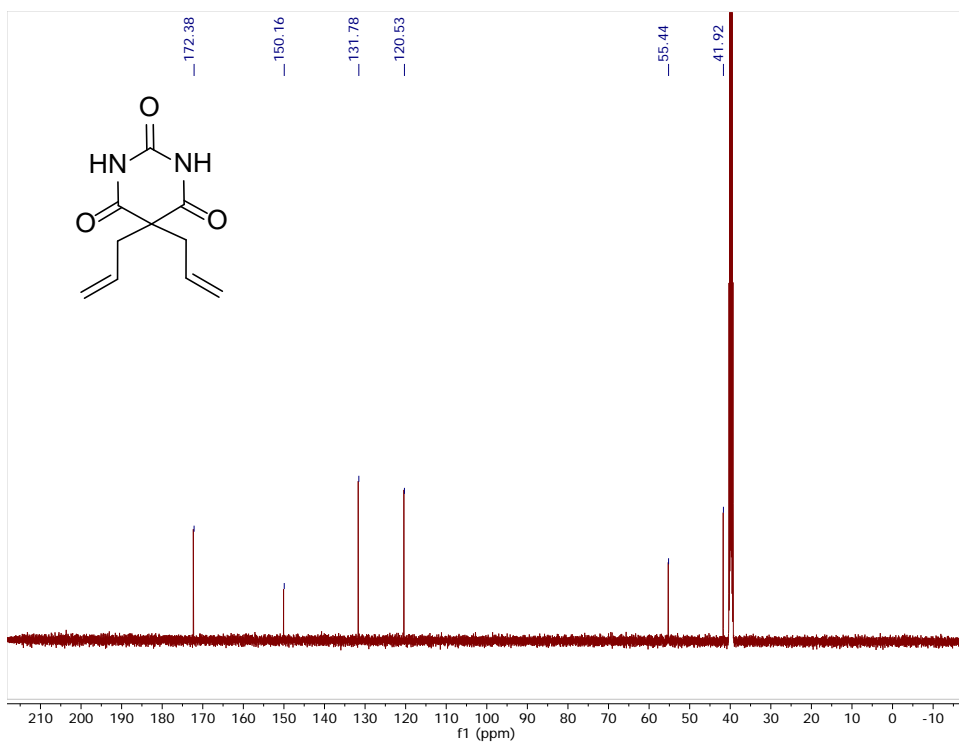


Figure B.22. $^{13}\text{C}\{^1\text{H}\}$ (126 MHz) NMR spectrum of 5,5'-diallylbarbituric acid in d_6 -DMSO.

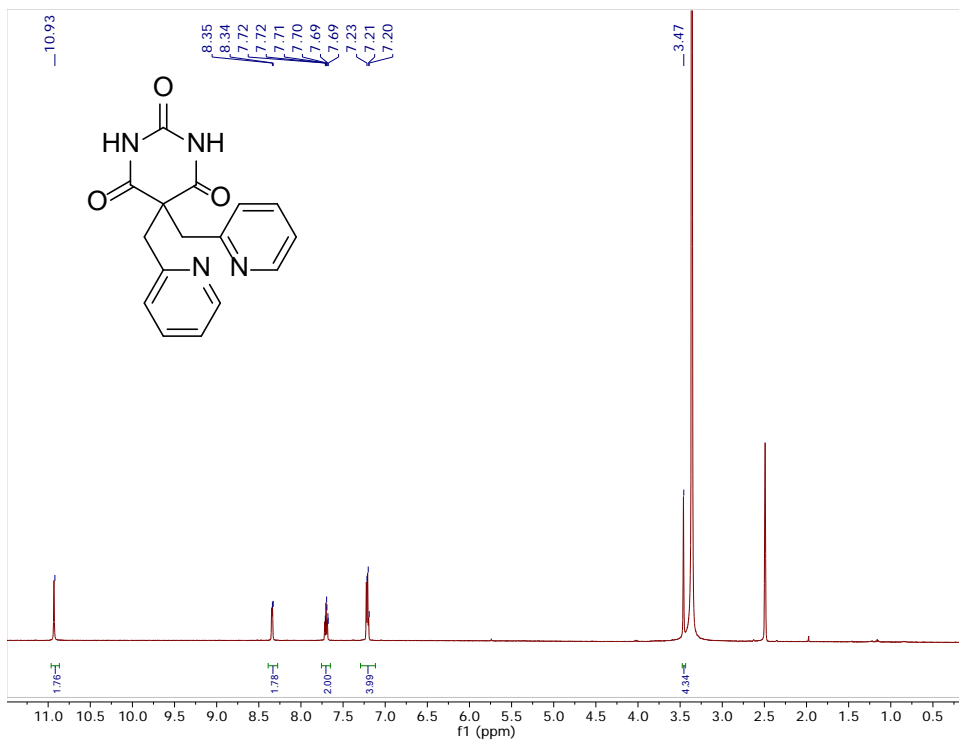


Figure B.23. ^1H (500 MHz) NMR spectrum of 1 in d_6 -DMSO.

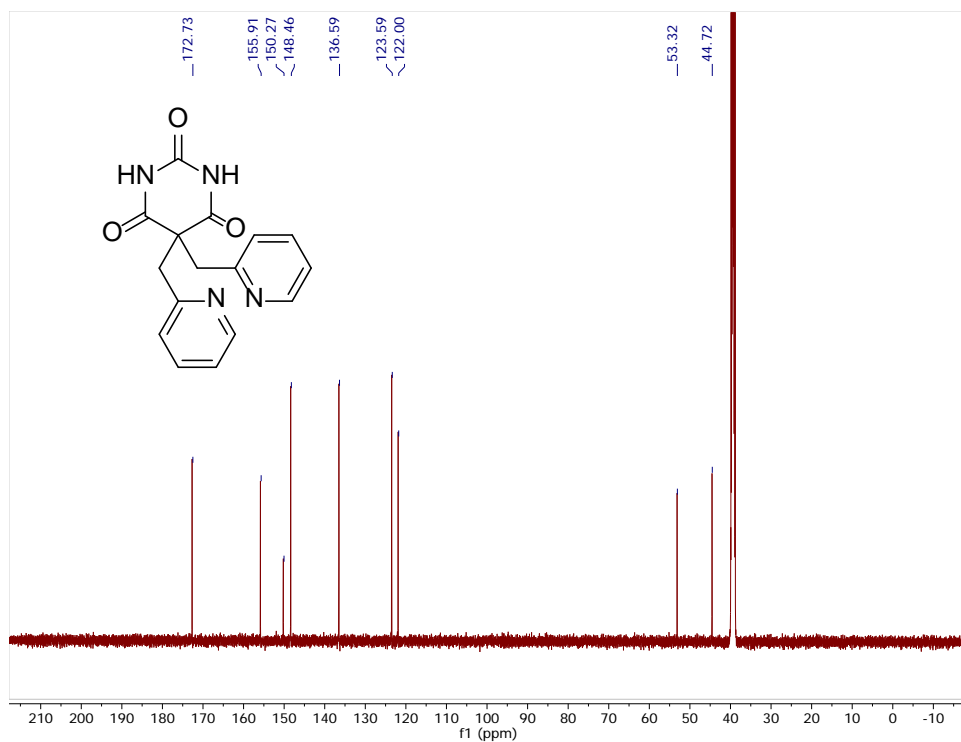


Figure B.24. $^{13}\text{C}\{^1\text{H}\}$ (126 MHz) NMR spectrum of 1 in d_6 -DMSO.

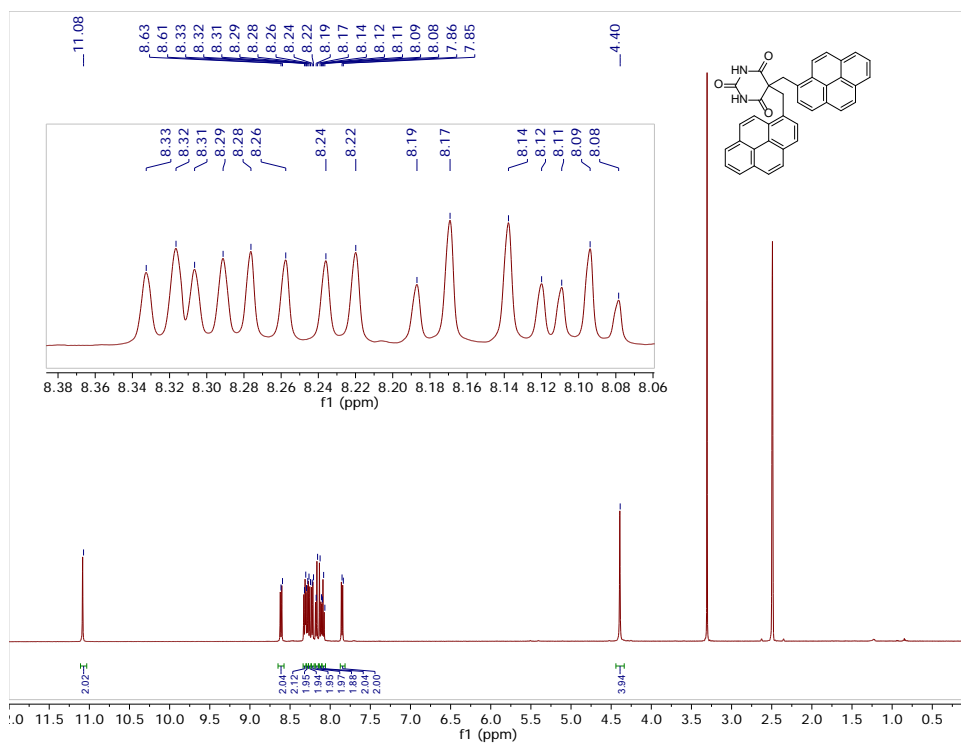


Figure B.25. ^1H (500 MHz) NMR spectrum of 3 in d_6 -DMSO.

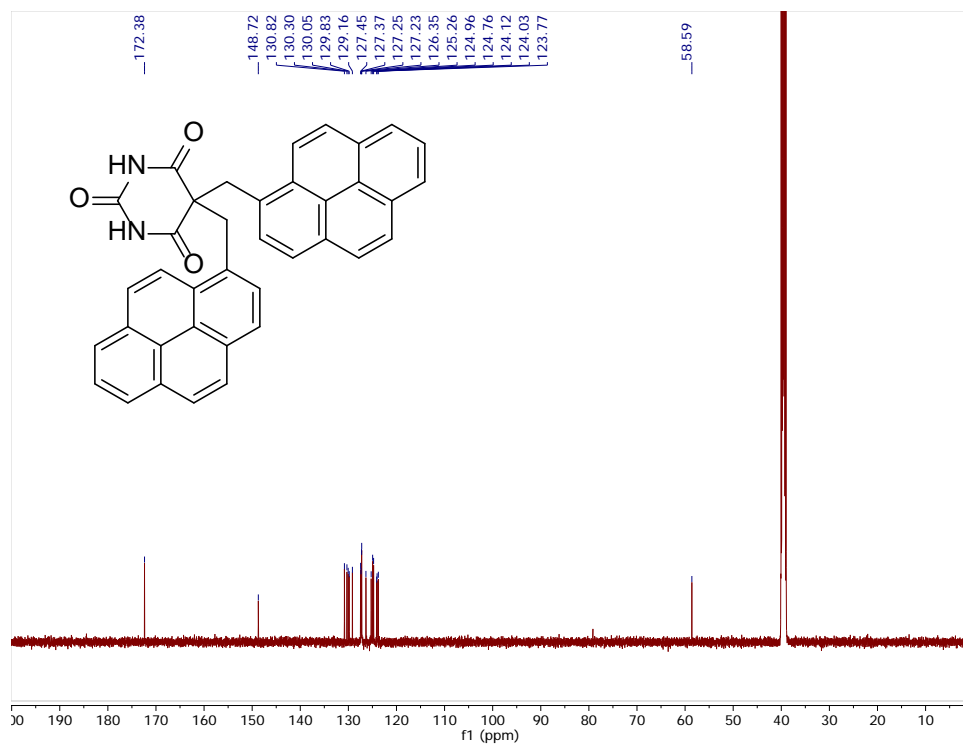


Figure B.26. $^{13}\text{C}\{^1\text{H}\}$ (126 MHz) NMR spectrum of 3 in d_6 -DMSO.

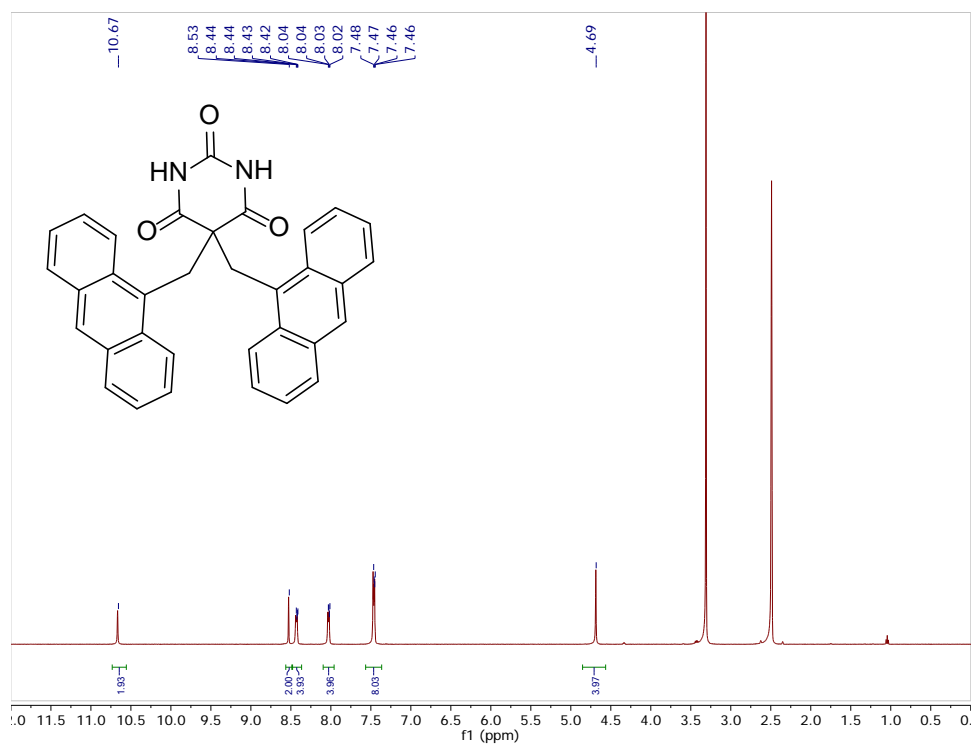


Figure B.27. ^1H (500 MHz) NMR spectrum of 3 in d_6 -DMSO.

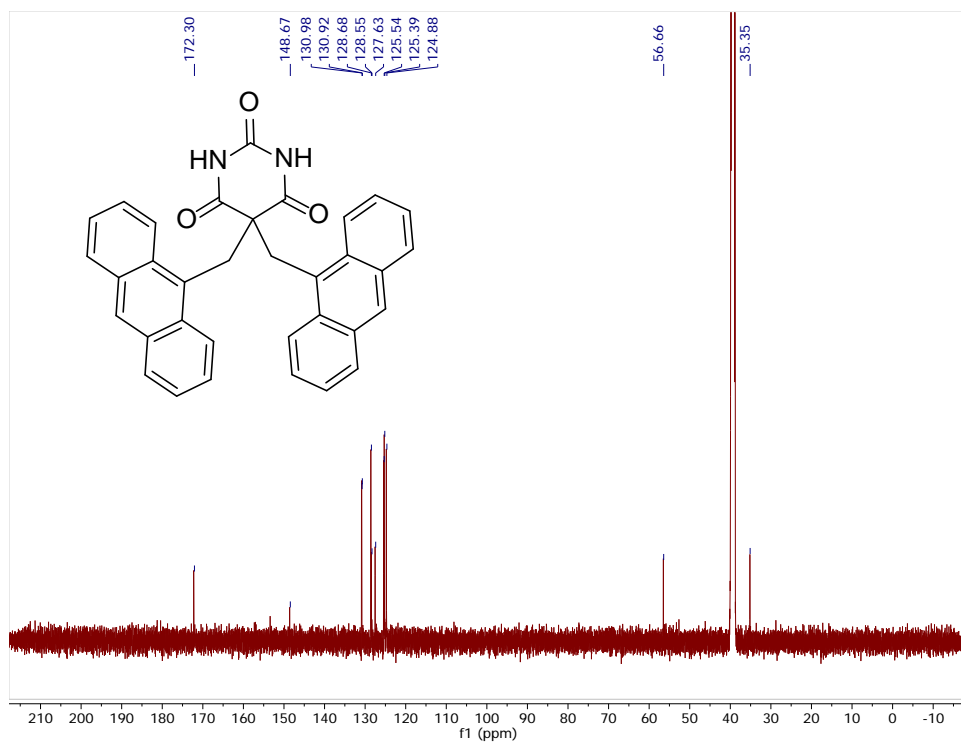


Figure B.28. $^{13}\text{C}\{^1\text{H}\}$ (126 MHz) NMR spectrum of 3 in d_6 -DMSO.

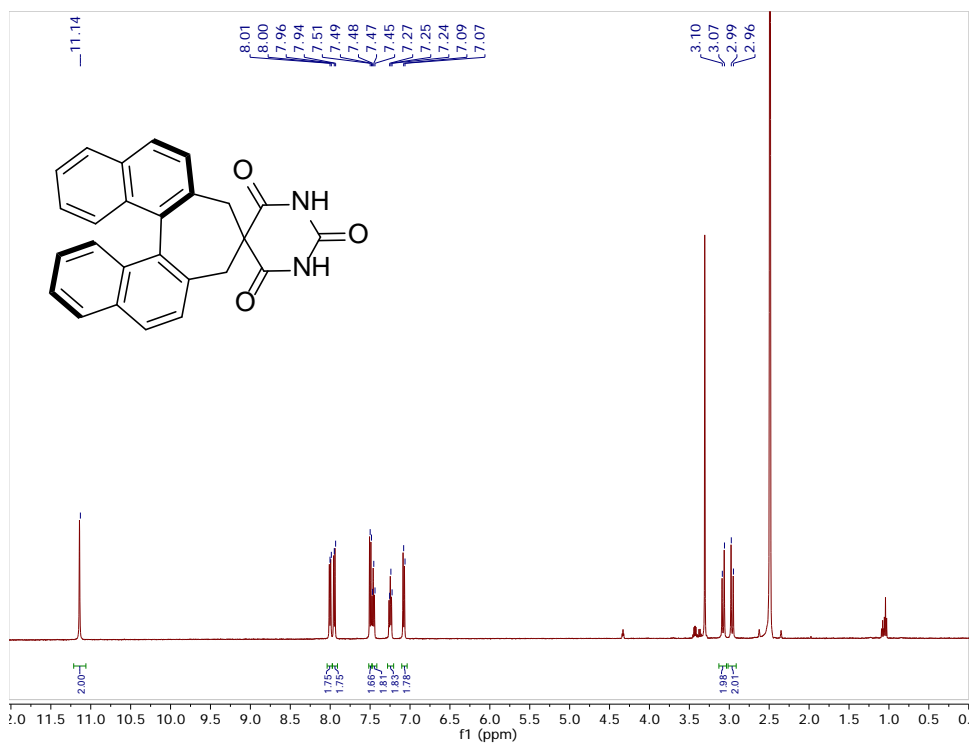


Figure B.29. ^1H (500 MHz) NMR spectrum of 4a in d_6 -DMSO.

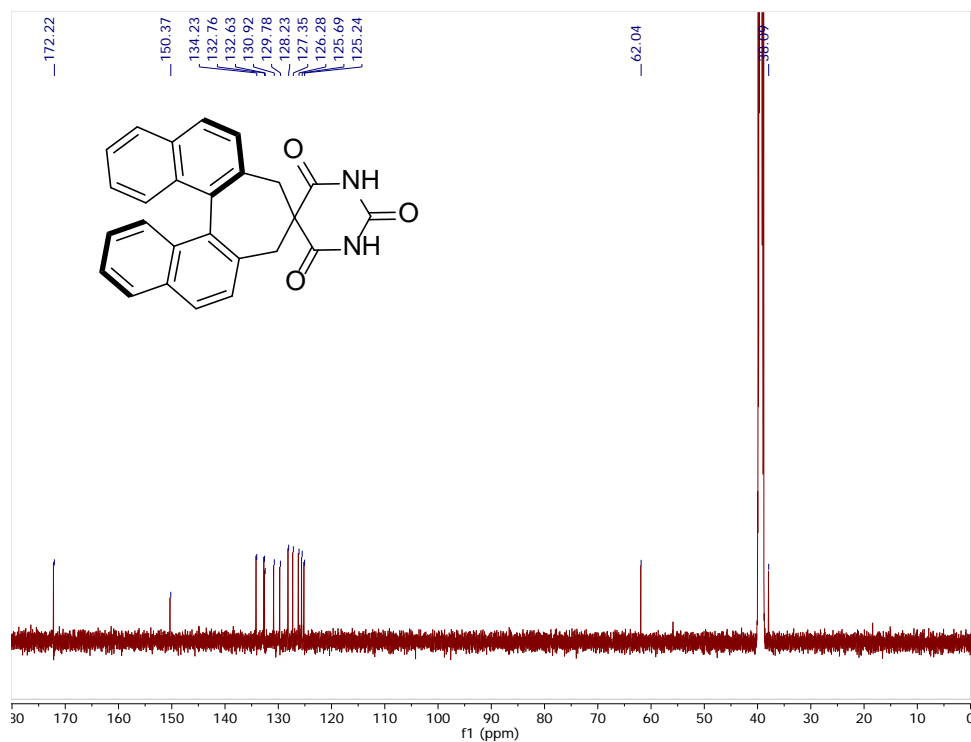


Figure B.30. $^{13}\text{C}\{^1\text{H}\}$ (126 MHz) NMR spectrum of 4a in d_6 -DMSO.

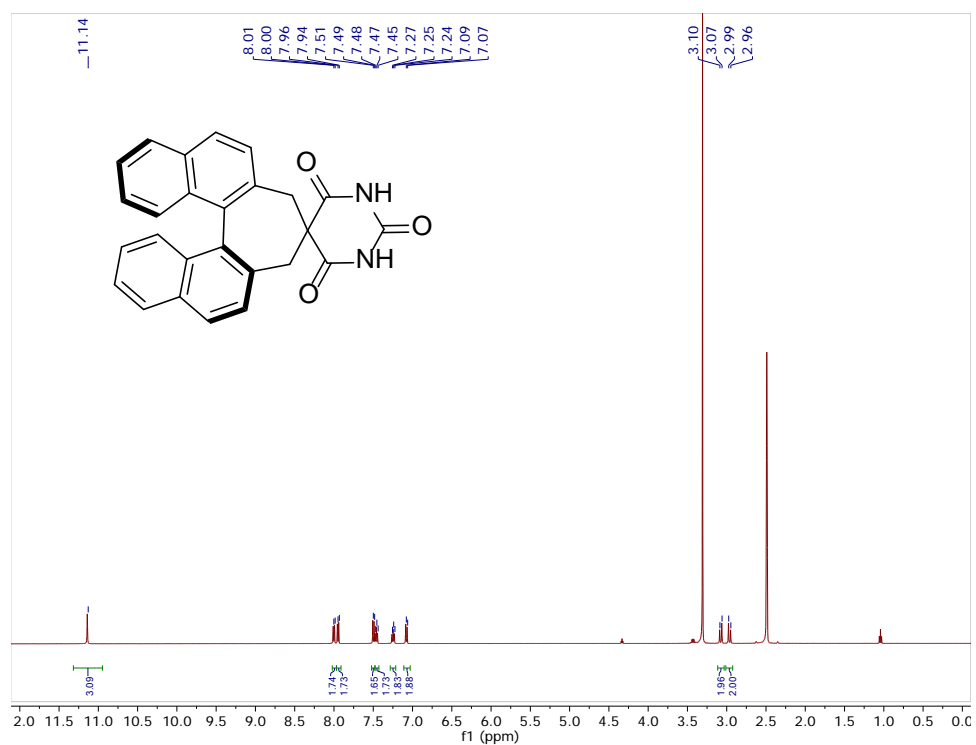


Figure B.31. ^1H (500 MHz) NMR spectrum of 4b in d_6 -DMSO.

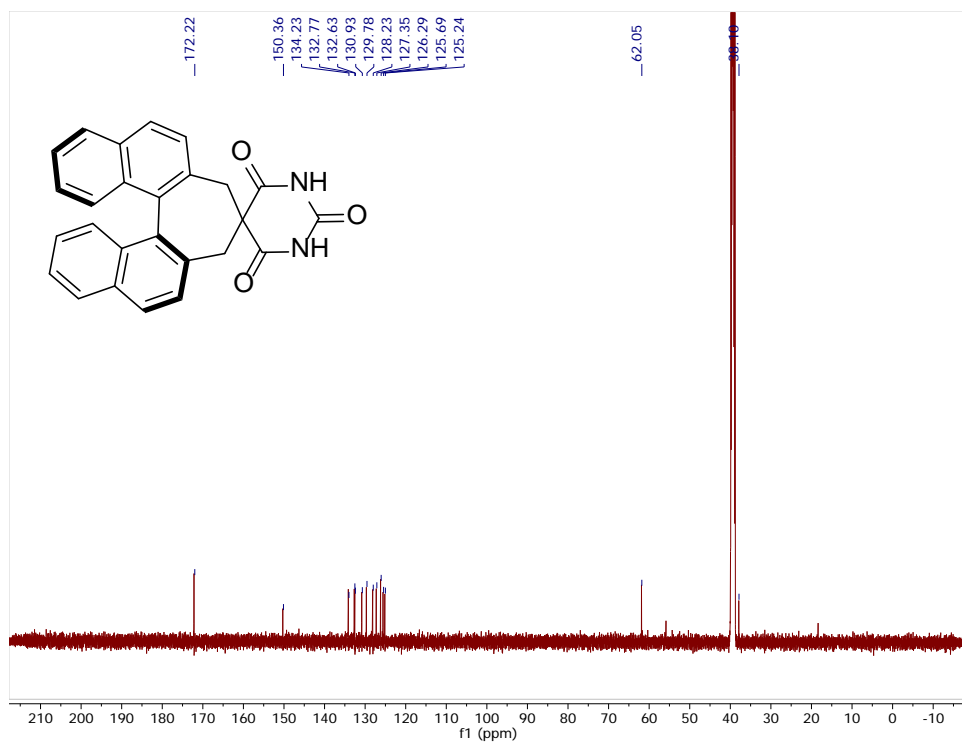


Figure B.32. $^{13}\text{C}\{^1\text{H}\}$ (126 MHz) NMR spectrum of 4b in d_6 -DMSO.

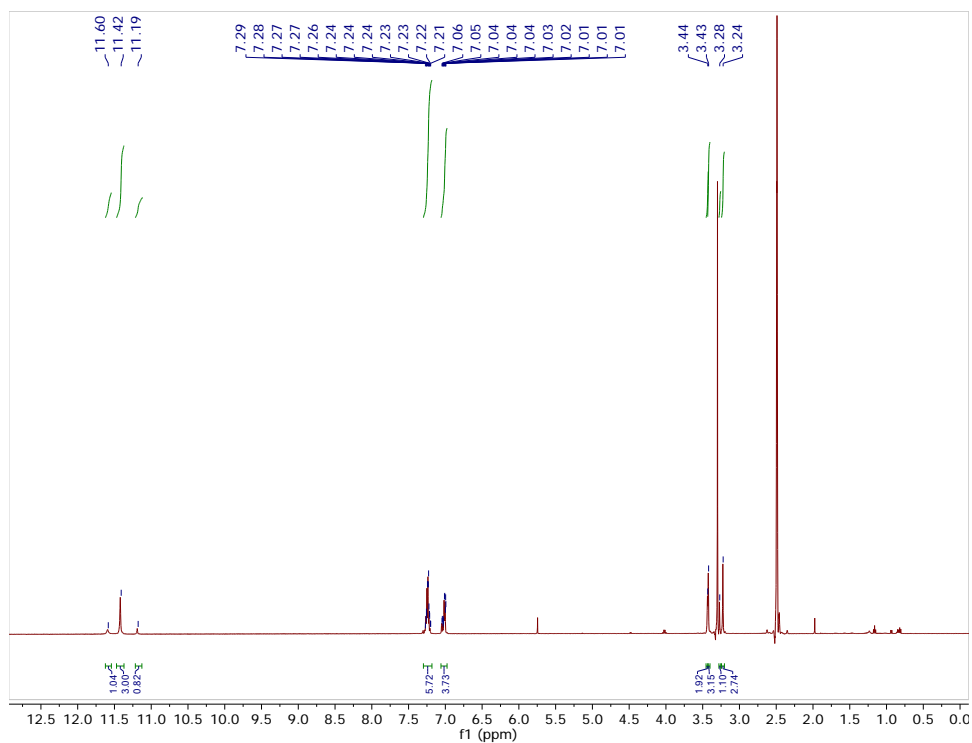


Figure B.33. ^1H (500 MHz) NMR spectrum of compound 5 crude reaction mixture in d_6 -DMSO.

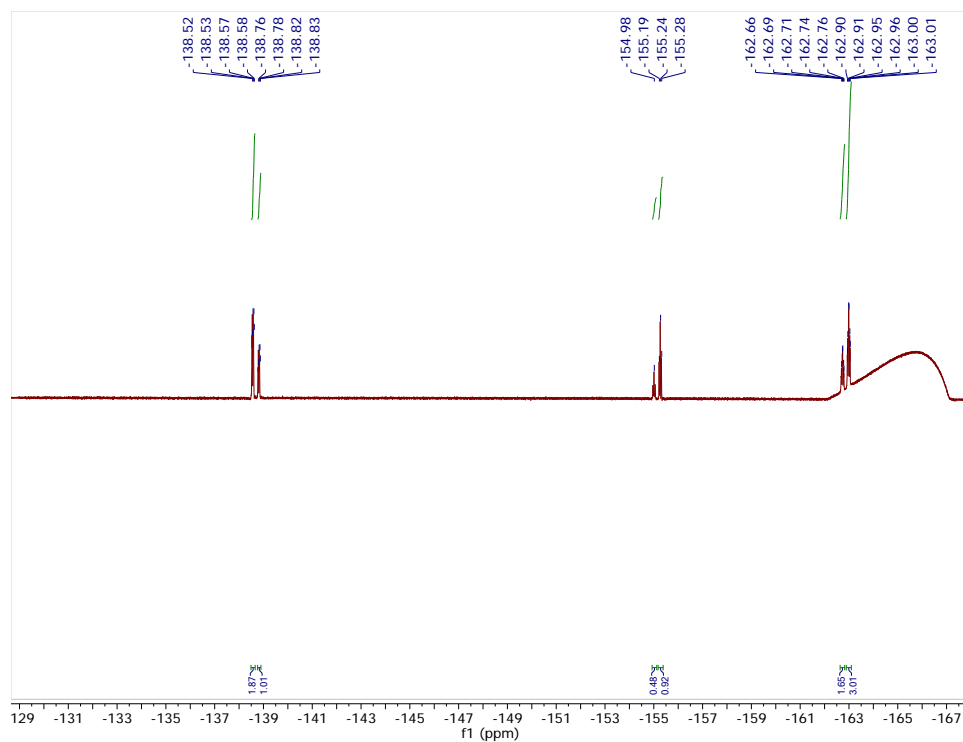


Figure B.34. ^{19}F ((471 MHz) NMR spectrum of compound 5 crude reaction mixture in d_6 -DMSO.

HPLC and X-Ray Bond Length Data

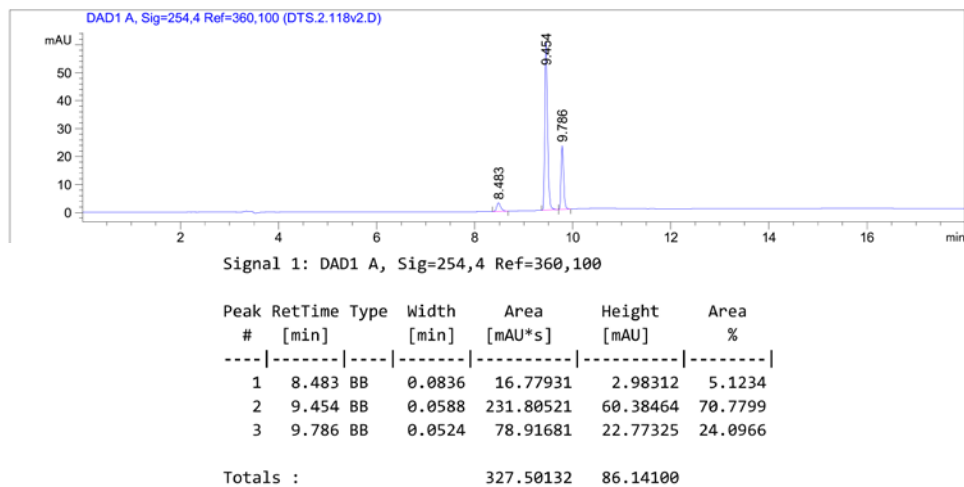


Figure B.35. HPLC trace and integration table of compound 5 crude reaction mixture.

Table B.1. Quantitative structural parameters for X-ray structures of compounds **1-5**. Envelope angle calculated from angle between C(6)N(1)C(2)N(3)C(4) and C(6)C(5)C(4) planes.

Compound	Envelop angle (°)	C-N bond lengths (Å)	C-O bond lengths (Å)
1	16.90	1.365, 1.376, 1.378, 1.368	1.215, 1.210, 1.212
2	0.16	1.367, 1.356, 1.356, 1.367	1.215, 1.223, 1.215
3	32.63	1.366, 1.377, 1.376, 1.378	1.216, 1.212, 1.211
4a	30.52	1.383, 1.365, 1.368, 1.373	1.208, 1.222, 1.211
5	10.11	1.363, 1.377, 1.371, 1.369	1.205, 1.206, 1.210

APPENDIX C

SUPPORTING INFORMATION FOR CHAPTER IV

Appendix C is the supporting information for Chapter IV of this dissertation. It includes the experimental details and additional spectra relevant to the content of Chapter IV.

Experimental Details

General. All commercially-available reagents were used as received. Compounds **1–3** were synthesized as described previously.¹ Compounds **4a–d** were synthesized as described in Chapter III of this dissertation. Anhydrous, deoxygenated solvents were collected from a Pure Process Technologies solvent purification system. Triethylamine was dried and distilled over CaH₂ under nitrogen. CO:H₂ (1:1 v/v) was supplied from Praxair. Reactions were monitored using Merck F₂₅₄ silica gel 60 TLC plates and visualized using UV light or a KMnO₄ stain. Reactions conducted under an inert atmosphere were performed by either using standard Schlenk techniques or a N₂-filled glove box. Chromatographic purification was performed using a Biotage automated flash chromatography purification system or as described. ¹H and ¹³C{¹H} NMR spectra were recorded at the reported frequencies, and chemical shifts are reported in ppm (δ) and referenced to the residual solvent resonance. ³¹P{¹H} chemical shifts are referenced to H₃PO₄. All ¹⁹F spectra were indirectly referenced via the Bruker TopSpin 3.5 software suite to CFCl₃. The following naming conventions were used to describe NMR

couplings: (s) singlet, (d) doublet, (t) triplet, (q) quartet, (dd) doublet of doublets, (m) multiplet, (b) broad. GC-MS analysis was done using a Shimadzu QP2010 SE spectrometer equipped with a SH-RXi-5Sil column.

General Procedure for Hydroformylation of 1-octene. To individual 1-dram vials equipped with stir bars was added Rh(acac)(CO)₂ (0.15 μmol, 100 μM), 20 equivalents of ligand, barbiturate guest (see table XX), and 1-octene (150 μmol, 100 mM). Decane was added (75 μmol, 50 mM) as an internal standard. The individual vials were then loosely capped (this was critical to ensure that evaporation of the solvent was kept to a minimum) and placed inside a Parr reactor. This process was done inside a glovebox to avoid oxygen contamination. The reactor was then removed from the glovebox and pressurized/vented with CO:H₂ (1:1) to 150 PSI (3x). The reactor was pressurized to a final pressure of 150 PSI and added to a preheated oil bath. The catalysts were preformed by stirring at 50 °C for 90 minutes. The reactor was then allowed to cool to the desired temperature and stirred overnight (12-24 hours). Subsequently, the reactions were then allowed to cool to room temperature, the reactor vented, and 100 μL aliquots were taken from the individual trials and analyzed by GC-MS.

Binding Constant Determination. Binding studies were performed in CDCl₃ and were monitored by ¹H NMR spectroscopy at 25 °C. In a typical titration, 10.00 mL of a 1.0 mM barbiturate guest solution was prepared. The guest solution was then divided such that 600 μL was placed into an NMR tube and 1.00 mL was used to create a second solution containing 24 mM host. An initial spectrum of the guest was recorded using the following parameters: nt=16 and d₁=1s, after which aliquots (5-250 μL) of the host

solution were added until minimal changes in the N-H resonance of barbiturate was observed. The resultant curve was fit using a 1:1 model and the K_{assoc} obtained.

Synthesis of Compounds 5–10

3-(Chloromethyl)-*N*-(6-(3,3-dimethylbutanamido)pyridin-2-yl)benzamide (**5a**).

Excess thionyl chloride (5.0 mL, 69 mmol) was added to a scintillation vial containing 3-(Chloromethyl)benzoic acid (1.00 g, 5.87 mmol). Two drops of anhydrous DMF was added to the reaction mixture, heated to 55 °C, and stirred for 1.5 hours. The excess thionyl chloride was removed under vacuum. The resultant residue was dissolved in anhydrous THF (10 mL) and slowly added to a solution of **1** (1.16 g, 5.60 mmol) and anhydrous triethylamine (940 μ L, 6.74 mmol) in THF (50 mL) at 0 °C. The resulting turbid mixture was warmed to room temperature and stirred overnight. The mixture was filtered and the filtrate concentrated onto silica gel. The crude product was purified via column chromatography (SiO₂, 1:3 EtOAc:Hex, R_f = 0.31) to yield a white solid (1.847 g, 92%). ¹H NMR (500 MHz, Chloroform-*d*) δ : 8.22 (s, 1H), 8.06 (d, J = 8.0 Hz, 1H), 7.98 (d, J = 8.0 Hz, 1H), 7.92 (s, 1H), 7.84 (dt, J = 7.7, 1.5 Hz, 1H), 7.77 (t, J = 8.1 Hz, 1H), 7.60 (dt, J = 7.7, 1.4 Hz, 1H), 7.53 (s, 1H), 7.51 (t, J = 7.7 Hz, 2H), 4.65 (s, 2H), 2.25 (s, 2H), 1.12 (s, 9H). ¹³C NMR (126 MHz, CDCl₃) δ : 170.35, 164.95, 149.69, 149.54, 141.11, 138.59, 134.98, 132.46, 129.52, 127.45, 127.12, 109.93, 109.75, 51.99, 45.58, 31.52, 29.96.

4-(Chloromethyl)-*N*-(6-(3,3-dimethylbutanamido)pyridin-2-yl)benzamide (**5b**).

Excess thionyl chloride (5.0 mL, 69 mmol) was added to a scintillation vial containing 4-(Chloromethyl)benzoic acid (1.00 g, 5.87 mmol). Two drops of anhydrous DMF was

added to the reaction mixture, heated to 55 °C, and stirred for 1.5 hours. The excess thionyl chloride was removed under vacuum. The resultant residue was dissolved in anhydrous THF (10 mL) and slowly added to a solution of **1** (1.16 g, 5.60 mmol) and anhydrous triethylamine (935 µL, 6.70 mmol) in THF (50 mL) at 0 °C. The resulting turbid mixture was warmed to room temperature and stirred overnight. The mixture was filtered and the filtrate concentrated onto silica gel. The crude product was purified via column chromatography (SiO₂, 1:3 EtOAc:Hex, R_f = 0.29) to yield a white solid (1.825 g, 91%). ¹H NMR (500 MHz, Chloroform-*d*) δ: 8.21 (s, 1H), 8.05 (d, *J* = 8.1 Hz, 1H), 7.98 (d, *J* = 8.1 Hz, 1H), 7.89 (d, *J* = 8.3 Hz, 2H), 7.76 (t, *J* = 8.1 Hz, 1H), 7.53 (d, *J* = 8.1 Hz, 3H), 4.64 (s, 2H), 2.25 (s, 2H), 1.12 (s, 9H). ¹³C NMR (126 MHz, CDCl₃) δ: 170.34, 164.89, 149.68, 149.57, 141.85, 141.09, 134.28, 129.12, 127.72, 109.90, 109.74, 51.98, 45.36, 31.52, 29.96.

N-(6-(3,3-Dimethylbutanamido)pyridin-2-yl)-3-((diphenylphosphino)methyl)benzamide (**6a**). The following compound was prepared inside a N₂-filled glovebox. **5a** (0.998 g, 1.13 mmol) and CuCl (27.1 mg, 2.74 mmol) were dissolved in 5 mL anhydrous, deoxygenated THF (25 mL). Diphenylphosphine (0.519 g, 2.77 mmol) in anhydrous, deoxygenated THF (5 mL) was then added to the solution of **6a** followed by NaOSiMe (2.8 mL, 2.8 mmol, 1M in THF) to produce a yellow solution with some precipitate present. The mixture was allowed to stir overnight at room temperature. The solvent was then removed via vacuum followed by the addition of DCM (25 mL). The insoluble NaCl was then filtered and the filtrate concentrated. The crude product was purified using a plug of silica eluting with DCM to yield the final product as a white solid (0.725 g, 51%). ¹H NMR (500 MHz, Chloroform-*d*) δ: 8.01 (d, *J*

= 8.1 Hz, 1H), 7.93 (d, $J = 8.1$ Hz, 1H), 7.72 (t, $J = 8.1$ Hz, 1H), 7.65 (s, 1H), 7.47 (s, 0H), 7.42 – 7.21 (m, 10H), 7.28–7.24 (m, 1H), 7.17 (d, $J = 6.9$ Hz, 1H), 3.45 (s, 2H), 2.26 (s, 2H), 1.10 (s, 9H). ^{13}C NMR (126 MHz, Chloroform-*d*) δ : 138.52 (d, $J = 8.1$ Hz), 137.71 (d, $J = 14.8$ Hz), 133.38, 133.06 (d, $J = 18.5$ Hz), 129.16, 128.94, 128.63 (d, $J = 6.5$ Hz), 127.96, 125.19. ^{31}P NMR (202 MHz, Chloroform-*d*) δ : -9.00.

N-(6-(3,3-Dimethylbutanamido)pyridin-2-yl)-4-((diphenylphosphino)methyl)benzamide (**6b**). The following compound was prepared inside a N_2 -filled glovebox. **5a** (01.00 g, 2.78 mmol) and CuCl (27.1 mg, 2.74 mmol) were dissolved in 5 mL anhydrous, deoxygenated THF (25 mL). Diphenylphosphine (0.5223 g, 2.80 mmol) in anhydrous, deoxygenated THF (5 mL) was then added to the solution of **6a** followed by NaOSiMe (2.8 mL, 2.8 mmol, 1M in THF) to produce a yellow solution with some precipitate present. The mixture was allowed to stir overnight at room temperature. The solvent was then removed via vacuum followed by the addition of DCM (25 mL). The insoluble NaCl was then filtered and the filtrate concentrated. The crude product was purified using a plug of silica eluting with DCM to yield the final product as a white solid (0.723 g, 51%). ^1H NMR (500 MHz, Chloroform-*d*) δ : 8.17 (s, 1H), 8.05 (d, $J = 8.1$ Hz, 1H), 7.94 (d, $J = 8.6$ Hz, 1H), 7.75 (q, $J = 8.1$ Hz, 1H), 7.75 (s, 1H), 7.42 – 7.30 (m, 10H), 7.13 (d, $J = 7.0$ Hz, 2H), 3.47 (s, 2H), 2.27 (s, 2H), 1.11 (s, 9H). ^{13}C NMR (126 MHz, Chloroform-*d*) δ : 137.68 (d, $J = 15.2$ Hz), 133.03 (d, $J = 18.7$ Hz), 129.92 (d, $J = 6.4$ Hz), 129.13, 128.64 (d, $J = 6.7$ Hz), 127.36. ^{31}P NMR (202 MHz, Chloroform-*d*) δ : -8.67.

cis- PtL_2Cl_2 (L = **6a**) (**7a**). In an inert atmosphere, a solution of **6a** (104 mg, 204 μmol) in CH_2Cl_2 (2 mL) was added dropwise to a stirring solution of $\text{Pt}(\text{COD})\text{Cl}_2$ (38.2

mg, 102 μmol) in CH_2Cl_2 (3 mL). The reaction was stirred at room temperature for two hours, after which the solvent was removed under vacuum (outside of the glovebox). The resulting solids were triturated three times with hexanes, in air, and filtered to obtain **7a** as an off white solid (107 mg, 85%). ^{31}P NMR (202 MHz, Chloroform-*d*) δ : ^1H NMR (500 MHz, Chloroform-*d*) δ : 8.32 (s, 2H), 8.02 (s, 2H), 7.99 (d, $J = 8.0$ Hz, 2H), 7.96 (d, $J = 8.0$ Hz, 2H), 7.92 (d, $J = 7.6$ Hz, 2H), 7.78 (s, 2H), 7.73 (t, $J = 8.1$ Hz, 2H), 7.31 – 7.16 (m, 10H), 7.07 (t, $J = 9.0$ Hz, 8H), 6.97 (t, $J = 6.8$ Hz, 8H), 4.15 (d, $J = 11.5$ Hz, 4H), 2.25 (s, 4H), 1.08 (s, 18H). ^{13}C NMR (126 MHz, Chloroform-*d*) δ : 170.78, 164.69, 149.95, 149.55, 140.83, 134.91, 134.18, 134.03 – 133.62 (m), 131.52, 129.15, 128.98, 128.30 – 128.04 (m), 109.90, 109.54, 51.64, 31.50, 29.96.

N-(6-Aminopyridin-2-yl)-2-phenylacetamide (**8a**). To a flame-dried flask containing 2,6-diaminopyridine (0.776 g, 7.10 mmol) in THF (50 mL, anhydrous) at 0 $^\circ\text{C}$ was added phenylacetyl chloride (1.0 mL, 7.6 mmol). The reaction mixture was allowed to warm to room temperature and stirred overnight. The reaction was then diluted with ethyl acetate and washed with sat. NaHCO_3 (aq) (3x). The organic layer was then washed with brine (3x), dried over MgSO_4 , filtered, and the filtrate concentrated. The crude product was purified using column chromatography eluting with 7:1 DCM:EtOAc to yield the final product as a white solid (0.540 g, 33%). ^1H NMR (500 MHz, Chloroform-*d*) δ : 7.81 (s, 1H), 7.53 (d, $J = 7.8$ Hz, 1H), 7.41 (t, $J = 8.0$ Hz, 1H), 7.38 – 7.32 (m, 2H), 7.32 – 7.27 (m, 3H), 6.20 (d, $J = 8.0$ Hz, 1H), 4.28 (s, 2H), 3.68 (s, 2H).

N-(6-Aminopyridin-2-yl)-2-(perfluorophenyl)acetamide (**8b**). Thionyl chloride (180 μL , 2.45 mmol) was added to flame-dried flask containing 2,3,4,5,6-

pentafluorophenylacetic acid (500 mg, 2.04 mmol) in DCM (anhydrous, 4 mL). One drop of anhydrous DMF was added to the reaction mixture, heated to reflux, and stirred for 3 hours. The solvent was removed under vacuum. The resultant residue was dissolved in anhydrous THF (3 mL) and slowly added to a solution of 2,6-diaminopyridine (223 mg, 2.04 mmol) and anhydrous triethylamine (650 μ L, 4.69 mmol) in THF (20 mL) at 0 °C. The resulting mixture was warmed to room temperature and stirred for 1 hour. The reaction was then diluted with ethyl acetate and washed with sat. NaHCO₃ (aq) (3x). The organic layer was then washed with brine (3x), dried over MgSO₄, filtered, and the filtrate concentrated. The crude product was purified via column chromatography (SiO₂, 1:1 EtOAc:Hex) to yield a white solid (0.193 g, 30%). ¹H NMR (500 MHz, Chloroform-*d*) δ : 8.62 (s, 1H), 7.50 – 7.36 (m, 2H), 6.29 – 6.23 (m, 1H), 4.46 (s, 2H), 3.77 (s, 2H). ¹⁹F NMR (282 MHz, Chloroform-*d*) δ : -141.99, -154.95 (t, *J* = 16.3 Hz), -162.04 (t, *J* = 20.3 Hz).

3-Iodo-*N*-(6-(2-phenylacetamido)pyridin-2-yl)benzamide (**9a**). Excess thionyl chloride (3.0 mL, 41 mmol) was added to flame-dried flask containing 3-iodobenzoic acid (526 mg, 2.12 mmol). One drop of anhydrous DMF was added to the reaction mixture, heated to 65 °C, and stirred for 3 hours. The excess thionyl chloride was removed under vacuum. The resultant residue was dissolved in anhydrous THF (2 mL) and slowly added to a solution of **8a** (400 mg, 1.76 mmol) and anhydrous triethylamine (320 μ L, 2.30 mmol) in THF (10 mL) at 0 °C. The resulting mixture was warmed to room temperature and stirred for 1 hour. The reaction was then filtered and adsorbed onto silica gel. The crude product was purified via column chromatography (SiO₂, 3:1 DCM:EtOAc) to yield a white solid (0.652 g, 81%). ¹H NMR (500 MHz, Chloroform-*d*)

δ : 8.19 (t, $J = 1.8$ Hz, 1H), 8.15 (s, 1H), 8.01 (d, $J = 8.0$ Hz, 1H), 7.96 (d, $J = 8.1$ Hz, 1H), 7.88 (dt, $J = 8.0, 1.3$ Hz, 1H), 7.81 (dt, $J = 7.8, 1.3$ Hz, 1H), 7.75 (t, $J = 8.1$ Hz, 1H), 7.56 (s, 1H), 7.45 – 7.40 (m, 2H), 7.39 – 7.32 (m, 3H), 7.22 (t, $J = 7.8$ Hz, 1H), 3.77 (s, 2H).

3-Iodo-*N*-(6-(2-(perfluorophenyl)acetamido)pyridin-2-yl)benzamide (**9b**). Excess thionyl chloride (3.0 mL, 41 mmol) was added to flame-dried flask containing 3-iodobenzoic acid (130 mg, 0.522 mmol). One drop of anhydrous DMF was added to the reaction mixture, heated to 65 °C, and stirred for 3 hours. The excess thionyl chloride was removed under vacuum. The resultant residue was dissolved in anhydrous THF (2 mL) and slowly added to a solution of **8b** (140 mg, 0.474 mmol) and anhydrous triethylamine (100 μ L, 0.617 mmol) in THF (10 mL) at 0 °C. The resulting mixture was warmed to room temperature and stirred for 1 hour. The reaction was then filtered and adsorbed onto silica gel. The crude product was purified via column chromatography (SiO₂, 1:1 DCM:EtOAc) to yield a white solid (0.166 g, 64%). ¹H NMR (500 MHz, Chloroform-*d*) δ : 8.25 (s, 1H), 8.08 (d, $J = 8.0$ Hz, 1H), 7.91 (d, $J = 7.9$ Hz, 1H), 7.87 (d, $J = 7.7$ Hz, 1H), 7.86 (s, 1H), 7.79 (t, $J = 8.0$ Hz, 1H), 7.29 – 7.22 (m, 3H), 3.85 (s, 2H). ¹⁹F NMR (282 MHz, Chloroform-*d*) δ : -141.78 (d, $J = 15.1$ Hz), -154.18 (t, $J = 21.7$ Hz), -161.01 – -162.08 (m).

3-(Diphenylphosphino)-*N*-(6-(2-phenylacetamido)pyridin-2-yl)benzamide (**10a**). Reactants **9a** (0.400 g, 0.875 mmol), diphenylphosphine (0.194 g, 1.04 mmol), Pd(OAc)₂ (12 mg, 53 μ mol), triethylamine (180 μ L, 1.26 mmol), and CH₃CN (60 mL) were combined in a dry flask under N₂. The resulting dark red solution was heated to reflux and stirred overnight. The crude solution was loaded onto dry silica, in air, and purified via column chromatography (dry SiO₂, 3:1 EtOAc:Hex, R_f = 0.41) to yield a

white solid (0.290 g, 64%). ^1H NMR (500 MHz, Chloroform-*d*) δ : 8.06 (s, 1H), 8.00 (d, $J = 8.1$ Hz, 1H), 7.94 (d, $J = 8.1$ Hz, 1H), 7.87 – 7.79 (m, 2H), 7.72 (t, $J = 8.1$ Hz, 1H), 7.50 – 7.41 (m, 4H), 7.38 – 7.33 (m, 7H), 7.34 – 7.27 (m, 4H), 3.76 (s, 2H). ^{31}P NMR (202 MHz, Chloroform-*d*) δ : -5.27.

3-(Diphenylphosphino)-*N*-(6-(2-(perfluorophenyl)acetamido)pyridin-2-yl)benzamide (**10b**). Reactants **9b** (0.500 g, 0.914 mmol), diphenylphosphine (0.205 g, 1.10 mmol), Pd(OAc)₂ (12 mg, 53 μmol), triethylamine (200 μL , 1.38 mmol), and CH₃CN (60 mL) were combined in a dry flask under N₂. The resulting dark red solution was heated to reflux and stirred overnight. The crude solution was loaded onto dry silica, in air, and purified via column chromatography (dry SiO₂, 4:1 DCM:EtOAc) to yield a white solid (0.474 g, 86%). ^1H NMR (500 MHz, Chloroform-*d*) δ : 8.18 (s, 1H), 8.05 (d, $J = 8.1$ Hz, 1H), 7.89 (d, $J = 8.0$ Hz, 1H), 7.88 – 7.84 (m, 2H), 7.74 (t, $J = 8.0$ Hz, 2H), 7.47 (t, $J = 7.2$ Hz, 1H), 7.45 – 7.41 (m, 1H), 7.39 – 7.35 (m, 6H), 7.35 – 7.29 (m, 4H), 3.82 (s, 2H). ^{19}F NMR (471 MHz, Chloroform-*d*) δ : -141.80 (dd, $J = 22.2, 8.6$ Hz), -154.28 (t, $J = 21.4$ Hz), -161.22 – -161.80 (m). ^{31}P NMR (202 MHz, Chloroform-*d*) δ : -5.18.

NMR Spectra

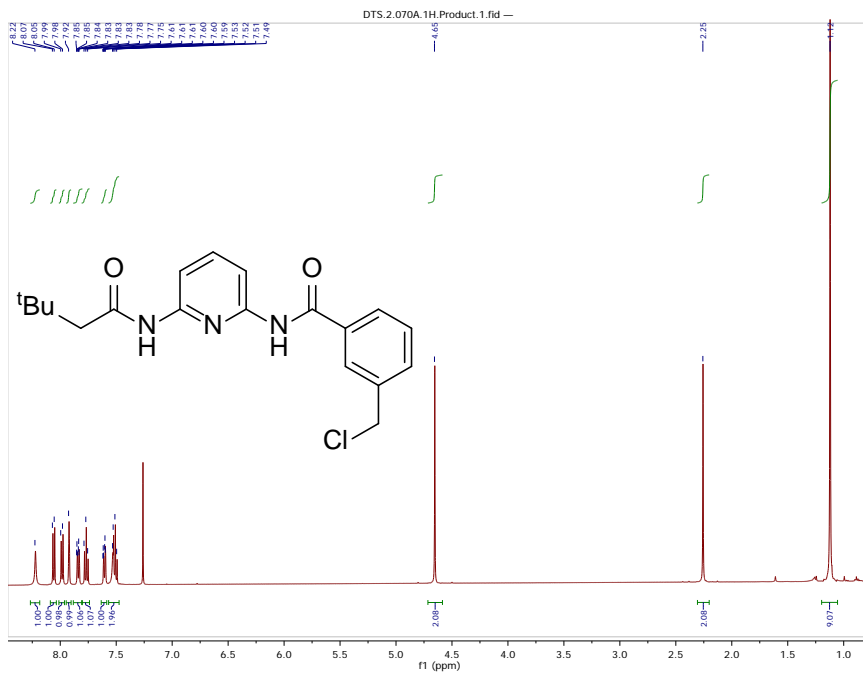


Figure C.1. ¹H (500 MHz) NMR spectrum of **5a** in CDCl₃.

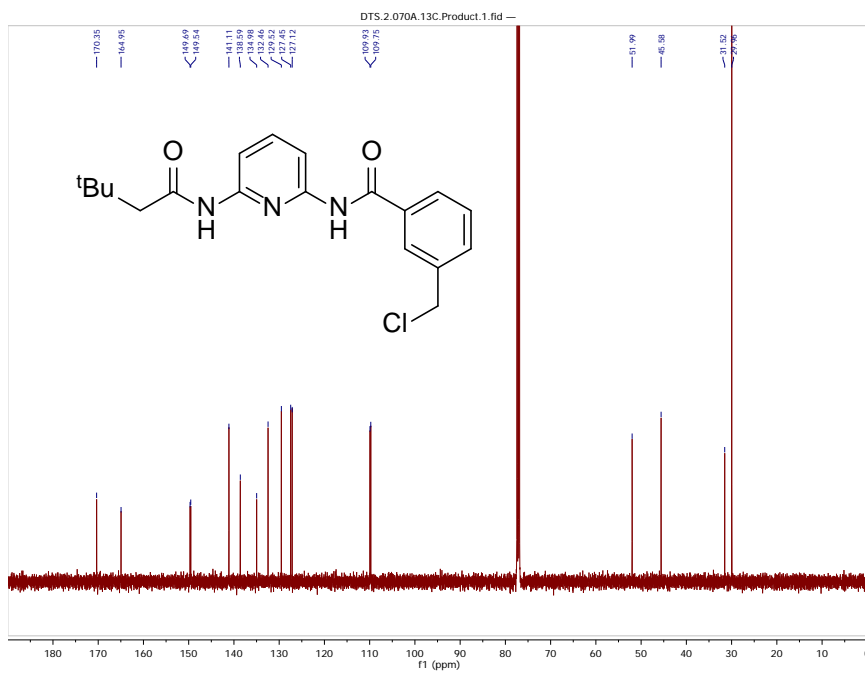


Figure C.2. ¹³C{¹H} (126 MHz) NMR spectrum of **5a** in CDCl₃.

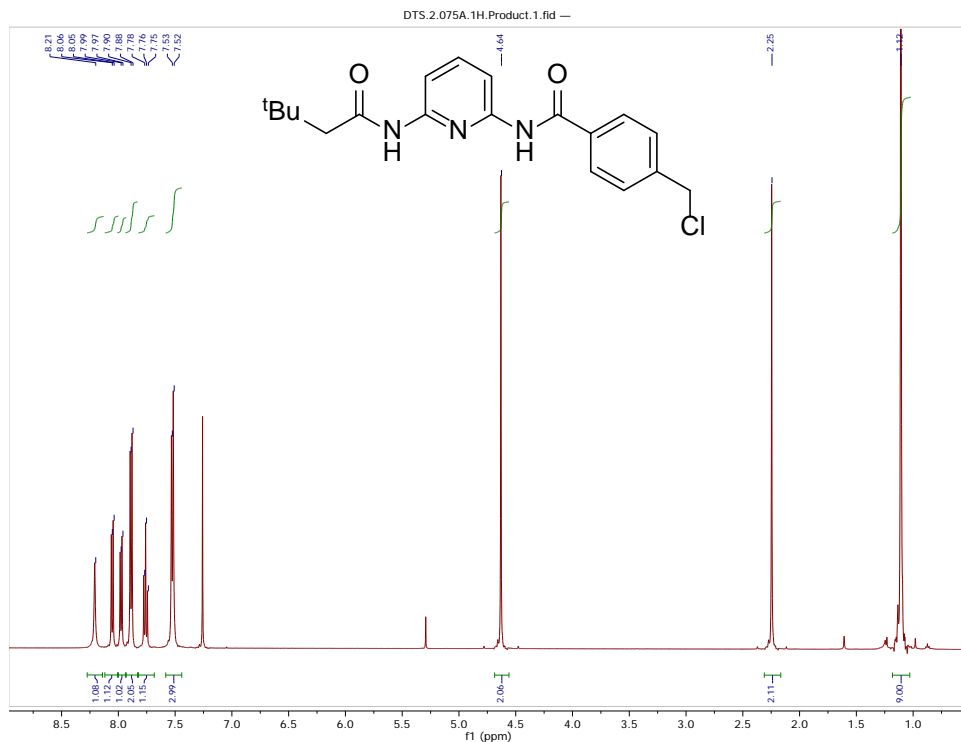


Figure C.3. ¹H (500 MHz) NMR spectrum of **5b** in CDCl₃.

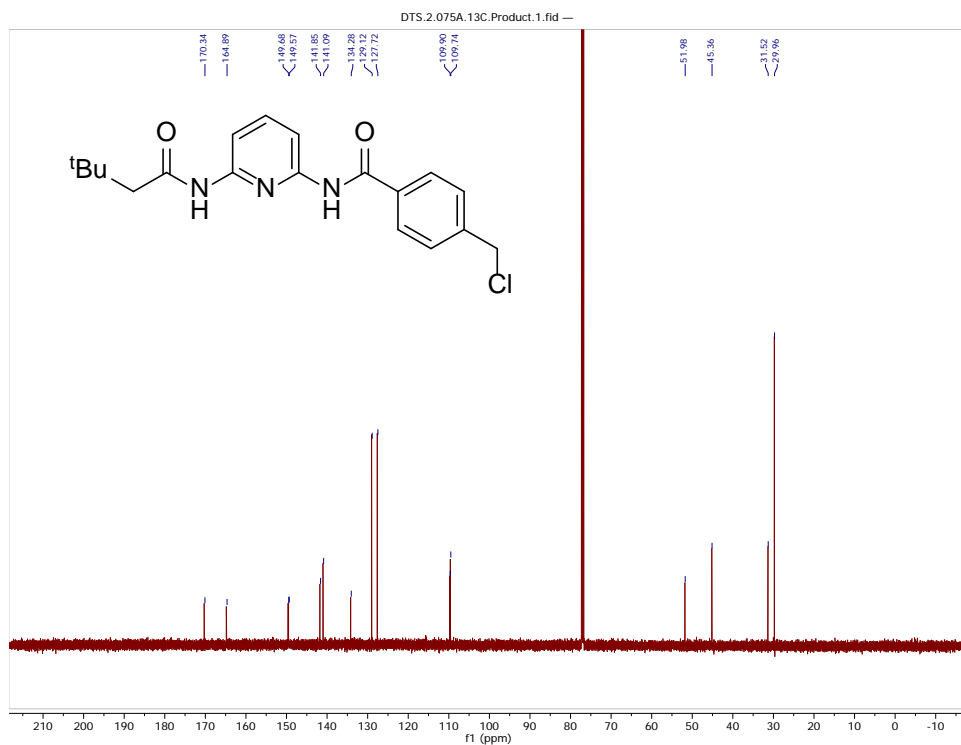


Figure C.4. ¹³C{¹H} (126 MHz) NMR spectrum of **5b** in CDCl₃.

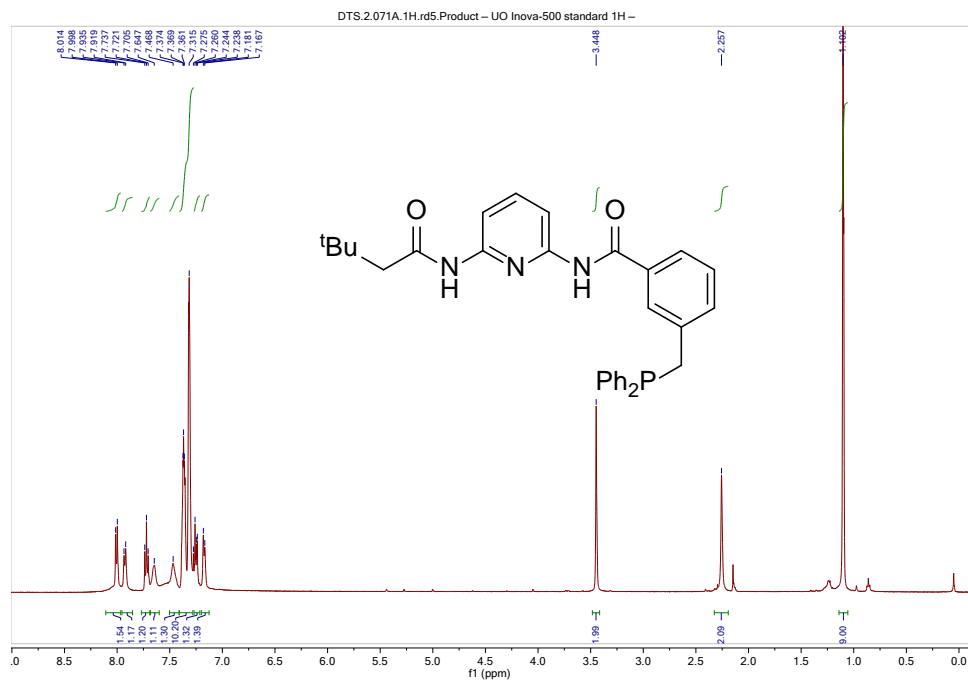


Figure C.5. ¹H (500 MHz) NMR spectrum of **6a** in CDCl₃.

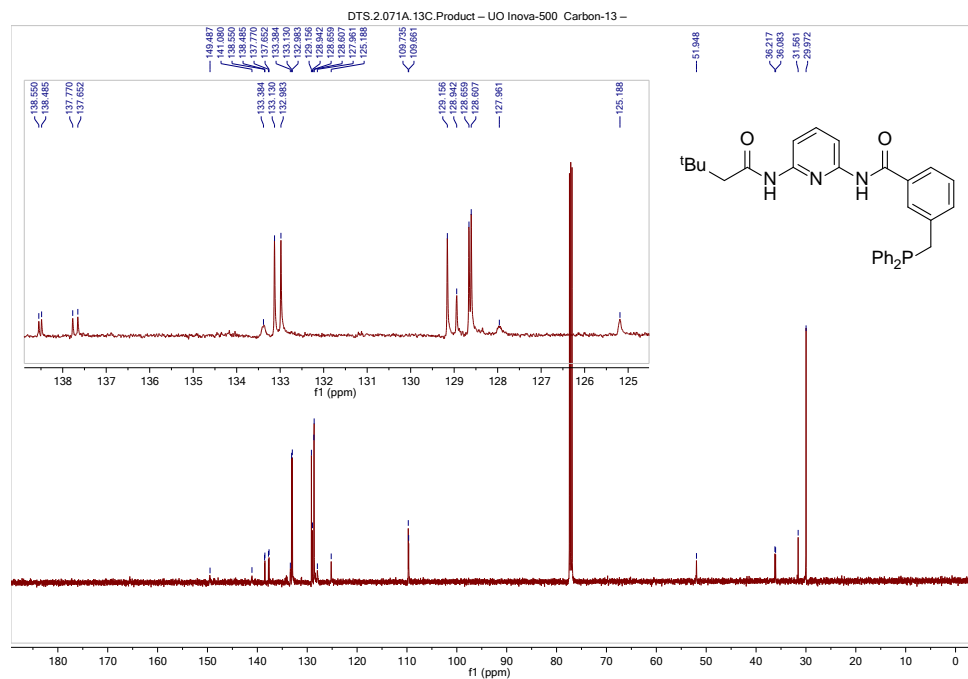


Figure C.6. ¹³C {¹H} (126 MHz) NMR spectrum of **6a** in CDCl₃.

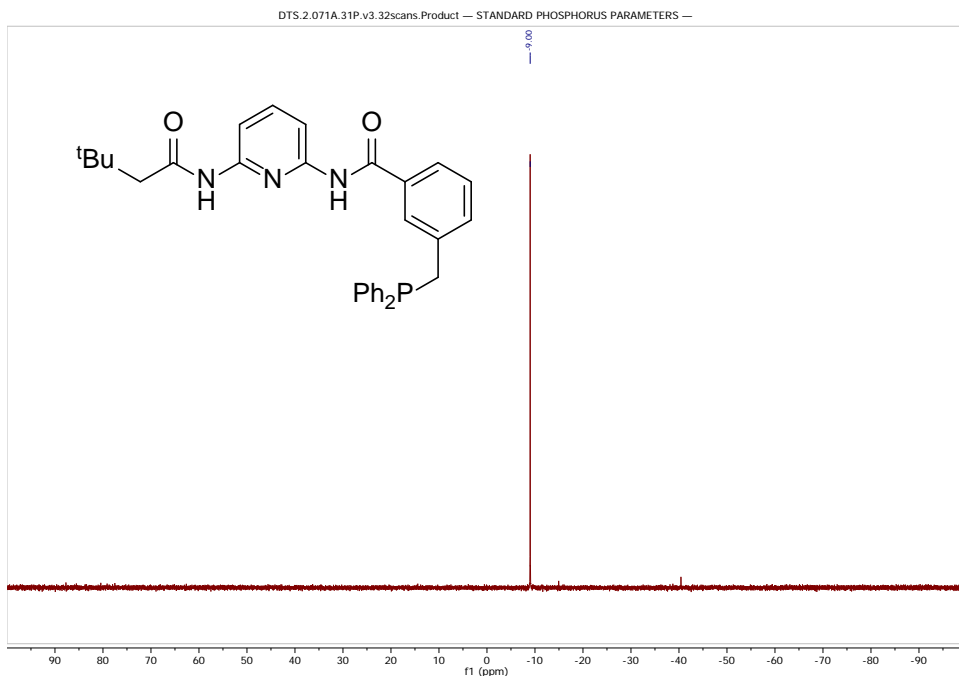


Figure C.7. $^{31}\text{P}\{^1\text{H}\}$ (202 MHz) NMR spectrum of **6a** in CDCl_3 .

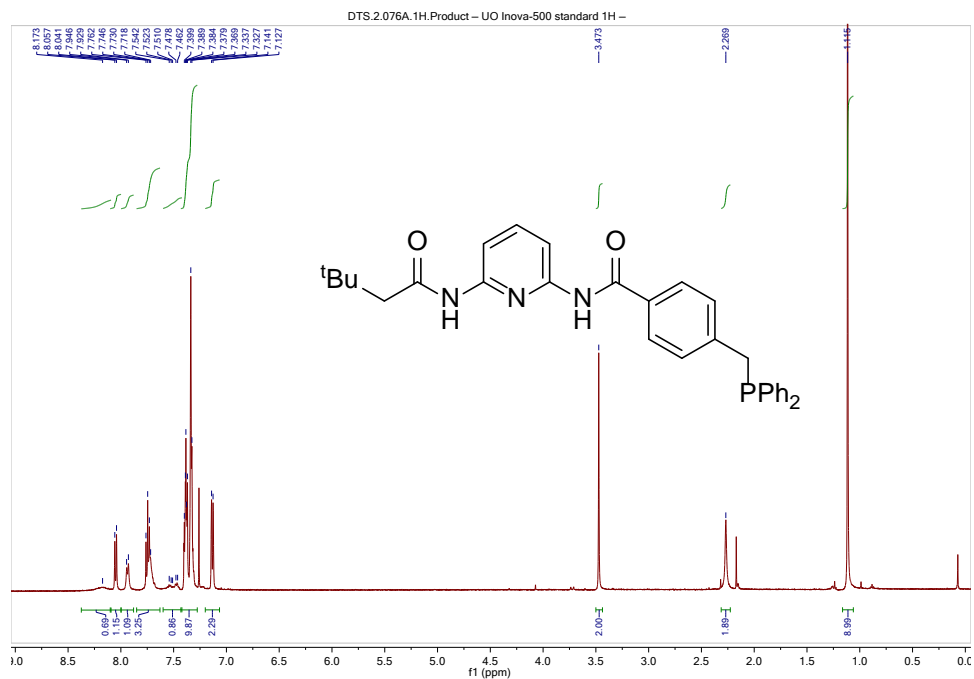
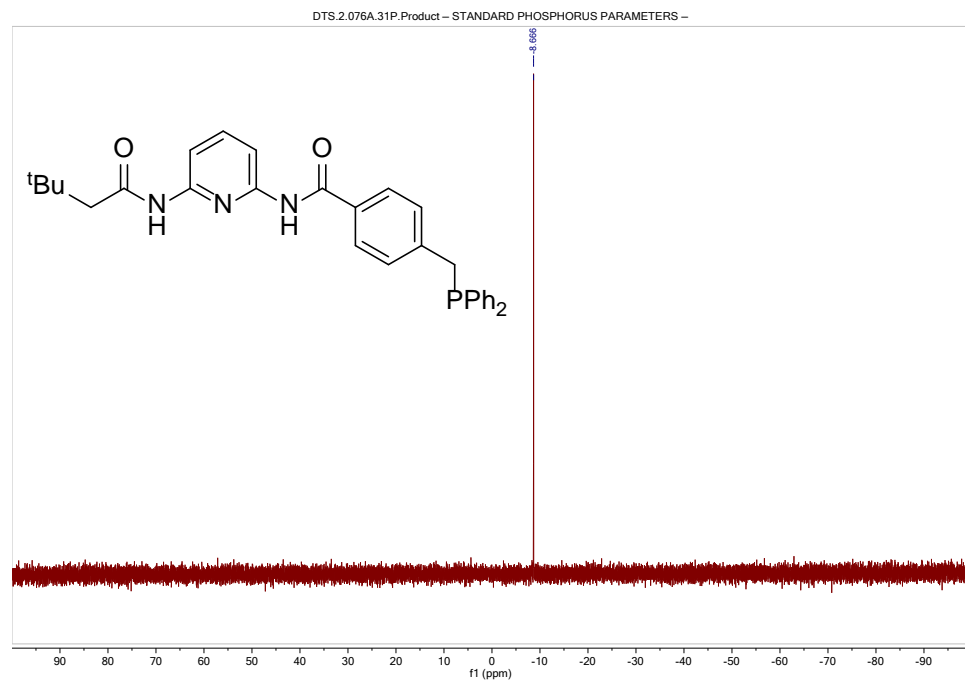
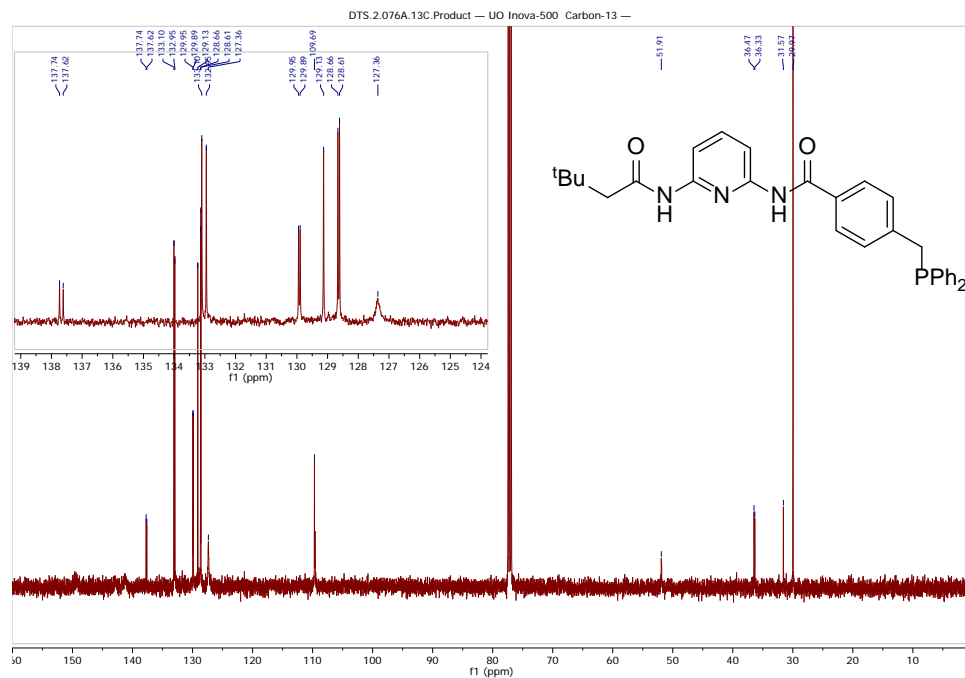


Figure C.8. ^1H (500 MHz) NMR spectrum of **6b** in CDCl_3 .



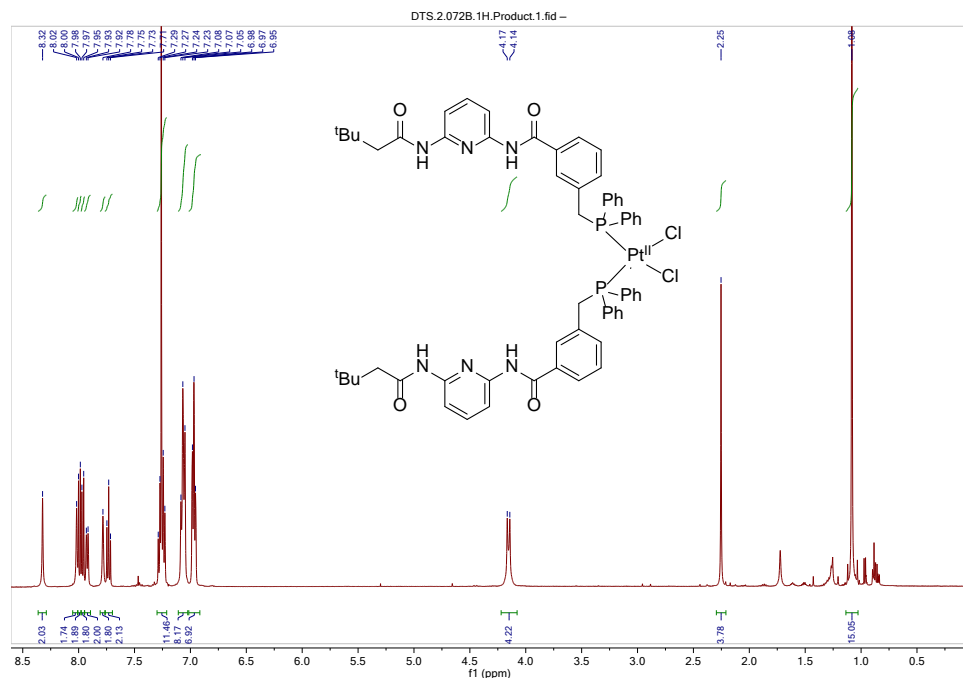


Figure C.11. ^1H (500 MHz) NMR spectrum of **7a** in CDCl_3 .

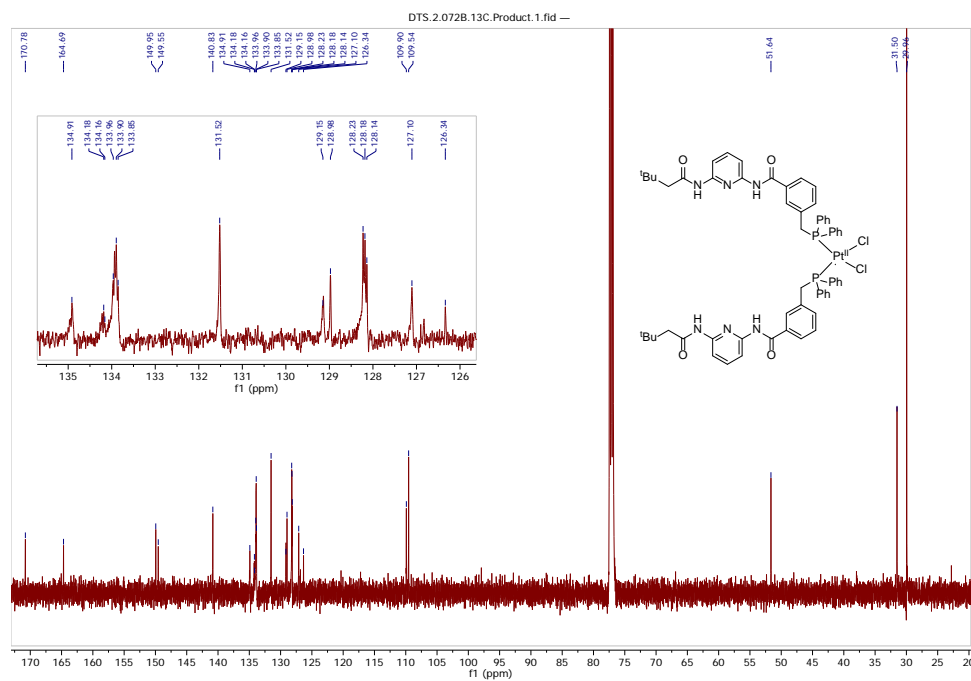


Figure C.12. $^{13}\text{C}\{^1\text{H}\}$ NMR (126 MHz), NMR spectrum of **7a** in CDCl_3 .

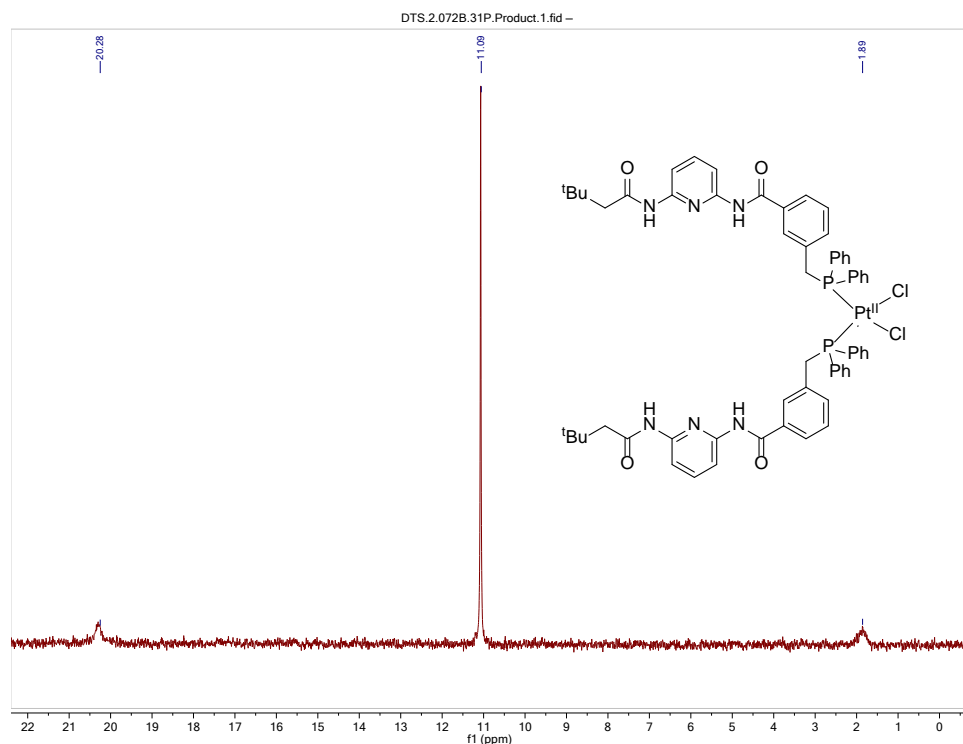


Figure C.13. $^{31}\text{P}\{^1\text{H}\}$ (202 MHz) NMR spectra of **7a** in CDCl_3 .

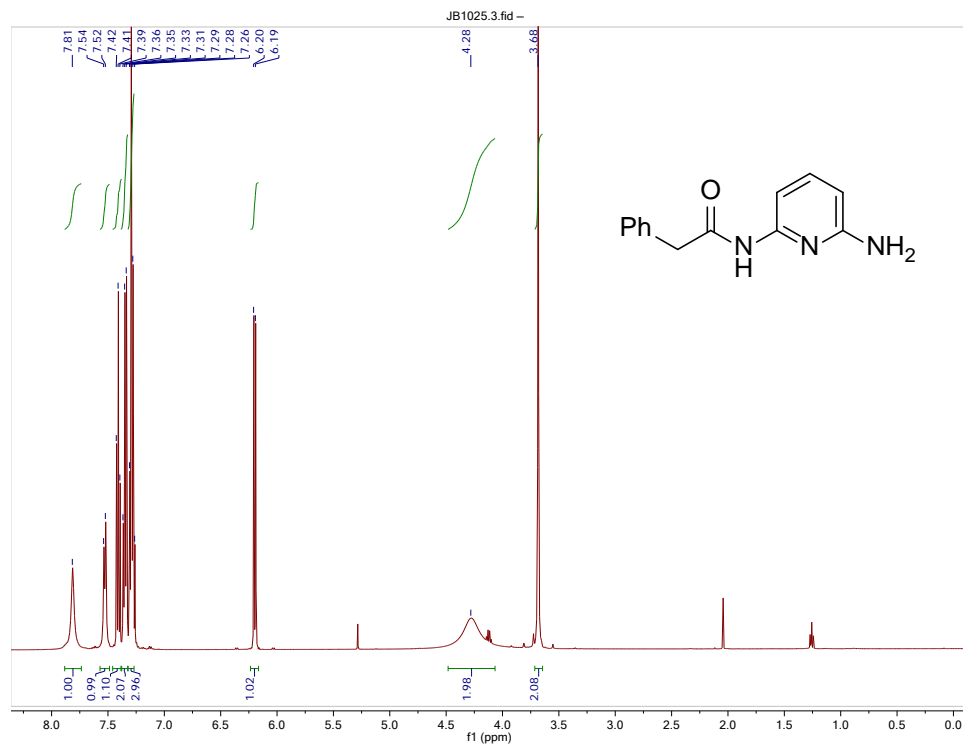


Figure C.14. ^1H (500 MHz) NMR spectrum of **8a** in CDCl_3 .

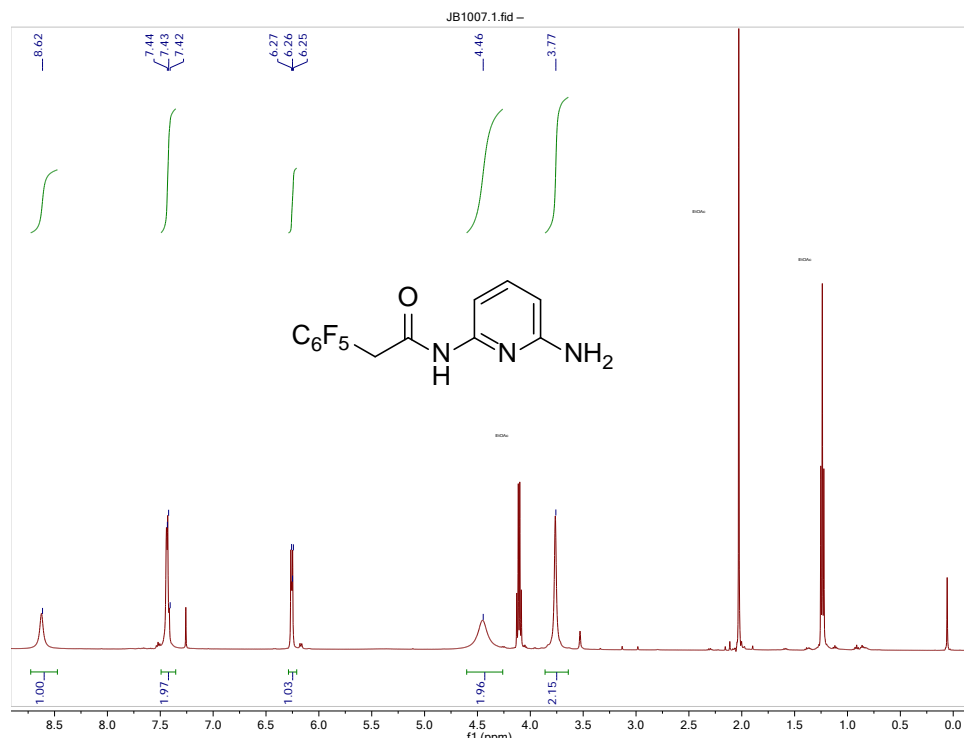


Figure C.15. ^1H (500 MHz) NMR spectrum of **8b** in CDCl_3 .

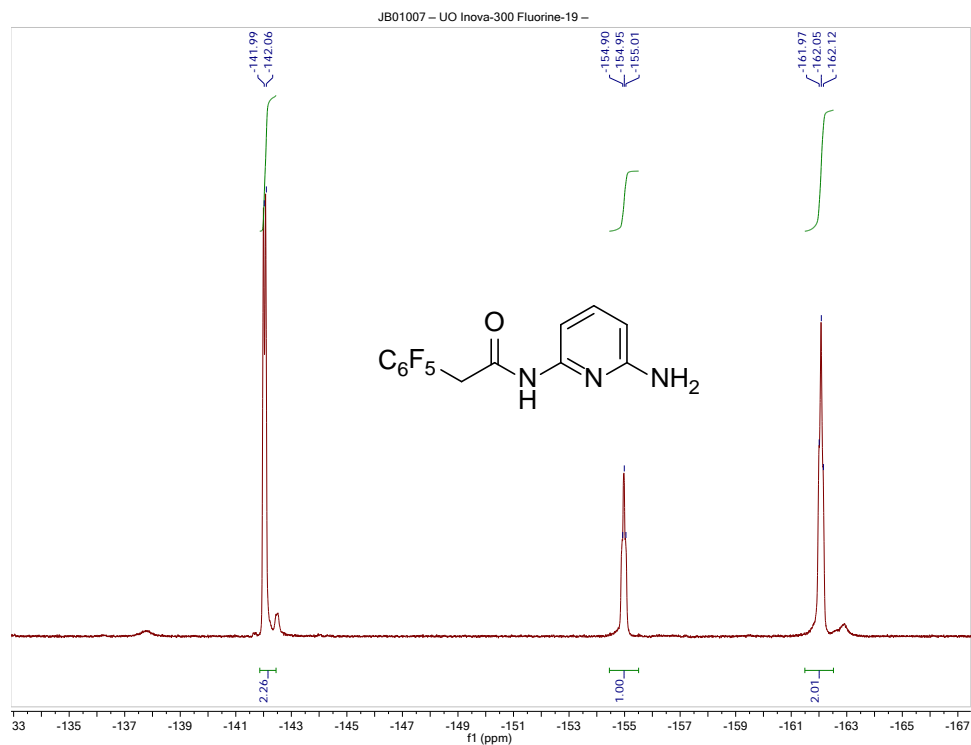


Figure C.16. ^{19}F (282 MHz) NMR spectrum of **8b** in CDCl_3 .

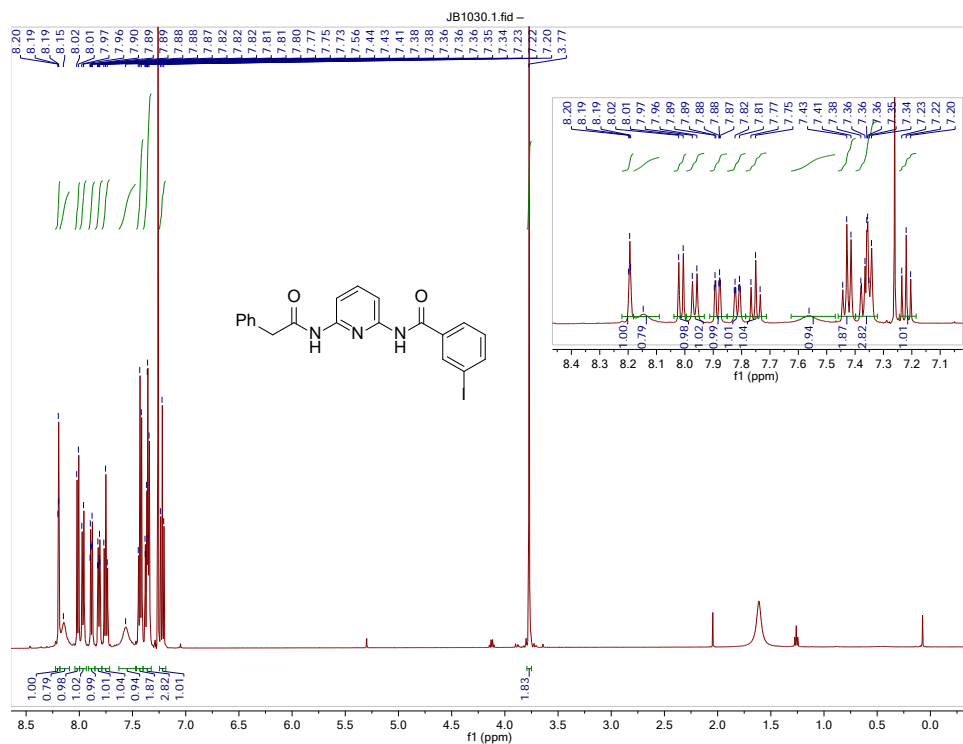


Figure C.17. ^1H (500 MHz) NMR spectrum of **9a** in CDCl_3 .

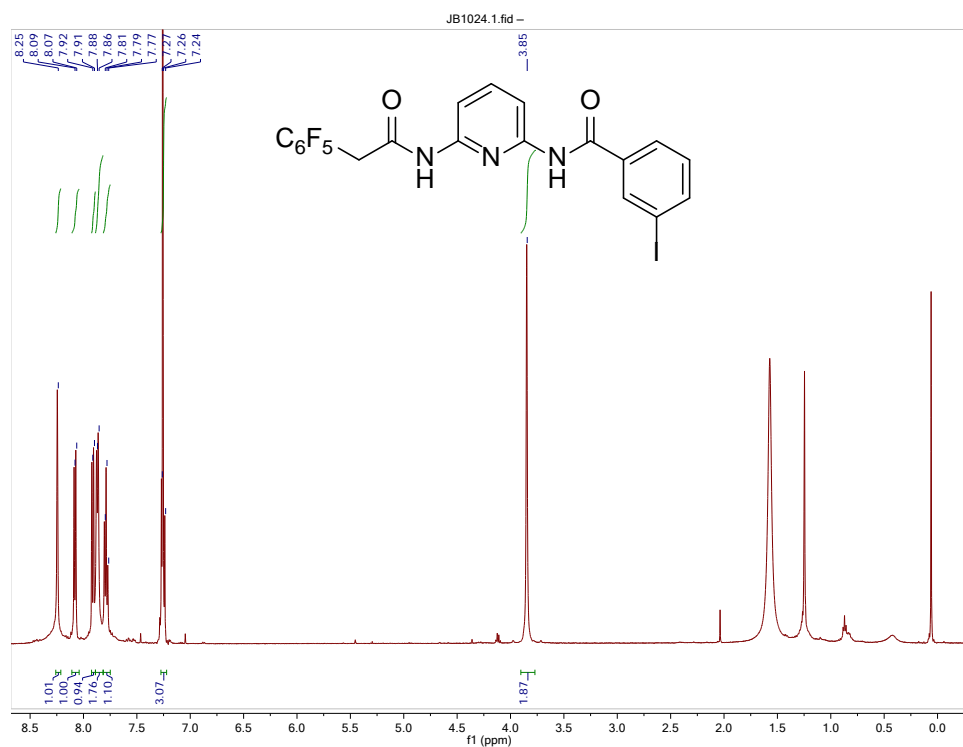


Figure C.18. ^1H (500 MHz) NMR spectrum of **9b** in CDCl_3 .

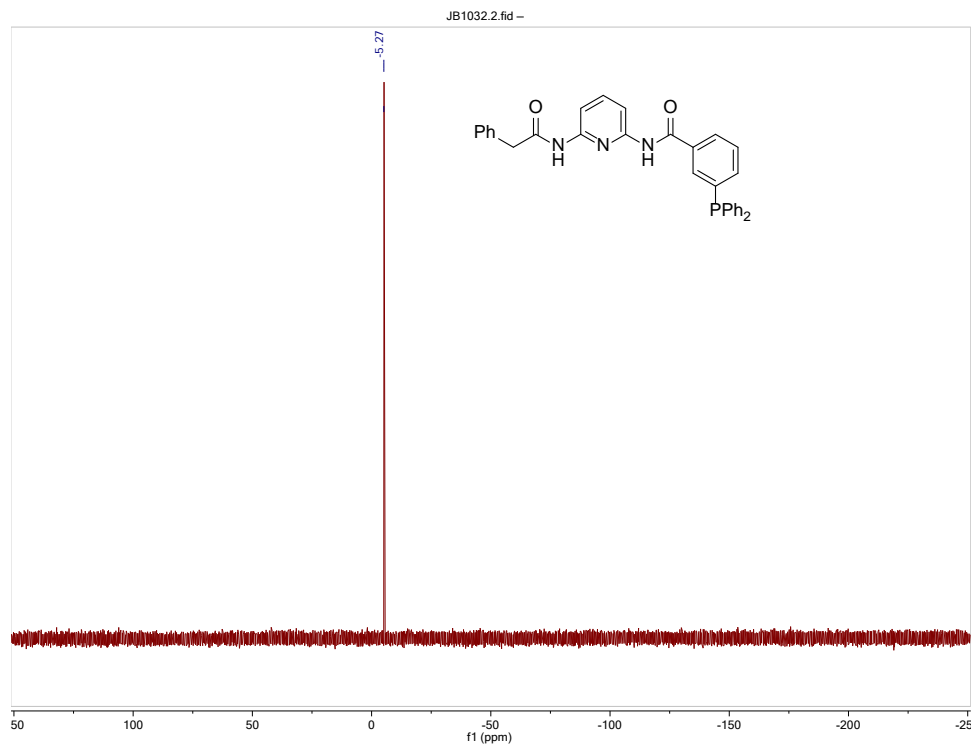


Figure C.21. $^{31}\text{P}\{^1\text{H}\}$ (202 MHz) NMR spectra of **10a** in CDCl_3 .

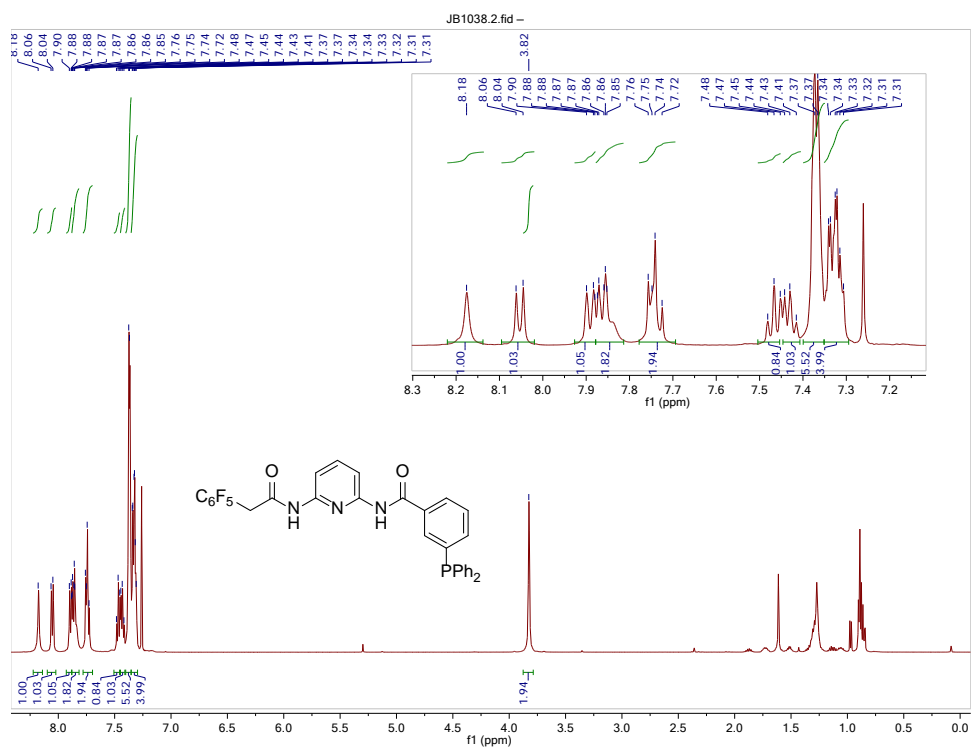


Figure C.22. ^1H (500 MHz) NMR spectrum of **10b** in CDCl_3 .

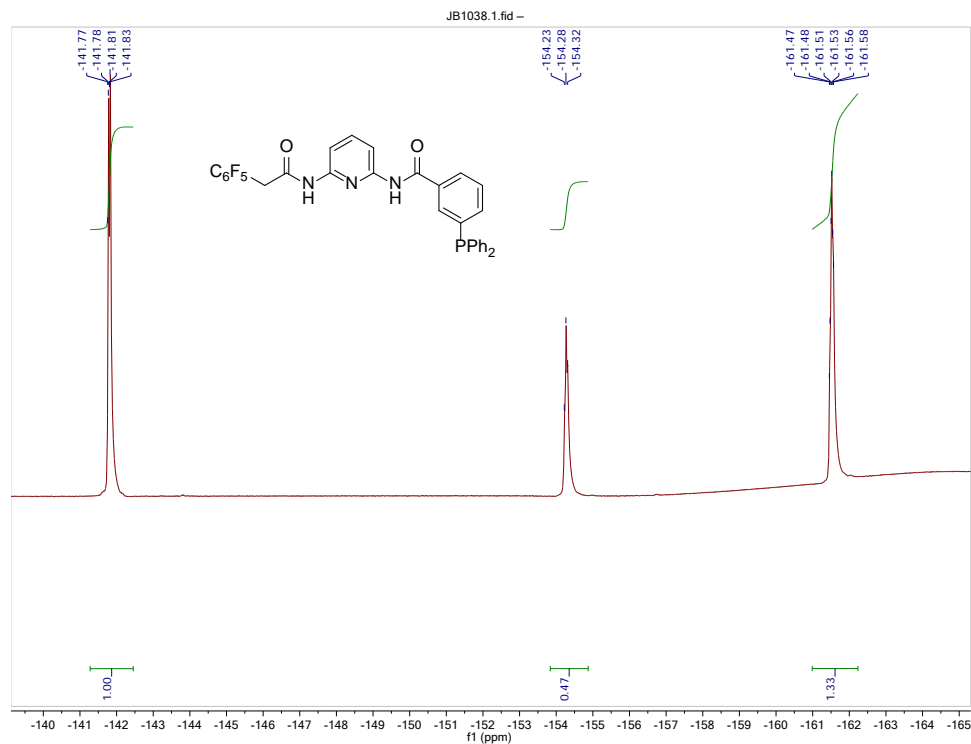


Figure C.23. ^{19}F (282 MHz) NMR spectrum of **10b** in CDCl_3 .

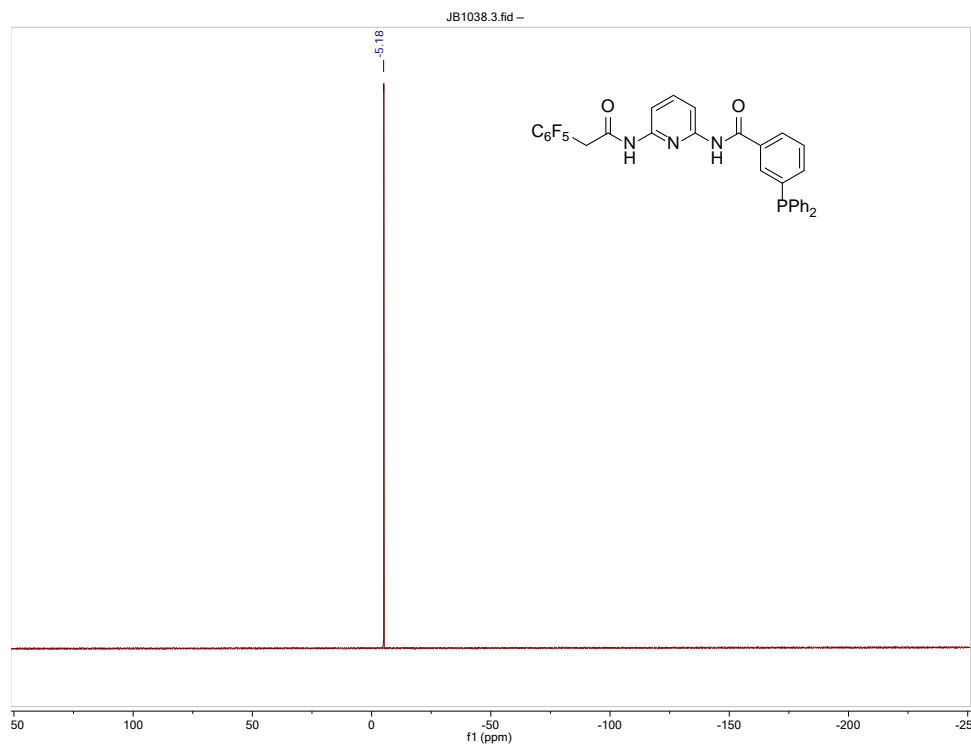


Figure C.24. $^{31}\text{P}\{^1\text{H}\}$ (202 MHz) NMR spectra of **10b** in CDCl_3 .

Binding Isotherm and Fitting for Titration of 4b with 7a

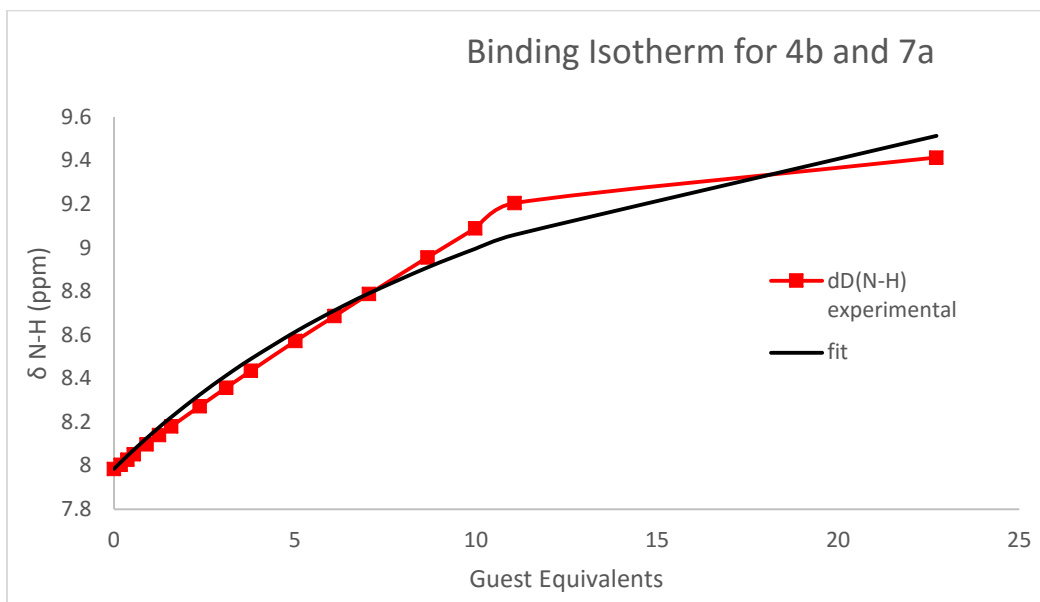


Figure C.25. Binding isotherm fit with a 1:1 binding stoichiometry in H₂O sat. CDCl₃ at 25 °C.

APPENDIX D

SUPPORTING INFORMATION FOR CHAPTER V

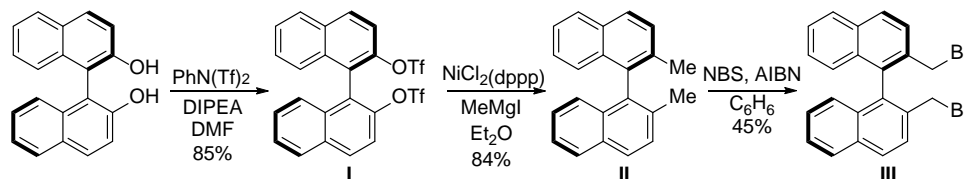
Appendix D is the supporting information for Chapter V of this dissertation. It includes the experimental details and additional spectra relevant to the content of Chapter V.

Experimental Details

General. All commercially-available reagents were used as received. Anhydrous, deoxygenated solvents were collected from a Pure Process Technologies solvent purification system. Reactions were monitored using Merck F₂₅₄ silica gel 60 TLC plates and visualized using UV light or a KMnO₄ stain. Chromatographic purification was performed using a Biotage automated flash chromatography purification system. ¹H and ¹³C{¹H} NMR spectra were recorded at the reported frequencies, and chemical shifts are reported in ppm (δ) and referenced to the residual solvent resonance. All ¹⁹F spectra were indirectly referenced via the Bruker TopSpin 3.5 software suite to CFC_l₃. The following naming conventions were used to describe NMR couplings: (s) singlet, (d) doublet, (t) triplet, (q) quartet, (dd) doublet of doublets, (m) multiplet, (b) broad.

Syntheses

Synthesis of dibromomethylbinaphthalene precursors were prepared according to Scheme D.1 using a modified procedure as reported previously (Ooi et al., 2003) and matched the reported spectroscopic signals.



Scheme D.1. Synthesis of dibromomethylbinaphthalene with (*R*)-stereochemistry shown.

2,2'-bis(trifluoromethanesulfonyloxy)-1,1'-binaphthyl, [(*R*)-**I**]. (*R*)-BINOL (2.01 g, 7.02 mmol), *N*-phenylbistrifluoromethanesulfonamide (5.02 g, 14.1 mmol), DIPEA (3.60 mL, 21.7 mmol) were combined in 10 mL dry DMF and stirred at r.t. for 24 hours. The reaction was diluted with Et₂O, washed 3x with H₂O and then with brine. The organic layer was dried over MgSO₄, filtered and concentrated under vacuum. The crude product was purified by column chromatography using hexanes:EtOAc gradient (0% - 20%) as the eluent (*R*_f = 0.12, Hex; *R*_f = 0.45, 20% EtOAc) to yield the final product as an oil that solidifies to a white solid upon standing (3.27 g, 85%) ¹H NMR (500 MHz, CDCl₃) δ: 8.15 (d, *J* = 9.1 Hz, 2H), 8.02 (d, *J* = 8.3 Hz, 2H), 7.66 – 7.57 (m, 4H), 7.43 (t, *J* = 7.6 Hz, 2H), 7.32 – 7.19 (m, 2H). ¹³C{¹H} NMR (126 MHz, CDCl₃) δ: 145.51, 133.27, 132.48, 132.12, 128.48, 128.11, 127.45, 126.88, 123.57, 119.46, 118.26 (q, *J* = 320.7 Hz). ¹⁹F NMR (471 MHz, CDCl₃) δ: -74.56.

2,2'-bis(trifluoromethanesulfonyloxy)-1,1'-binaphthyl, [(*S*)-**I**]. Was prepared similar to (*R*)-**I** using the following amounts: (*S*)-BINOL (996 mg, 3.48 mmol), *N*-phenylbistrifluoromethanesulfonamide (2.50 g, 7.00 mmol), DIPEA (1.8 mL, 10 mmol) in

5 mL DMF. The product was isolated as a white solid (1.35 g, 71%). ^1H NMR (500 MHz, CDCl_3) δ : 8.15 (d, $J = 9.1$ Hz, 2H), 8.01 (d, $J = 8.3$ Hz, 2H), 7.62 (d, $J = 9.1$ Hz, 2H), 7.59 (ddd, $J = 8.1, 6.7, 1.0$ Hz, 2H), 7.42 (ddd, $J = 8.2, 6.8, 1.2$ Hz, 2H), 7.32 – 7.19 (m, 2H). $^{13}\text{C}\{^1\text{H}\}$ NMR (126 MHz, CDCl_3) δ : 145.51, 133.28, 132.48, 132.12, 128.48, 128.11, 127.45, 126.89, 123.57, 119.53, 118.26 (q, $J = 320.7$). ^{19}F NMR (471 MHz, CDCl_3) δ : -74.57.

(*R*)-2,2'-Dimethyl-1,1'-binaphthyl, [(*R*)-**II**]. (*R*)-**I** (2.502 g, 4.54 mmol) and $\text{NiCl}_2(\text{dppp})$ (82.0 mg, 0.139 mmol) were combined in a Schlenk and evacuated/refilled 3x with and atmosphere of N_2 . Dry and degassed Et_2O (25 mL) was added via cannula and cooled to 0 °C. MeMgI (2 M in Et_2O , 6.8 mL, 14 mmol) was added slowly. The reaction mixture was then heated to reflux and stirred for 19 hours. The reaction was then cooled to 0 °C and quenched with 2 mL of 1 M HCl (aq), diluted with Et_2O , and filtered through celite. The organic layer was then washed 3x with H_2O and brine, dried over MgSO_4 , filtered, and concentrated under vacuum. The crude mixture was dissolved in hexanes and the residual salts removed via filtration. The product was purified using column chromatography using hexanes as the eluent ($R_f = 0.23$) to yield the final product as a colorless oil that solidifies upon standing (1.08 g, 84%). ^1H NMR (500 MHz, CDCl_3) δ : 7.89 (t, $J = 8.0$ Hz, 4H), 7.51 (d, $J = 8.4$ Hz, 2H), 7.39 (t, $J = 7.5$ Hz, 2H), 7.21 (t, $J = 7.6$ Hz, 2H), 7.05 (d, $J = 8.5$ Hz, 2H), 2.04 (s, 6H). ^{13}C NMR (126 MHz, CDCl_3) δ : 135.26, 134.42, 132.89, 132.35, 128.86, 128.06, 127.56, 126.21, 125.78, 125.02, 20.18.

(*S*)-2,2'-Dimethyl-1,1'-binaphthyl, [(*S*)-**II**]. Was prepared similar to (*R*)-**II** using the following amounts: (*S*)-**I** (4.86 g, 8.83 mmol), $\text{NiCl}_2(\text{dppp})$ (157 mg, 0.265 mmol), degassed Et_2O (40 mL), MeMgI (2 M in Et_2O , 13 mL, 26 mmol). The final product was

isolated as an oil that solidified upon standing (2.185 g, 88%) ^1H NMR (500 MHz, CDCl_3) δ : 7.89 (t, $J = 8.0$ Hz, 4H), 7.51 (d, $J = 8.4$ Hz, 2H), 7.39 (ddd, $J = 8.1, 6.6, 1.1$ Hz, 2H), 7.21 (ddd, $J = 8.2, 6.8, 1.3$ Hz, 2H), 7.05 (d, $J = 8.4$ Hz, 2H), 2.04 (s, 6H). $^{13}\text{C}\{^1\text{H}\}$ NMR (126 MHz, CDCl_3) δ : 135.27, 134.43, 132.90, 132.36, 128.86, 128.06, 127.57, 126.22, 125.78, 125.03, 20.18.

(*R*)-2,2'-Bis(bromomethyl)-1,1'-binaphthyl, [(*R*)-**III**]. (*R*)-**II** (428 mg, 1.52 mmol), *N*-bromosuccinimide (594 mg, 3.34 mmol), and AIBN (24.3 mg, 0.148 mmol, 10%) were dissolved in benzene (15 mL) and heated to reflux for 3 hours. The reaction was cooled to room temperature and diluted with Et_2O . The organic layer was washed 3x with H_2O , 3x brine, dried over MgSO_4 and filtered. The crude product was purified using column chromatography ($R_f = 0.23$, Hex). The combined fractions were concentrated and the product was triturated in hexanes and then filtered to yield the final product as a white solid (302 mg, 45%) ^1H NMR (500 MHz, CDCl_3) δ : 8.02 (d, $J = 8.6$ Hz, 2H), 7.93 (d, $J = 8.2$ Hz, 2H), 7.75 (d, $J = 8.6$ Hz, 2H), 7.49 (ddd, $J = 8.2, 6.7, 1.0$ Hz, 2H), 7.32 – 7.18 (m, 2H), 7.08 (d, $J = 8.5$ Hz, 2H), 4.26 (s, 4H). $^{13}\text{C}\{^1\text{H}\}$ NMR (126 MHz, CDCl_3) δ : 134.33, 134.23, 133.41, 132.66, 129.52, 128.17, 127.89, 126.99, 126.97, 126.94, 32.78.

(*S*)-2,2'-Bis(bromomethyl)-1,1'-binaphthyl, [(*S*)-**III**]. Was prepared similar to (*R*)-**III** using the following amounts: (*S*)-**II** (501 mg, 1.77 mmol), *N*-bromosuccinimide (668 mg, 3.75 mmol), and AIBN (32.0 mg, 0.195 mmol), and benzene (15 mL). After 3 hours 125 mg (0.702 mmol) NBS and 5.0 mg (3.0 μmol) AIBN were added and heated to reflux for an additional hour. The final product was isolated as a white solid (294 mg, 38%). ^1H NMR (500 MHz, CDCl_3) δ : 8.02 (d, $J = 8.6$ Hz, 2H), 7.93 (d, $J = 8.2$ Hz, 2H), 7.75 (d, $J = 8.6$ Hz, 2H), 7.49 (t, $J = 7.5$ Hz, 2H), 7.28 (t, $J = 7.9$ Hz, 2H), 7.08 (d, $J = 8.5$ Hz, 2H),

4.26 (s, 4H). ^{13}C NMR (126 MHz, CDCl_3) δ : 134.33, 134.23, 133.40, 132.65, 129.51, 128.17, 127.89, 126.99, 126.96, 126.94, 32.78.

General synthesis of barbituric acid derivatives I-3. To a solution of barbituric acid (1 equiv.) in DMSO was added diisopropylethylamine (DIPEA, 2.3 equiv.) The mixture was stirred at room temperature for 10 min, after which time a precipitate formed (depending on the concentration of barbituric acid). The corresponding benzyl bromide (2 equiv.) was then added to the mixture, which was then heated to 50 °C and stirred overnight (~22 h). The crude, clear orange reaction mixture was diluted with H_2O and extracted 3x with EtOAc. The combined organic extracts were washed 3x with brine, dried over MgSO_4 , filtered and concentrated. The residue was triturated with a DCM:hexanes mixture and the resulting solids collected via vacuum filtration to yield the final product. In general, this gave acceptably pure product. Further purification could be achieved via recrystallization from EtOH or column chromatography.

5,5'-(*S*)-1,1'-binaphthylbarbituric acid [(*S*)-**BINABARB**, (**1a**)]. This compound was prepared as described in the general procedure using the following quantities barbituric acid (49.7 mg, 0.388 mmol) in 5 mL DMSO, DIPEA (160 μL , 0.92 mmol), and (*S*)-**III** (172 mg, 0.391 mmol). The compound was purified by column chromatography ($R_f = 0.33$, 1:1 EtOAc:Hex) followed by recrystallization from ethanol to yield the final product as a white solid (36 mg, 23%). ^1H NMR (500 MHz, $\text{DMSO}-d_6$) δ : 11.14 (s, 2H), 8.01 (d, $J = 8.2$ Hz, 2H), 7.95 (d, $J = 8.3$ Hz, 2H), 7.50 (d, $J = 8.4$ Hz, 2H), 7.47 (t, $J = 7.5$ Hz, 2H), 7.25 (t, $J = 7.6$ Hz, 2H), 7.08 (d, $J = 8.6$ Hz, 2H), 3.09 (d, $J = 13.6$ Hz, 2H), 2.97 (d, $J = 13.5$ Hz, 2H). ^{13}C NMR (126 MHz, $\text{DMSO}-d_6$) δ : 172.22, 150.36, 134.23,

132.77, 132.63, 130.93, 129.78, 128.23, 127.35, 126.29, 125.69, 125.24, 62.05. HRMS (ESI-TOF) m/z : $[M + Na]^+$ Calcd for $C_{26}H_{19}N_2O_3$, 407.1396; found 407.1396.

5,5'-(*R*)-1,1'-binaphthylbarbituric acid [(*R*)-**BINABARB**, (**1b**)]. This compound was prepared as described in the general procedure using the following quantities: barbituric acid (57.9 mg, 0.452 mmol) in 3 mL DMSO, DIPEA (180 μ L, 1.0 mmol), and (*R*)-**III** (199 mg μ L, 0.452 mmol). The compound was purified by column chromatography (R_f = 0.33, 1:1 EtOAc:Hex) followed by recrystallization from ethanol to yield the final product as a white solid (62 mg, 33%) 1H NMR (500 MHz, DMSO- d_6) δ : 11.14 (s, 2H), 8.01 (d, J = 8.2 Hz, 2H), 7.95 (d, J = 8.4 Hz, 2H), 7.50 (d, J = 8.4 Hz, 2H), 7.47 (t, J = 7.5 Hz, 2H), 7.25 (t, J = 7.6 Hz, 2H), 7.08 (d, J = 8.5 Hz, 2H), 3.09 (d, J = 13.5 Hz, 2H), 2.97 (d, J = 13.5 Hz, 2H). ^{13}C NMR (126 MHz, DMSO- d_6) δ : 172.22, 150.37, 134.23, 132.76, 132.63, 130.92, 129.78, 128.23, 127.35, 126.28, 125.69, 125.24, 62.04, 38.09. HRMS (ESI-TOF) m/z : $[M + Na]^+$ Calcd for $C_{26}H_{19}N_2O_3$, 407.1396; found 407.1385.

5,5'-dibenzylbarbituric acid (**3**). This compound was prepared as described in the general procedure using the following quantities: barbituric acid (253 mg, 1.95 mmol) in 5 mL DMSO, DIPEA (780 μ L, 4.45 mmol), and benzyl bromide (470 μ L, 3.95 mmol). The product was isolated as a white solid (474 mg, 78%). 1H NMR (500 MHz, DMSO- d_6) δ : 11.19 (s, 2H), 7.35 – 7.17 (m, 6), 7.11 – 7.01 (m, 4H), 3.28 (s, 4H). $^{13}C\{^1H\}$ NMR (126 MHz, DMSO- d_6) δ : 171.99, 148.85, 135.13, 129.26, 128.47, 127.33, 58.99, 43.78.

NMR Spectra of Compounds 1-3

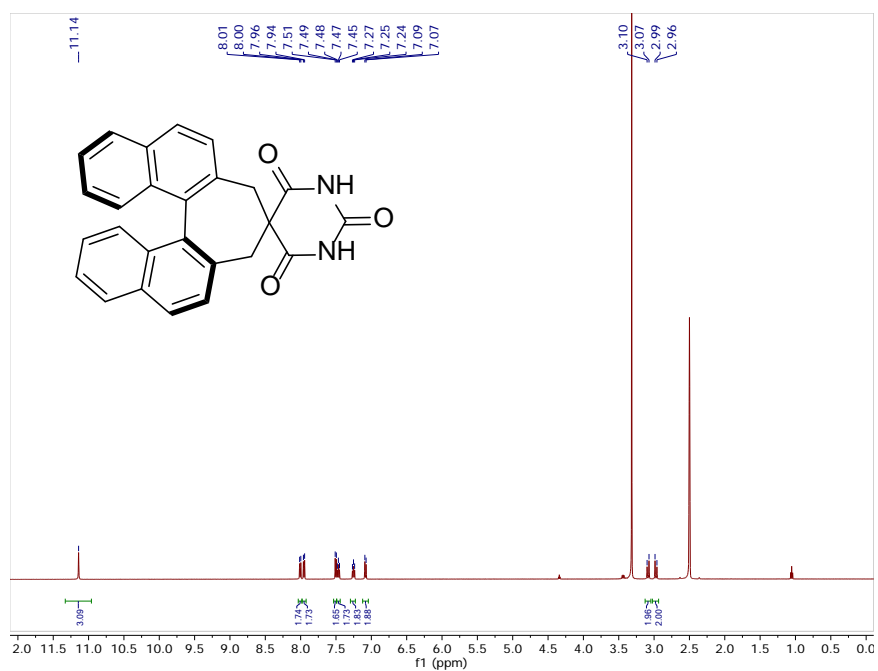


Figure D.1. ¹H (500 MHz) NMR spectrum of **1a** in *d*₆-DMSO.

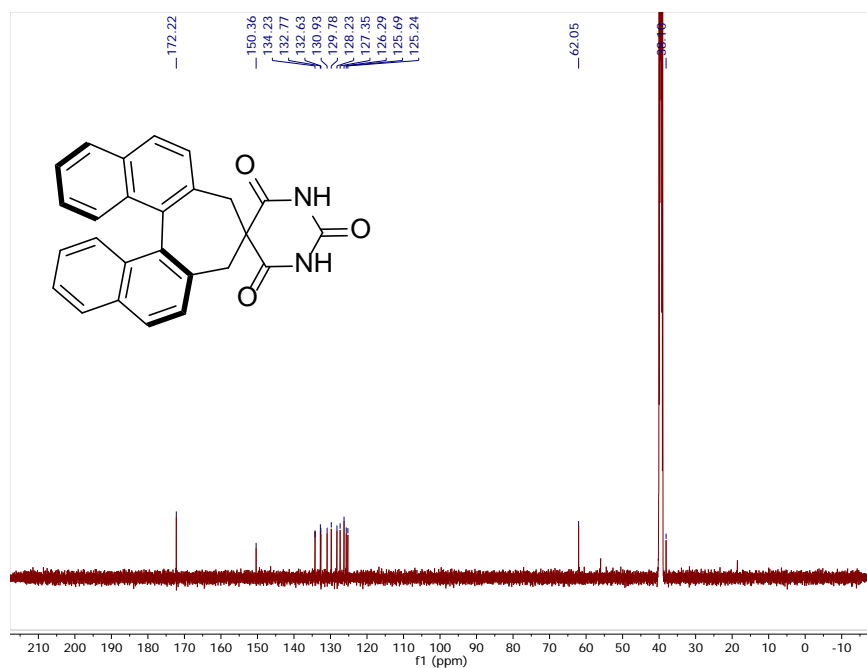


Figure D.2. ¹³C{¹H} (126 MHz) NMR spectrum of **1a** in *d*₆-DMSO.

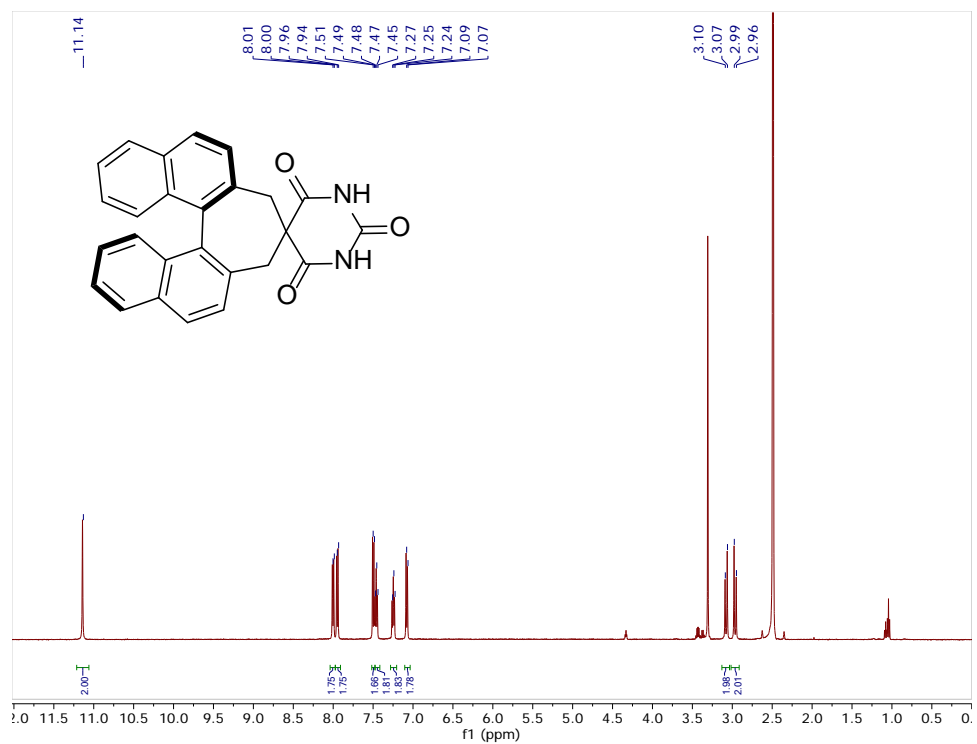


Figure D.3. ¹H (500 MHz) NMR spectrum of **1b** in *d*₆-DMSO.

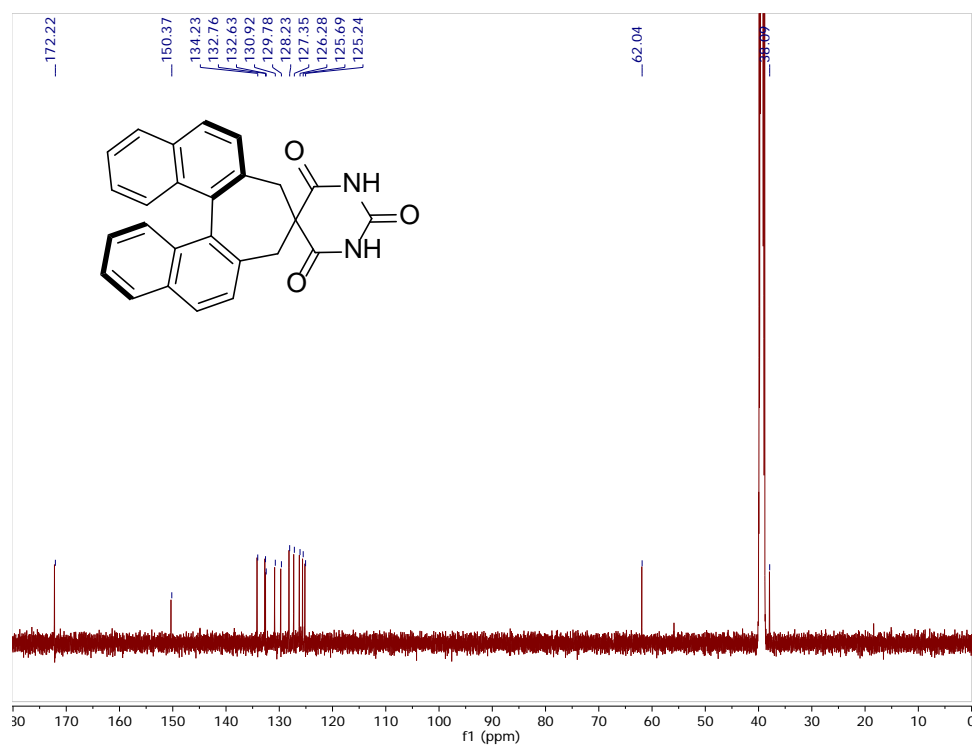


Figure D.4. ¹³C{¹H} (126 MHz) NMR spectrum of **1b** in *d*₆-DMSO.

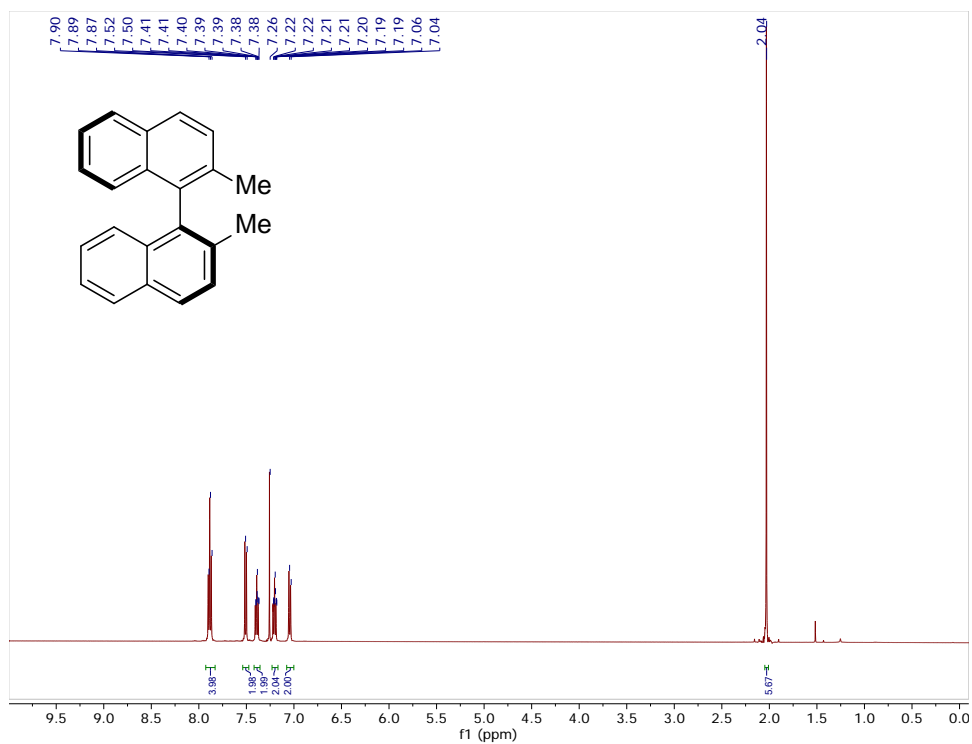


Figure D.5. ^1H (500 MHz) NMR spectrum of 3 in d_6 -DMSO.

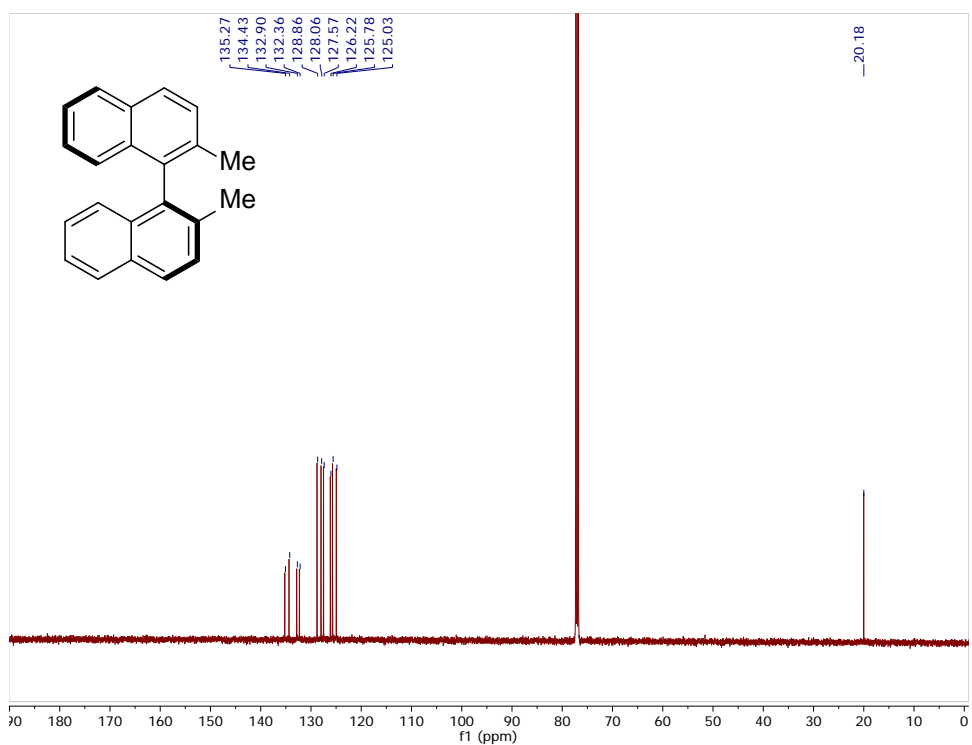


Figure D.6. $^{13}\text{C}\{^1\text{H}\}$ (126 MHz) NMR spectrum of 2 in CDCl_3 .

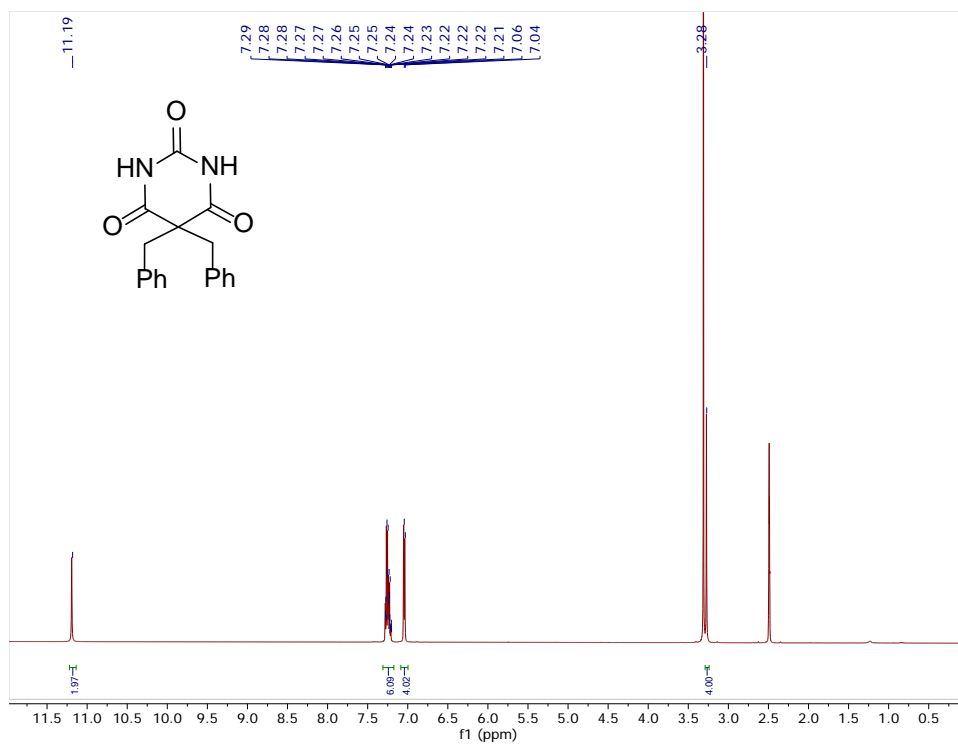


Figure D.7. ^1H (500 MHz) NMR spectrum of **3** in d_6 -DMSO.

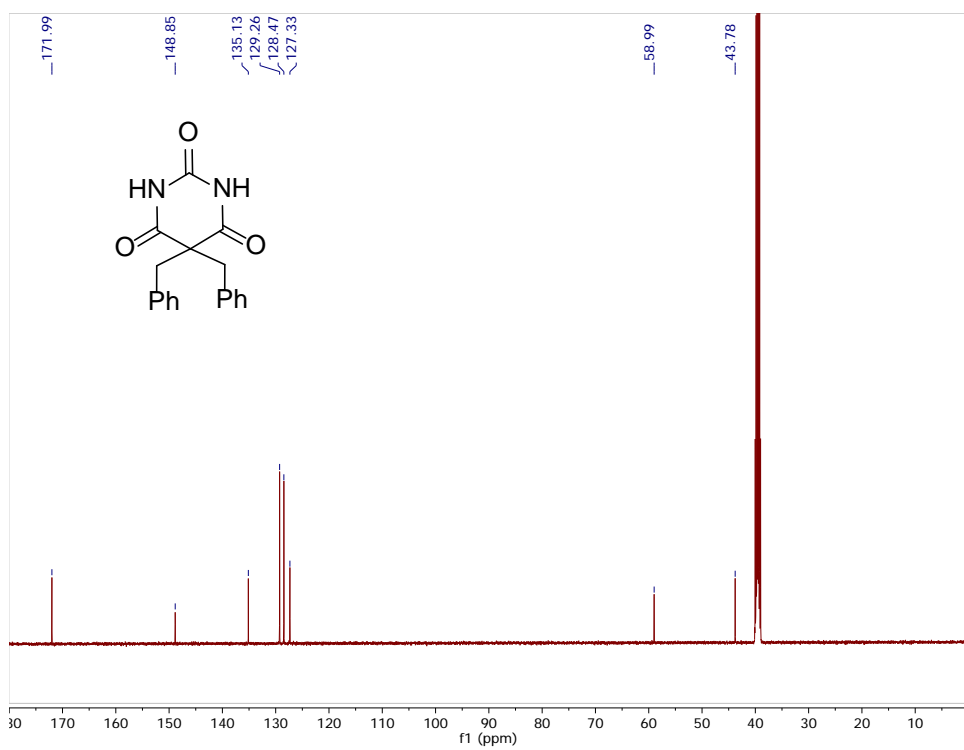


Figure D.8. $^{13}\text{C}\{^1\text{H}\}$ (126 MHz) NMR spectrum of **3** in d_6 -DMSO.

Determining gelation behavior

A 25 mM sample of the numbered compound was prepared in the desired solvent. The sample was sonicated and heated in a GC-vial to reflux or until all visible solids were dissolved. The sample was then allowed to cool and stand for at least 10 minutes before being inverted. If the sample appeared homogenous and no flow was observed, then the solvent and compound combination was marked as a gel.

Sample preparation for DOSY NMR.

For control compounds **2** and **3**, a corresponding amount of a concentrated stock solution was diluted with CDCl_3 to a total volume of 600 μL to achieve the desired concentrations. For the (*S*)-BINABarb samples ≤ 10 mM, a similar procedure to that of **2** and **3** was used. For the more concentrated samples of (*S*)-BINABarb, a corresponding amount of solid was added to an NMR tube and dissolved in CDCl_3 to achieve the desired concentration with a total volume of 600 μL . Heating and sonication was necessary to achieve complete dissolution of the more concentrated samples. The samples were then allowed to cool to room temperature and stand for at least 15 minutes prior analysis.

Determination of diffusion coefficients

Diffusion-ordered spectroscopy (DOSY) was performed on a 600 MHz Bruker spectrometer with a prodigy cryoprobe using the **ledbpgp2s** pulse sequence. The 90° pulse widths were optimized individually for each sample. A typical experiment has a Δ (d20) = 0.060 s, δ (p30*2) = 3.0 ms with a varying gradient strength between 35-45% with data taken in 25 increments. All data was processed in MestReNova using the max peak height method for the doublet centered at 3.40 ppm (Bn H) with the following values: $\gamma = 42.58$ (MHz T⁻¹), $k = 6.57$ (DAC to G), $\Delta = 0.060$ s, $\delta = 3.0$ ms. The exponential decays were then fit using the three parameter exponential fit function in the MestReNova data analysis package. The data reported represents the average of at least 3 or more trials, and the reported uncertainty is the standard deviation.

Representative DOSY Plots and Fitting

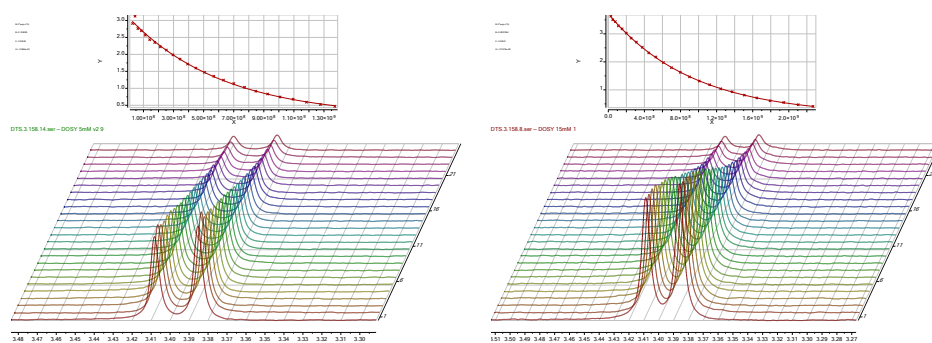


Figure D.9. Representative exponential decay plots from DOSY experiments of **1a** at 5 mM (left) and 15 mM (right) showing doublet at 3.40 ppm and the corresponding exponential decay fits.

Determination of diffusion coefficients for VT DOSY

Variable temperature diffusion-ordered spectroscopy (VT DOSY) was performed on a 500 MHz Varian spectrometer using the **DONESHOT** pulse sequence. A 20 mM sample in CDCl₃ was prepared similarly to the room temperature samples. A typical experiment has a $\Delta = 0.050$ s, $\delta = 2.0$ ms with the low and high pulse gradients set to 2,000 and 22,000, respectively. The temperature was incrementally increased up to 50 °C and allowed to equilibrate for at least 10 minutes before each acquisition (black squares). After the acquisition at 50 °C, the sample was then re-cooled inside the spectrometer to 25 °C and the diffusion coefficient was remeasured (red circle). All data was processed in MestReNova using the max peak height method for the doublet centered at 3.40 ppm (Bn Hs) with the following values: $\gamma = 26752.2205$ (G⁻¹s⁻¹), $k = 0.00222$, $\Delta = 0.05$ s, $\delta = 2.0$ ms. The exponential decays were then fit using the three parameter exponential fit function in the MestReNova data analysis package.

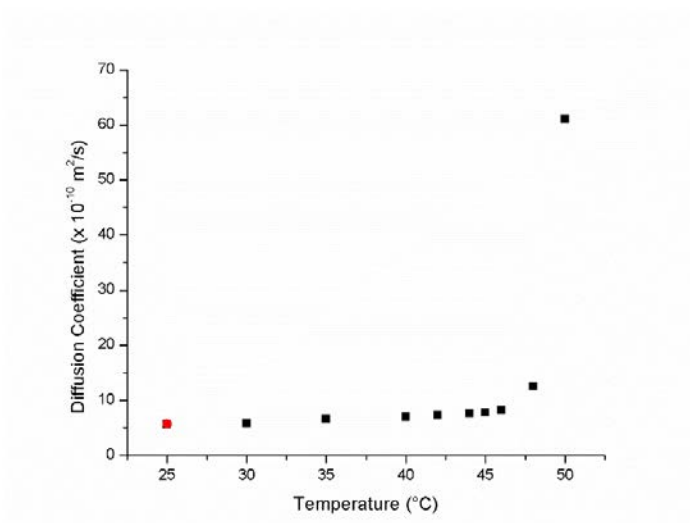


Figure D.10. Variable temperature DOSY of a 20 mM gel sample of **1a** in CDCl₃. The black squares represent a sequential increase in temperature until the T_{gel} was reached.

The red circle represents the diffusion coefficient after cooling the sample back to 25 °C from 50 °C.

Variable Pressure- Scanning electron microscopy details

To image the gels, an FEI Quanta 200 ESEM was used in variable-pressure mode. The best image quality was obtained operating at 100pa pressure, while actively cooling the gel to 4 °C (resulting in 12% relative humidity). Images were captured at 15kV, using spot size 4, with a GSED (gaseous-state electron detector.) Samples were prepared for SEM imaging by placing several micro-liters of fully hydrated/solvated gel onto cooled aluminum pucks, which were placed onto an FEI Peltier-cooled stage.

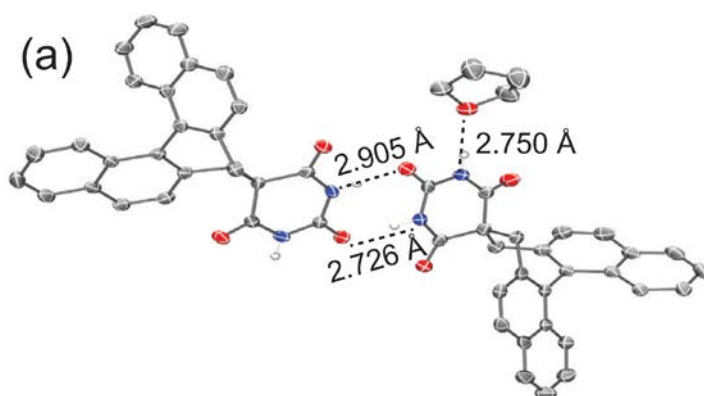


Figure D.11. ORTEP representation of smallest repeat unit of **1b**. Thermal ellipsoids shown at 50% probability. Non-H bonding hydrogens omitted for clarity.

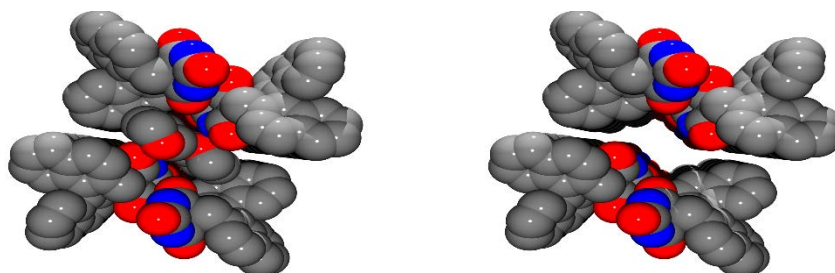


Figure D.12. Space-filling representation of columnar stack of **1b** viewed down screw axis with (left) and without (right) THF co-solvent. H bonds omitted for clarity.

APPENDIX E

SUPPORTING INFORMATION FOR CHAPTER VI

Appendix E is the supporting information for Chapter VI of this dissertation. It includes the experimental details and additional spectra relevant to the content of Chapter VI.

Experimental Details

General. All commercially-available reagents were used as received. Anhydrous, deoxygenated solvents were collected from a Pure Process Technologies solvent purification system. Triethylamine was dried and distilled over CaH₂ under nitrogen. Barbiturates were synthesized according to the procedures outline in Chapter II of this dissertation. Reactions were monitored using Merck F₂₅₄ silica gel 60 TLC plates and visualized using UV light or a KMnO₄ stain. Reactions conducted under an inert atmosphere were performed by either using standard Schlenk techniques. Chromatographic purification was performed using a Biotage automated flash chromatography purification system. Preparative HPLC chromatography was performed using a JAI Recycling Preparative HPLC (Model LC-9101) with a JAIGEL - 1H preparative column. ¹H and ¹³C{¹H} NMR spectra were recorded at the reported frequencies, and chemical shifts are reported in ppm (δ) and referenced to the residual solvent resonance. ³¹P{¹H} chemical shifts are referenced to H₃PO₄. The following naming conventions were used to describe NMR couplings: (s) singlet, (d) doublet, (t)

triplet, (q) quartet, (dd) doublet of doublets, (m) multiplet, (b) broad. Absorbance measurements were made using an Agilent Technologies Cary 60 spectrometer.

Fluorescent measurements were made using a Quanta Master 40 spectrofluorometer (Photon Technology International) equipped with a Quantum Northwest TLC-50 temperature controller at 25.0 ± 0.05 °C.

Fluorescence Titrations of Barbiturates 4a–d with CF₃ Host (3b). Stock solutions of **3b** (1.1 μM) and barbiturate (2.0 mM) in H₂O sat. CHCl₃ were prepared separately. 1.8 mL of the host stock solution was combined with 200 μL of the guest stock solution to give a final guest:host solution containing 200 μM guest and 1 μM host, respectively. To a blank cuvette was added 1.5 mL of host stock and diluted with H₂O sat. CHCl₃ to achieve a final concentration that matched that of the guest:host solution (1 μM). Aliquots of the guest:host solution were then added to the cuvette containing host until minimal changes in the emission spectra were observed. Plots of F_{obs}/F_0 vs [Guest] were then fit to equation 1 using Origin[®] to determine the association constant. This procedure was performed in triplicate and the average K_a values and their standard deviation are reported.

$$(1) \frac{F_{obs}}{F_0} = \frac{1 + (k_{HG}/k_H^0)K_a[G]}{1 + K_a[G]}$$

Fluorescence Titrations of Host (3b–e) with barbital. Stock solutions of **3a–e** (2 μM) and barbital (2.0 mM) in H₂O sat. CHCl₃ were prepared separately. 1.0 mL of the host stock solution was combined with 1 mL of the guest stock solution to give a final guest:host solution containing 1.0 mM guest and 1 μM host, respectively. To a blank cuvette was added 1.0 mL of host stock and diluted with H₂O sat. CHCl₃ to achieve a

final concentration that matched that of the guest:host solution (1 μM). Aliquots of the guest:host solution were then added to the cuvette containing host until minimal changes in the emission spectra were observed. Plots of F_{obs}/F_0 vs [Guest] were then fit to equation 1 using Origin[®] to determine the association constant. This procedure was performed in triplicate and the average K_a values and their standard deviation are reported.

Fluorescence Titration of 3b in the Presence of 4d with Acetic Acid. To a solution of 5 μM **3b** in H_2O sat. CDCl_3 was added 100 equivalents of **4d** (500 μM). Then aliquots of a dilute solution of acetic acid (10mM) was added followed by the addition of aliquots of concentrated acetic acid and followed using the following acquisition parameters Acquisition parameters: λ_{ex} : 325 nm; λ_{em} : 330-600 nm; excitation slits = 5.0 nm; integration time: 0.1 sec; step size: 1 nm. The ratiometric response curve between 0-0.3 M is shown below.

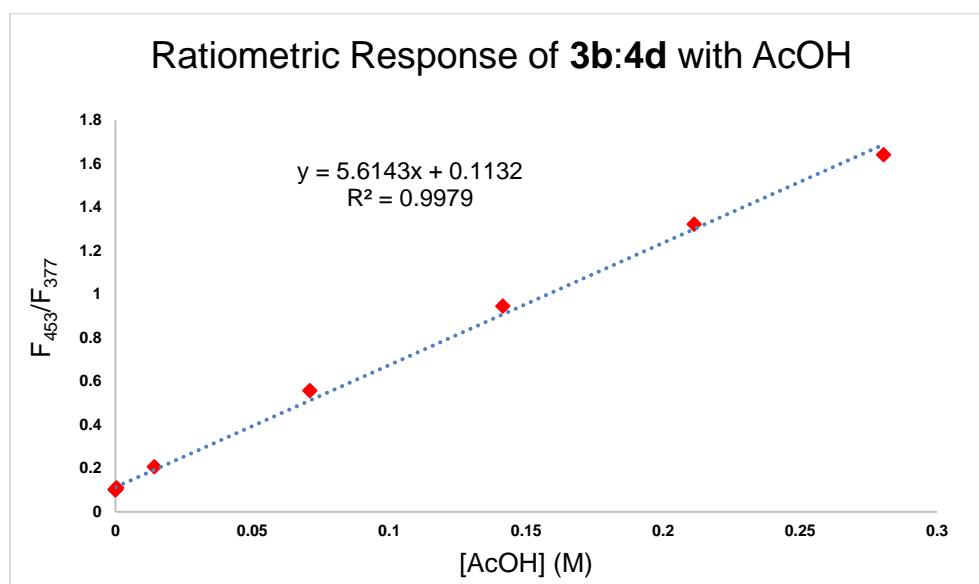


Figure E.1. Ratiometric response of **3b:4d** to the addition of AcOH in CHCl_3 .

¹H NMR Titration of 3e with 4b. A 1.0 mM solution of host **3e** in H₂O sat. CDCl₃ was prepared. The host solution was then divided such that 560 μL was placed into an NMR tube and 2.0 mL was used to create a second solution containing 50 mM guest. An initial spectrum of the host was recorded using the following parameters: nt=16 and d1=1s, after which aliquots (1-25 μL total) of the guest solution were added until the N-H resonance of host no longer shifted.

Syntheses

N-(6-Amino-4-bromopyridin-2-yl)-3,3-dimethylbutanamide (**1**). A flame dried flask containing 4-bromo-2,6-diaminopyridine (753 mg, 4.00 mmol) and anhydrous triethylamine (670 μL, 4.80 mmol) was charged with anhydrous THF (50 mL) and cooled to 0 °C. 3,3-dimethylbutyryl chloride (560 μL, 4.03 mmol) was then added dropwise. The reaction mixture was warmed to room temperature and allowed to stir for 3 hours. The crude reaction mixture was diluted with EtOAc (50 mL) and washed with water (3x) followed by brine (3x). The organic layer was then dried with MgSO₄, filtered, and concentrated via rotary evaporation. The crude product was purified via column chromatography (SiO₂, 1:1 EtOAc:Hex, R_f= 0.48) to yield a white solid (777 mg, 68%) ¹H NMR (500 MHz, CDCl₃) δ: 7.81 (s, 1H), 7.43 (s, 1H), 6.42 (s, 1H), 4.31 (s, 2H), 2.20 (s, 2H), 1.09 (s, 9H). ¹³C{¹H} NMR (126 MHz, CDCl₃) δ: 170.30, 157.47, 150.43, 135.42, 107.14, 106.66, 51.87, 31.49, 29.92.

*N*¹,*N*³-bis(4-Bromo-6-(3,3-dimethylbutanamido)pyridin-2-yl)isophthalamide (**2**). A flame dried flask containing **1** (900 mg, 3.14 mmol) and anhydrous triethylamine (500 μL, 3.58 mmol) was charged with anhydrous THF (40 mL) and cooled to 0 °C.

Isophthaloyl chloride (325 mg, 1.60 mmol) in 5 mL anhydrous THF (5 mL) was then added slowly. The reaction mixture was warmed to room temperature and allowed to stir for 23 hours. The crude reaction mixture was diluted with EtOAc and washed with water (3x) followed by brine (3x). The organic layer was then dried with MgSO₄, filtered, and concentrated via rotary evaporation. The crude product was purified via column chromatography (SiO₂, 1:1 EtOAc:Hex, R_f = 0.57) to yield a white solid (784 mg, 72%)
¹H NMR (500 MHz, CDCl₃) δ: 8.41 (s, 1H), 8.33 (s, 2H), 8.29 (s, 2H), 8.26 (s, 2H), 8.09 (d, *J* = 7.7 Hz, 2H), 7.66 (t, *J* = 7.7 Hz, 1H), 7.60 (s, 2H), 2.27 (s, 4H), 1.12 (s, 18H).
¹³C{¹H} NMR (126 MHz, CDCl₃) δ: 170.51, 164.18, 150.14, 149.72, 136.59, 134.69, 131.04, 129.92, 126.07, 113.34, 112.95, 51.88, 31.58, 29.93.

*N*¹,*N*³-bis(6-(3,3-Dimethylbutanamido)-4-((4-nitrophenyl)ethynyl)pyridin-2-yl)isophthalamide (**3a**). A flame dried flask containing **2** (96.9 mg, 0.138 mmol), Pd(PPh₃)₄ (7.6 mg, 6.6 μmol), CuI (2.7 mg, 14 μmol) was equipped with a reflux condenser and evacuated/refilled with N₂ 3x. 4-trifluoromethylphenylacetylene (63.6 mg 0.43 mmol) was then added followed by a mixture of degassed, anhydrous THF:DIPA (10:1 mL). The solution was heated to reflux and monitored via ¹H NMR by observing the disappearance of the starting N-H protons. After 16 hours there was still a small amount of unreacted starting material, therefore an additional aliquot of 4-nitrophenylacetylene (66 mg, 0.45 mmol) were added and the reaction continued to reflux for an additional 58 hrs. After this time no further conversion was observed. The crude reaction mixture was cooled to room temperature diluted with EtOAc and filtered through celite. The crude product was then dry-loaded onto silica and purified via column chromatography (SiO₂, 1:1 EtOAc:Hex) to yield an off white solid (69 mg, 60%)

containing a small amount of starting material impurity. Further purification was achieved using a recycling GPC with a flow rate of 3.5 min. The crude material was collected on the 3rd cycle to yield the final product as a white solid (35 mg, 30%). ¹H NMR (500 MHz, DMSO-*d*₆) δ: 10.73 (s, 2H), 10.26 (s, 2), 8.54 (s, 1H), 8.30 (d, *J* = 7.9 Hz, 4H), 8.19 (d, *J* = 7.7 Hz, 2H), 8.07 (s, 2H), 8.01 (s, 2H), 7.97 (d, *J* = 8.0 Hz, 4H), 7.71 (t, *J* = 7.8 Hz, 1H), 2.35 (s, 4H), 1.03 (s, 18H). ¹³C NMR (126 MHz, DMSO) δ: 171.37, 165.61, 151.00, 150.75, 147.50, 134.02, 133.22, 132.50, 131.53, 128.87, 127.88, 127.74, 123.94, 112.08, 111.52, 91.43, 90.66, 48.99, 30.96, 29.55.

*N*¹,*N*³-bis(6-(3,3-Dimethylbutanamido)-4-((4-(trifluoromethyl)phenyl)ethynyl)pyridin-2-yl)isophthalamide (**3b**). A flame dried flask containing **2** (98.9 mg, 0.140 mmol), Pd(PPh₃)₄ (8.3 mg, 7.2 μmol), CuI (4.0mg, 21 μmol) was equipped with a reflux condenser and evacuated/refilled with N₂ 3x. 4-trifluormethylphenylacetylene (70 μL 0.43 mmol) was then added followed by a mixture of degassed, anhydrous THF:DIPA (10:1 mL). The solution was heated to reflux and monitored via ¹H NMR by observing the disappearance of the starting N-H protons. After 21 hours there was still a small amount of unreacted starting material, therefore additional aliquots (2 total) of 4-trifluormethylphenylacetylene (25 μL, 0.14 mmol) were added and the reaction continued to reflux for an additional 12 hrs. After this time no further conversion was observed. The crude reaction mixture was cooled to room temperature diluted with EtOAc and filtered through celite. The crude product was then dry-loaded onto silica and purified via column chromatography (SiO₂, 1:1 EtOAc:Hex) to yield an off white solid (88 mg, 79%) containing a small amount of starting material impurity. Further purification was achieved using a recycling GPC with a flow rate of 3.5 min. The

crude material was collected on the 3rd cycle to yield the final product as a white solid (59 mg, 52%). ¹H NMR (500 MHz, DMSO-*d*₆) δ: 10.72 (s, 2H), 10.25 (s, 2H), 8.54 (s, 1H), 8.18 (d, *J* = 7.7 Hz, 2H), 8.05 (s, 2H), 7.99 (s, 2H), 7.91 (d, *J* = 8.0 Hz, 4H), 7.84 (d, *J* = 7.9 Hz, 4H), 7.71 (t, *J* = 7.7 Hz, 1H), 2.34 (s, 4H), 1.03 (s, 18H). ¹⁹F NMR (471 MHz, DMSO) δ: -61.40.

*N*¹,*N*³-bis(6-(3,3-Dimethylbutanamido)-4-(phenylethynyl)pyridin-2-yl)isophthalamide (**3c**). A flame dried flask containing **2** (98.0mg, 0.140 mmol), Pd(PPh₃)₄ (8.0 mg, 6.9 μmol), and CuI (3.2 mg, 17 μmol) was equipped with a reflux condenser and evacuated/refilled with N₂ 3x. Phenylacetylene (50 μL, 0.455 mmol) was then added followed by a mixture of degassed, anhydrous THF:DIPA (10:1 mL). The solution was heated to reflux and monitored until completion (6 hrs) via ¹H NMR by observing the disappearance of the starting N-H protons. The crude reaction mixture was cooled to room temperature diluted with EtOAc and filtered through celite. The crude product was then dry-loaded onto silica and purified via column chromatography (SiO₂, 1:1 EtOAc:Hex) to yield an off white solid. Further purification was achieved by recrystallization from a CHCl₃:Hex layering to yield the final product as a white solid (58 mg, 55%). ¹H NMR (500 MHz, DMSO-*d*₆) δ: 10.68 (s, 2H), 10.21 (s, 2H), 8.53 (s, 1H), 8.18 (d, *J* = 7.7 Hz, 2H), 8.01 (s, 2H), 7.95 (s, 2H), 7.71 (t, *J* = 7.8 Hz, 1H), 7.68 (d, *J* = 7.6 Hz, 4H), 7.54 – 7.43 (m, 6H), 2.34 (s, 4H), 1.03 (s, 18H). ¹³C NMR (126 MHz, DMSO) δ: 171.31, 165.57, 150.92, 150.65, 134.06, 133.44, 131.89, 131.50, 129.76, 128.92, 128.87, 127.68, 121.15, 111.94, 111.37, 92.86, 87.24, 49.02, 30.95, 29.56.

*N*¹,*N*³-bis(6-(3,3-Dimethylbutanamido)-4-((4-methoxyphenyl)ethynyl)pyridin-2-yl)isophthalamide (**3d**). A flame dried flask containing **2** (98.9 mg, 0.140 mmol),

Pd(PPh₃)₄ (8.6 mg, 7.4 μmol), CuI (3.8 mg, 20 μmol) and 4-methoxyphenylacetylene (40.0 mg, 0.30 mmol) was equipped with a reflux condenser and evacuated/refilled with N₂ 3x. Then a mixture of degassed, anhydrous THF:DIPA (10:1 mL) was added. The solution was heated to reflux and monitored until completion (7.5 hrs) via ¹H NMR by observing the disappearance of the starting N-H protons. The crude reaction mixture was cooled to room temperature diluted with EtOAc and filtered through celite. The crude product was then dry-loaded onto silica and purified via column chromatography (SiO₂, 1:1 EtOAc:Hex) to yield an off white solid (88 mg, 79%) containing a small amount of starting material impurity. Further purification was achieved using a recycling GPC with a flow rate of 3.5 min. The crude material was collected on the 3rd cycle to yield the final product as a white solid (59 mg, 52%). ¹H NMR (500 MHz, DMSO-*d*₆) δ: 10.64 (s, 2H), 10.17 (s, 2H), 8.53 (s, 1H), 8.23 – 8.13 (m, 2H), 7.97 (s, 2H), 7.91 (s, 2H), 7.66 – 7.56 (m, 4H), 7.03 (d, *J* = 8.1 Hz, 4H), 3.82 (s, 6H), 2.33 (s, 4H), 1.03 (s, 18H). ¹³C NMR (126 MHz, DMSO) δ: 208.92, 203.17, 197.94, 188.51, 188.23, 171.72, 171.53, 171.27, 169.11, 166.51, 165.29, 152.22, 150.64, 149.40, 148.83, 131.03, 123.84, 93.03, 86.66, 68.59, 67.20.

*N*¹,*N*³-bis(4-((4-(Dimethylamino)phenyl)ethynyl)-6-(3,3-dimethylbutanamido)pyridin-2-yl)isophthalamide (**3e**). A flame dried flask containing **2** (98.4 mg, 0.140 mmol), Pd(PPh₃)₄ (9.2 mg, 8.0 μmol), CuI (3.1 mg, 16 μmol) and 4-Dimethylaminophenylacetylene (61.0 mg, 0.42 mmol) was equipped with a reflux condenser and evacuated/refilled with N₂ 3x. Then a mixture of degassed, anhydrous THF:DIPA (10:1 mL) was added. The solution was heated to reflux and monitored until completion (5 hrs) via ¹H NMR by observing the disappearance of the starting N-H

protons. The crude reaction mixture was cooled to room temperature diluted with EtOAc and filtered through celite. The crude product was then dry-loaded onto silica and purified via column chromatography (SiO₂, 1:1 EtOAc:Hex) to yield a yellow solid (78 mg, 67%). ¹H NMR (500 MHz, DMSO-*d*₆) δ: 10.60 (s, 2H), 10.13 (s, 2H), 8.52 (s, 1H), 8.17 (d, *J* = 7.7 Hz, 2H), 7.93 (s, 2H), 7.86 (s, 2H), 7.70 (t, *J* = 7.7 Hz, 1H), 7.46 (d, *J* = 8.0 Hz, 4H), 6.74 (d, *J* = 8.1 Hz, 4H), 2.98 (s, 12H), 2.33 (s, 4H), 1.03 (s, 18H). ¹³C NMR (126 MHz, DMSO-*d*₆) δ: 171.22, 165.48, 150.79, 150.73, 150.49, 134.51, 134.10, 133.12, 131.43, 128.86, 127.60, 111.85, 111.45, 110.87, 106.90, 95.40, 85.84, 49.03, 30.94, 29.56.

Additional Fluorescence and Absorption Spectra

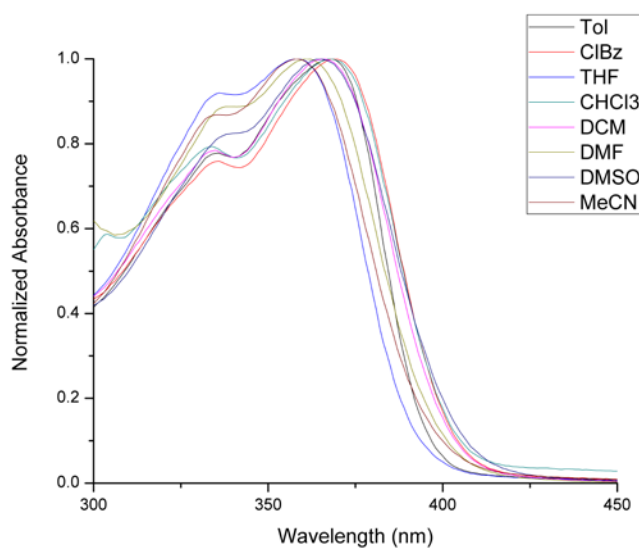


Figure E.2. Normalized absorbance spectra of **3e** showing solvatochromic behavior. [3e] = 5.0 μM.

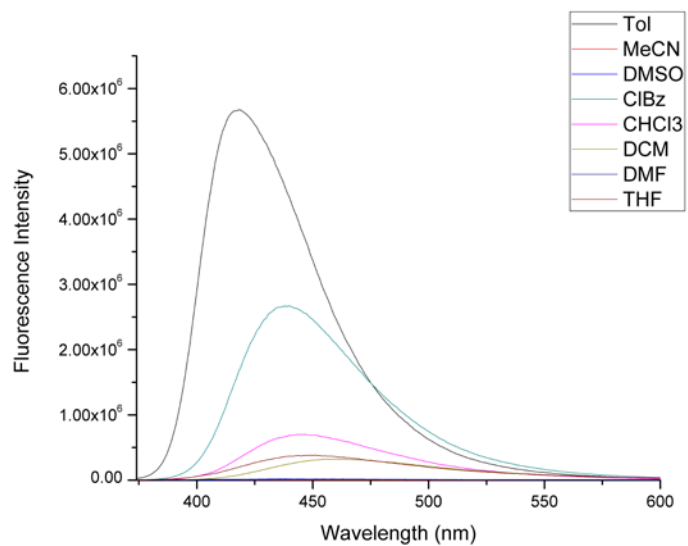


Figure E.3. Raw absorbance spectra of **3e** showing decreasing emission intensity as a function of solvent polarity. $[3e] = 5.0 \mu\text{M}$.

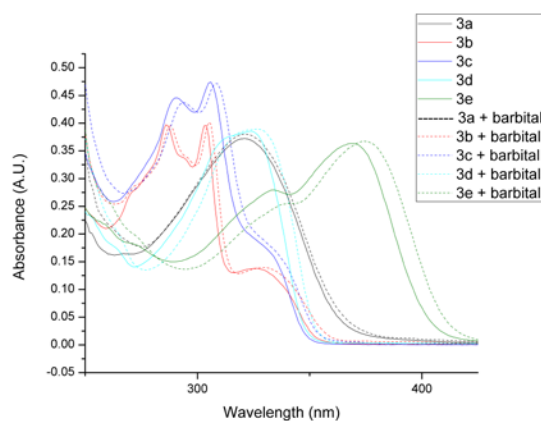


Figure E.4. Absorption spectra of **3a-e** in the absence and presence of barbital (100 equiv.) in H_2O sat. CHCl_3 . $[H] = 5 \mu\text{M}$.

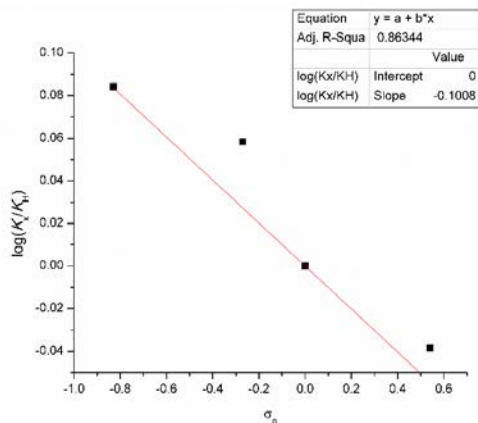


Figure E.5. Hammett Plot of binding affinities of **3b-e** with barbital in H₂O sat. CHCl₃ @ 25 °C.

Table E.1. Solvent dependent absorption and emission properties of **3e** ([H] = 5 μM).

solvent	absorption λ_{\max} (nm)	emission λ_{\max} (nm)
toluene	368	418
chloroform	368	447
chlorobenzene	369	440
tetrahydrofuran	359	451
dichloromethane	366	459
acetonitrile	358	479
dimethylformamide	361	438
dimethylsulfoxide	365	464

Representative Binding Isotherms and Raw Fluorescence Data

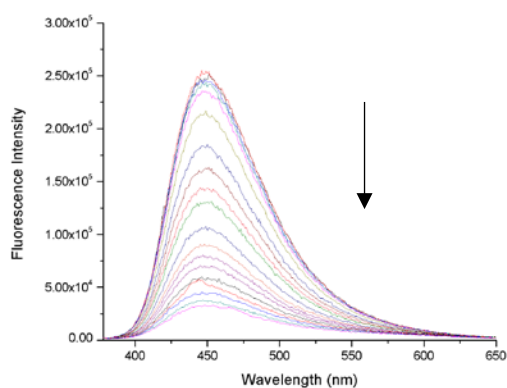


Figure E.6. Raw fluorescence data from **3e** with barbital titration.

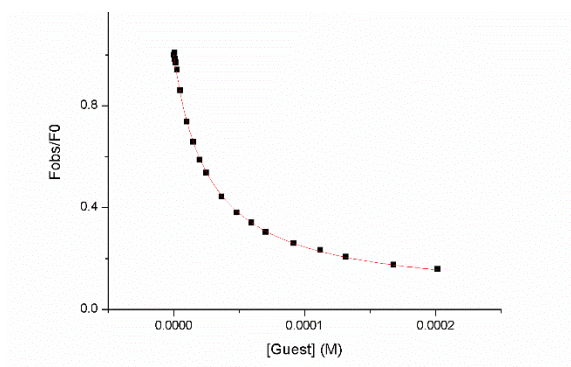


Figure E.7. Representative binding isotherm of **3e** with barbital.

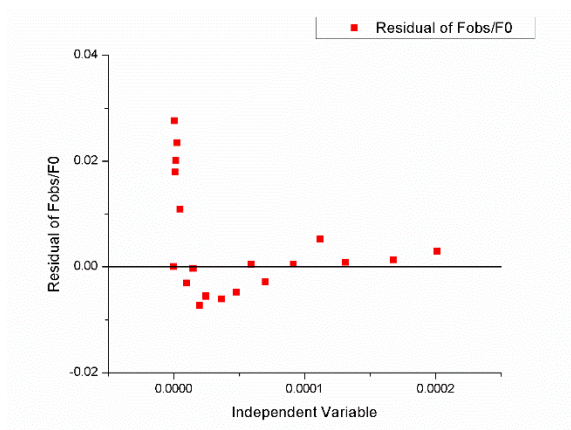


Figure E.8. Residuals plot from 1:1 binding model of **3e** with barbital titration.

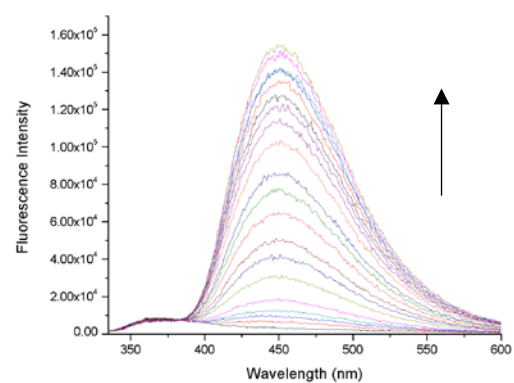


Figure E.9. Raw fluorescence data from **3d** with barbital titration.

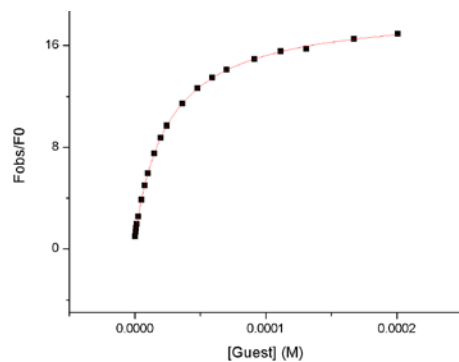


Figure E.10. Representative binding isotherm of **3d** with barbital.

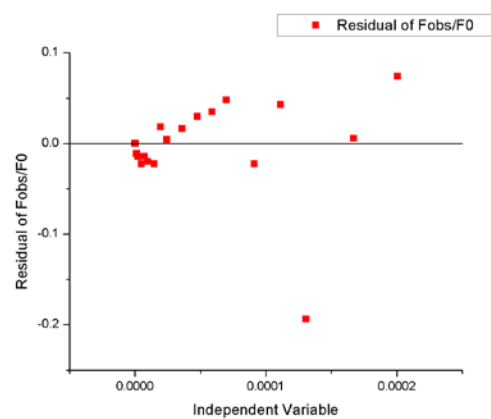


Figure E.11. Residuals plot from 1:1 binding model of **3d** with barbital titration.

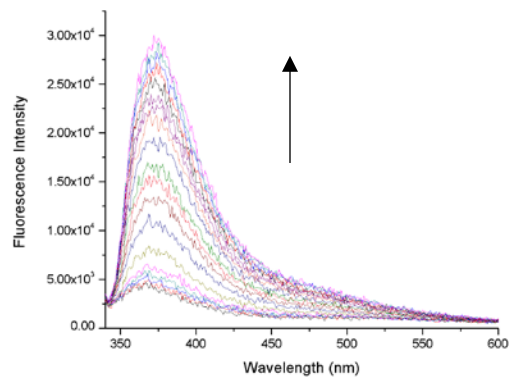


Figure E.12 Raw fluorescence data from **3c** with barbital titration.

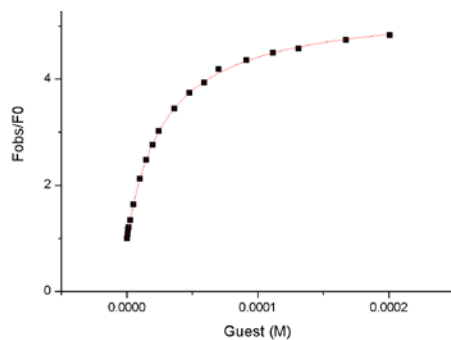


Figure E.13. Representative binding isotherm of **3c** with barbital.

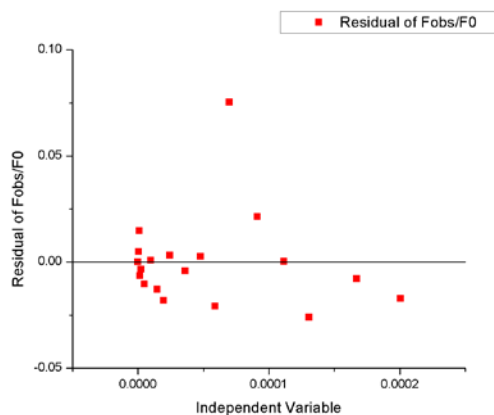


Figure E.14. Residuals plot from 1:1 binding model of **3c** with barbital titration.

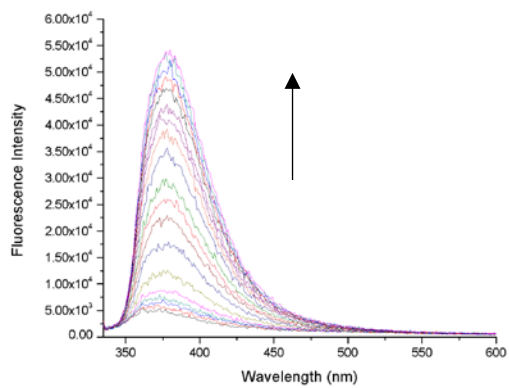


Figure E.15. Raw fluorescence data from **3b** with barbital titration

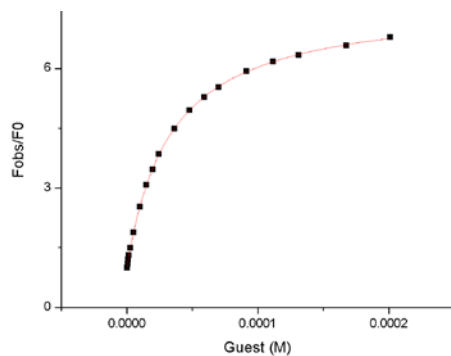


Figure E.16. Representative binding isotherm of **3b** with barbital.

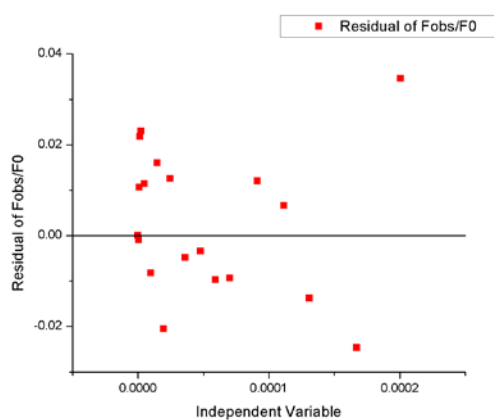


Figure E.17. Residuals plot from 1:1 binding model of **3c** with barbital titration.

NMR Spectra.

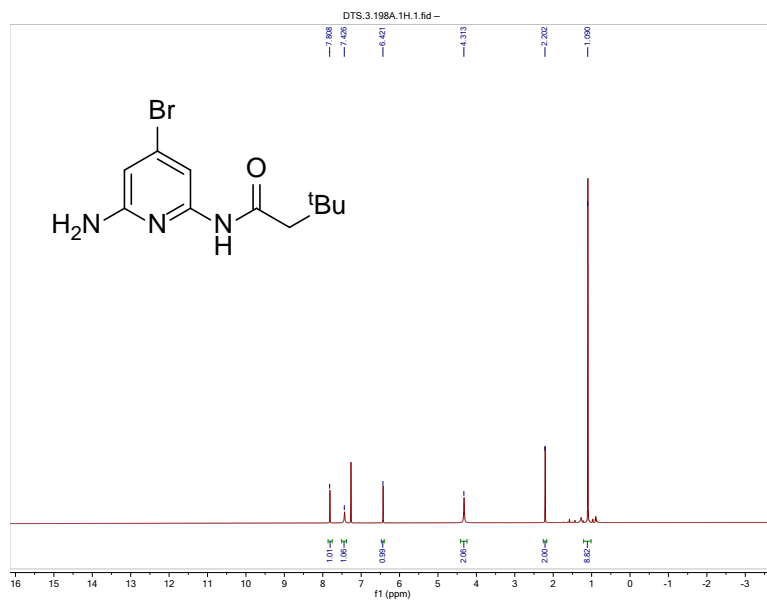


Figure E.18. ^1H (500 MHz), NMR spectrum of **1**.

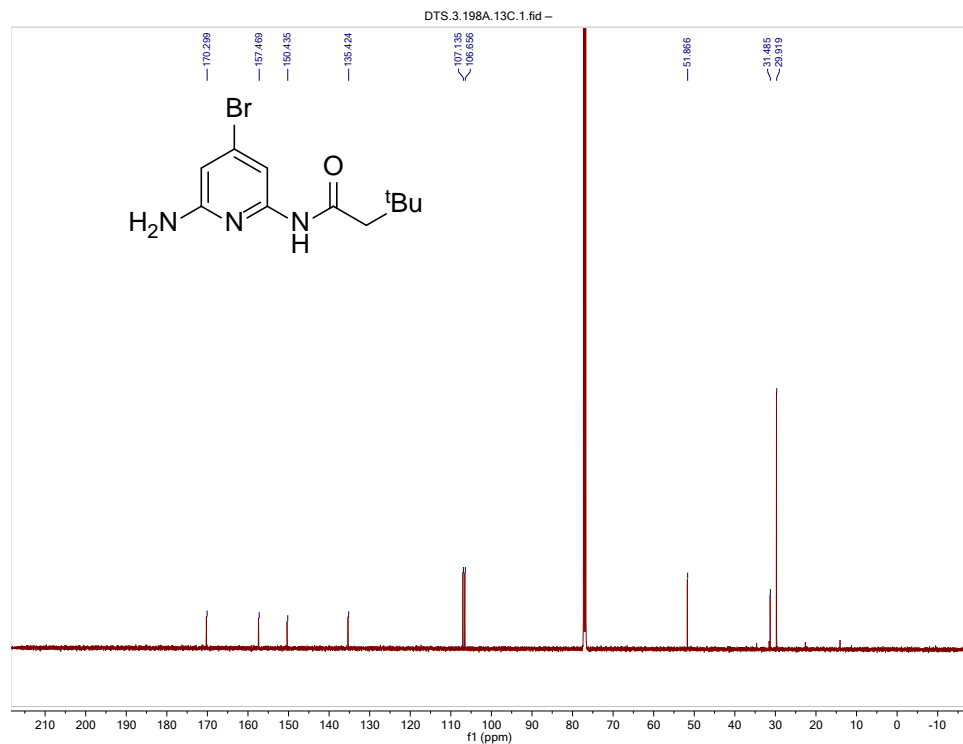


Figure E.19. $^{13}\text{C}\{^1\text{H}\}$ (126 MHz) NMR spectrum of **1**.

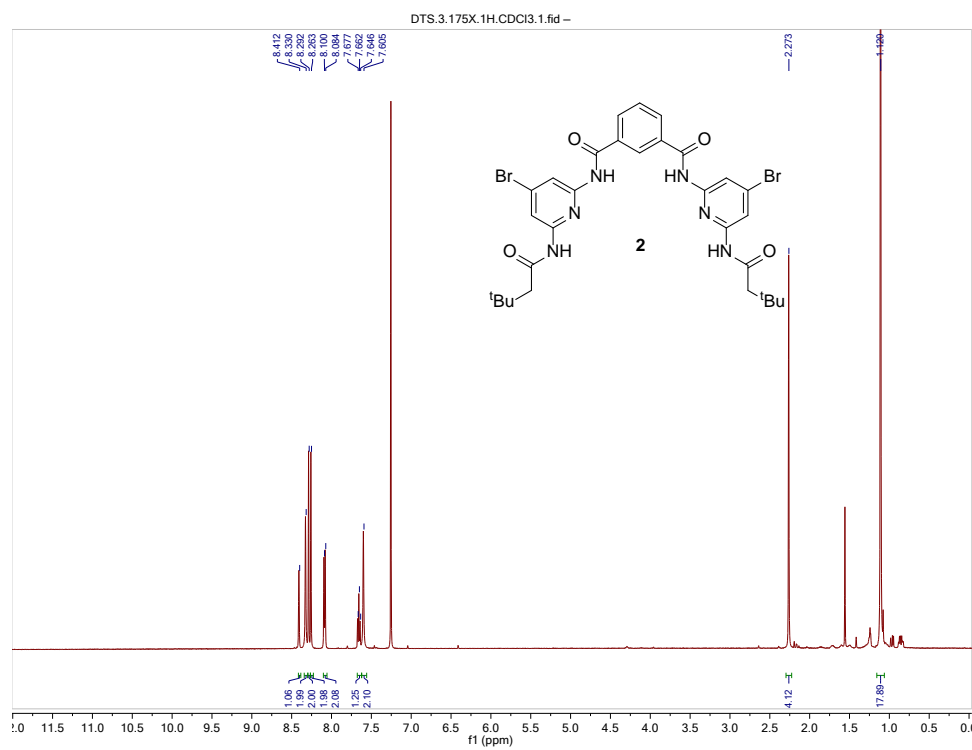


Figure E.20. ^1H (500 MHz), NMR spectrum of **2**.

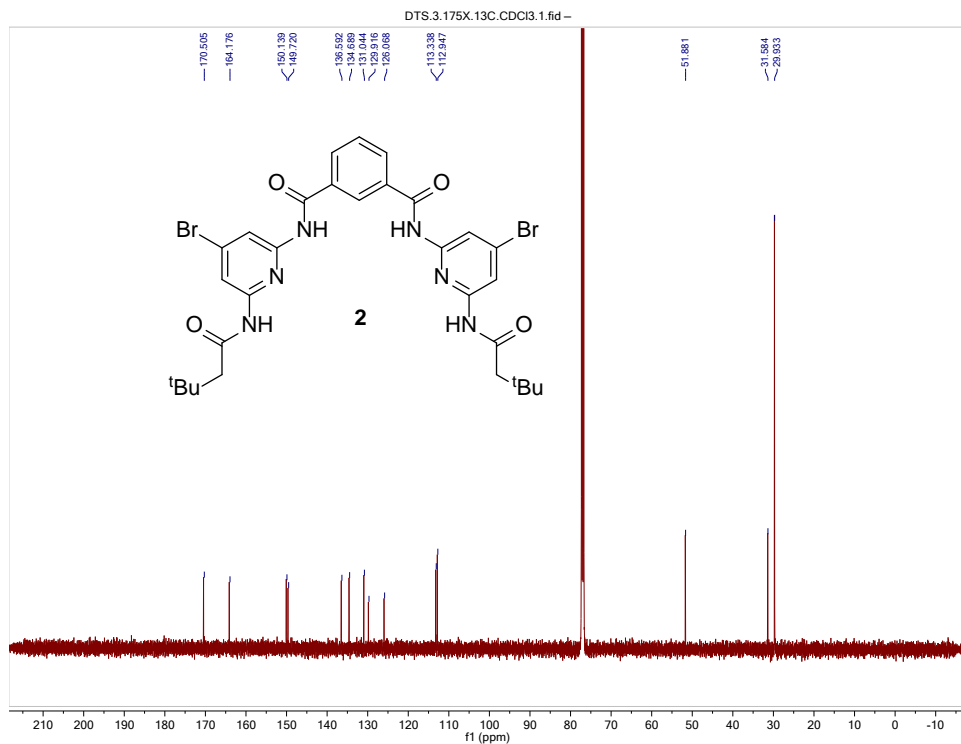


Figure E.21. $^{13}\text{C}\{^1\text{H}\}$ (126 MHz) NMR spectrum of **2**.

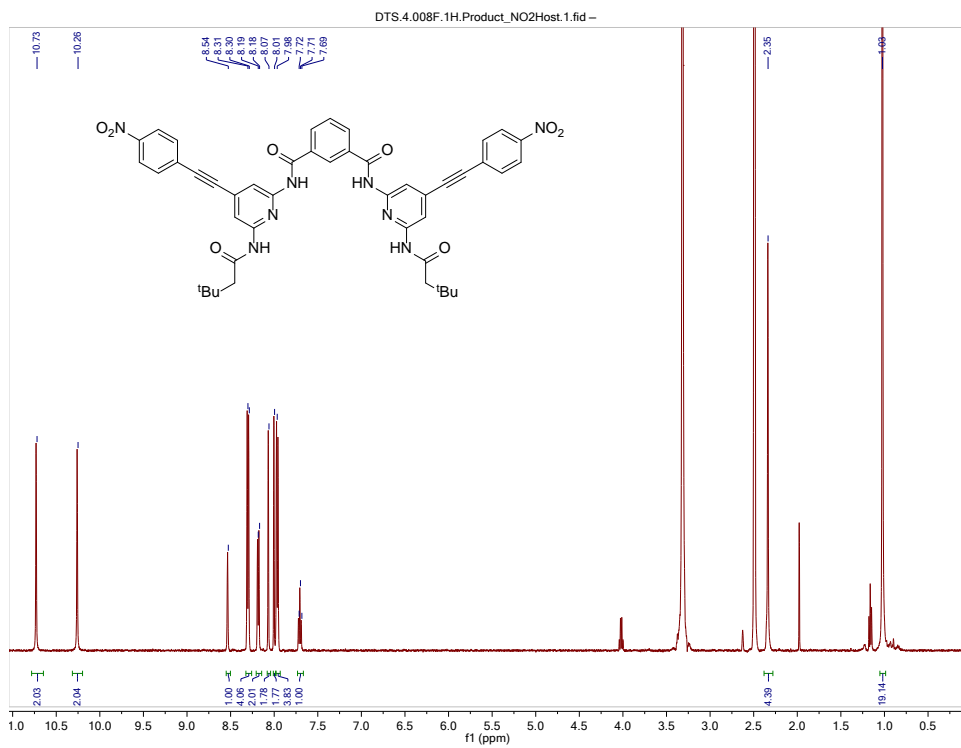


Figure E.22. ^1H (500 MHz) NMR spectrum of **3a**.

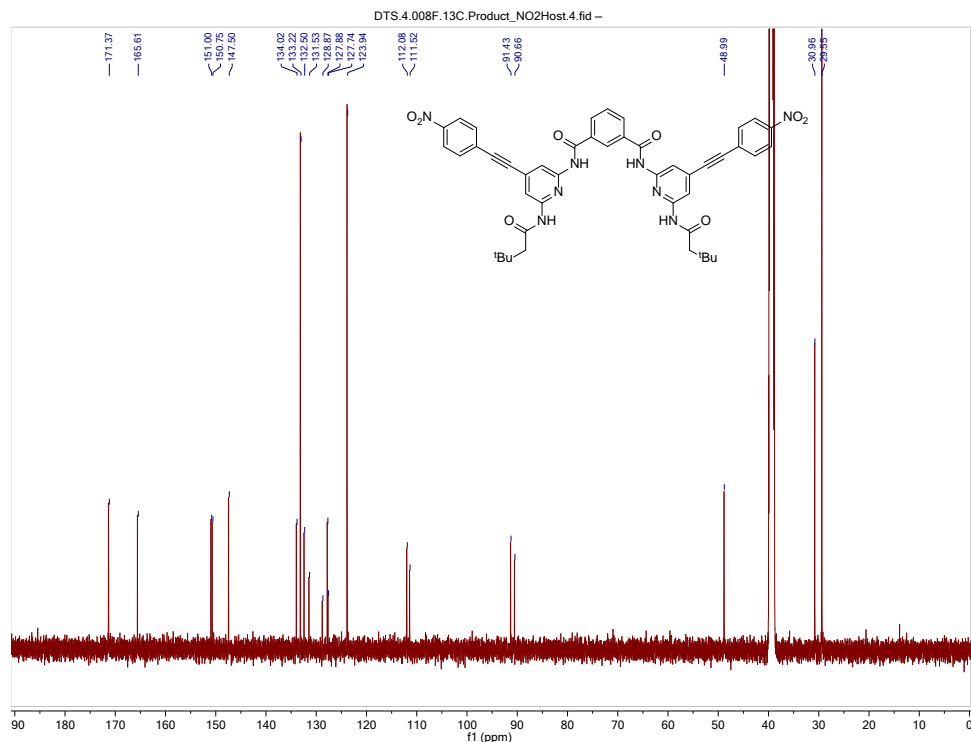


Figure E.23. $^{13}\text{C}\{^1\text{H}\}$ (126 MHz) NMR spectrum of **3a**.

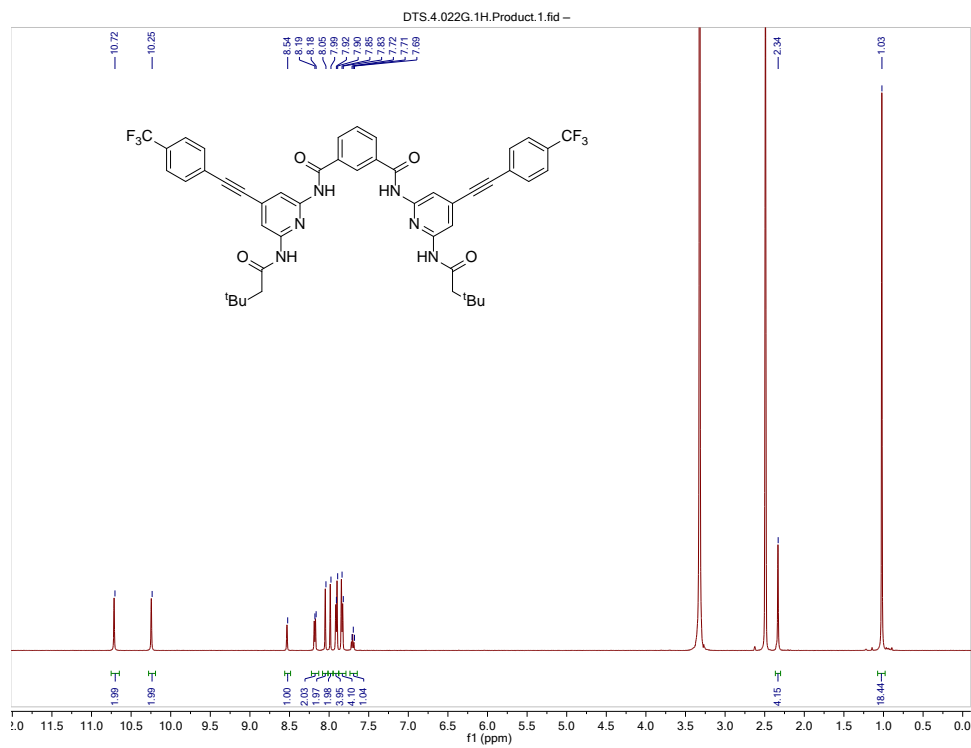


Figure E.24. ^1H (500 MHz) NMR spectrum of **3b**.



Figure E.25. ^{19}F (471 MHz) NMR spectrum of **3b**.

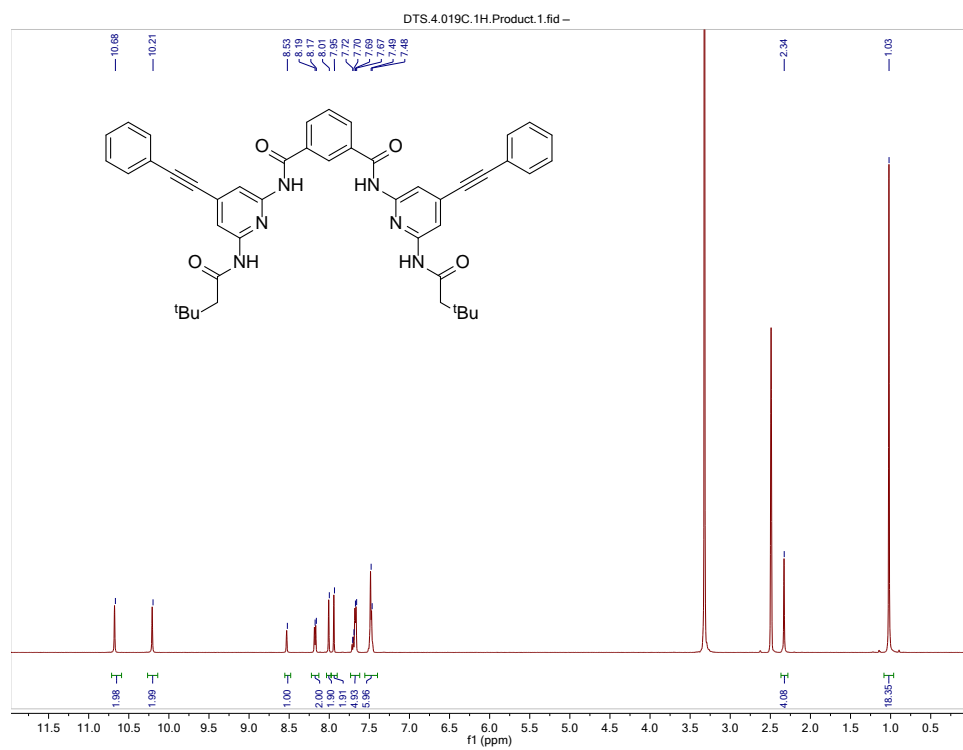


Figure E.26. ^1H (500 MHz) NMR spectrum of **3c**.

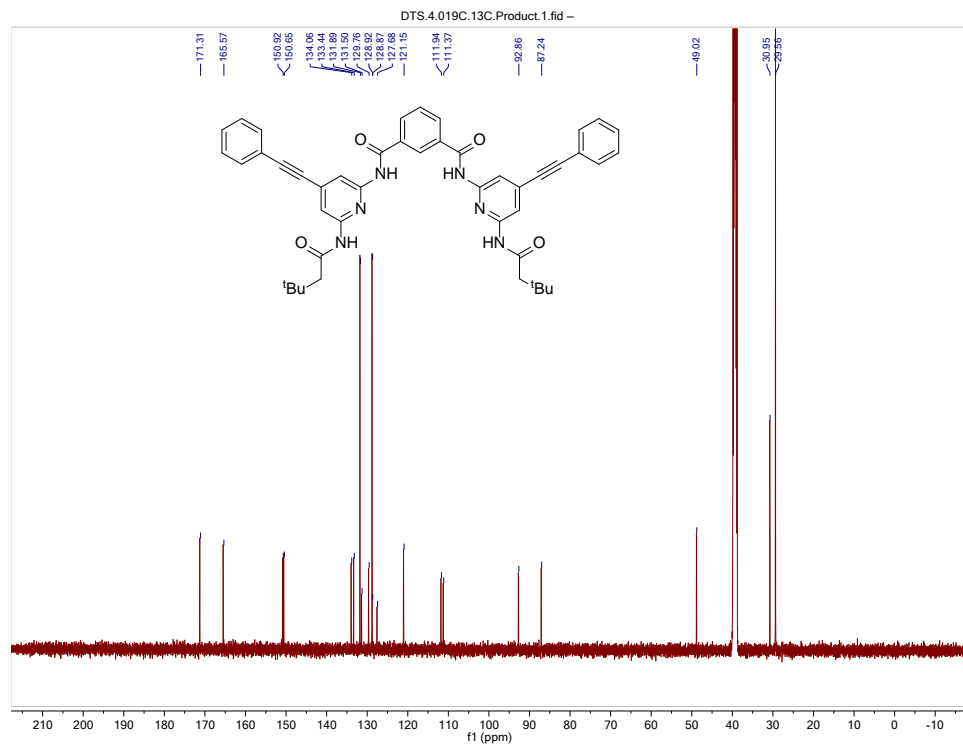


Figure E.27. $^{13}\text{C}\{^1\text{H}\}$ (126 MHz) NMR spectrum of **3c**.

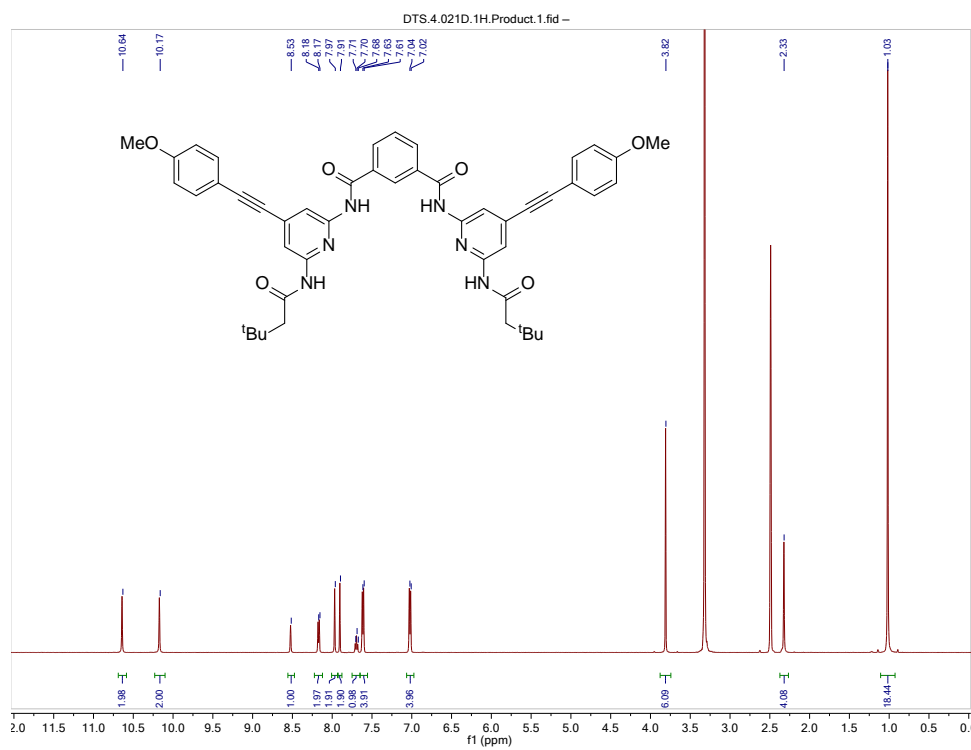


Figure E.28. ^1H (500 MHz) NMR spectrum of **3d**.

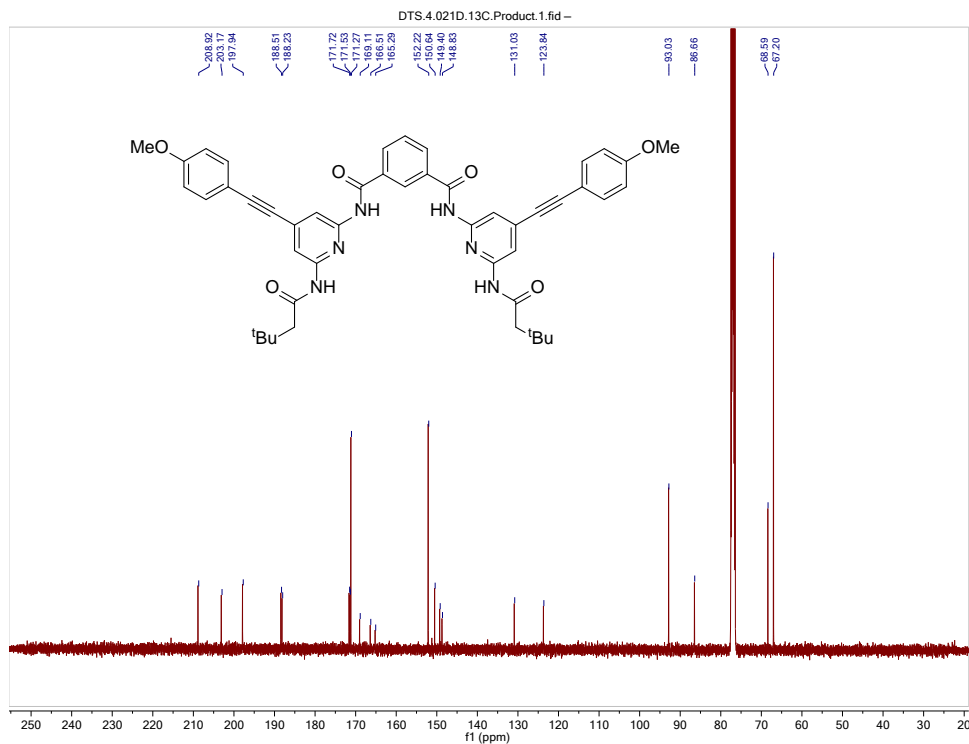


Figure E.29. $^{13}\text{C}\{^1\text{H}\}$ (126 MHz) NMR spectrum of **3d**.

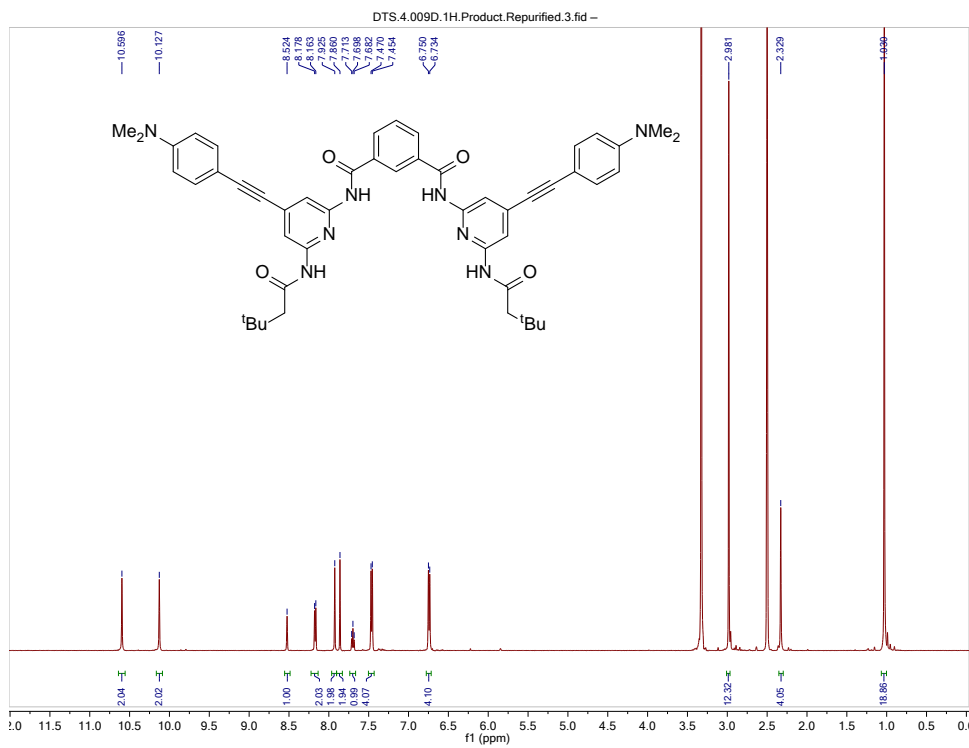


Figure E.30. ^1H (500 MHz) NMR spectrum of **3e**.

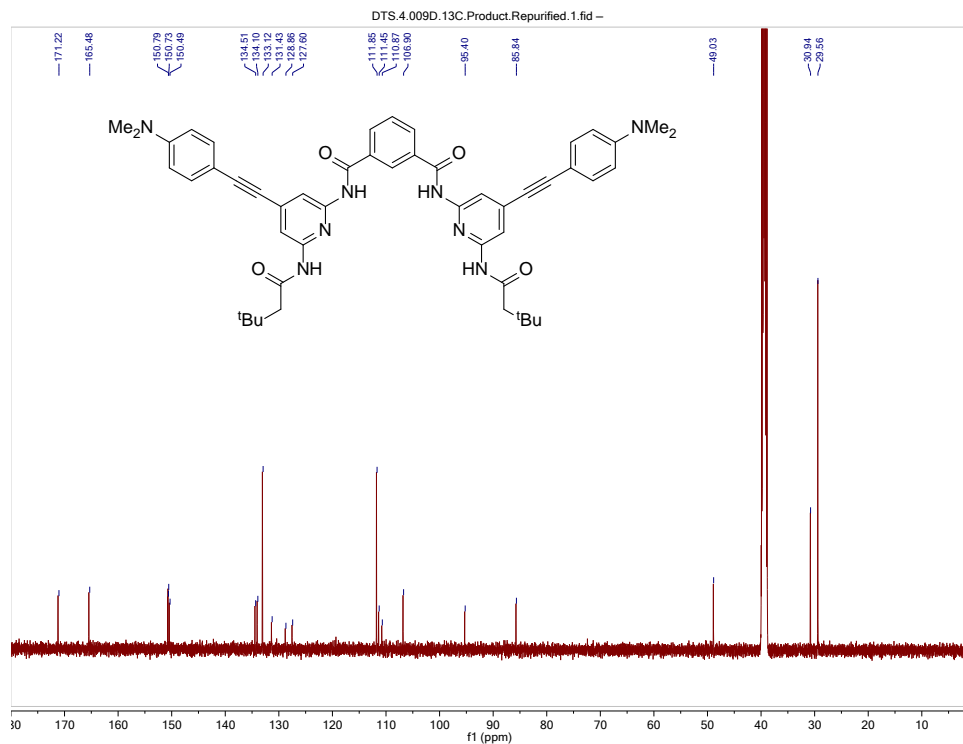


Figure E.31. $^{13}\text{C}\{^1\text{H}\}$ (126 MHz) NMR spectrum of **3e**.

REFERENCES CITED

CHAPTER I

1. Huang, F. H.; Anslyn, E. V., *Chem. Rev.* **2015**, *115*, 6999-7000.
2. Lehn, J. M., *Chem. Soc. Rev.* **2017**, *46*, 2378-2379.
3. Biedermann, F.; Schneider, H. J., *Chem. Rev.* **2016**, *116*, 5216-5300.
4. Muller-Dethlefs, K.; Hobza, P., *Chem. Rev.* **2000**, *100*, 143-167.
5. Cooke, G.; Rotello, V. M., *Chem. Soc. Rev.* **2002**, *31*, 275-286.
6. Chang, S. K.; Hamilton, A. D., *J. Am. Chem. Soc.* **1988**, *110*, 1318-1319.
7. López-Muñoz, F.; Ucha-Udabe, R.; Alamo, C., *Neuropsychiatr. Dis. Treat.* **2005**, *1*, 329-343.
8. Chang, S. K.; Vanengen, D.; Fan, E.; Hamilton, A. D., *J. Am. Chem. Soc.* **1991**, *113*, 7640-7645.
9. Tecilla, P.; Hamilton, A. D., *J. Chem. Soc. Chem. Commun.* **1990**, 1232-1234.
10. McGrath, J. M.; Pluth, M. D., *J. Org. Chem.* **2014**, *79*, 711-719.
11. McGrath, J. M.; Pluth, M. D., *J. Org. Chem.* **2014**, *79*, 11797-11801.
12. Tron, A.; Rocher, M.; Thornton, P. J.; Tucker, J. H. R.; McClenaghan, N. D., *Asian J. Org. Chem.* **2015**, *4*, 192-202.
13. Al-Sayah, M. H.; McDonald, R.; Branda, N. R., *Eur. J. Org. Chem.* **2004**, 173-182.
14. Sorensen, H. S.; Larsen, J.; Rasmussen, B. S.; Laursen, B.; Hansen, S. G.; Skrydstrup, T.; Amatore, C.; Jutand, A., *Organometallics* **2002**, *21*, 5243-5253.
15. Larsen, J.; Rasmussen, B. S.; Hazell, R. G.; Skrydstrup, T., *Chem. Commun.* **2004**, 202-203.
16. Li, Y.; He, Y. M.; Li, Z. W.; Zhang, F.; Fan, Q. H., *Org. Biomol. Chem.* **2009**, *7*, 1890-1895.

17. Rasmussen, B. S.; Elezcano, U.; Skrydstrup, T., *J. Chem. Soc. Perkin Trans. 1* **2002**, 1723-1733.
18. Ema, T.; Tanida, D.; Sakai, T., *Org. Lett.* **2006**, 8, 3773-3775.
19. Ema, T.; Tanida, D.; Sakai, T., *J. Am. Chem. Soc.* **2007**, 129, 10591-10596.
20. Ema, T.; Okuda, K.; Watanabe, S.; Yamasaki, T.; Minami, T.; Esipenko, N. A.; Anzenbacher, P., *Org. Lett.* **2014**, 16, 1302-1305.
21. Zirbs, R.; Kienberger, F.; Hinterdorfer, P.; Binder, W. H., *Langmuir* **2005**, 21, 8414-8421.
22. Binder, W. H.; Kluger, C.; Josipovic, M.; Straif, C. J.; Friedbacher, G., *Macromolecules* **2006**, 39, 8092-8101.
23. Binder, W. H.; Lomoschitz, M.; Sachsenhofer, R.; Friedbacher, G., *J. Nanomater.* **2009**, 14.
24. Glockner, C.; Luning, U., *J. Incl. Phenom. Macrocycl. Chem.* **2011**, 71, 239-242.
25. Zeininger, L.; Klaumunzer, M.; Peukert, W.; Hirsch, A., *Int. J. Mol. Sci.* **2015**, 16, 8186-8200.
26. Zeininger, L.; Lodermeier, F.; Costa, R. D.; Guldi, D. M.; Hirsch, A., *Chem. Commun.* **2016**, 52, 8842-8845.
27. Hager, K.; Hartnagel, U.; Hirsch, A., *Eur. J. Org. Chem.* **2007**, 1942-1956.
28. Wessendorf, F.; Gnichwitz, J. F.; Sarova, G. H.; Hager, K.; Hartnagel, U.; Guldi, D. M.; Hirsch, A., *J. Am. Chem. Soc.* **2007**, 129, 16057-16071.
29. Wessendorf, F.; Grimm, B.; Guldi, D. M.; Hirsch, A., *J. Am. Chem. Soc.* **2010**, 132, 10786-10795.
30. Pagona, G.; Rotas, G.; Tagmatarchis, N., *Fuller. Nanotub. Carbon Nanostruct.* **2014**, 22, 88-98.
31. Pagona, G.; Stergiou, A.; Gobeze, H. B.; Rotas, G.; D'Souza, F.; Tagmatarchis, N., *Phys. Chem. Chem. Phys.* **2016**, 18, 811-817.
32. Grimm, B.; Schornbaum, J.; Jasch, H.; Trukhina, O.; Wessendorf, F.; Hirsch, A.; Torres, T.; Guldi, D. M., *Proc. Natl. Acad. Sci. U. S. A.* **2012**, 109, 15565-15571.
33. Bosch, S.; Zeininger, L.; Hauke, F.; Hirsch, A., *Chem. Eur. J.* **2014**, 20, 2537-2541.

34. Altintas, O.; Artar, M.; ter Huurne, G.; Voets, I. K.; Palmans, A. R. A.; Barner-Kowollik, C.; Meijer, E. W., *Macromolecules* **2015**, *48*, 8921-8932.
35. Lee, S. H.; Ouchi, M.; Kim, S.; Sawamoto, M., *Polym. Chem.* **2016**, *7*, 7152-7160.
36. Chen, S.; Strohl, D.; Binder, W. H., *ACS Macro Lett.* **2015**, *4*, 48-52.
37. Altintas, O.; Schulze-Suenninghausen, D.; Luy, B.; Barner-Kowollik, C., *Eur. Polym. J.* **2015**, *62*, 409-417.
38. Pagona, G.; Stergiou, A.; Gobeze, H. B.; Rotas, G.; D'Souza, F.; Tagmatarchis, N., *Phys. Chem. Chem. Phys.* **2016**, *18*, 811-817.
39. Berl, V.; Krische, M. J.; Huc, I.; Lehn, J. M.; Schmutz, M., *Chem. Eur. J.* **2000**, *6*, 1938-1946.
40. Berl, V.; Schmutz, M.; Krische, M. J.; Khoury, R. G.; Lehn, J. M., *Chem. Eur. J.* **2002**, *8*, 1227-1244.
41. Binder, W. H.; Bernstorff, S.; Kluger, C.; Petraru, L.; Kunz, M. J., *Adv. Mater.* **2005**, *17*, 2824-2828.
42. H., B. W.; Laura, P.; Harald, W.; Dietrich, G.; Robert, S., *Macromolecular Symposia* **2007**, *254*, 62-66.
43. Binder, W. H.; Petraru, L.; Roth, T.; Groh, P. W.; Palfi, V.; Keki, S.; Ivan, B., *Adv. Funct. Mater.* **2007**, *17*, 1317-1326.
44. Herbst, F.; Seiffert, S.; Binder, W. H., *Polym. Chem.* **2012**, *3*, 3084-3092.
45. Chen, S. B.; Mahmood, N.; Beiner, M.; Binder, W. H., *Angew. Chem. Int. Ed.* **2015**, *54*, 10188-10192.
46. Altintas, O.; Krolla-Sidenstein, P.; Gliemann, H.; Barner-Kowollik, C., *Macromolecules* **2014**, *47*, 5877-5888.
47. Fischer, T. S.; Schulze-Sunninghausen, D.; Luy, B.; Altintas, O.; Barner-Kowollik, C., *Angew. Chem. Int. Ed.* **2016**, *55*, 11276-11280.
48. Pahnke, K.; Altintas, O.; Schmidt, F. G.; Barner-Kowollik, C., *ACS Macro Lett.* **2015**, *4*, 774-777.
49. Groom, A.; Manning, K. B.; Weck, M., *Macromolecules* **2016**, *49*, 7117-7128.

50. Tron, A.; Thornton, P. J.; Rocher, M.; de Rouville, H. P. J.; Desvergne, J. P.; Kauffmann, B.; Buffeteau, T.; Cavagnat, D.; Tucker, J. H. R.; McClenaghan, N. D., *Org. Lett.* **2014**, *16*, 1358-1361.
51. Tron, A.; Thornton, P. J.; Lincheneau, C.; Desvergne, J. P.; Spencer, N.; Tucker, J. H. R.; McClenaghan, N. D., *J. Org. Chem.* **2015**, *80*, 988-996.
52. Tron, A.; Pianet, I.; Martinez-Cuezva, A.; Tucker, J. H. R.; Pisciottoni, L.; Alajarin, M.; Berna, J.; McClenaghan, N. D., *Org. Lett.* **2017**, *19*, 154-157.
53. Martinez-Cuezva, A.; Berna, J.; Orenes, R. A.; Pastor, A.; Alajarin, M., *Angew. Chem. Int. Ed.* **2014**, *53*, 6762-6767.

CHAPTER II

1. Gillespie, J. A.; Zuidema, E.; van Leeuwen, P. W. N. M.; Kamer, P. C. J., Phosphorus Ligand Effects in Homogeneous Catalysis and Rational Catalyst Design. In *Phosphorus(III) Ligands in Homogeneous Catalysis: Design and Synthesis*, John Wiley & Sons, Ltd **2012**; pp 1-26.
2. Falkowski, J. M.; Sawano, T.; Zhang, T.; Tsun, G.; Chen, Y.; Lockard, J. V.; Lin, W. B., *J. Am. Chem. Soc.* **2014**, *136*, 5213-5216.
3. Tan, X.; Li, L.; Zhang, J. Y.; Han, X. R.; Jiang, L.; Li, F. W.; Su, C. Y., *Chem. Mater.* **2012**, *24*, 480-485.
4. Xu, X. L.; Nieuwenhuyzen, M.; James, S. L., *Angew. Chem. Int. Ed.* **2002**, *41*, 764-767.
5. Cook, T. R.; Zheng, Y. R.; Stang, P. J., *Chem. Rev.* **2013**, *113*, 734-777.
6. Holliday, B. J.; Mirkin, C. A., *Angew. Chem. Int. Ed.* **2001**, *40*, 2022-2043.
7. Bocokic, V.; Kalkan, A.; Lutz, M.; Spek, A. L.; Gryko, D. T.; Reek, J. N. H., *Nat. Commun.* **2013**, *4*, 9.
8. Wang, Q. Q.; Gonell, S.; Leenders, S.; Durr, M.; Ivanovic-Burmazovic, I.; Reek, J. N. H., *Nat. Chem.* **2016**, *8*, 225-230.
9. Yamamura, M.; Sukegawa, K.; Nabeshima, T., *Chem. Commun.* **2015**, *51*, 12080-12083.
10. Bellini, R.; van der Vlugt, J. I.; Reek, J. N. H., *Isr. J. Chem.* **2012**, *52*, 613-629.
11. Breit, B., *Angew. Chem. Int. Ed.* **2005**, *44*, 6816-6825.

12. Carboni, S.; Gennari, C.; Pignataro, L.; Piarulli, U., *Dalton Trans.* **2011**, *40*, 4355-4373.
13. Raynal, M.; Ballester, P.; Vidal-Ferran, A.; van Leeuwen, P., *Chem. Soc. Rev.* **2014**, *43*, 1660-1733.
14. Sandee, A. J.; Reek, J. N. H., *Dalton Trans.* **2006**, 3385-3391.
15. Slagt, V. F.; Röder, M.; Kamer, P. C. J.; van Leeuwen, P. W. N. M.; Reek, J. N. H., *J. Am. Chem. Soc.* **2004**, *126*, 4056-4057.
16. Weis, M.; Waloch, C.; Seiche, W.; Breit, B., *J. Am. Chem. Soc.* **2006**, *128*, 4188-4189.
17. Breit, B.; Seiche, W., *J. Am. Chem. Soc.* **2003**, *125*, 6608-6609.
18. Wieland, J.; Breit, B., *Nat. Chem.* **2010**, *2*, 832-837.
19. Slagt, V. F.; van Leeuwen, P.; Reek, J. N. H., *Angew. Chem. Int. Ed.* **2003**, *42*, 5619-5623.
20. Slagt, V. F.; van Leeuwen, P.; Reek, J. N. H., *Chem. Commun.* **2003**, 2474-2475.
21. Chang, S. K.; Hamilton, A. D., *J. Am. Chem. Soc.* **1988**, *110*, 1318-1319.
22. Larsen, J.; Rasmussen, B. S.; Hazell, R. G.; Skrydstrup, T., *Chem. Commun.* **2004**, 202-203.
23. Sorensen, H. S.; Larsen, J.; Rasmussen, B. S.; Laursen, B.; Hansen, S. G.; Skrydstrup, T.; Amatore, C.; Jutand, A., *Organometallics* **2002**, *21*, 5243-5253.
24. McGrath, J. M.; Pluth, M. D., *J. Org. Chem.* **2014**, *79*, 711-719.
25. Pregosin, P. S.; Kunz, R. W., *³¹P and ¹³C NMR of transition metal phosphine complexes*. Springer Science & Business Media **2012**; Vol. 16.
26. Thordarson, P., *Chem. Soc. Rev.* **2011**, *40*, 1305-1323.

CHAPTER III

1. Lopez-Munoz, F.; Ucha-Udabe, R.; Alamo, C., *Neuropsychiatr. Dis. Treat.* **2005**, *1*, 329-43.
2. Babu, S. S.; Praveen, V. K.; Ajayaghosh, A., *Chem. Rev.* **2014**, *114*, 1973-2129.

3. Ivanova, B. B.; Spiteller, M., *Cryst. Growth Des.* **2010**, *10*, 2470-2474.
4. Gryl, M.; Koziel, M.; Stadnicka, K.; Matulkova, I.; Nemeč, I.; Tesarova, N.; Nemeč, P., *Crystengcomm* **2013**, *15*, 3275-3278.
5. Zadnarm, R.; Akbari-Moghaddam, P.; Darvishi, S., *Supramol. Chem.* **2017**, *29*, 17-23.
6. Wang, J. N.; Zhang, L.; Qi, Q.; Li, S. H.; Jiang, Y. B., *Anal. Methods* **2013**, *5*, 608-611.
7. Mahmudov, K. T.; Kopylovich, M. N.; Maharramov, A. M.; Kurbanova, M. M.; Gurbanov, A. V.; Pombeiro, A. J. L., *Coord. Chem. Rev.* **2014**, *265*, 1-37.
8. Seidenkranz, D. T.; McGrath, J. M.; Zakharov, L. N.; Pluth, M. D., *Chem. Commun.* **2017**, *53*, 561-564.
9. Baeyer, A., *Ann. Chem.* **1863**, *127*, 1-27.
10. Levina, R. Y.; Velichko, F. K., *Russ. Chem. Rev.* **1960**, *29*, 437.
11. Beres, J. A.; Pearson, D. E.; Bush, M. T., *J. Med. Chem.* **1967**, *10*, 1078-1080.
12. Tate, J. V.; Tinnerman, W. N.; Jurevics, V.; Jeskey, H.; Biehl, E. R., *J Heterocyclic Chem* **1986**, *23*, 9-11.
13. Singh, P.; Paul, K., *J Heterocyclic Chem* **2006**, *43*, 607-612.
14. Wang, J.; Zhang, L.; Qi, Q.; Li, S.; Jiang, Y., *Anal. Methods* **2013**, *5*, 608-611.
15. Tecilla, P.; Dixon, R. P.; Slobodkin, G.; Alavi, D. S.; Waldeck, D. H.; Hamilton, A. D., *J. Am. Chem. Soc.* **1990**, *112*, 9408-9410.
16. Aoki, I.; Kawahara, Y.; Sakaki, T.; Harada, T.; Shinkai, S., *BCSJ* **1993**, *66*, 927-933.
17. Aboul-Enein, H. Y.; Wainer, I. W., *The impact of stereochemistry on drug development and use*. Wiley: New York, 1997; p 695.
18. Han, J.; Zhao, L.; Yau, C. W.; Mak, T. C. W., *Cryst. Growth Des.* **2009**, *9*, 308-319.
19. Gryl, M.; Cenedese, S.; Stadnicka, K., *J. Phys. Chem. C* **2015**, *119*, 590-598.
20. Gryl, M.; Seidler, T.; Stadnicka, K.; Matulkova, I.; Nemeč, I.; Tesarova, N.; Nemeč, P., *Crystengcomm* **2014**, *16*, 5765-5768.

21. Chierotti, M. R.; Gobetto, R.; Pellegrino, L.; Milone, L.; Venturello, P., *Cryst. Growth Des.* **2008**, *8*, 1454-1457.
22. Powell, K. A.; Bartolini, G.; Wittering, K. E.; Saleemi, A. N.; Wilson, C. C.; Rielly, C. D.; Nagy, Z. K., *Cryst. Growth Des.* **2015**, *15*, 4821-4836.
23. Rossi, D.; Gelbrich, T.; Kahlenberg, V.; Griesser, U. J., *Crystengcomm* **2012**, *14*, 2494-2506.
24. Zencirci, N.; Gelbrich, T.; Kahlenberg, V.; Griesser, U. J., *Cryst. Growth Des.* **2009**, *9*, 3444-3456.
25. Lewis, T. C.; Tocher, D. A.; Price, S. L., *Cryst. Growth Des.* **2004**, *4*, 979-987.
26. Ooi, T.; Kameda, M.; Maruoka, K., *J. Am. Chem. Soc.* **2003**, *125*, 5139-5151.

CHAPTER IV

1. Nurttila, S. S.; Linnebank, P. R.; Krachko, T.; Reek, J. N. H., *ACS Catal.* **2018**, *8*, 3469-3488.
2. Franke, R.; Selent, D.; Borner, A., *Chem. Rev.* **2012**, *112*, 5675-5732.
3. Gorbunov, D. N.; Volkov, A. V.; Kardasheva, Y. S.; Maksimov, A. L.; Karakhanov, E. A., *Pet. Chem.* **2015**, *55*, 587-603.
4. Gusevskaya, E. V.; Jimenez-Pinto, J.; Borner, A., *ChemCatChem* **2014**, *6*, 382-411.
5. Kegl, T., *RSC Adv.* **2015**, *5*, 4304-4327.
6. Pospech, J.; Fleischer, I.; Franke, R.; Buchholz, S.; Beller, M., *Angew. Chem. Int. Ed.* **2013**, *52*, 2852-2872.
7. Sharma, S. K.; Jasra, R. V., *Catal. Today* **2015**, *247*, 70-81.
8. Vanbesien, T.; Monflier, E.; Hapiot, F., *Eur. J. Lipid Sci. Technol.* **2016**, *118*, 26-35.
9. Gil, W.; Trzeciak, A. M., *Coord. Chem. Rev.* **2011**, *255*, 473-483.
10. Gillespie, J. A.; Dodds, D. L.; Kamer, P. C. J., *Dalton Trans.* **2010**, *39*, 2751-2764.

11. Woodward, S.; Dieguez, M.; Pamies, O., *Coord. Chem. Rev.* **2010**, *254*, 2007-2030.
12. Agbossou, F.; Carpentier, J. F.; Mortreaux, A., *Chem. Rev.* **1995**, *95*, 2485-2506.
13. Breit, B.; Seiche, W., *Synthesis* **2001**, 1-36.
14. Deng, Y. C.; Wang, H.; Sun, Y. H.; Wang, X., *ACS Catal.* **2015**, *5*, 6828-6837.
15. Gladiali, S.; Bayon, J. C.; Claver, C., *Tetrahedron Asymmetry* **1995**, *6*, 1453-1474.
16. Gual, A.; Godard, C.; Castillon, S.; Claver, C., *Tetrahedron Asymmetry* **2010**, *21*, 1135-1146.
17. Klosin, J.; Landis, C. R., *Accounts Chem. Res.* **2007**, *40*, 1251-1259.
18. Yeung, C. S.; Dong, V. M., *Angew. Chem. Int. Ed.* **2011**, *50*, 809-812.
19. Bondzic, B. P., *J. Mol. Catal. A Chem.* **2015**, *408*, 310-334.
20. Kalck, P.; Urrutigoity, M., *Chem. Rev.* **2018**, *118*, 3833-3861.
21. Vasylyev, M.; Alper, H., *Synthesis* **2010**, 2893-2900.
22. Vilches-Herrera, M.; Domke, L.; Borner, A., *ACS Catal.* **2014**, *4*, 1706-1724.
23. Birkholz, M. N.; Freixa, Z.; van Leeuwen, P., *Chem. Soc. Rev.* **2009**, *38*, 1099-1118.
24. Dierkes, P.; van Leeuwen, P., *J. Chem. Soc. Dalton Trans.* **1999**, 1519-1529.
25. Breit, B., *Angew. Chem. Int. Ed.* **2005**, *44*, 6816-6825.
26. Meeuwissen, J.; Reek, J. N. H., *Nat. Chem.* **2010**, *2*, 615-621.
27. Sandee, A. J.; Reek, J. N. H., *Dalton Trans.* **2006**, 3385-3391.
28. Breit, B.; Seiche, W., *J. Am. Chem. Soc.* **2003**, *125*, 6608-6609.
29. Gellrich, U.; Seiche, W.; Keller, M.; Breit, B., *Angew. Chem. Int. Ed.* **2012**, *51*, 11033-11038.
30. Smejkal, T.; Breit, B., *Angew. Chem. Int. Ed.* **2008**, *47*, 311-315.
31. Weis, M.; Waloch, C.; Seiche, W.; Breit, B., *J. Am. Chem. Soc.* **2006**, *128*, 4188-4189.

32. Wieland, J.; Breit, B., *Nat. Chem.* **2010**, *2*, 832-837.
33. Bellini, R.; Chikkali, S. H.; Berthon-Gelloz, G.; Reek, J. N. H., *Angew. Chem. Int. Ed.* **2011**, *50*, 7342-7345.
34. Jiang, X. B.; Lefort, L.; Goudriaan, P. E.; de Vries, A. H. M.; van Leeuwen, P.; de Vries, J. G.; Reek, J. N. H., *Angew. Chem. Int. Ed.* **2006**, *45*, 1223-1227.
35. Kuil, M.; Soltner, T.; van Leeuwen, P.; Reek, J. N. H., *J. Am. Chem. Soc.* **2006**, *128*, 11344-11345.
36. Slagt, V. F.; Kamer, P. C. J.; van Leeuwen, P.; Reek, J. N. H., *J. Am. Chem. Soc.* **2004**, *126*, 1526-1536.
37. Slagt, V. F.; Roder, M.; Kamer, P. C. J.; van Leeuwen, P.; Reek, J. N. H., *J. Am. Chem. Soc.* **2004**, *126*, 4056-4057.
38. Slagt, V. F.; van Leeuwen, P.; Reek, J. N. H., *Angew. Chem. Int. Ed.* **2003**, *42*, 5619-5623.
39. Slagt, V. F.; van Leeuwen, P.; Reek, J. N. H., *Chem. Commun.* **2003**, 2474-2475.
40. Goudriaan, P. E.; van Leeuwen, P.; Birkholz, M. N.; Reek, J. N. H., *Eur. J. Inorg. Chem.* **2008**, 2939-2958.
41. Seidenkranz, D. T.; McGrath, J. M.; Zakharov, L. N.; Pluth, M. D., *Chem. Commun.* **2017**, *53*, 561-564.

CHAPTER V

1. Murata, K.; Aoki, M.; Nishi, T.; Ikeda, A.; Shinkai, S., *J. Chem. Soc. Chem. Commun.* **1991**, 1715-1718.
2. Pozzo, J. L.; Clavier, G. M.; Desvergne, J. P., *J. Mater. Chem.* **1998**, *8*, 2575-2577.
3. Haines, S. R.; Harrison, R. G., *Chem. Commun.* **2002**, 2846-2847.
4. Ayabe, M.; Kishida, T.; Fujita, N.; Sada, K.; Shinkai, S., *Org. Biomol. Chem.* **2003**, *1*, 2744-2747.
5. Sugiyasu, K.; Fujita, N.; Takeuchi, M.; Yamada, S.; Shinkai, S., *Org. Biomol. Chem.* **2003**, *1*, 895-899.

6. de Jong, J. J. D.; Lucas, L. N.; Kellogg, R. M.; van Esch, J. H.; Feringa, B. L., *Science* **2004**, *304*, 278-281.
7. Chen, X.; Huang, Z.; Chen, S. Y.; Li, K.; Yu, X. Q.; Pu, L., *J. Am. Chem. Soc.* **2010**, *132*, 7297-7299.
8. Ran, X.; Gao, Q. Q.; Zhang, Y.; Guo, L. J., *RSC Adv.* **2017**, *7*, 56016-56022.
9. Kartha, K. K.; Babu, S. S.; Srinivasan, S.; Ajayaghosh, A., *J. Am. Chem. Soc.* **2012**, *134*, 4834-4841.
10. Liu, Q. T.; Wang, Y. L.; Li, W.; Wu, L. X., *Langmuir* **2007**, *23*, 8217-8223.
11. Duan, P. F.; Yanai, N.; Nagatomi, H.; Kimizuka, N., *J. Am. Chem. Soc.* **2015**, *137*, 1887-1894.
12. Friggeri, A.; Gronwald, O.; van Bommel, K. J. C.; Shinkai, S.; Reinhoudt, D. N., *J. Am. Chem. Soc.* **2002**, *124*, 10754-10758.
13. An, B. K.; Lee, D. S.; Lee, J. S.; Park, Y. S.; Song, H. S.; Park, S. Y., *J. Am. Chem. Soc.* **2004**, *126*, 10232-10233.
14. Cardolaccia, T.; Li, Y. J.; Schanze, K. S., *J. Am. Chem. Soc.* **2008**, *130*, 2535-2545.
15. Kishimura, A.; Yamashita, T.; Aida, T., *J. Am. Chem. Soc.* **2005**, *127*, 179-183.
16. Kitamura, T.; Nakaso, S.; Mizoshita, N.; Tochigi, Y.; Shimomura, T.; Moriyama, M.; Ito, K.; Kato, T., *J. Am. Chem. Soc.* **2005**, *127*, 14769-14775.
17. Puigmarti-Luis, J.; Laukhin, V.; del Pino, A. P.; Vidal-Gancedo, J.; Rovira, C.; Laukhina, E.; Amabilino, D. B., *Angew. Chem. Int. Ed.* **2007**, *46*, 238-241.
18. Lee, D. C.; McGrath, K. K.; Jang, K., *Chem. Commun.* **2008**, 3636-3638.
19. Ajayaghosh, A.; Praveen, V. K., *Accounts Chem. Res.* **2007**, *40*, 644-656.
20. Ajayaghosh, A.; Praveen, V. K.; Vijayakumar, C., *Chem. Soc. Rev.* **2008**, *37*, 109-122.
21. Vintiloiu, A.; Leroux, J. C., *J. Control. Release* **2008**, *125*, 179-192.
22. Sangeetha, N. M.; Maitra, U., *Chem. Soc. Rev.* **2005**, *34*, 821-836.
23. Kimura, M.; Kobayashi, S.; Kuroda, T.; Hanabusa, K.; Shirai, H., *Adv. Mater.* **2004**, *16*, 335-338.

24. Simmons, B.; Li, S. C.; John, V. T.; McPherson, G. L.; Taylor, C.; Schwartz, D. K.; Maskos, K., *Nano Lett.* **2002**, *2*, 1037-1042.
25. Svobodova, H.; Noponen, V.; Kolehmainen, E.; Sievanen, E., *RSC Adv.* **2012**, *2*, 4985-5007.
26. Hirst, A. R.; Smith, D. K., *Chem. Eur. J.* **2005**, *11*, 5496-5508.
27. Draper, E. R.; Adams, D. J., *Chem. Soc. Rev.* **2018**.
28. Buerkle, L. E.; Rowan, S. J., *Chem. Soc. Rev.* **2012**, *41*, 6089-6102.
29. Abdallah, D. J.; Weiss, R. G., *Adv. Mater.* **2000**, *12*, 1237-1247.
30. Hanabusa, K.; Miki, T.; Taguchi, Y.; Koyama, T.; Shirai, H., *J. Chem. Soc. Chem. Commun.* **1993**, 1382-1384.
31. Jeong, S. W.; Murata, K.; Shinkai, S., *Supramol. Sci.* **1996**, *3*, 83-86.
32. Inoue, K.; Ono, Y.; Kanekiyo, Y.; Ishi-i, T.; Yoshihara, K.; Shinkai, S., *J. Org. Chem.* **1999**, *64*, 2933-2937.
33. Yagai, S.; Higashi, M.; Karatsu, T.; Kitamura, A., *Chem. Mat.* **2004**, *16*, 3582-3585.
34. Yagai, S.; Nakajima, T.; Kishikawa, K.; Kohmoto, S.; Karatsu, T.; Kitamura, A., *J. Am. Chem. Soc.* **2005**, *127*, 11134-11139.
35. Schmidt, R.; Stolte, M.; Grune, M.; Wurthner, F., *Macromolecules* **2011**, *44*, 3766-3776.
36. Brizard, A.; Oda, R.; Huc, I., Chirality Effects in Self-assembled Fibrillar Networks. In *Low Molecular Mass Gelator*, Springer Berlin Heidelberg: Berlin, Heidelberg, 2005; pp 167-218.
37. Ajayaghosh, A.; Varghese, R.; George, S. J.; Vijayakumar, C., *Angew. Chem. Int. Ed.* **2006**, *45*, 1141-1144.
38. Cai, W.; Wang, G. T.; Du, P.; Wang, R. X.; Jiang, X. K.; Li, Z. T., *J. Am. Chem. Soc.* **2008**, *130*, 13450-13459.
39. Das, R. K.; Kandanelli, R.; Linnanto, J.; Bose, K.; Maitra, U., *Langmuir* **2010**, *26*, 16141-16149.
40. Hifsudheen, M.; Mishra, R. K.; Vedhanarayanan, B.; Praveen, V. K.; Ajayaghosh, A., *Angew. Chem. Int. Ed.* **2017**, *56*, 12634-12638.

41. Sun, Y.; Li, S.; Zhou, Z.; Saha, M. L.; Datta, S.; Zhang, M.; Yan, X.; Tian, D.; Wang, H.; Wang, L.; Li, X.; Liu, M.; Li, H.; Stang, P. J., *J. Am. Chem. Soc.* **2018**, *140*, 3257-3263.
42. Bielejewski, M.; Kowalczyk, J.; Kaszynska, J.; Lapinski, A.; Luboradzki, R.; Demchuk, O.; Tritt-Goc, J., *Soft Matter* **2013**, *9*, 7501-7514.
43. Hisamatsu, Y.; Banerjee, S.; Avinash, M. B.; Govindaraju, T.; Schmuck, C., *Angew. Chem. Int. Ed.* **2013**, *52*, 12550-12554.
44. Murata, K.; Aoki, M.; Suzuki, T.; Harada, T.; Kawabata, H.; Komori, T.; Ohseto, F.; Ueda, K.; Shinkai, S., *J. Am. Chem. Soc.* **1994**, *116*, 6664-6676.

CHAPTER VI

1. Cooke, G.; Rotello, V. M., *Chem. Soc. Rev.* **2002**, *31*, 275-286.
2. Chang, S. K.; Hamilton, A. D., *J. Am. Chem. Soc.* **1988**, *110*, 1318-1319.
3. Chang, S. K.; Van Engen, D.; Fan, E.; Hamilton, A. D., *J. Am. Chem. Soc.* **1991**, *113*, 7640-7645.
4. McGrath, J. M.; Pluth, M. D., *J. Org. Chem.* **2014**, *79*, 711-719.
5. McGrath, J. M.; Pluth, M. D., *J. Org. Chem.* **2014**, *79*, 11797-11801.
6. Hager, K.; Hartnagel, U.; Hirsch, A., *Eur. J. Org. Chem.* **2007**, 1942-1956.
7. Li, Y.; He, Y. M.; Li, Z. W.; Zhang, F.; Fan, Q. H., *Org. Biomol. Chem.* **2009**, *7*, 1890-1895.
8. Binder, W. H.; Kunz, M. J.; Kluger, C.; Hayn, G.; Saf, R., *Macromolecules* **2004**, *37*, 1749-1759.
9. Binder, W. H.; Petraru, L.; Roth, T.; Groh, P. W.; Palfi, V.; Keki, S.; Ivan, B., *Adv. Funct. Mater.* **2007**, *17*, 1317-1326.
10. Chen, S. B.; Mahmood, N.; Beiner, M.; Binder, W. H., *Angew. Chem. Int. Ed.* **2015**, *54*, 10188-10192.
11. Bosch, S.; Zeininger, L.; Hauke, F.; Hirsch, A., *Chem.-Eur. J.* **2014**, *20*, 2537-2541.
12. Wessendorf, F.; Gnichwitz, J. F.; Sarova, G. H.; Hager, K.; Hartnagel, U.; Guldi, D. M.; Hirsch, A., *J. Am. Chem. Soc.* **2007**, *129*, 16057-16071.

13. Wessendorf, F.; Grimm, B.; Guldi, D. M.; Hirsch, A., *J. Am. Chem. Soc.* **2010**, *132*, 10786-10795.
14. Pagona, G.; Stergiou, A.; Gobeze, H. B.; Rotas, G.; D'Souza, F.; Tagmatarchis, N., *Phys. Chem. Chem. Phys.* **2016**, *18*, 811-817.
15. Ema, T.; Okuda, K.; Watanabe, S.; Yamasaki, T.; Minami, T.; Esipenko, N. A.; Anzenbacher, P., *Org. Lett.* **2014**, *16*, 1302-1305.
16. Ema, T.; Tanida, D.; Sakai, T., *Org. Lett.* **2006**, *8*, 3773-3775.
17. Ema, T.; Tanida, D.; Sakai, T., *J. Am. Chem. Soc.* **2007**, *129*, 10591-10596.
18. Izuo, A.; Yohko, K.; Toru, S.; Takaaki, H.; Seiji, S., *Bull. Chem. Soc. Jpn.* **1993**, *66*, 927-933.
19. Chambers, R. C.; Bell, E. J.; Records, T. M.; Cherian, A.; Ragan, K.; Swartout, B., *Liq. Cryst.* **2007**, *34*, 1221-1226.
20. Westwood, J.; Coles, S. J.; Collinson, S. R.; Gasser, G.; Green, S. J.; Hursthouse, M. B.; Light, M. E.; Tucker, J. H. R., *Organometallics* **2004**, *23*, 946-951.
21. Young, M. C.; Liew, E.; Hooley, R. J., *Chem. Commun.* **2014**, *50*, 5043-5045.
22. Kondo, S.; Endo, K.; Lioka, J.; Sato, K.; Matsuta, Y., *Tetrahedron Lett.* **2017**, *58*, 4115-4118.
23. Seidenkranz, D. T.; McGrath, J. M.; Zakharov, L. N.; Pluth, M. D., *Chem. Commun.* **2017**, *53*, 561-564.
24. Spitler, E. L.; Shirtcliff, L. D.; Haley, M. M., *J. Org. Chem.* **2007**, *72*, 86-96.
25. Wilson, J. N.; Bunz, U. H. F., *J. Am. Chem. Soc.* **2005**, *127*, 4124-4125.
26. Solvent and Environmental Effects. In *Principles of Fluorescence Spectroscopy*, Lakowicz, J. R., Ed. Springer US: Boston, MA, 2006; pp 205-235.